Acta morphologica et anthropologica 29 (1–2)

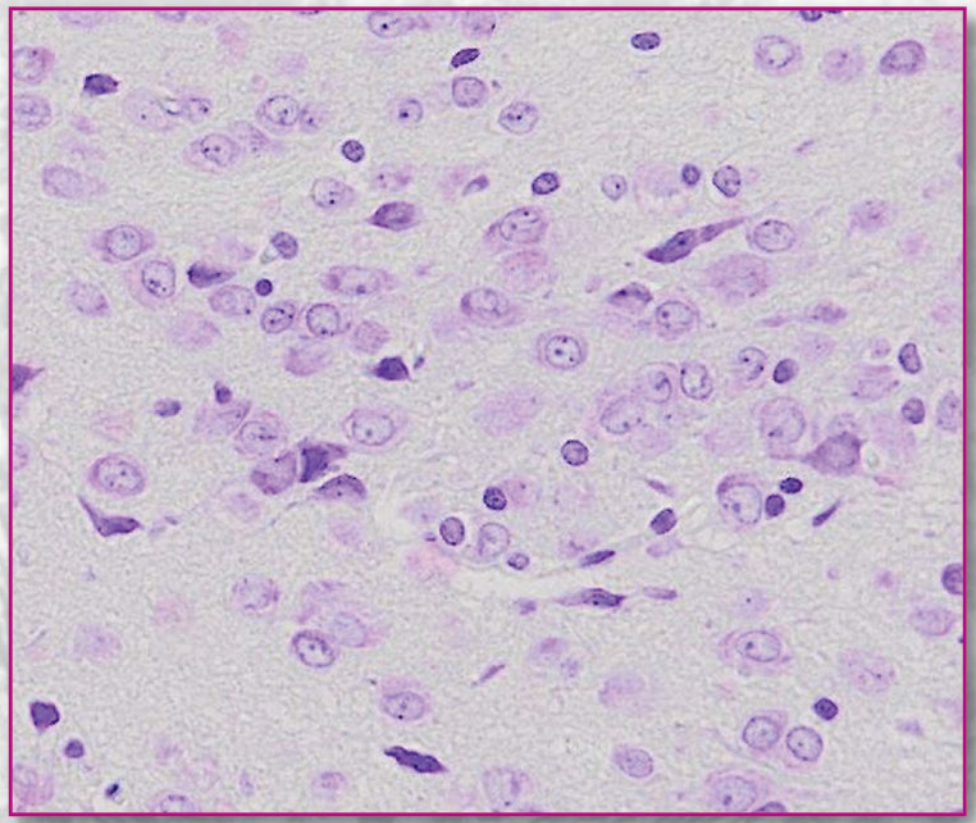

Prof. Marin Drinov Publishing House
of Bulgarian Academy of Sciences

Acta morphologica et anthropologica
is the continuation of Acta cytobiologica et morphologica

Editor-in-Chief: Prof. Nina Atanassova
e-mail: ninaatanassova@yahoo.com
+359 2 979 2342
Deputy Editor-in-Chief: Prof. Dimitar Kadiysky
e-mail: dkadiysky@yahoo.com
+359 2 979 2340
Managing Editor: Assoc. Prof. Y. Gluhcheva
e-mail: ygluhcheva@hotmail.com
+359 2 979 2344

Editorial Correspondence
Institute of Experimental Morphology, Pathology and Anthropology with Museum
Bulgarian Academy of Sciences
Acta morphologica et anthropologica
Acad. Georgi Bonchev Str., Bl. 25
1113 Sofia, Bulgaria

E-mail: ygluhcheva@hotmail.com, iempam@bas.bg
Tel.: +359 2 979 2344

Издаването на настоящия том 29, книжки 1 и 2 е осъществено с финансовата подкрепа на Фонд „Научни изследвания“

Prof. Marin Drinov Publishing House of Bulgarian Academy of Sciences
Bulgaria, 1113 Sofia, Acad. Georgi Bonchev Str., Bl. 6

Graphic designer Veronika Tomcheva
Format 70×100/16 Printed sheets 11,37

Printing Office of Prof. Marin Drinov Publishing House of Bulgarian Academy of Sciences
Bulgaria, 1113 Sofia, Acad. Georgi Bonchev Str., Bl. 5

ISSN 1311-8773 (print)
ISSN 2535-0811 (online)

Acta morphologica et anthropologica

29
(1-2)

29 (1-2) ● Sofia ● 2022
Institute of Experimental Morphology, Pathology and Anthropology with Museum
Bulgarian Anatomical Society

Contents

MORPHOLOGY 29 (1)

Original Articles

ANTHROPOLOGY AND ANATOMY 29 (2)

Institute of Experimental Morphology, Pathology and Anthropology with Museum
Bulgarian Anatomical Society

Acta morphologica et anthropologica, 29 (1-2)
Sofia ● 2022

MORPHOLOGY 29 (1)

Original Articles

The Bed Nucleus of the Stria Terminalis: Cytoarchitecture and Morphometry of its Subnuclear Organizationin the rat Brain

Albert Gradev[1], Lazar Jelev[1], Nikolai Lazarov[1,2]*

[1]Department of Anatomy, Histology and Embryology, Medical University of Sofia, Sofia, Bulgaria
[2]Institute of Neurobiology, Bulgarian Academy of Sciences, Sofia, Bulgaria

*Corresponding author e-mail: a.gradev@medfac.mu-sofia.bg

The complexity of the bed nucleus of the stria terminalis (BNST), its function, sex difference, cyto- and chemoarchitectonic structure has intrigued scientists during the last decades. As part of the extended amygdala, it is involved in many limbic functions being the main target of treating anxiety and addiction as lately revealed. This paper is a brief review of the BNST structure and also a morphometric study of its subnuclear groups in the adult male rat brain. The Kluver-Barrera staining revealed the main white matter tracts which serve us for landmarks to identify the BNST subdivisions. The majority of BNST neurons were small in size, less than 15μm in diameter, oval in shape and with prominent nucleoli. The present results clearly show the complexity in the BNST structural organization to better understand its function, and to emphasize it as a novel research area of the functional morphology.

Key words: Bed nucleus of stria terminalis, morphometry, cytoarchitecture, rat

Introduction

The bed nucleus of the str ia terminalis (BNST) is a complex brain structure located in the basal forebrain which belongs to the extended amygdala [1, 23]. Its position is almost the same in the rodent and human brain [35, 43] and can be defined as a structure that surrounds the anterior commissure, medial to the internal capsule, posterior to the

nucleus accumbens, anterior to the thalamus and in proximity to the ventral pallidum and hypothalamus [2]. Such a location gives a bright suggestion for its function as a general integral unit for the limbic system and makes it easily accessible for different studies. Based on its complexity, a number of classification systems about the subnuclear groups of the BNST has been developed [14, 26, 32, 35, 37]. It is generally accepted that the BNST is primarily divided into anterior and posterior divisions. The anterior division consists of dorsal and ventral areas and contains a number of nuclei, including the oval, fusiform, rhomboid, magnocellular, ventral and dorsomedial nucleus. The principal, transverse, supracapsular (strial extension) and interfascicular nuclei can be identified in the posterior part [37].

In this study, we further describe the nuclear organization of the BNST in the adult rat brain.

Material and Methods

Ten 3-month-old male Wistar rats were used for the study. The experiments were performed in agreement with the European Communities Council Directive 2010/63/EU for the protection of animals used for scientific purposes. After deep ether anesthesia, the animals were euthanized by cervical dislocation and then transcardially perfused. After washing the blood vessels with cold normal saline (0.9% NaCl solution) for about 20 min, 4% paraformaldehyde fixation solution was introduced for about 30 min. After decapitation, the brains were quickly removed from the skull and postfixed overnight with 4% paraformaldehyde in a refrigerator at 4°C. The brain was then trimmed into blocks at the levels of the BNST as follows: coronal section of the whole brain at a level 5 mm posterior to the olfactory tubercle; coronal section of the hemisphere (thickness of 4 mm) – from 1 mm anteriorly to 3 mm posteriorly to the anterior commissure; sagittal section of the hemisphere (thickness of 3 mm) – 0.5 mm laterally to the midline; horizontal sections of the hemisphere (thickness of 4 mm) – from 1 mm under to 3 mm above the anterior commissure.

Paraffin embedded tissue slices from specific brain regions were cut at a thickness of 7 μm and appropriately stained to demonstrate the brain structures. We used routine H&E and Nissl stains to visualize the neuronal morphology while Kluver-Barrera staining method [29] was applied to observe both myelinated fibers and nerve cells. The samples were examined and photographed under an Olympus light microscope, digital images were created with a slide scanner (Olympus VS 120 Slide scanner) and an Imaging Analyzing System (Olympus VS-ASW) was used for morphometry. The BNST subdivisions are mapped according to Paxinos and Watson's rat brain in stereotaxic coordinates [35] and the rat brain schematics available from Swanson [37].

Results

On the frontal, sagittal and horizontal slices, we found a large number of neurons in the different regions in the BNST (**Figs. 1-3**). We also observed very clearly the transition between the anterior and posterior nuclear groups in horizontal and sagittal sections through the stria terminalis (**Fig. 1**). In the anterior division, the

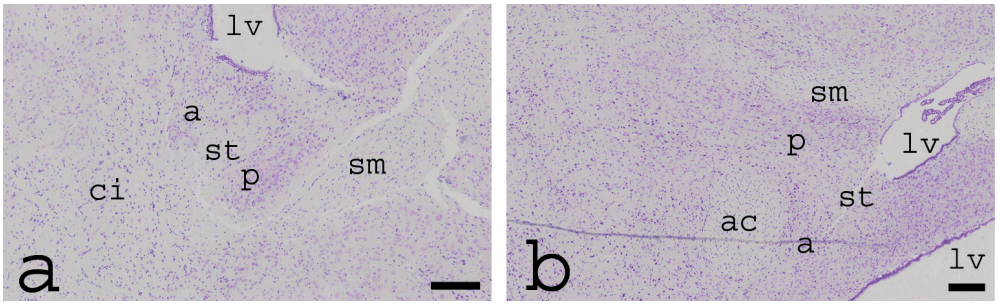

Fig. 1. Photomicrographs of Nissl-stained horizontal (a) and sagittal (b) sections at the level the BNST. The stria terminalis (st) divides the nucleus into an anterior (a) and a posterior (p) parts. Stria medullaris (sm), capsula interna (ci), and lateral ventricle (lv) are also visible while the anterior commissure is seen only on (b). Scale bar = 200 μm.

posterodorsal nucleus of the BNST, also called oval nucleus, is shown on **Fig. 2**. It is a part of anterolateral area according to the atlas of Swanson [37]. The oval nucleus was composed of small-sized neurons with an oval to polygonal shape and diameter of 9-15 μm that cover an area of approximately 120 μm^2. The neurons have large nuclei (7-13 μm in diameter) with a prominent nucleolus. The Nissl bodies were well distinguished, which correlates with the great metabolic activity of these neurons. In the anterior part several nuclei were identified – the ventromedial, ventrolateral nucleus, medialis anterior, lateralis posterior, or the anteromedial area and anterolateral area according to Swanson [37]. In the anterolateral area with its ventral part, we observed neurons of various shapes and size and most of these showed oval bodies (**Fig. 2**). We also found a small number of spindle-shaped perikaryal profiles. The morphometric analysis revealed a population of small-sized cells with diameter ranges from 8 to 16 μm that occupied a cell surface area of approximately 100 μm^2. The boundaries between the other different areas or nuclei were not clearly

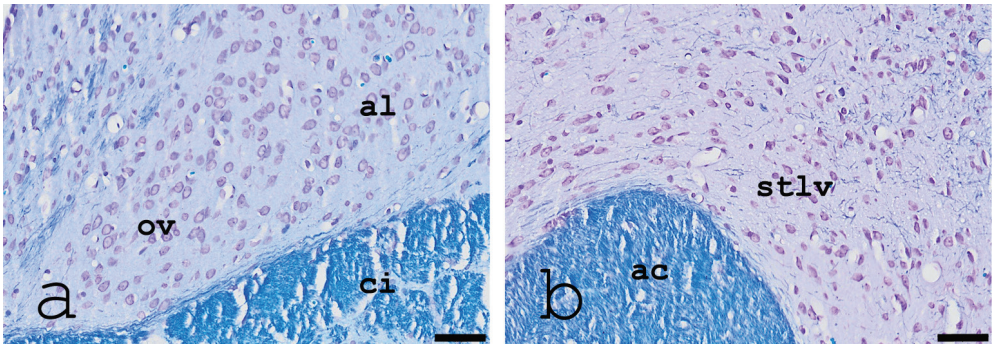

Fig. 2. Photomicrographs of Kluver-Barrera-stained frontal sections through the BNST. In (a) the oval nucleus (ov) is presented. Note the blue-depicted initial fibers of stria terminalis which are seen between the neurons. The capsula interna (ci) and the remaining part of anterolateral area (al) are evident as well. In (b) the neurons in the ventrolateral area (stlv) are shown. The anterior commissure (ac) is also visible. Scale bar = 50 μm.

discernible. In the posterior division of BNST, we identifed the BNSTprincipal and supracapsular nuclei. In the supracapsular nucleus, also known as the strial extension of the BNST, a small number of small-to-medium in size, oval to polygonal neurons with a diameter between 8 μm and 15 μm, and a cell surface area of 115-191 μm^2 was seen. The neurons also had large nuclei (6-12 μm in diameter) with prominent nucleoli. The nerve fibers of the stria terminalis, depicted in blue after the Kluver-Barrera staining, were clearly visible between neurons. In the superior portions of the principal nucleus of the BNST and initial parts of the strial extension, i.e. the supracapsular nucleus on transverse and sagittal sections, we found a few small-sized, lightly-stained neurons with a diameter 8-13 μm and a surface area ranging from 50 μm^2 to 89 μm^2 (**Fig. 3**).

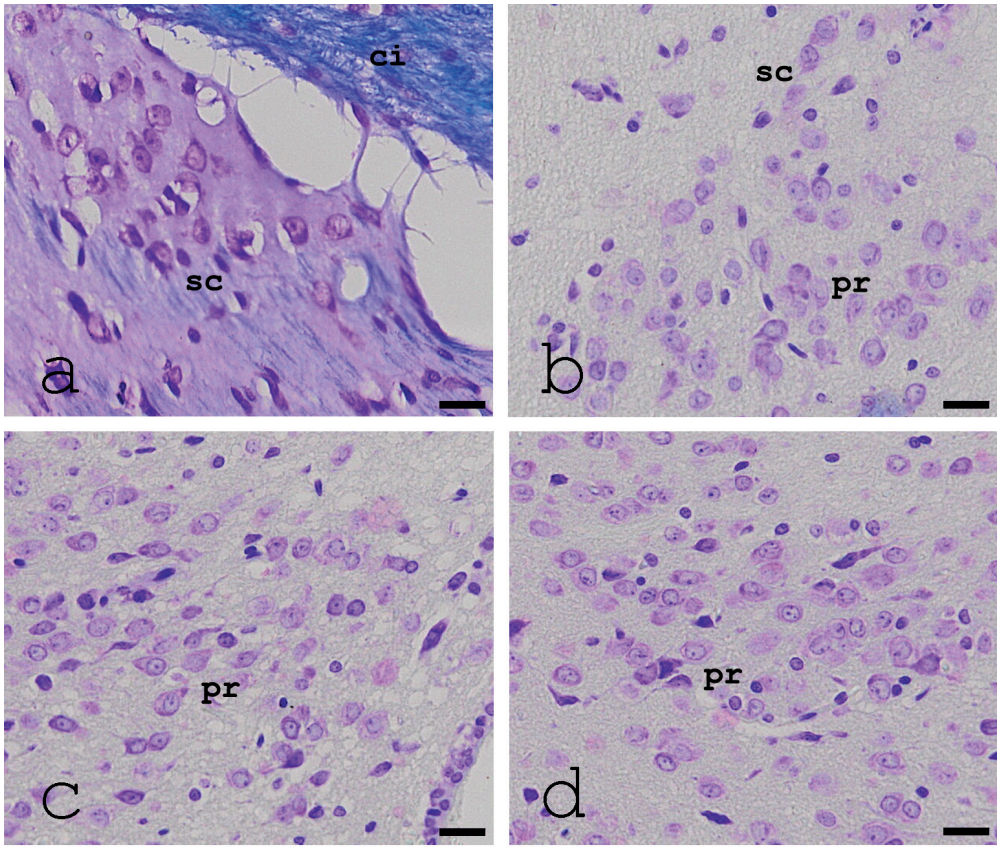

Fig. 3. Photomicrographs of a Kluver-Barrera-stained coronal section (a), and Nissl-stained horizontal (b) and sagittal (c,d) sections of the BNST. The supracapsular nucleus (sc) is shown in (a). The blue-stained fibers of the stria terminalis and the capsula interna (ci) are displayed. In (b) neurons in the principal nucleus (pr) and initial portion of the supracapsular nucleus (sc) are identified. In (c) and (d) the neurons of the principal nucleus (pr) at lower levels are shown. Scale bar = 20 μm.

Discussion

The BNST is originally described by Johnston [25] as a cell cluster surrounding the initial part of the stria terminalis. Subsequently, it has been extensively studied but the interest for it as a possible contributor to some psychiatric disorders has been renewed in the last 20 years [4, 11, 12, 16, 17, 18, 21, 22, 31, 44]. Evidence for its complexity is obvious in the works of different morphologists, who have described a number of subnuclei and specific neuronal types [26, 35, 37]. The divisions of the BNST are based on morphological (location to anterior commissure or stria terminalis), functional or neurochemical criteria [14, 26, 32, 35, 37].

Complexity of the BNST is clearly shown in many studies, most of which on the rat brain, although they appear contradictory in relation to its subnuclear structure [7, 14, 26, 32, 35, 37]. Classically, the BNST is divided into medial and lateral subdivisions [1, 32], which corresponds to the theory of the extended amygdala [7, 23]. Another major classification divides the BNST in antero-posterior direction [26, 37]. This division is consistent with its embryonic origin and is more useful with regards to its connections [5, 20]. Another way to divide the nuclear groups within the BNST is the dorso-ventral orientation with respect to the anterior commissure [14]. Additionaly each division displays its own subnuclei. Over the time, many neuroscientists have used the atlases of Paxinos and Watson [35] or Swanson [37] and the terminology therein. In the latter, an improved version of the Ju and Swanson classification was added [26]. In the further descriptions the Swanson nomenclature [37] and Bota's table [7] for comparison of terms are used.

Of all nuclear groups, the principal nucleus, the oval nucleus, and some of the medioventral and ventrolateral nuclei are particularly fascinating due to the fact that some of them exhibit different characteristics between sexes and thus show sexual dimorphism [3, 15, 27, 39, 40]. The sex difference starts after birth, and continues into adulthood [8]. It is a result of apoptosis [9], which might be epigenetically controlled [33]. Some of the neurons might continue their development and adapt their cellular and synaptic activity during puberty, depending on previous stress history [18, 22, 42]. This fact, together with the current evidence for stem cell niches in the ventral pallidum [22], indicates that the BNST is very dynamic in its development. This dynamic, taking into account the function of the nucleus, bring us to the idea of future in-depth studying of periadolescent development, and specifically how stress factors could correlate with different psychiatric disorders, and how do they change the anatomy of the BNST.

The complexity of BNST is not only valid for its subnuclear division, but also for its neurochemical profile, types of neurons and their connections, functions and gene expression [5, 6, 12, 14, 26, 32, 34]. The main types of neurons in BNST are GABAergic, mainly seen in the oval nucleus [28, 36]. A few BNST neurons in its principal, medioventral and fusiform nuclei use glutamate as a neurotransmitter [28, 36]. A broad spectrum of neuropeptides including corticotropin-releasing hormone, neuropeptide Y, enkephalins, dynorphin, neurotensin, oxytocin, pituitary adenylate-cyclase-activating polypeptide, vasoactive intestinal peptide, cholecystokinin, substance P, orexin and galanin has also been established in the nucleus [6, 23 30, 31]. Among them, oxytocin and arginine vasopressin are the most intriguing since they are proposed as novel medication treatments for some anxiety disorders [13]. This finding suggests a brain-storming complexity of the limbic connectivity, circuits and controls of emotions. In

addition, in the BNST of some monogamous rodent species, such as the California mouse, some oxytocinergic neurons were recently identified [17] and they belong to the so-called extra-hypothalamic oxytocin system. Moreover, many oxytocin (OXT) receptors are present on BNST-neurons [11, 15, 19, 38, 41]. The occurrence of such OXT receptors on GABAergic terminals, some of them co-expressed with corticotropin-releasing hormones, a neuropeptide [6, 10, 11], suggests a large contribution of OXT to all functions of the BNST, and primarily the anxiety-related ones. Taken together with its sexual dimorphism and intriguing peripubertal development, the present data identify the BNST as a novel research area, particularly in the field of functional morphology and psychiatry.

References

1. **Alheid, G. F.** Extended Amygdala and Basal Forebrain. – *Ann. N. Y. Acad. Sci.,* **985(1),** 2006, 185-205.
2. **Alheid, G. F., L. Heimer.** New perspectives in basal forebrain organization of special relevance for neuropsychiatric disorders: the striatopallidal, amygdaloid, and corticopetal components of substantia innominata. – *Neuroscience*, **27**, 1988, 1-39.
3. **Allen, L. S., R. A. Gorski.** Sex difference in the bed nucleus of the stria terminalis of the human brain. – *J. Comp. Neurol.,* **302(4)**, 1990, 697-706.
4. **Avery, S. N., J. A. Clauss, J. U. Blackford.** The Human BNST: Functional Role in Anxiety and Addiction. – *Neuropsychopharmacology*, **41(1)**, 2016, 126-141.
5. **Bayer, S. A.** Neurogenetic and morphogenetic heterogeneity in the bed nucleus of the stria terminalis. – *J. Comp. Neurol*., **265(1)**, 1987, 47-64.
6. **Beyeler, A., J. Dabrowska**. Neuronal diversity of the amygdala and the bed nucleus of the stria terminalis. – *Handb Behav. Neurosci.,***26**, 2020, 63-100.
7. **Bota, M., L. W. Swanson LW.** Collating and curating neuroanatomical nomenclatures: Principles and use of the brain architecture knowledge management system (BAMS). – *Front Neuroinform*., **4**, 2010, 3.
8. **Chung, W. C. J., G. J. De Vries, D. F. Swaab.** Sexual differentiation of the bed nucleus of the stria terminalis in humans may extend into adulthood. – *J. Neurosci.***, 22(3)**, 2002, 1027–1033.
9. **Chung, W. C., D. F. Swaab, G. J. De Vries.** Apoptosis during sexual differentiation of the bed nucleus of the stria terminalis in the rat brain. – *J. Neurobiol*., **43(3)**, 2000, 234-243.
10. **Dabrowska, J., R. Hazra, J. D. Guo, S. Dewitt, D. G. Rainnie.** Central CRF neurons are not created equal: phenotypic differences in CRF-containing neurons of the rat paraventricular hypothalamus and the bed nucleus of the stria terminalis. – *Front Neurosci*., **7**, 2013, 156.
11. **Dabrowska, J., R. Hazra, T. H. Ahern, J. D. Guo, A. J. McDonald, F. Mascagni, J. F. Muller, L. G. Young, D. G. Rainnie.** Neuroanatomical evidence for reciprocal regulation of the corticotrophin-releasing factor and oxytocin systems in the hypothalamus and the bed nucleus of the stria terminalis of the rat: Implications for balancing stress and affect. – *Psychoneuroendocrinology,* **36(9)**, 2011, 1312-1326.
12. **Daniel, S., D. Rainnie.** Stress modulation of opposing circuits in the bed nucleus of the stria terminalis. – *Neuropsychopharmacology,* **41**, 2016, 103-125.
13. **De Cagna, F., L. Fusar-Poli, S. Damiani, M. Rocchetti, G. Giovanna, A. Mori, P. Politi, N. Brondino.** The role of intranasal oxytocin in anxiety and depressive disorders: A systematic review of randomized controlled trials. – *Clin. Psychopharmacol. Neurosci*., **17(1),** 2019, 1-11.

14. De Olmos, J. S., W. R. Ingram. The projection field of the stria terminalis in the rat brain. An experimental study. – *J. Comp. Neurol.*, **146(3),** 1972, 303-333.
15. Dumais, K. M., R. Bredewold , T. E. Mayer, A. H. Veenema. Sex differences in oxytocin receptor binding in forebrain regions: correlations with social interest in brain region- and sex- specific ways. – *Horm. Behav*., **64(4),** 2013, 693-701.
16. Dumont, É. C. What is the bed nucleus of the stria terminalis? – *Prog. Neuro-Psychopharmacol. Biol. Psychiatry*, **33(8)**, 2009, 1289-1290.
17. Duque-Wilckens, N., L. Y. Torres, S. Yokoyama, V. A. Minie, A. M. Tran, S. P. Petkova, R. Hao, S. Ramos-Maciel, R. A. Rios, K. Jackson, F. J. Flores-Ramirez, I. Garcia-Carachure, P. A. Pesavento, S. D. Iniguez, V. Grinevich, B. C. Trainor. Extrahypothalamic oxytocin neurons drive stress-induced social vigilance and avoidance. – *Proc. Natl. Acad. Sci.,* **117 (42)**, 2020, 26406-26413.
18. Flanigan, M. E., T. L. Kash. Coordination of social behaviors by the bed nucleus of the stria terminalis. – *Eur. J. Neurosci*., 2020, 1-17.
19. Francesconi, W., F. Berton, V. Olivera-Pasilio, J. Dabrowska. Oxytocin excites BNST interneurons and inhibits BNST output neurons to the central amygdala. – *Neuropharmacology.,***192**, 2021, 108601.
20. García-López, M., A. Abellán , I. Legaz , J. L. Rubenstein, L. Puelles, L. Medina. Histogenetic compartments of the mouse centromedial and extended amygdala based on gene expression patterns during development. – *J. Comp. Neurol.,* **506(1),** 2008, 46-74.
21. Grinevich, V., M. G. Desarménien, B. Chini, M. Tauber, F. Muscatelli. Ontogenesis of oxytocin pathways in the mammalian brain: late maturation and psychosocial disorders. – *Front. Neuroanat*., **8**, 2015, 164.
22. Heimer, L. A new anatomical framework for neuropsychiatric disorders and drug abuse. *Am J Psychiatry.,* **160(10),** 2003, 1726-1739.
23. Heimer, L., J. de Olmos, G. F. Alheid, L. Záborszky. "Perestroika" in the basal forebrain: opening the border between neurology and psychiatry. – *Prog. Brain Res*., **87**, 1991, 109-165.
24. Hammack, S. E., K. M. Braas, V. May. Chemoarchitecture of the bed nucleus of the stria terminalis: Neurophenotypic diversity and function. – *Handb Clin Neurol*. **179**, 2021, 385-402.
25. Johnston, J. B. Further contributions to the study of the evolution of the forebrain. – *J. Comp. Neurol.*, **35(5)**, 1923, 337-481.
26. Ju, G., L. W. Swanson. Studies on the cellular architecture of the bed nuclei of the stria terminalis in the rat: I. cytoarchitecture. – *J. Comp. Neurol.*, **280(4)**, 1989, 587-602.
27. Juraska, J. M., C. L. Sisk, L. L. DonCarlos. Sexual differentiation of the adolescent rodent brain: Hormonal influences and developmental mechanisms. – *Horm. Behav*., **64(2)**, 2013, 203-210.
28. Kim, S.R., S. Y. Kim. Functional Dissection of Glutamatergic and GABAergic Neurons in the Bed Nucleus of the Stria Terminalis. – *Mol. Cells,***44(2)**, 2021, 63-67.
29. Klüver, H., E. Barrera. A Method for the Combined Staining of Cells and Fibers in the Nervous System. – *J. Neuropathol. Exp. Neurol.*, **12(4)**, 1953, 400-403.
30. Lazarov, N., K. Usunoff, D. Itzev, A. Rolfs, A. Wree, O. Schmitt. Orexinergic innervation of the rat extended amygdala. – *Acta morphol. anthropol.*, 2011, **17**, 10-14.
31. Lebow, M. A., A. Chen. Overshadowed by the amygdala: the bed nucleus of the stria terminalis emerges as key to psychiatric disorders. – *Mol. Psychiatry*., **21**, 2016, 450-463.
32. Moga, M. M., C. B. Saper, T. S. Gray. Bed nucleus of the stria terminalis: Cytoarchitecture, immunohistochemistry, and projection to the parabrachial nucleus in the rat. – *J. Comp. Neurol.*, **283(3)**, 1989, 315-332.
33. Murray, E. K., A. Hien, G. J. de Vries, N. G. Forger. Epigenetic control of sexual differentiation of the bed nucleus of the stria terminalis. – *Endocrinology*, **150(9)**, 2009, 4241-4247.

34. Ortiz-Juza, M. M., R. A. Alghorazi, J. Rodriguez-Romaguera. Cell-type diversity in the bed nucleus of the stria terminalis to regulate motivated behaviors. – *Behav. Brain Res.,* **411**, 2021, 11340.
35. Paxinos, G., C. Watson. The rat brain in stereotaxic coordinates. 6th ed. London. Elsevier Inc. 2007.
36. Poulin, J. F., D. Arbour, S. Laforest, G. Drolet. Neuroanatomical characterization of endogenous opioids in the bed nucleus of the stria terminalis. – *Prog. Neuropsychopharmacol. Biol. Psychiatry*, **33**, 2009, 1356-1365.
37. Swanson, L. W. Brain maps 4.0-Structure of the rat brain: An open access atlas with global nervous system nomenclature ontology and flatmaps. – *J. Comp. Neurol*., **526(6)**, 2018, 935-943.
38. Tribollet, E., C. Barberis, S. Jard, M. Dubois-Dauphin, J. J. Dreifuss. Localization and pharmacological characterization of high affinity binding sites for vasopressin and oxytocin in the rat brain by light microscopic autoradiography. – *Brain Res.*, **442(1)**, 1988, 105-118.
39. Tsukahara, S., M. Morishita. Sexually dimorphic formation of the preoptic area and the bed nucleus of the stria terminalis by neuroestrogens. – *Front. Neurosci.***, 14**, 2020, 797.
40. Uchida, K., H. Otsuka, M. Morishita, S. Tsukahara, T. Sato, K. Sakimura, K. Itoi. Female-biased sexual dimorphism of corticotropin-releasing factor neurons in the bed nucleus of the stria terminalis. – *Biol. Sex Differ.*, **10(1)**, 2019, 6.
41. Veinante, P., M. J. Freund-Mercier. Distribution of oxytocin- and vasopressin-binding sites in the rat extended amygdala: a histoautoradiographic study. – *J. Comp. Neurol.,* **383(3),** 1997, 305-325.
42. Walker, D. L., M. Davis. Role of the extended amygdala in short-duration versus sustained fear: a tribute to Dr. Lennart Heimer. – *Brain Struct. Funct*., **213(1-2)**, 2008, 29-42.
43. Walter, A., J. K. Mai, L. Lanta, T. Görcs. Differential distribution of immunohistochemical markers in the bed nucleus of the stria terminalis in the human brain. – *J. Chem. Neuroanat.*, **4(4)**, 1991, 281-298.
44. Yassa, M. A., R. L. Hazlett , C. E. Stark, R. Hoehn-Saric. Functional MRI of the amygdala and bed nucleus of the stria terminalis during conditions of uncertainty in generalized anxiety disorder. – *J. Psychiatr. Res.* **46(8)**, 2012, 1045-1052.

Institute of Experimental Morphology, Pathology and Anthropology with Museum
Bulgarian Anatomical Society

Acta morphologica et anthropologica, 29 (1-2)
Sofia ● 2022

Morphology of NOS-immunoreactive Neurons in the Human Thalamic Reticular Nucleus and its Clinical Implications

Lina G. Malinova

Department of Anatomy, Histology and Embryology, Medical University Sofia, Bulgaria

Corresponding author e-mail: lmalinova@abv.bg

Nitric oxide (NO) is an important signaling molecule that is widely distributed in the central and peripheral nervous system. The aim of this study was to determinate the morphology of the different neurons scattered in the thalamic reticular nucleus (TRN) and close to it, i.e. the internal capsule and external medullary lamina of the thalamus. We discuss the main functions pertaining to the modulation of synaptic transmission in the TRN, the internal capsule and external medullary lamina, the targets of nitrergic signaling, and the involvement of nitric oxide (NO) in the different neurodegenerative diseases, psychiatric disorders, and sensory neurotransmission in the thalamocortical and corticothalamic connections passing through the TRN.

Key words: NOS, thalamic reticular nucleus, NO, neurodegenerative diseases

Introduction

The thalamic reticular nucleus (TRN) belongs to the lateroventral group of thalamic nuclei and it forms a shell enclosing the thalamus anteriorly and along its entire lateral aspect, enveloping the other thalamic nuclei. It consists of cell groups that are traversed by the thalamocortical and corticothalamic pathways [10]. It is located laterally to the external medullary lamina of the thalamus and medially to the internal capsule. The work of Buren and Borke [10] also describes a few main types of neurons, although not in great detail. In the dorsosagittal part of the TRN its largest in size neurons are found, with a diameter of 30-40 μm, while in the anteroinferior part of the nucleus are located its smallest neurons, measuring 20-25 μm. Most of the described cells are long rather than wide, and that difference is 10 to 30 μm. Before these findings, M. E. Scheibel and A. B. Scheibel [29] described in the TRN a population of multipolar neurons of various sizes, similar to the ones in the reticular formation in the brainstem. Berezhnaya [5] describes in detail the neuronal organization of the TRN in the human using silver nitrate impregnation by the Golgi method. Using the Ortolux (Leitz, Germany) microscope, in this study the authors investigated and drew all the sections in sagittal and frontal planes. Due to the fact that there is a similarity between human

neurons and the ones in other species, the classification and terminology of the TRN in the dog was applied [21]. Besides, in this classification the term "reticular cells" is also used to describe the TRN cells as being similar to the cells of the reticular formation in the brainstem [28]. Prior studies on cats report that the dendrites of the TRN neurons form a local inhibitory internal network [13]. Berezhnaya [5] describes in detail the morphology of the TRN neurons, and according to this study when comparing the TRN cells in the human and the other species it can be found that the classical aspiny neurons of types R1 and R2 are indeed identical [21]. Apart from these cells, this study reports that in the human TRN is also found another type of R1 reticular neurons with spine-like processes on their bodies and the proximal parts of their dendrites. The comparison of the large R1 reticular neurons with their identical types in the ventral anterior and ventral lateral nuclei of the human thalamus showed that the nature of branching in the former was the same [3]. Our previous studies on the presence and morphology of NADPH-diaphorase positive neurons in the human TRN [22], and also the study of Berezhnaya [4] on these neurons and the ones in the internal capsule, located lateral to the TRN, demonstrate without any doubt the presence of NADPH-diaphorase positive neurons in these structures of the human brain. Nitric oxide is a small, highly diffusible, and reactive molecule with a short lifespan that is generated by nitric oxide synthase (NOS) through enzymatic conversion of L-arginine to L-citrulline [1, 9]. It is highly reactive, readily diffusible and has limited solubility in water [25]. Neuronal NADPH-diaphorase is identical to the neuronal isoform of nitric oxide synthase (nNOS), and hence NADPH-d histochemistry provides a specific marker for the neurons producing nitric oxide, which has been described in 1991 year by Hope B. et al. [17].

Material and Methods

The brains of 2 males and 1 female (between 30 and 54 years of age) with no evidence of neurogical disorders were obtained at autopsy. The portion of each diencephalic part containing the TRN was dissected out and sectioned into blocks (1-2 cm in the transversal plane), and then fixed for two days in 4% paraformaldehyde in 0.1 M phosphate buffer. Serial coronal sections of 40 μm were cut on a freezing microtome and collected in the same buffer. All planes from the rostral to the caudal pole were examined. Each fifth section was processed for nNOS immunohistochemistry. Free-floating sections were preincubated for 1 hour in 5% normal goat serum in PBS. After that, incubation in the primary antibody was done for 48 hours at room temperature. We used monoclonal anti-NOS1 antibody (Santa Cruz) in a dilution of 1:1000. After rinsing in PBS, the sections were incubated for 2 hours in biotinylated goat anti-mouse IgG antibody (Vector) diluted 1:500. The sections were rinsed in PBS and incubated for 1 hour in avidin-biotin-peroxidase complex (Vector). This was followed by a rinse in PBS and then 0.05M Tris-HCl buffer, pH 7.6. These steps were followed by incubation in 0.05% 3,3′- diaminobenzidine (Sigma) containing 1% H_2O_2 (1:100) for the reaction product visualization. Sections were then collected in Tris-HCl buffer 0.05M, pH 7.6, air-dried for 24 hours, rinsed three times in distilled water (5 minutes per rinse), and air-dried again. Finally, they were mounted on gelatin-coated glass slides, dried for 24 hours and coverslipped with Entellan.

Results

We found NOS-immunopositive neurons everywhere along the longitudinal axis in the transverse sections of the TRN (**Fig. 1A, B**). Some of them were scattered, while others where organized in small groups of cells distant from each other (**Fig. 2C**). This is probably because of the critical position of the TRN, as it is crossed by thalamocortical and corticothalamic pathways. Some neurons that were close to the internal medullary lamina or internal capsule, or even located deep into these structures, were spindle shaped (**Fig. 1D**) or angular (**Fig. 2B**), while others were visualized as multipolar (**Fig. 2A, C, D**). There were even incoming neurons towards the internal capsule or the external medullary lamina of the thalamus. On the other hand, the neuropil showed very weak intensity of staining except for the places where fibers with varicosities along their length traversed akin the longitudinal axis of the nucleus. These fibers comprise part of the afferent and efferent connections of the TRN with the other thalamic nuclei, and also they are part of the thalamocortical and corticothalamic projections and the projectional fibers in the brainstem. Besides, in certain places immunopositive fibers running along the longitudinal axis of the nucleus were observed. They also possessed multiple varicosities, so it can be speculated that they belong to the association fibers connecting the neurons inside the TRN.

The spindle shaped neurons had processes that appeared from the opposite poles of the cells (**Fig. 1D**). After a short distance, the processes divided dichotomously, and while at first they were rather thick, after their division they became thin along their course. When followed visually, the processes further divided into smaller in

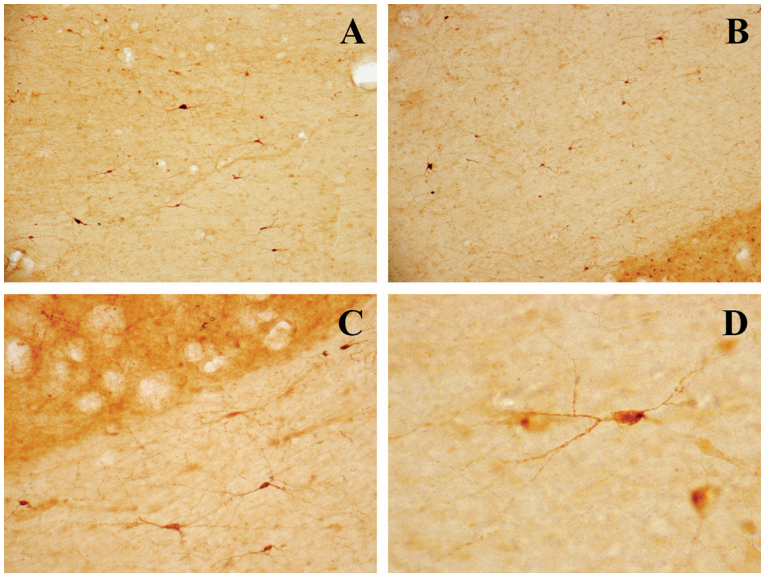

Fig. 1A. Overview of nNOS- imunoreactive neurons in the TRN (x10). **Fig. 1B.** Overview of nNOS- immunoreactive neurons. On the right side is the thalamus. (x10). **Fig. 1C.** Immunopositive neurons of different shape in the TRN (x20). **Fig. 1D.** Elongated reticular neuron with branches extending from the opposite poles of the cell (x40)

size branches. As a whole, the dendritic tree was not with too many arborizations. The axons of these neurons could be followed for some short distance and some of them were seen to end upon blood vessels via a single or a few varicose terminals (**Fig. 1D**). The perikarya of most of these cells demonstrated moderate and more rarely intense nNOS expression (**Fig. 1D**). Along the processes appearing from the neuronal somata, notwithstanding their thickness, varicosities were observed. They were larger in the proximal segments of the processes, while more distally their size diminished.

In the multipolar neurons the arborization of the dendritic tree was much more obvious (**Fig. 2 A, C**). The branches ran in all directions and varicosities of different sizes were seen along their length. The somata of the multipolar neurons demonstrated a considerable immunoreactivity for nNOS (**Fig. 2 A, C, D**).

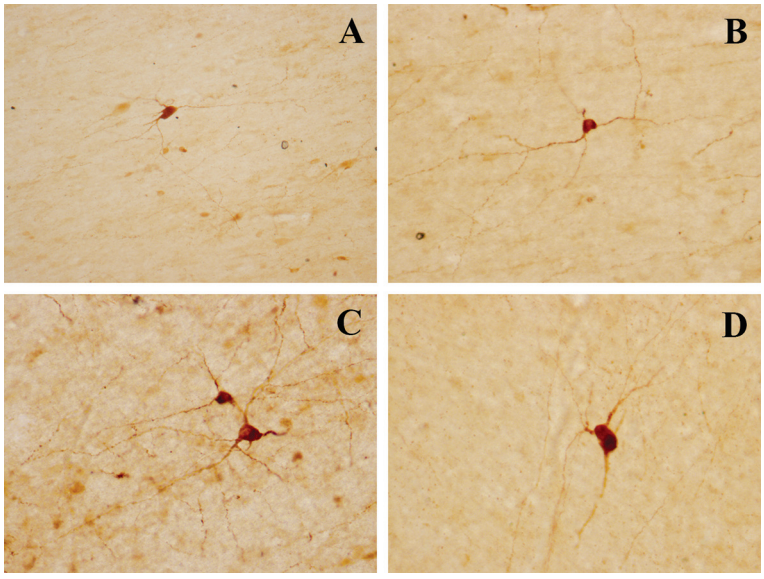

Fig. 2A. Multipolar neuron (x20). **Fig. 2B**. Angular neuron (x20). **Fig. 2C**. Multipolar neurons (x40). **Fig. 2D**. Multipolar neuron (x40)

Discussion

NO is a molecule with pleiotropic effects in the brain. This study describes the morphology and the intensity of the immunoreaction for nNOS in the cells of the TRN and the surrounding brain structures. NO is a signaling molecule in all mammals including the humans, and it is involved in a number of physiological and pathological processes [1]. NO facilitates the synaptic functions by long-term potentiation, maintenance and protein translation at the dendritic spines. It is also critical for the proper supply of blood to neurons and it has been demonstrated to be an antiapoptotic molecule and a regulator of neuronal function by nitrosylation. However, when NO is produced in a pro-oxidant environment, for example during aging, it damages the brain cells [27]. In the TRN there are two main types of reticular neurons, namely long-axon sparsely branched and short–axon smooth dendrite cells, described in our studies [22]

and by Berezhnaya [4] using NADPH-d histochemistry. It should be considered that the positive cellular reaction for NADPH-d indeed is a marker of the presence of nNOS in these cells, described by Hope et al. [17]. Hyperpolarization of the neurons in the thalamic nuclei, in particular the interneurons of the TRN, plays a role as a pacemaker for the transition of visual stimuli to the cortex [26]. This function is regulated by NO [6], whose presence we report in this study. NADPH-d reactivity is co-localized with GABA in a sub-population of local inhibitory interneurons [24]. In that region, the action of NO does not seem to involve cGMP [12]. NO regulates presynaptic plasticity in GABAergic and glutamatergic neurons [16]. Besides its proposed role in protecting NOS neurons from neurotoxicity, NO may itself induce neurotoxicity, especially in the adults. Neurotoxicity associated with cerebral ischemia is thought to involve glutamatergic stimulation via NMDA receptors [11, 19]. The reduction of GABA release from the TRN to other thalamic nuclei, due to inactivation of NMDA receptors on TRN neurons, would increase the firing rate of thalamic relay neurons to the cortex in schizophrenia [14].

NO plays multiple roles in the nervous system. Under physiological conditions, it contributes to regulating the proliferation, survival, and differentiation of neurons. The association of neurons expressing nNOS with blood vessels, which is found in this study, probably proves the intensity of blood supply and the trophic of the long-axon collaterals of the reticular neurons, and also the trophic of the fibers of the projection neurons [1]. NO is involved in synaptic activity, neural plasticity, and memory function; it exerts long-lasting effects through regulation of transcription factors and modulation of gene expression. Abnormal NO signaling could therefore contribute to a variety of neurodegenerative pathologies such as stroke/excitotoxicity, multiple sclerosis [7], Parkinson's and Alzheimer's disease [8], oxidative stress in vascular dementia [2], and intrinsic neuronal excitability [30]. The TRN is referred to as a pacemaker in the thalamus that generates rhythmic activity amongst thalamocortical and corticothalamic chains by mediation of inhibitory postsynaptic potentials [31] and it is regulated by NO [6]. Previous research has shown that the role of NO in sleep regulation is challenged. Actually, the group of Kilduff [18] has reported that long range projecting nNOS-type I GABAergic neurons are specifically activated during sleep [15, 23] by demonstrating that these cells in the cerebral cortex definitely accumulate c-Fos during sleep [15].

Conclusion

The key position of the TRN and its grid structure is involved in all the functional modalities that the nucleus is responsible for (motor, limbic, somatosensory, auditory and visual). All these modalities are associated in one way or another with the expression of NO.

References

1. **Alderton, W. K., C. E. Cooper, R. G. Knowles.** Nitric oxide synthases: structure, function and inhibition. – *Biochem. J*., **357**, 2001, 593-615.
2. **Bennett, S., M. M. Grant, S. Aldred**. Oxidative stress in vascular dementia and Alzheimer's disease: a common pathology. – *J. Alzheimers Dis*., **17**, 2009, 245-257.

3. **Berezhnaya, L. A.** Neuronal organization of the ventral anterior and ventral lateral nuclei of the human thalamus. – *Morfologiya,* **121**, 2002, 1, 38-43.
4. **Berezhnaya, L. A.** NADPH-diaphorase-positive cells in the thalamic nuclei and internal capsule in human. – *Neurosci. Behav. Physiol*., **35**, 2005, 3, 273-279.
5. **Berezhnaya, L. A**. Neuronal organization of the reticular nucleus of the thalamus in adult humans. – *Neurosci. Behav. Physiol*., **36**, 2006, 5, 519-525.
6. **Biel, M., C. Wahl-Schott, S. Michalakis, X. Zong**. Hyperpolarization-activated cation channels: from genes to function. - *Physiol. Rev*., **89**, 2009, 847-885.
7**. Bo, L., T. M. Dawson, S. Wesselingh, S. Mork, S. Choi, P. A. Kong, D. Hanley, B. Trapp**. Induction of nitric oxide synthase in demyelinating regions of multiple sclerosis brains. – *Ann. Neurol*., **36**, 1994, 778-786.
8. **Braak, H., E. Braak, D. Yilmazer, R. A. de Vos, E. N. Jansen, J. Bohl.** Pattern of brain destruction in Parkinson's and Alzheimer's diseases. – *J. Neural. Transm*., **103**, 1996, 455-490.
9. **Bredt, D. S., S. H. Snyder.** Nitric oxide: a novel neuronal messenger. – *Neuron*, **8**, 1992, 3-11.
10**. Buren, G. M. V., R. C. Borke.** *Variations and connections of the human thalamus*. Springer-Verlag, New York, Heidelberg, Berlin, 1972
11. **Choi, D. W.** Glutamate neurotoxicity and diseases of the nervous system. – *Neuron,* **1**, 1991, 623-634.
12. **Cudeiro, J., K. L. Grieve, C. Rivadulla, R. Rodriguez, S. Martinez-Conde, C. Acuna**. The role of nitric oxide in the transformation of visual information within the dorsal lateral geniculate nucleus of the cat. – *Neuropharmacol*., **33**, 1994, 1413–1418.
13. **Deschenes, M., A. Madariaga-Domich, M. Steriade**. Dendro dendritic synapses in the cat reticularis thalamic nucleus: a structural basis for thalamic spindle synchronization. – *Brain Res.,* **334**, 1985, 1, 165-168.
14. **Ferrarelli, F., G. Tononi.** The thalamic reticular nucleus and schizophrenia. – *Schizophrenia Bulletin,* **37**, 2011, 2, 306-315.
15. **Gerashchenko, D., J. P. Wisor, D. Burns, R. K. Reh, P. J. Shiromani, T. Sakurai, H. O. de la Iglesia, T. S. Kilduff.** Identification of a population of sleep-active cerebral cortex neurons. – *Proc. Natl. Acad. Sci*., **105**, 2008, 29, 10227-10232.
16. **Hardingham, N., J. Dachtler, K. Fox.** The role of nitric oxide in pre-synaptic plasticity and homeostasis. – *Front. Cell. Neurosci*., **7**, 2013, 1-19.
17. **Hope, B. T., G. J. Michael, K. M. Knigge, S. R. Vincent.** Neuronal NADPH diaphorase is a nitric oxide synthase. – *Proc. Nati. Acad. Sci.,* **88**, 1991, 2811-2814.
18. **Kilduff Thomas S., E. S. Lein, H. de la Iglesia, T. Sakurai, Y. H. Fu, P. Shaw.** New developments in sleep research: molecular genetics, gene expression, and systems neurobiology. – *J. Neurosci*., **28**, 2008, 46, 11814 -11818.
19. **Jacobsen, R. B., D. Ulrich, J. R. Huguenard.** GABA(B) and NMDA receptors contribute to spindle-like oscillations in rat thalamus in vitro. – *J. Neurophysiol*., **86**, 2001, 1365-1375.
20. **Leontovich, T. A., L. Y. Mukhina**. Characteristics of the neuronal structure of some nuclei of the dog amygdaloid complex. – *Arkh. Anat*., **59**, 1970, 8, 62-70.
21. **Leontovich, T. A.** *Neuronal organization of the subcortical formations of the forebrain*. – Moscow, Meditsina, 1978, [in Russian]
22. **Malinova, L., T. Kirov, A. Dandov.** Morphology of NADPH-diaphorase reactive neurons in the human thalamic reticular nucleus. – *Acta morphol. anthropol*., **27**, 2020, 1-2, 22-28.
23. **McCormick, D. A., T. Bal.** Sleep and arousal: Thalamocortical mechanisms. - *Annu Rev. Neurosci.*, **20**, 1997, 185-215.
24. **Mitrofanis, J**. Calbindin immunoreactivity in a subset of cat thalamic reticular neurones. – *J. Neurocytol*., **21**, 1992, 495-505.

25. **Moncada, S., R. M. J. Palmer, E. A. Higgs.** Nitric oxide: physiology, pathophysiology and pharmacology. – *Am. Sot. Pharmac. Exp Ther*., **43**, 1991, 109-143.
26. **Pape, H. C., R. Mager.** Nitric oxide controls oscillatory activity in thalamocortical neurons. – *Neuron*, **9**, 1992, 441-448.
27. **Picon-Pages, P., J. Garcia-Buendia, F. J. Munoz.** Functions and dysfunctions of nitric oxide in brain. *Biochimica et Biophysica Acta (BBA) - Molecular Basis of Disease*, **1865**, 2019, 8, 1949-1967.
28. **Zhukova, G. P., T. A. Leontovich.** Characteristics of the neuronal structure and topography of the reticular formation. – *Zh. Vyssh. Nerv. Deyat*., **14**, 1964, 122-147.
29. **Scheibel, M. E., A. B. Scheibel.** The organization of the ventral anterior nucleus of the thalamus. A Golgi study. – *Brain Res*., **1**, 1966, 250-268.
30. **Steinert, J. R., T. Chernova, I. D. Forsythe.** Nitric Oxide Signaling in Brain Function, Dysfunction, and Dementia. – *Neuroscientist,* **16**, 2010, 4, 435-452.
31. **Steriade, M., M. Deschbnes, L. Domich, C. Mulle.** Abolition of spindle oscillations in thalamic neurons disconnected from nucleus reticularis thalami. – *J. Neurophysiol*., **54**, 1985, 1473-1497.

Institute of Experimental Morphology, Pathology and Anthropology with Museum
Bulgarian Anatomical Society

Acta morphologica et anthropologica, 29 (1-2)
Sofia ● 2022

Microscopic Anatomy of the Pulmonary Neuroepithelial Bodies in Spontaneously Hypertensive Rats

Nikola Stamenov[1], Lazar Jelev[1], Dimitrinka Atanasova[2,3], Angel Dandov[1], Nikolai Lazarov[1,3]*

[1] *Department of Anatomy, Histology and Embryology, Medical University of Sofia, Sofia, Bulgaria*
[2] *Department of Anatomy, Faculty of Medicine, Trakia University, Stara Zagora, Bulgaria*
[3] *Institute of Neurobiology, Bulgarian Academy of Sciences, Sofia, Bulgaria*

*Corresponding author e-mail: nstamenov@medfac.mu-sofia.bg

Neuroepithelial bodies (NEBs) are clusters of highly specialized cells spread in the epithelium of intrapulmonary airways. The present study aimed at the identification and morphological description of the pulmonary NEBs in spontaneously hypertensive rats (SHRs). Tissue slices from the lungs of 1-month-old male SHRs were stained routinely with hematoxylin and eosin (H&E) or with the vital dye neutral red. The H&E staining revealed the neuroendocrine cells as visible clusters of clear cells seen in the airway epithelium. Neutral red staining visualized the NEBs as reddish cell clusters protruding in the airway lumen. Our results support the general morphological structure of sensory receptors in SHRs. Their role and significance in the development of essential hypertension remains to be clarified.

Key words: neuroepithelial bodies, hematoxylin and eosin, neutral red, lung, spontaneously hypertensive rat

Introduction

Neuroendocrine cells are specialized epithelial cells that can be found throughout the tracheobronchial epithelium as solitary or grouped cells [1]. When grouped into discrete cell clusters within intrapulmonary airways they are called pulmonary neuroepithelial bodies (NEBs) [1, 2]. As previously revealed, in the NEBs the neuroendocrine cells are supported by Clara-like cells, which surround them and leave only the apical domains of the neuroendocrine cells in contact with the pulmonary airway's lumen [9]. The neuroendocrine cells of the NEBs and the Clara-like cells comprise the so-called NEB microenvironment. The NEBs are composed of up to 25 neuroendocrine cells with lucid cytoplasm and they are protruding into the lumen of the pulmonary airways. Their cytoplasm is rich in vesicles storing a wide variety of bioactive substances such as acetylcholine, serotonin, calcitonin and others [2, 3, 5].

Our prior research has demonstrated the structural features of the NEBs in normotensive Wistar rats [7]. Therefore, the aim of the present study was to visualize and describe the morphology of the NEBs in spontaneously hypertensive rats (SHRs), the commonly used model of essential hypertension.

Material and Methods

In this study, we used 1-month old male SHRs weighing approximately 120 g. The animals were bred and housed at the vivarium of the Medical University of Sofia. The experiments were performed in agreement with the European Communities Council Directive 2010/63/ EU for the protection of animals used for scientific purposes and approved by the Research Ethics Commission of the Medical University of Sofia. The rats were deeply anesthetized with an intraperitoneal injection of sodium pentobarbital (70 mg/kg) and then transcardially perfused with cold 4% paraformaldehyde. Subsequently, intratracheal infusion with 4% paraformaldehyde was performed. The lungs were quickly removed, put into a cuvette with 4% paraformaldehyde and then proceeded to mild deaeration using a vacuum aspiration pump. Afterwards, we prepared 6 μm thick paraffin sections and routinely stained them with hematoxylin and eosin (H&E) following a protocol that included dewaxing and rehydration in decreasing concentrations of ethanol, staining with hematoxylin, differentiation with 0.3% acid alcohol, rinsing in water and blueing, staining with eosin, dehydration in ascending ethanol solutions, clearing in xylene and coverslipping in Entellan (Merck, Darmstadt, Germany). For the staining with neutral red, the deparaffinized sections of the lungs were rehydrated and then stained with neutral red dye for 3-4 min until the desired intensity was obtained. Finally, they were dehydrated, cleared in xylene and coverslipped.

Results and Discussion

Using the H&E staining we were able to observe NEBs as clusters of oval cells with lucid cytoplasm, protruding into the lumen of the terminal bronchioles (**Fig. 1A)** and alveoli (**Fig. 1C**). Using neutral red as a vital stain, we observed on adjacent sections the NEBs in terminal bronchioles (**Fig. 1B)** and alveoli (**Fig. 1D)**. They were seen as intensely-stained red clusters of cells protruding into the lumen of intrapulmonary airways.

The visualization of the NEBs with routine staining procedures using H&E and neutral red stain is possible yet hard to achieve, due to the low count of NEBs in the lungs and the lack of distinctive feature of the neuroendocrine cells. The present results show for the first time the microscopic structure of NEBs in SHRs. Our observations coincide with the general pattern of the NEBs as clusters of neuroendocrine cells with lucid cytoplasm spread throughout the intrapulmonary airways, including the terminal bronchioles and the alveoli. A striking feature is the protrusion of the apical domain of their cells into the lumen of the intrapulmonary airways. Such a localization implies an oxygen sensing role; yet more recent studies ascribe such a function mainly to the neonatal lungs [5]. Indeed, in adults NEBs are more often associated with mechanical and chemical reception, and sensing changes in the local extracellular matrix [6].

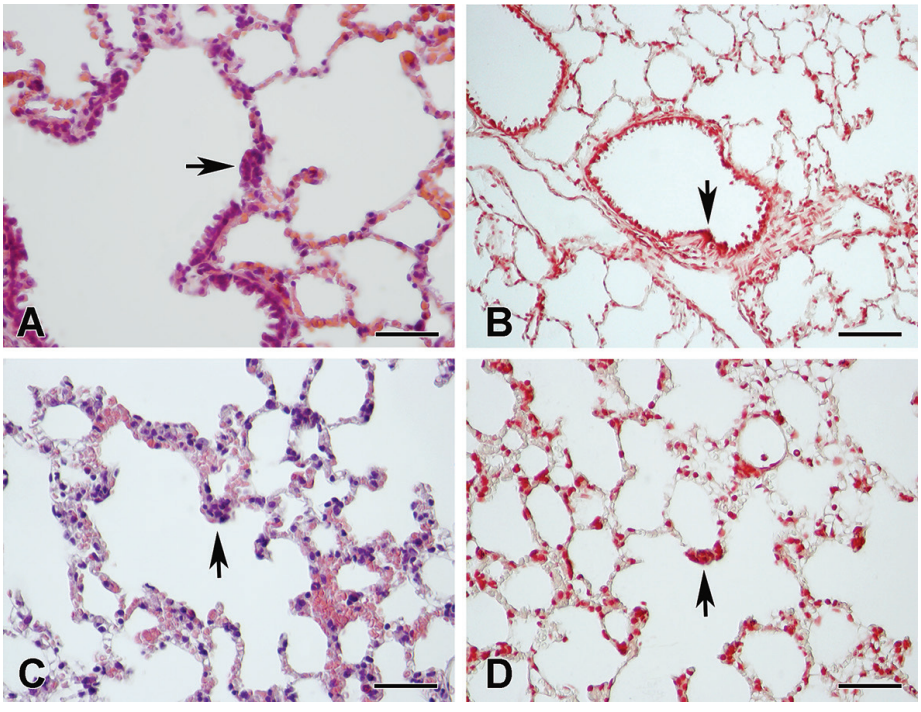

Fig.1. Staining of the NEBs in the intrapulmonary airways. **(A)** Higher magnification of a H&E-stained section through a terminal bronchiole revealing a cluster of neuroendocrine cells in the epithelium (arrow). **(B)** Neutral red staining of a terminal bronchiole showing an intensely-stained cluster of cells making up the NEB (arrow). **(C, D)** Adjacent sections of the alveoli displaying a group of oval cells with lucid cytoplasm (arrow), protruding into the lumen, **(C)**, H&E staining and **(D)**, Neutral red staining. Scale bars = 50 μm.

The SHR is the most commonly used animal model of human essential hypertension [4]. Literature data suggest that NEBs play a role in the pathogenesis of pulmonary hypertension through an increased serotonin expression [8, 10]. Based on these findings future studies will focus on analysing the potential role of NEBs in essential hypertension and involvement of certain bioactive substances in the mechanisms of high blood pressure.

In conclusion, the visualisation of the NEBs in SHRs using routine histological methods is possible and the obtained results are on a par with the literature data. Their unique localization and the broad spectrum of bioactive substances they utilize make them an interesting target for future immunohistochemical research in an attempt to find a connection between the NEBs and pathological conditions of the lungs.

Acknowledgements: This study was financially supported by the Medical Science Council at the Medical University of Sofia (Grant No. D-79/04.06.2021).

References

1. **Adriaensen, D., D. W. Scheuermann.** Neuroendocrine cells and nerves of the lung. – *Anat Rec.,***236**, 1993,70-85.
2. **Adriaensen, D., I. Brouns, J. Van Genechten, J. P. Timmermans.** Functional morphology of pulmonary neuroepithelial bodies: extremely complex airway receptors. – *Anat. Rec. A Discov. Mol. Cell Evol. Biol.,* **270**, 2003, 25-40.
3. **Cutz, E., J. Pan, H. Yeger, N. J. Domnik, J. T. Fisher.** Recent advances and contraversies on the role of pulmonary neuroepithelial bodies as airway sensors. – *Semin. Cell Dev. Biol.,* **24**, 2013, 40-50.
4. **Kundu, S., J. P. Rao.** The story of spontaneously hypertensive rat (SHR): are view.– *Al Ameen J. Med. Sci.,***1**, 2008, 65-66.
5. **Linnoila, R. I.** Functional facets of the pulmonary neuroendocrine system. –*Lab. Invest.,* **86**, 2006, 425-44.
6. **Scherer-Singler, U., S. R. Vincent, H. Kimura, E. G. McGeer.** Demonstration of a unique population of neurons with NADPH-diaphorase histochemistry. – *J. Neurosci. Methods*, **9**, 1983, 229-234.
7. **Stamenov, N., N.Lazarov.** Structure and innervation of the pulmonary neuroepithelial bodies in rats. – *Acta morphol. anthropol.,* **28**, 2021, 28-31.
8. **Van Genechten, J., I. Brouns, G.Burnstock, J. P. Timmermans, D. Adriaensen.** Quantification of neuroepithelial bodies and their innervation in fawn-hooded and Wistar rat lungs. – *Am. J. Respir. Cell Mol. Biol.,* **30**, 2004, 20-30.
9. **Verckist, L., R. Lembrechts, S. Thys, I. Pintelon, J. P. Timmermans, I. Brouns, D. Adriaensen.** Selective gene expression analysis of the neuroepithelial body microenvironment in postnatal lungs with special interest for potential stem cell characteristics. – *Respir. Res.*, **18**, 2017, 87.
10. **Yelmen, N. K., G. Sahin, T. Oruç, M. Hacibekiroğlu.** Hypoxic initiation of pulmonary hypertension is mediated by serotonin secretion from neuroepithelial bodies in chemodenervated dogs. – *Chin. J. Physiol.*, **46**, 2003, 27-33.

Institute of Experimental Morphology, Pathology and Anthropology with Museum
Bulgarian Anatomical Society

Acta morphologica et anthropologica, 29 (1-2)
Sofia ● 2022

Morphology of the Sequelae of Increased Intracranial Pressure

Natasha Davceva

Institute of Forensic Medicine and Criminalistcs, Faculty of Medicine, University "Ss Cyril and Methodius" Skopje, North Macedonia;
Faculty of Medical Sciences, University Goce Delcev Stip, North Macedonia;
Faculty of Medicine, University of Maribor, Republic of Slovenia.

*****Corresponding author e-mail: drdavcevamk@yahoo.com

With the introduction of the concept of primary and secondary brain injuries, it became clear that the outcome of one particular cranial-cerebral injury greatly depends on the secondarily initiated mechanisms, which are actually resulting of raised intracranial pressure (ICP). We can conclude about the existence of the raised ICP during person was alive, at the postmortem examination only by its effects on the brain tissue i.e. the signs of internal herniation as sequelae of it. This paper discusses our findings on the sequelae of raised ICP based on neuropathological examination of 80 forensic cases of closed head injury with a survival until 1,5 month. Our findings indicate that the herniation of the brain is going to occur in the first 10,5 days in 90% of the cases and in nearly half of them this deadly consequence can occur in the first 48 hours, which is of great clinical importance.

Keywords: ischemia, herniation, secondary brain injuries

Introduction

With the introduction of the concept of primary and secondary brain injuries, it became clear that primary brain injuries (focal and diffuse brain injuries inflicted directly by forces of impact) are not decisive for the outcome of one particular cranial-cerebral injury, but greatly depend on the secondarily initiated mechanisms. The latter are actually result of raised intracranial pressure (ICP) [1, 4, 9, 10, 11].

The intracranial cavity is a space of limited volume, where three main contents are present: the brain 80%; the blood 2-11%; and the cerebrospinal liquor 10%. When the equilibrium of these contents is impaired, an increase in ICP occurs. The ICP is a clinical parameter which can be measured only ante mortem. Normal values are below 2 kPa (1 kPa =7,5 mm Hg), elevation to 3 kPa is considered mild, to 4 kPa moderate, and values exceeding 5 kPa are considered as severe intracranial hypertension [14]. The lethal upper limit of ICP is of 8-10 kPa.

During the post-mortem examination, what we can conclude about the increased ICP is only by its effects on the brain tissue and the occurrence of the signs of internal herniation [9, 11, 14, 15].

The herniation of the brain represents the movements of particular parts of the brain, from one compartment to another. The increased pressure in the supratentorial region leads to herniation against the edge of the tentorium cerebelli i.e. transtentorial herniation where the most exposed part is the temporal lobe uncus, including the hippocampus and the parahippocampal region. The increased pressure in the infratentorial compartment leads to herniation through the foramen magnum i.e. infratentorial herniation. This is associated with brainstem compression and death. The midline shift of the medial parts of the brain hemispheres (gyrus cinguli) to the left or right under the falx cerebri is known as subfalcine herniation [10, 14].

In this study, the sequelae of increased intracranial pressure i.e. signs of internal herniation have been analyzed in order to emphasize the characteristic morphological appearance of those injuries in the postmortem examination of the brain and their correlation with the time of survival. The overall purpose of this study has been to contribute to the neuropathological criteria for determining the sequelae of increased intracranial pressure in the daily forensic medicine practice.

Material and Methods

Eighty cases with fatal closed head injury (57 male, 23 female, age ranged from 5 to 94 years), already presented in another study [5], have been now analyzed for the appearance and distribution of hypoxic-ischemic brain injury and the signs of internal herniation.

The inclusion criteria included post-mortem interval up to 24 h and the availability of data concerning: clear evidence of the type of the traumatic event [5] the known time of survival and full autopsy information. Clinical information was obtained for cases that survived long enough to be clinically investigated.

The survival period ranged from instantaneous death to 1.5 months (12 of the examined cases died quickly after the traumatic event, 25 of them survived 24 hours, 22 cases survived 1 week and the rest 21 cases survived more than 1 week, the longest survived 1,5 months).

All cases have been subjected to a forensic neuropathological examination of fixed brains in 10% buffered formalin [6, 8, 13].

Finding uncal notching or hemorrhages and necroses in the hippocampus and the parahippocampal area and infarctions of the inferior surfaces of both occipital lobes resulting from posterior cerebral artery compression have been considered to be a sign of transtentorial herniation. The characteristic finding of the cerebellar tonsillar notching and the secondary brainstem hemorrhages which typically occur in the midline of the midbrain and pons (the so called Duret hemorrhages) have been considered to be a sign of infratentorial herniation [5, 10].

Results and Discussion

Using the criteria given above, signs of the internal herniation have been perceived in 46 (57,5%) of the cases (**Table 1**.)

Table1. Finding signs of herniation in the examined cases

Type of internal herniation	Number of cases (n = 46)	%
Transtentorial herniation	16	20
Infratentorial herniation	9	11,25
Subfalcine herniation	1	1,25
Transtentorial and infratentorial herniation	12	15
Transtentorial and subfalcine herniation	2	2,5
Infratentorial and subfalcine heniation	3	3.75
Transtentorial, infratentorial and subfalcine herniation	3	3,75

Table 2 presents the time of survival for all cases diagnosed with internal herniation. Using the data on **Table 2**, the distribution of the time of survival in cases with herniation was explored i.e. the dependence between the time of survival and the occurrence of herniation was demonstrated on **Table 3**.

Table 2. Time of survival for all cases diagnosed with internal herniation

Case	Type of the herniation	Time of survival
1	Transtentorial herniation	9 days
2	Infratentorial herniation	10 days
3	Subfalcine and transtentorial herniation	2 days
4	Infratentorial herniation	2-4 hours
5	Infratentorial herniation	6 days
6	Transtentorial herniation	until 1 hour
7	Subfalcine and infratentorial herniation	2 days
8	Infratentorial herniation	until 1 hour
9	Transtentorial and infratentorial herniation	3 days
10	Transtentorial and infratentorial herniation	12 days
11	Transtentorial and infratentorial herniation	10 days
12	Transtentorial and infratentorial herniation	10 days
13	Transtentorial herniation	immediately
14	Transtentorial and infratentorial herniation	2 days
15	Transtentorial and infratentorial herniation	1,5 months

Table 2.

Case	Type of the herniation	Time of survival
16	Subfalcine herniation	3 weeks
17	Subfalcine and infratentorial herniation	3 days
18	Subfalcine herniation, transtentorial and infratentorial herniation	8 days
19	Transtentorial herniation	until 1 hour
20	Transtentorial herniation	immediately
21	Transtentorial herniation	immediately
22	Transtentorial herniation	15 days
23	Subfalcine herniation, transtentorial and infratentorial herniation	4 days
24	Transtentorial and infratentorial herniation	5 days
25	Subfalcine and infratentorial herniation	7 days
26	Transtentorial herniation	4 hours
27	Subfalcine herniation, transtentorial and infratentorial herniation	6 hours
28	Transtentorial herniation	immediately
29	Transtentorial herniation	6 hours
30	Transtentorial herniation	immediately
31	Transtentorial herniation	until 1 hour
32	Infratentorial herniation	10 days
33	Transtentorial and infratentorial herniation	2-4 hours
34	Infratentorial herniation	4 days
35	Transtentorial and infratentorial herniation	7 hours
36	Infratentorial herniation	10 days
37	Infratentorial herniation	2 days
38	Transtentorial herniation	6 days
39	Transtentorial herniation	6 days
40	Transtentorial and infratentorial herniation	24 hours
41	Subfalcine and transtentorial herniation	7 days
42	Transtentorial herniation	2 days
43	Infratentorial herniation	3 days
44	Transtentorial and infratentorial herniation	minutes
45	Transtentorial and infratentorial herniation	8 days
46	Transtentorial herniation	2 days

The results shown in Table 3 demonstrate that:

– in 90% of the cases with herniation, the herniation occurred within the first 10,5 days after the injury;

– in 50% of them, the herniation occurred in less than two days and 6 hours;

– in 35% of the cases, the herniation occurred within in the first 24 hours.

Table 3. The interdependence of survival time with the occurrence of the herniation in 46 of the examined cases.

No of cases, in total	Cases with herniation	Percentage
Until 10,5 days	42	91%
Until 2days, 6 hours	23	50%
Until 24 hors	14	30%

Hence, 80 cases of fatal closed head injury in this study were analyzed with detailed forensic neuropathological examination [6, 13] for the occurrence of secondary brain changes resulting from the increased ICP.

Signs of internal herniation as the sequelae of the raised ICP were present in 57,5% of the examined cases, which is in accordance with other studies (56% by Adams et al. 1982 [2] and 55% of 85 examined cases by Adams et al. 2011[3]). Signs of transtentorial herniation (**Fig. 1**) have been found in 33 (41, 25%) of the cases. Signs of infratentorial herniation (**Fig. 2**) have been found in 27 (33,75%) of the cases, whereas signs of subfalcine herniation have been found in 9 (11,25%) of the examined cases. In a study with 434 analyzed cases [11], signs of transtentorial herniation have been found in two thirds of the cases, and signs of infratentorial herniation in 68% of cases.

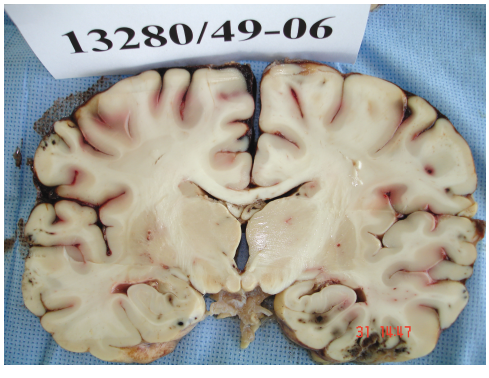

Fig. 1a

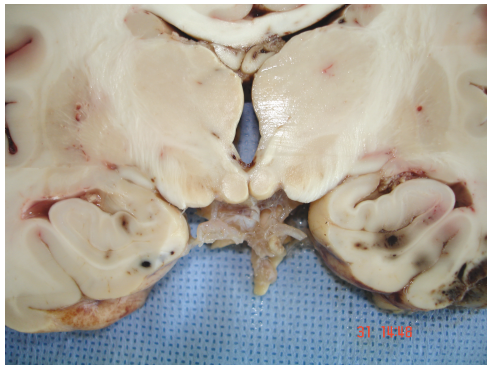

Fig. 1b

Fig. 1. a. b. Signs of transtentorial herniation. Transtentorial herniation. Case with survival time of 3-4 hours and brain weight of 1.503 grams. On the section of the level of mammilary bodies have been seen hemorrhages in the hippocampus and the parahippocampal region on both sides.

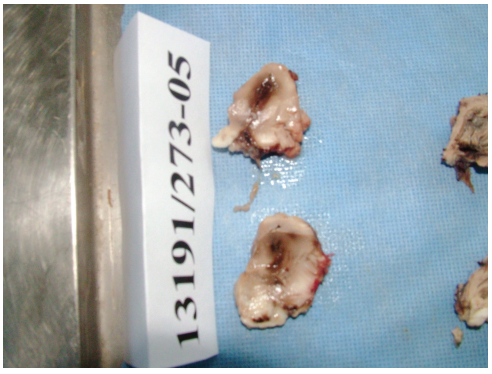

Fig. 2a **Fig. 2b**

Fig. 2. Signs of infratentorial herniation. Infratentorial herniation. The secondary Duret hemorrhages which are typically midline located in the midbrain and pons can be seen. **a**. Case with a survival of 7 hours and the weight of the brain of 1.487 grams; **b**. Case with a survival of 8 days and brain weight of 1.512 grams.

In 90% of the cases with internal herniation, as shown by the results in this study, herniation occurred within the time frame of 10,5 days postinjury, implying that the threat of internal herniation is highest in the first 10 days after injury. Accordingly, in 50% of the cases herniation occurred in less than 2 days and 6 hours and in 35% of the cases it occurred in the first 24 hours. This analysis is mostly of clinical importance, obtaining information about the occurrence threat of internal herniation in cases with closed head injuries and possible time window for therapeutic intervention. From a forensic neuropathological point of view, besides the correlation with the survival time and proof for the existence of raised ICP ante mortem, this study emphasizes the morphological feature of herniation as it has been classically outlined [7, 8, 12].

Conclussion

Hence, the results of the present study show that in order to perceive the existence of the raised ICP during person has been alive, it is essential to perform postmortem the detail forensic neuropathological examination of the brain and to observe the signs of herniation as the sequelae of the raised ICP. Herniation of the brain is a deadly complication of closed head injury and in 90% of the closed injury cases it is going to occur in the first 10,5 days and in nearly half of them this deadly consequence can occur in the first 48 hours, which is of great clinical importance to take measures of avoiding them.

References

1. **Adams, H. J., J. A .N. Corsellis, L. W. Duchen**. *Greenfield's neuropathology* Eds. S. Love, A. Perry, J. Ironside, H. Budka), 4th Edition. New York, John Wiley&Sons, 1984.
2. **Adams J. H., D. I. Graham, L. S. Muray, G. Scott**. Diffuse axonal injury due to nonmissile head injury in humans: an analysis of 45 cases. – *Ann. Neurol.,* **12**, 1982, 557-563.
3. **Adams J. H., B. Jannet, L. S. Murray, M. G. Teasdale, T. A. Gennarelli, D. I. Graham.** Neuropathological findings in disabled survivors of a head injury. – *J Neurotrauma.,* **28**, 2011, 701-709.
4. **Adams, H., D. E. Mitchell, D. I. Graham, D. Doyle.** Diffuse brain damage of immediate impact type. Its relationship to "primary brain stem damage" in head injury. – *Brain*, **100**, 1977, (3), 489-502.
5. **Davceva N., V. Janevska, B. Ilievski, G. Petrushevska, Z. Popeska.** The occurrence of acute subdural haematoma and diffuse axonal injury as two typical acceleration injuries. – *J. Forensic Leg Med.,* **19**, 2012, 480-484.
6. **Davceva N., V. Janevska, B. Ilievski, R. Jovanovic.** The importance of the detail forensic-neuropathological examination in the determination of the diffuse brain injuries. – *Soud Lek.,* **57**, 2012, 2-6.
7. **Dolinak D., E. Matshes.** *Medicolegal neuropathology.* New York, CRC Press 2002.
8. **Finnie J. W.** Forensic pathology of traumatic brain injury – Review. *Veterinary Pathology,* 2016, **53** (5) 962-978.
9. **Graham D. I., J. H. Adams, D. Doyle.** Ischemic brain damage in fatal non-missile head injuries. – J *Neurol Sci.,* **39**,1978, 213-234.
10. **Graham D. I., T. A. Gennarelli, T. K. McIntosh.** Diffuse (multifocal) brain damage. In: *Greenfield's neuropathology* (Eds. D. I. Graham, P. L. Lantos), 7th Edition, vol.1, London, Arnold, 2002, 854-875.
11. **Graham D. I., A. E. Lawrence, J. H. Adams, D. Doyle, D. R. Mclellan.** Brain damage in non-missile head injury secondary to high intracranial pressure. – *Neuropathol. Appl. Neurobiol.,* **13**, 1987, 209-217.
12. **Itabashi H. H., J. M. Andrews, U. Tomiyasu, S. Erlich, L. Sathyavagiswaran.** *Forensic neuropathology. A practical review of the fundamentals.* Elsevier 2007.
13. **Kalimo H., P. Saukko, D. Graham.** Neuropathological examination in forensic context. *Forensic Sci. Int.,* **146**, 2004, 73-81.
14. **Miller J. D., J. W. Ironside.** Raised intracranial pressure, oedema and hydrocephalus. – In*: Greenfield neuropathology* (Eds. D. I. Graham, P. L. Lantos), 6th Edition, London, Arnold, 1997, 157-195.
15. **Oehmichen M., R. N. Auer, H. G. Konig.** *Forensic neuropathology and associated neurology.* Springer-Verlag Berlin Heidelberg 2006.

Institute of Experimental Morphology, Pathology and Anthropology with Museum
Bulgarian Anatomical Society

Acta morphologica et anthropologica, 29 (1-2)
Sofia ● 2022

Light Microscopical Study of the GABA-expression in the Thalamic Reticular Nucleus of the Rat in the Postnatal Period

Lina G. Malinova

Department of Anatomy, Histology and Embryology, Medical University Sofia, Bulgaria

Corresponding author e-mail: lmalinova@abv.bg

The thalamic reticular nucleus (TRN) is a slender sheet of GABA-ergic neurons that coexist with parvalbumin and somatostatin. In this study we describe the changes in immunopositive neurons and the neuropil in the nucleus during the postnatal period of development, namely on the twentieth and sixtieth day. We found that the immunopositive reaction in twenty-day old animals was considerably stronger than that in sixty-day old ones. This phenomenon is probably associated with the maturation of the neurons, and also their plasticity and synaptogenesis.

Key words: thalamic reticular nucleus, GABA, maturation, plasticity

Introduction

Gamma-aminobutyric acid (GABA) is a biogenic amino acid that is synthesized from glutamic acid with the aid of glutamate decarboxylaze [12, 14]. The thalamic reticular nucleus (TRN) is a thin sheet of cells surrounding the anterolateral surface of the thalamus. It mainly consists of GABA-ergic neurons that coexist with parvalbumin and somatostatin [1]. Due to this specific location it is often regarded as "the gateway" through which the information from the thalamus to the cortex and vice versa has to pass. On the other hand, it is involved in sensory detection, arousal and attention [4, 11, 17, 22]. The disruption of the normal functions of the TRN is associated with the onset of epilepsy [13] and schizophrenia [7]. GABA is considered to be the most important inhibitory neurotransmitter in the CNS, and the excitation of the TRN neurons leads to the induction of a long-lasting period of hyperpolarization in the dorsal thalamic relay nuclei [5, 12, 14]. It has been found that GABA starts its expression very early in the prenatal development of the rat [3], and it is thought that the neurotransmitter role of GABA is highly significant and exerts both a trophic effect and regulation of various developmental processes [21].

The TRN can be divided into a few sectors, and each of them is associated with a different function, i.e. visual, auditory, somatosensory, motor and limbic. The limbic and motors sectors are located in the rostral part of the nucleus, and they are associated

with the anterior thalamic nuclei and the functionally related cortical areas [18, 23]. Cicirata et al. [2] describe the motor sector. All the sensory sectors, associated with thalamic nuclei and cortical structures, are situated in the central and caudal part of the nucleus [20].

Material and Methods

We used 2 groups of 5 rats, 20- and 60-day old respectively. All animals received humane care in compliance with the "Principles of laboratory animal care" formulated by the National Society for Medical Research and the "Guide for the care and use of laboratory animals" prepared by the National Institute of Health (NIH publication No. 86-23, revised 1996). The animals were perfused transcardially with 4% paraformaldehyde in 0.1 M phosphate buffer, pH 7.2-7.4. Immediately after the perfusion, the brains were dissected out and placed in the same fixative for 1 hour at room temperature for postfixation. After a few rinses in 0.1 M phosphate buffer pH 7.4, the material was left to stay overnight in 0.01 M phosphate sodium-chloride buffer (PBS) pH 7.2-7.4 at a temperature of 4ºC. On a freezing microtome coronary brain sections with a thickness of 40 µm were sliced along the anteroposterior axis of the TRN. Free-floating sections were obtained and preincubated for 30 min in 3% H_2O_2 in phosphate-buffered saline, pH 7.4 (PBS) to inactivate endogenous peroxidase. After rinsing in PBS, non-specific sites were blocked in PBS containing 10% normal goat serum (NGS) and 0.2% Triton-X100. The sections were then incubated overnight at room temperature with the following antiserum diluted in 1% NGS in PBS: anti-GABA, 1:6000. After several rinses in PBS, the sections were incubated in biotinylated goat anti-rabbit IgG (Vector) diluted 1:200 in 1% NGS in PBS. The avidin-biotin-peroxidase protocol (ABC; Vector) was followed and finally 3,3´ -diaminobenzidine tetrahydrochloride (DAB; Sigma) was used as a chromogen. Thereafter, the sections were mounted on gelatin-coated glass slides, dried for 24 hours and coverslipped with Entellan. In order to control the specificity of the antibodies, some sections were processed by omitting the primary antibody or replacing it with NGS diluted 1:100. No specific staining was detected in this case. All the sections were examined under the light microscope.

Results

The TRN is a thin layer of cells surrounding the anterolateral surface of the thalamus (**Figs. 1A, 2A**). In twenty-day old rats we found the presence of immunoreactive neurons. The reaction product was confined both to the neuronal perikarya in the different sectors of the TRN, and along the short neuronal processes that formed small varicosities. In the rostral part of the TRN we predominantly observed oval-shaped neurons, and most of them had homogenous immunoreaction. Another part of the neurons expressed GABA in the periphery of their somata, above all in one pole of the cell bodies. The neuropil was moderately stained, albeit intense staining of the neuronal elements was observed (**Fig.1B**). Neurons of different shape and direction were marked in the central sector of the TRN, and they formed smaller or larger cellular groups. Some of the neurons were positioned in the vicinity of blood vessels.

The cellular groups themselves were located at some distance from one another. This sector of the nucleus had the weakest staining of the neuropil when compared to the rostral and caudal parts (**Fig. 1C**). In the caudal sector of the TRN the immunopositive neurons were mainly elongated to oval-shaped and aligned parallel to the long axis of the nucleus. The GABA immunoexpression was positive only in the peripheral parts of the neuronal somata, while the cell processes were longer than in the other neurons of the nucleus, and could only be followed for some distance. The solitary neurons were wholly immunoreactive, while the neuropil displayed weak staining (**Fig. 1D**).

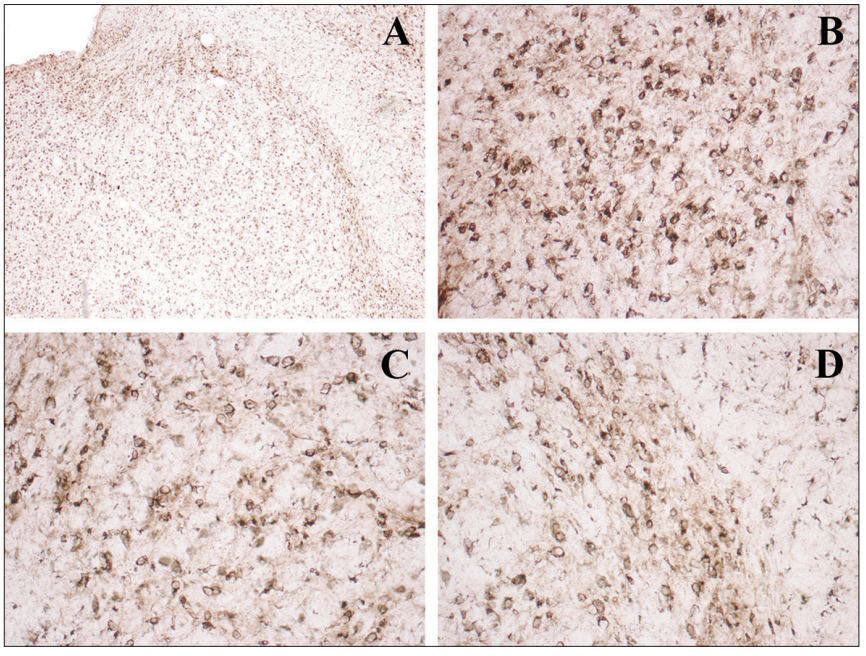

Fig. 1A. Anteroposterior view of the entire nucleus in 20 day animals (x10). **Fig. 1B.** Rostral sector of the TRN (x20). **Fig. 1C.** Central sector of the TRN (x20). **Fig. 1D**. Caudal sector of the TRN (x20)

In sixty-day old animals, the immunoreaction was located only in the peripheral part of the neuronal somata, and the intensity of the observed expression was considerably weaker when compared to the twenty-day old rats. It was solely in the rostral portion of the nucleus that solitary wholly-marked neurons were observed (**Fig. 2B**). In general, the immunostaining both of the neurons and the neuropil at this age was considerably weaker. In the rostral portion of the TRN, the GABA expression was most pronounced in comparison with the other nuclear parts. The spaces in-between the cellular groups in the central portion were significantly larger because of the traversing projection fibers (**Fig. 2C**). The GABA immunoreaction in the caudal portion was similar to that in the central (**Fig. 2D**). On the overall, the nerve fibers showed a weaker intensity of immuno-positivity in all the parts of the nucleus.

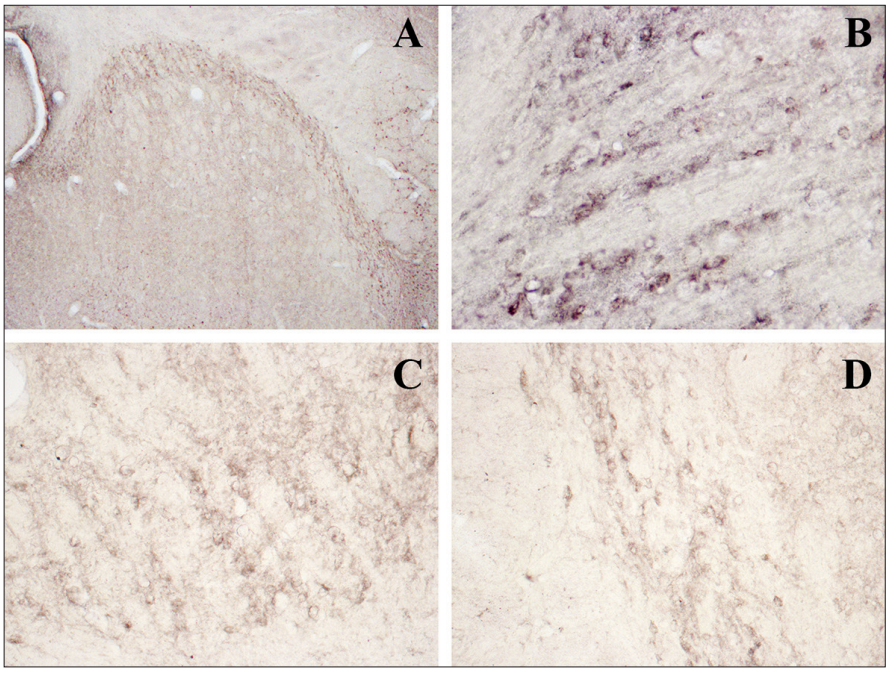

Fig. 2A. Anteroposterior view of the entire nucleus in 60 day animals (x10). **Fig. 2B.** Rostral sector of the TRN (x20). F**ig. 2C**. Central sector of the TRN (x20). **Fig. 2D.** Caudal sector of the TRN (x20)

Discussion

This study aimed to assess the neuronal expression of GABA and the plasticity in the TRN during the postnatal development in the rat. The TRN is extremely rich in GABA-ergic neurons [5, 24]. Since it is located on the border of the afferent and efferent pathways between the cortex and the thalamus [19, 24], the TRN receives collateral projections from both of them. Besides, the TRN also receives direct projections from other thalamic nuclei, though it relays information only to thalamic nuclei and other subcortical areas, and not the cortex [15]. On the other hand, the TRN contains GABA-ergic neurons of two distinct types – ones coexisting with parvalbumin, and others coexisting with somatostatin [1]. These two neuronal types are responsible for various thalamocortical relations. The parvalbumin GABA-ergic TRN neurons generate rhythmic thalamocortical sensory information, while the neurons containing somatostatin exert both anticonvulsive and convulsive effects [9]. Moreover, deep cerebral stimulation of the TRN is applied as a novel therapeutic strategy in laboratory animals to influence the neuronal function of the nucleus; it is also used to modulate the neuronal excitability in animal models [16]. The inhibitory role of GABA in the TRN appears after the second postnatal week, when most of the GABA-ergic terminals reach full development [6]. The vulnerability of the immature brain to epileptic seizures is probably the reason for the disruption of neuronal connectivity. This is associated with

the processes of maturation, synaptogenesis, neuronal migration and differentiation, and to a lesser degree with neuronal death [8]. The decrease in the GABA expression in sixty-day old rats is probably associated with the maturation of the brain structures. When GABA neurotransmission in the TRN is disrupted, a number of various psychiatric disorders, such as schizophrenia and depression, Parkinson's disease, and Alzheimer's disease may develop [10]. The technique of deep cerebral stimulation gives an opportunity to modulate neuronal excitability in experimental animal models for neurological and psychiatric conditions. When the normal development of the TRN neurons is affected in the early stages of the postnatal development of the rat, it results in the disruption of the interneuronal connections within the TRN, and also in communication alterations between the TRN and the thalamus on the one hand, and between the TRN and the thalamocortical and corticothalamic pathways on the other hand. These phenomena lead to the development and onset of the diseases that were described previously.

Conclusion

It is apparent that GABA plays significant roles in the developmental processes of the TRN and the brain in general. These roles are associated with trophic functions, synaptogenesis and maturation, especially in the early postnatal stages. The disruption of the functional modalities in the adult TRN may lead to various neurological and psychiatric conditions, so acquiring further knowledge on the intrinsic processes in the nucleus may offer perspectives for novel therapeutic strategies.

References

1. **Ahrens, S., S. Jaramillo, K.Yu, S. Ghosh, G. R. Hwang, R. Paik, C. Lai, M. He, Z. J. Huang, B. Li.** ErbB4 regulation of a thalamic reticular nucleus circuit for sensory selection. – *Nat. Neurosci*., **18**(1), 2015, 104-111.
2. **Cicirata, F., P. Angaut, M. F. Serapide, M. R. Panto.** Functional organization of the direct and indirect projection via the reticularis thalami nuclear complex from the motor cortex to the thalamic nucleus ventralis lateralis. – *Exp. Brain Res.,* **79**, 1990, 325-337.
3. **Cobas A., A. Fairén, G. Alvarez-Bolado, M. P. Sánchez.** Prenatal development of the intrinsic neurons of the rat neocortex: a comparative study of the distribution of GABA-immunoreactive cells and the GABAA receptor. – *Neuroscience*, **40**(2), 1991, 375-397.
4. **Crick, F.** Function of the thalamic reticular complex: The searchlight hypothesis. – *Proc. Natl. Acad. Sci*., **81**, 1984, 4586-4590.
5. **De Biasi, S., C. Frassoni, R. Spreafico.** GABA immunoreactivity in the thalamic reticular nucleus of the rat. A light and electron microscopical study. – *Brain Res*., **399**, 1986, 143-147.
6. **De Biasi, S., A. Amadeo, P. Arcelli, C. Frassoni, R. Spreafico.** Postnatal development of GABA-immunoreactive terminals in the reticular and ventrobasal nuclei of the rat thalamus: A light and electron microscopic study. – *Neuroscience*, **76**, 1997, 2, 503-515.
7. **Ferrarelli, F., G. Tononi.** The Thalamic reticular nucleus and schizophrenia. – *Schizophrenia Bulletin*, **37**, 2011, 306-315.
8. **Galanopoulou, A., S. Moshe**. The epileptic hypothesis: Developmentally related arguments based on animal models. – *Epilepsia*, **50**, 2009, 37-42.

9. Gerardo, C. M., M. V. Manuel. The thalamic reticular nucleus: A common nucleus of neuropsychiatric diseases and deep brain stimulation. – *J. Clin. Neurosci*., **73**, 2020, 1-7.
10. Hamani, C., J. N. Nobrega. Deep brain stimulation in clinical trials and animal models of depression. – *Eur. J. Neurosci*., **32**, 2010, 7, 1109-1117.
11. Halassa, M. M., J. H. Siegle, J. T. Ritt, J. T. Ting, G. Feng, C. Moore. Selective optical drive of thalamic reticular nucleus generates thalamic bursts and cortical spindles. – *Nat. Neurosci.,* **14**, 2011, 9, 1118-1120.
12. Houser, C. R., J. E. Vaughn, R. P. Barber, E. Roberts. GABA neurons are the major cell type of the nucleus reticularis thalami. – *Brain Res*., **200**, 1980, 2, 341-354.
13. Huguenard, J. R., D. A. McCormick. Thalamic synchrony and dynamic regulation of global forebrain oscillations. – *Trends in Neurosciences*, **30**, 2007, 7, 350-356.
14. Jones, E .G. *The thalamus*. New York: Plenum Press, 1985.
15. Jones, E. G. Thalamic circuitry and thalamocortical synchrony. *Phil.Trans. R. Soc. Lond. B.*, **357**, 2002, 1659-1673.
16. Klein, J., M. L. Soto-Montenegro, Pascau J., L. Gunther, A. Kupsch, M. Desco, C. Winter. A novel approach to investigate neuronal network activity patterns affected by deep brain stimulation in rats. – *J. Psychiatr. Res*., **45**, 2011, 927-930.
17. Lewis, L. D., J. Voigts., F. G. Flores, L. I. Schmitt, M. A. Wilson, M. M. Halassa, E. N. Brown. Thalamic reticular nucleus induces fast and local modulation of arousal state. – *eLife*, **4**, 2015, e08760.
18. Lozsadi, D. A. Organization of cortical afferents to the rostral, limbic sector of the rat thalamic reticular nucleus. – *Res. Sys. Neurosci*., **341**, 1994, 520-533.
19. Pinault, D. The thalamic reticular nucleus: structure, function and concept. – *Brain Res. Rev.*, **46**, 2004, 1, 1-31.
20. Stehberg, J., C. Acuna-Goycolea, F. Ceric, F. Torrealba. The visceral sector of the thalamic reticular nucleus in the rat. – *Neurosci.*, **106**, 2001, 4, 745-755.
21. Varju, P., Z. Katarova, E. Madarasz, G. Szabo. GABA signalling during development: new data and old questions. - *Cell Tissue Res*., **305**, 2001, 2, 239-246.
22. Zikopoulos, B., H. Barbas. Prefrontal projections to the thalamic reticular nucleus form a unique circuit for attentional mechanisms. – *J. Neurosci.,* **26**, 2006, 28, 7348-7361.
23. Zikopoulos, B., H. Barbas. Circuits for multisensory integration and attentional modulation through the prefrontal cortex and the thalamic reticular nucleus in primates. – *Rev. Neurosci*., **18**, 2007, 417-438.
24. Malinova L., T. Kirov, A. Dandov. Morphology of NADPH-diaphorase reactive neurons in the human thalamic reticular nucleus. – *Acta morphol. et anthropol.*, **27** (1-2), 2020, 22-28.

Institute of Experimental Morphology, Pathology and Anthropology with Museum
Bulgarian Anatomical Society

Acta morphologica et anthropologica, 29 (1-2)
Sofia ● 2022

Histopathological model of COVID-19 pneumonia

Sylvia Genova[1,2], Mina Pencheva[3], George Kulinski[4]*

[1]*Department of General and ClinicalPathology, Medical Faculty, Medical University of Plovdiv, Plovdiv, Bulgaria*
[2]*University Multiprofile Hospital for Active Medical Treatment "Sveti Georgi" EAD-Plovdiv, Bulgaria*
[3]*Department of Medical Physics and Biophysics, Medical University of Plovdiv, Plovdiv, Bulgaria*
[4]*Medical faculty, Medical University of Plovdiv, Bulgaria*

*Corresponding author e-mail: Mina.Pencheva@mu-plovdiv.bg

Patients with severe coronavirus disease 2019 (COVID-19) have respiratory failure with hypoxemia and acute bilateral pulmonary infiltrates, consistent with ARDS. We aimed to study histological and immunohistochemical changes in the lungs in patients with severe coronavirus infection. All cases with COVID-19 were presented with viral desquamative pneumonia at different stages. Stage I - the lungs had pronounced hyperemia, dilated capillaries in the septa and many macrophages in the alveoli. Stage II has been characterized by desquamation of alveolocytes and their viral transformation into giant mononuclear cells, as well as the formation of syncytial structures. In stage III, alveolar damage and capillary proliferation were diffuse. In stage IV, fibrosis and collagen formation begin, which is more pronounced in the periphery of the lobe and propagate to the center. The autopsies revealed a consistent pattern of alveolar pulmonary injury and identified four stages in the course of COVID-19 pneumonia.

*Key word*s: COVID-19 pneumonia, SARS-CoV-2, diffuse alveolar damage, histological stages.

Introduction

Severe acute respiratory distress syndrome-associated coronavirus-2 (SARS-CoV-2), the etiologic agent of coronavirus disease 2019 (COVID-19), was initially identified in the Hubei province of China in December [13] and declared a pandemic by the World Health Organization in March 2020 [5]. Currently, 272,811,994 patients have fallen ill and 5,340,001 have died, which is 1.95% mortality.

SARS-CoV-2 is a coronavirus which utilizes angiotensin converting enzyme 2 (ACE2) as a source of cellular entry. ACE2 is expressed in lung alveolar cells, bronchial epithelium and vascular endothelial cells explaining why the respiratory tract and lung serve as a primary point of viral entry.

Radiologic evaluation of COVID-19 cases has similarly shown findings generally described as being more similar to organizing pneumonia, particularly in the earlier

phases of the disease. Much of the recognition of this pneumonia has been radiologic, described as ground glass nodules with progression to consolidation [1, 2, 4].

Typical features of Covid-19 pneumonia include hyaline membranes and alveolar cell 2 hyperplasia in 87% of patients. Alveolar pneumocytes frequently appeared atypical, enlarged, and sometimes multinucleated with syncytial features [10].

Autopsy reports of the lungs in COVID-19 to date have primarily shown diffuse alveolar damage (DAD) or acute lung injury.

We aimed to study histological and immunohistochemical changes in the lungs of patients deceased from Covid-19.

Material and Methods

Autopsy procedures

This is a prospective study of 15 consecutive COVID-19 autopsies performed in "Sv. Georgi "University Hospital, Plovdiv, Bulgaria. Specimen was taken from both lungs, from the central parts and the periphery. The study was conducted at the Morphological Center of the Medical University of Plovdiv. From each lung, 4 blocks were released for routine hematoxylin-eosin (HE) staining.

Genetic testing: Thirteen of the cases were diagnosed with a PCR (Polymerase Chain Reaction) test, one case was confirmed with an antibody (IgM/G) test and one with an rapid antigen test.

Histological examination

Autopsy material was fixed in 10% neutral buffered formalin and submitted for standard processing with haematoxylin and eosin staining.

Immunohistochemistry

Immunohistochemical staining was performed on formalin fixed, paraffin-embedded 5-μm sections following citrate pH 6.0 antigen retrieval, endogenous biotin, and peroxidase block. Dako's immunostainer is used. Immunohistochemically, both lungs were examined with CD34 for endothelial damage.

Results

Clinical Data

Out of 15 presented patients, 6 are women, 9 are men. SARS (Severe Acute Respiratory Syndrome) developed in 8 patients as a complication of COVID-19 pneumonia. Most patients developed the complication after 14 days of illness, 7 patients were on mechanical ventilation, 4 died in the emergency department, and the complication developed within hours. The earliest development of the syndrome is on day 7 of the onset of the disease. The clinical data, main disease and its complications, as well as the cause of death are summarized in **Table 1**.

Table. 1. The clinical data, main disease and its complications and the cause of death in Covid19

№	Age	Gender	Day of symptoms	Cause of death
1.	55	f	21	**SARS-Cov2**. ARV. DAD, *Generalised thrombosis*, *Brain infarction*.
2.	63	f	21	COVID19. ARV. DAD, *Generalised thrombosis:* Pulmonary thrombosis.Thrombosis in small cerebral arteries. Abacterial thrombotic endocarditis of the mitral and aortic valves. Infarct in the brainstem. Infarcts in the spleen and kidneys
3.	56	f	14	*COVID19 DAD**. Pulmonary thromboembolism***. Phlegmon in the area of the operative wound with antibiotic therapy. Ulcerative-necrotic, fibrinous-purulent colitis with local pelvic fibrinous-purulent peritonitis.
4.	62	m	7	COVID19 – Billateral fibrinous-purulent pneumonia. ***SARS-COV2 Pulmonary thromboembolism*** with acute right heart dilatation.
5.	56	m	8	***COVID19 ARV. DAD, stage III***. Exacerbated chronic total heart failure. Complete dilated hypertrophy of the heart.
6.	69	m	30	COVID19 DAD, ***SARS-COV2. Brain infarction.*** Died in the ED.
7.	37	m	14	***SARS-Cov2***. COVID19 DAD. Treatment in another hospital. Died in the ED.
8.	81	f	18	COVID19 - DAD. ARV. Bilateral pleural effusions. *Generalised thrombosis*: Thrombotic complications: splenic infarction, thrombotic infarction of the right kidney, thrombosis of the left coronary artery, thrombosis of cerebral arteries.
9.	70	m	7	***SARS-Cov2***. COVID19 DAD. Left coronary artery thrombosis. Acute anterior myocardial infarction. Died in the ED.
10.	61	m	14	***SARS-Cov2***. ARV. COVID19 DAD. Pulmonary thrombosis.
11.	88	m	10	***SARS-Cov2***. COVID19 DAD.
12.	51	f	9	***SARS-Cov2***. ARV. COVID19 DAD.
13.	75	m	14	***SARS-Cov2***. ARV. COVID19 DAD.
14.	86	f	13	***SARS-Cov2***. COVID19 DAD. Died in the ED.
15.	66	m	14	***SARS-Cov2***. COVID19 DAD.

Legend: DAD – Diffuse Alveolar Damage; ARV – Assisted Respiratory Ventilation; ED – Emergency Department

Pulmonary findings

Lung tissue was obtained from autopsies with a postmortem interval ranging from 1 to 16 days during October 2020 and November, 2021.

Macroscopically, all of the cases demonstrated diffuse and severe pulmonary changes. The lungs were enlarged bilaterally, heavy (600-700 g), with greatly reduced elasticity and increased density. Their cut surface were homogeneous, with a brownish-reddish color and scattered, firm nodular areas.

Microscopically, we have identified four stages in the development of COVID-19 pneumonia. Stage I – the lungs have pronounced hyperemia, dilated capillaries in the septa and many macrophages in the alveoli.

Stage II is characterized by desquamation of alveolocytes and their viral transformation into giant mononuclear cells (cytopathic effect), as well as the formation of syncytial structures **(Fig. 1A)** and diffuse alveolar damage (DAD) (**Fig. 1B**). The basement membranes are exposed. The inflammatory component is mild, with T lymphocytes and many macrophages. B lymphocytes are totally effaced. Multiple thrombosis in small and medium-sized vessels also occurs at this stage. The capillaries of the septa begin to proliferate.

In stage III, capillary proliferation is diffuse with budding formation. There is fresh granulation tissue in the alveoli, which proliferates diffusely and completely obliterates the alveolar spaces **(Fig. 1C).** CD34 marks endothelial cell proliferation (**Fig. 1D**).

In stage IV, fibrosis and collagen formation begin, which are more pronounced in the periphery of the lobe and propagate to the center (**Fig. 1E**). In SARS-Cov2 cases, the lung parenchyma is saturated with blood, and the basement membranes and capillaries are torn (**Fig. 1F**).

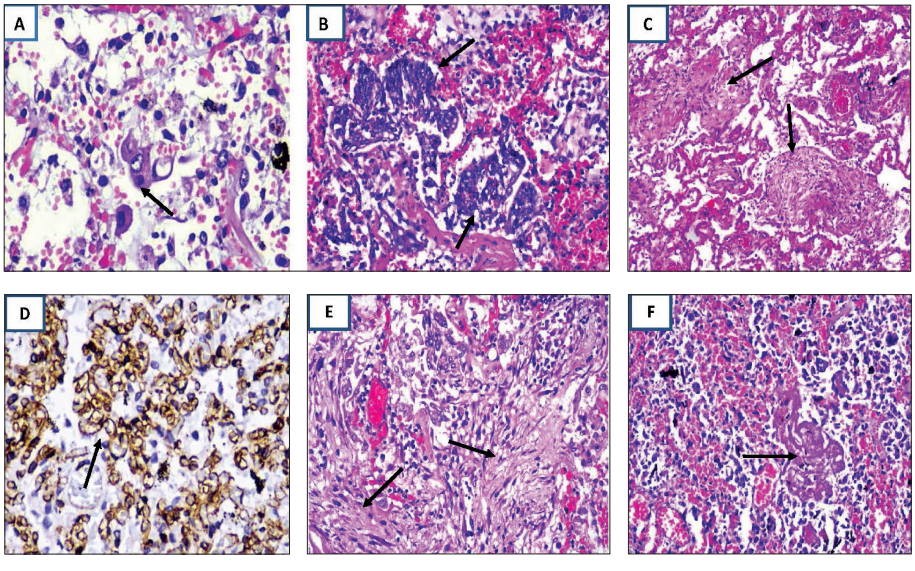

Fig.1. A) Cytopathic viral effect in alveolar pneumocytes type II with giant transformed cells, (HE, x20). **B)** Formation of syncytial epithelial structures and diffuse hemorrhages in SARS-Cov2, (HE, x20). **C)** Fresh granulation tissue in the alveoli partly or completely obliterates the alveolar spaces, formation of "fibrin balls" (HE, x20). **D)** Proliferation and budding of young capillaries, (CD34x10). **E)** Fibrous changes in organizing pneumonia, (HE, x4). **F)** Diffuse hemorrhages and intra-alveolar fibrin in SARS-Cov2 (HE, x20).

Discussion

Autopsy reports of the lungs in COVID-19 to date have primarily shown diffuse alveolar damage (DAD) or acute lung injury. The pulmonary autopsy findings are primarily limited to case reports or single center cohort studies. More recent findings have reported a wider spectrum of histological lesions involving both the epithelial and vascular components in lung and other organs. This has led to an increased awareness of the intrinsic complexity of the disease [1-7].

On average, patients with COVID 19 develop diffuse, bilateral, viral desquamative pneumonia on day 14 from the onset of the disease. *SARS-Cov2* and thromboses are observed on day 7 at the earliest. Most of the studies demonstrate venous thromboembolism and microthrombi in arterioles and venules [8,10].

In presented study patients developed SARS-Cov2 accompanied by respiratory syndrome and rapid lethal outcome in 60%. DAD is the predominant histopathologic pattern identified in lung pathology from patients with COVID-19. DAD is caused by "endothelial and alveolar lining cell injury which leads to fluid and cellular exudation," culminating in physical disruption of the blood-air barrier [7,11]. According to literature data DAD in Covid 19 is divided into three histopathological phases that generally correlate with the time from pulmonary injury:1) Acute (exudative) phase, 2) Subacute (organizing) phase, and 3) Chronic (fibrotic) phase [12]. However, in our study, we divided phase 2 (organizing) in two stages - the stage 2 of capillary proliferation and stage 3 – the formation of fresh granulation tissue. The fourth stage is the formation of collagen fibers and fibrous tissue.

According to the Hariri's study acute phase of DAD occurs within 1 week of the initial injury and is characterized by intra-alveolar hyaline membranes, edema, and alveolar wall thickening without significant inflammation. Vascular thrombosis and microthrombosis are frequently observed in DAD, even in the absence of a systemic hypercoagulable state, and they are thought to result from local inflammation [8].

In acute stage, our study correlates with the changes found by other authors such as focal hyperplasia of type II pneumocytes, some of which showed mild cytologic atypia. Some enlarged pneumocytes showed abundant cytoplasm with a ground-glass appearance, and prominent eosinophilic nucleoli. The main histological findings in the lungs in this cases include: 1) serous exudation, 2) infiltration of lymphocytes around blood vessels and in the alveolar septa, 3) aggregation of multinucleated giant cells within alveolar spaces, 4) hyperplasia of type II pneumocytes, 5) intracytoplasmic viral-like inclusion bodies. Our results completely coincide with the findings in the lungs described by other authors [6].

The subacute phase of DAD occurs approximately 1 week after the initial pulmonary injury and is characterized by microscopic organization of the fibrin followed by fibroblast migration and secretion of young "loose" collagen. Hyaline membranes become slowly incorporated into organizing fibrotic tissue, which begins to appear in airspaces, alveolar ducts, and alveolar walls. Reactive atypical changes in type II pneumocytes and squamous metaplasia may be present. In this research, we divided phase 2 (organizing), in the stage of capillary proliferation and stage 3 - the formation of fresh granulation tissue, as the two stages are well separated and follow a certain sequence in all studied cases.

Most findings, from single institution case series, have also described that first stage of DAD will ultimately resolve, whereas others evolve into a chronic fibrotic phase (weeks to months after the initial injury) with progressive architectural remodeling and interstitial fibrosis. In the extreme, these changes may resemble usual interstitial pneumonitis, the histopathological correlate of idiopathic pulmonary fibrosis [3,7,8,12].

In this research, the major pulmonary findings were diffuse alveolar damage in the acute or organising phases. Histological examination revealed focal pulmonary microthrombi in 13 patients. The major histopathological observation in most series of patients who died with COVID-19 was diffuse alveolar damage-type lung injury in the acute or organizing phases (86%). Lung tissue showed pulmonary oedema, prominent reactive type 2 pneumocytes, intra-alveolar fibrin, and hyaline membranes.

Stage IV, AFOP (acute fibrinous and organizing pneumonia) is characterized by formation of "fibrin balls" within the alveolar spaces, with organization resulting from fibroblast migration and secretion of young collagen within fibrin aggregates. OP (organizing pneumonia) can be seen in isolation or in combination with DAD or AFOP and is characterized by intraluminal tufts of plump fibroblasts and young/immature collagen tissue within alveolar ducts and distal airspaces [9]. Most of the published COVID-19 autopsy case series describe the acute phase of DAD as the prominent acute lung injury pattern. However, features of organizing fibrosis were reported on histopathologic examination in 52% of the COVID-19 autopsy cases. In most cases, organizing fibrosis was described as either focal or in the setting of mixed acute and organizing phases of DAD [6].

Severe respiratory syndrome develops most commonly in the second and third stage. We detected its earliest occurrence on day 7 of the disease up to day 21. Patients on respiratory ventilation (RV) developed the syndrome later and those on home therapy – earlier. Patients 1, 2, 7 and 10 with *SARS-Cov2* were treated in hospital. Three patients passed away in the Emergency Department due to severe respiratory syndrome. These patients were on home treatment and the respiratory insufficiency developed within hours.

The deceased cases described at this stage, usually at 7-10 days after the onset of symptoms, are characteristic for patients who have developed respiratory distress syndrome. The early fatal development of *SARS-Cov2* was observed in delta variants of Covid19, in patients with many concomitant diseases and obesity. It is noteworthy that patients with the Delta variant of Covid19 develop generalized thrombosis (patients 1-10). While in patients with the Omicron variant, these complications are absent (patients 11-15). Possible explanations are: 1) the mild course of the disease 2) the preventive use of anticoagulants since the diagnosis of Covid19 infection.

Conclusion

This study identified four stages in the course of COVID-19 pneumonia. Pneumonia lasts between two and three weeks. Severe cases manifested by subsequent proliferation of connective tissue and fibrosis, usually located in the subpleural areas of the lungs. We believe that the detailed study and categorization of the stages in the course of COVID-19 pneumonia, as well as the determination of the time interval of each stage, will support the therapeutic approaches in each of the stages.

Acknowledgments: The article is part of a study on Project KP-06-DK1/6 – 29.03.2021 COVID-19 HUB – Information, innovations and implementation of integrative research activities, National Scientific Fund, Ministry of Education Bulgaria.

References

1. **Barton, L. M., E. J. Duval, E. Stroberg, S. Ghosh, S. Mukhopadhyay.** COVID-19 autopsies, Oklahoma, USA. – *Am. J. Clin. Pathol*., **153**(6), 2020, 725-733.
2. **Bernheim, A., X. Mei, M. Huang, Y. Yang, Z. A. Fayad, N. Zhang, K. Diao, B. Lin, X. Zhu, K. Li, S. Li, H. Shan, A. Jacobi, M. Chung.** Chest CT findings in coronavirus disease-19 (COVID-19) relationship to duration of infection. – *Radiology*, **295**(3), 2020, 200463.
3. **Borczuk, A. C., S. P. Salvatore, S. V. Seshan.** COVID-19 pulmonary pathology: a multi-institutional autopsy cohort from Italy and New York City. – *Mod. Pathol*., **33**(11), 2020, 2156-2168.
4. **Chung, M., A. Bernheim, X. Mei, N. Zhang, M. Huang.** CT imaging features of 2019 novel coronavirus (2019-nCoV). - *Radiology*, **295**(1), 2020, 202-207.
5. **Cucinotta, D., M. Vanelli.** WHO declares COVID-19 a pandemic. – *Acta Biomed*., **91**(1), 2020, 157-160.
6. **Deshmukh, V., R. Motwani, A. Kumar, C. Kumari, K. Raza.** Histopathological observations in COVID-19: a systematic review. – *J. Clin. Pathol*., **74**(2), 2021, 76-83.
7. **Hariri, L. P., C. M. North, A. R. Shih, R. A. Israel, J. H. Maley, J. A. Villalba, V. Vinarsky, J. Rubin, D. A. Okin, A. Sclafani, J. W. Alladina, J. W. Griffith, M. A. Gillette, Y. Raz, C. J. Richards, A. K. Wong, A. Ly, Y. P. Hung, R. R. Chivukula, C. R. Petri, M. Mino-Kenudson.** Lung histopathology in coronavirus disease 2019 as compared with severe acute respiratory syndrome and H1N1 influenza Q1. A systematic review. – *Chest*, **159**(1), 2021, 73-84.
8. **Hariri, L., C. C. Hardin.** Covid-19, angiogenesis, and ARDS endotypes. – *N. Engl. J. Med*., **383**(2), 2020, 182-183.
9. **Huang, C., Y. Wang, X. Li, L. Ren, J. L. Zhao, Zhang, G. Fan, J. Xu, X. Gu, Z. Cheng, T. Yu, J. Xia, Y. Wei, W. Wu, X. Xie, W. Yin, H. Li, M. Liu, Y. Xiao, H. Gao, L. Guo, J. Xie, G. Wang, R. Jiang, Z. Gao, Q. Jin, J. Wang, B. Cao.** Clinical features of patients infected with 2019 novel coronavirus in Wuhan, China. – *Lancet*, 395(10223), 2020, 497-506.
10. **Katzenstein, A. L., C. M. Bloor, A. A. Leibow.** Diffuse alveolar damage: the role of oxygen, shock, and related factors. A review. – *Am. J. Pathol*., **85**(1), 1976, 209-228.
11. **Marshall, R. P., G. Bellingan, S. Webb, A. Puddicombe, N. Goldsack, R. J. McAnulty, G. J. Laurent.** Fibroproliferation occurs early in the acute respiratory distress syndrome and impacts on outcome. – *Am. J. Respir. Crit. Care Med*., **162**(5), 2000, 1783-1788.
12. **Zeng, Z., L. Xu, X. Y. Xie, H. L. Yan, B. L. Xie**, **W. Z. Xu, X. A. Liu, G. J. Kang, W. L. Jiang, J. P. Yuan.** Pulmonary pathology of early phase COVID-19 pneumonia in a patient with a benign lung lesion. – *Histopathology*, **77**(5), 2020, 823-831.
13. **Zhu, N., D. Zhang, W. Wang, X. Li, B. Yang, J. Song, X. Zhao, B. Huang, W. Shi, R. Lu, P. Niu, F. Zhan, X. Ma, D. Wang, W. Xu, G. Wu, G. F. Gao, W. Tan.** A novel coronavirus from patients with pneumonia in China, 2019. – *N. Engl. J. Med*, **382**(8), 2020, 727-733.

Institute of Experimental Morphology, Pathology and Anthropology with Museum
Bulgarian Anatomical Society

Acta morphologica et anthropologica, 29 (1-2)
Sofia ● 2022

Histochemical Characteristics and Density of Mast cells in the Porcine Conjunctiva and Eyeball

Ivaylo Stefanov[1,2], Stefan Stefanov[3]*

[1] Department of Anatomy, Faculty of Medicine, Trakia University, Stara Zagora, Bulgaria
[2]Department of Anatomy, Histology and Embryology, Pathology, Burgas University Prof. Dr. Asen Zlatarov, Burgas, Bulgaria
[3] Fifth year student at Medical Faculty, Trakia University, Stara Zagora, Bulgaria

*Corresponding author e-mail: ivstefanov@abv.bg

The anatomic similarities to human eyes, along with comparable physiologic processes, enable swine to be suitable experimental model. The aim was to define the histochemical characteristics and number of mast cells in the porcine conjunctiva and eye ball using toluidine blue and alcian blue staining. It was found that in the sclera, cornea, choroid, retina, lens and optic nerve mast cells were absent. When compared the mast cell density in all layers of eyeball we found that their number was the highest in the ciliary muscle, followed by the iris, and the lowest – in the stroma of ciliary body. The number of mast cells in bulbar conjunctiva was similar to that in the posterior part of the iris.

The current study showed that the mast cells are resident cells in the ciliary stroma and muscle, iris and ciliary body participating in maintaining the homeostasis in the porcine eye.

Key words: mast cells, metachromasia, toluidine blue, alcian blue, eye, swine

Introduction

The miniature swine is widely used as ophthalmology models [47]. The anatomic similarities to human eyes, along with comparable physiologic processes, enable miniature swine to be suitable model for surgical procedures and subsequent testing of potential therapeutic agents at treating multiple ophthalmic diseases such as uveitis, retinal detachment, cataracts, glaucoma and diabetic retinopathy [15, 26, 42, 47, 51].

Besides their well-known role in IgE-mediated hypersensitivity responses, mast cells have been implicated in a range of non-IgE-mediated immunological and pathological processes including responses to parasites and neoplasms, chronic inflammation, fibrosis, angiogenesis and wound healing [12, 17]. Leonardi [28] reported that mast-cell activation and release of the main mediator, histamine, has been described in all allergic ocular diseases: seasonal allergic conjunctivitis (SAC), perennial conjunctivitis (PAC),

vernal keratoconjunctivitis (VKC), atopic keratoconjunctivitis (AKC), and contact lens-associated giant papillary conjunctivitis (GPC). Although ocular allergic reactions involve many cell types and mediators, mast cells play a crucial role in the common pathogenesis of these different forms of ocular allergy.

In addition to preformed stored mediators (e.g. histamine, heparin) mast cells are known to be a potent source of many de novo synthesized proinflammatory cytokines and chemokines [17]. They also appear to regulate blood flow in some tissues and organs (Stead and Bienenstock 1990). It is known that mast cells constitute heterogeneous populations, and at least three types have been well characterized in common laboratory mammals and humans: bone marrow mast cells; mucosal mast cells; and connective tissue mast cells [13, 14].

Enerback [10] demonstrated in 1986 that rodent MC subpopulations could be differentially stained with alcian blue and berberine sulfate. The toluidine blue staining allows the visualization of metachromatic granules in the cytoplasm of mast cells. Enerback [10] also demonstrated that MCs from mucosal surfaces were sensitive to formaldehyde fixation in that they failed to stain metachromatically on additional exposure to dyes, whereas MCs from connective tissues were insensitive to formaldehyde fixation. This principle has now been extended to human MCs that have also been distinguished by their formaldehyde sensitivity [10, 19, 27, 48].

There have been a number of studies of the distribution of mast cells in the normal iris of various species (29, 16, 30-34, 45, 52]. These cells are absent or extremely rare in rabbits, rats and mice, but are present in some carnivores (e.g. dogs, cats), marsupials and humans, although no true estimates of density are available in the literature. In the human iris, they appear more randomly distributed than in the choroid where they are periarteriolar [33].

Mcmenamin and Poll [35] revealed that in bony fish, mast cells stained by toluidine blue were clearly identifiable and were present in all of the layers of the choroid, including the choriocapillaris. In the sharks or cartilaginous fish, no mast cells were identified in the choroid.

In the context of the mammalian eye, mast cells are invariably absent from the neural retina in all species studied to date. In 1937, Jorpes et al. first observed mast cells at the limbus in human and bovine corneas [22]. Later, Smelser and Silver [45] described many mast cells in the limbus and choroid of guinea pigs, rats, and rabbits. Smelser and Silver [45] studied the distribution of mast cells in sclera, uvea (iris, choroid and ciliary body) and retina of guinea pigs, rat, ferret and rabbit, using formalin for fixation and toluidine blue staining. In guinea pigs, rat and rabbit, large number of mast cells were seen in the posterior half of the choroid [45]. The anterior portion of the choroid contains fewer cells. A dense accumulation of mast cells forms a ribbon-like band completely in the deeper part of the ciliary body. The processes themselves contain very few mast cells. In many guinea-pigs the iris was totally devoid of mast cells, but in some animals occasionally a few cells were found. In the guinea pig, rat, and rabbit, practically no mast cells were found except for a few which at times followed a large vessel or nerve as it penetrated through the sclera. None was present in the normal cornea, but a limbal concentration of such ceils in the loose episcleral tissue was found regularly. Whole mounts of the retina were free from mast cells in all species examined. The lens was not preserved.

There have been a number of studies of the distribution of mast cells in the normal iris of various species [16, 29, 30-34, 45, 52]. They are absent or extremely rare in rabbits, rats and mice, but are present in some carnivores (e.g. dogs, cats), marsupials and humans, although no true estimates of density are available in the literature. In the human iris, they appear more randomly distributed than in the choroid where they are periarteriolar [33].

Mcmenaminand Poll [35] revealed that in bony fish, mast cells stained by toluidine blue were clearly identifiable and were present in all of the layers of the choroid, including the choriocapillaris. In the sharks or cartilaginous fish, no mast cells were identified in the choroid.

The distribution, morphology, and staining characteristics of choroidal mast cells were similar from teleost fish through to eutherian mammals resembling the mammalian connective tissue mast cells [35].

Since we have not found the information about the distribution of mast cells in porcine eyeball`s layers decided to perform this study.

The aim of the study was to define the histochemical characteristics and number of the mast cells in the porcine conjunctiva and eyeball using toluidine blue staining and alcian blue staining with pH 1.0 and 2.5.

Materials and Methods

Material

Twelve whole eyeballs were collected from 6 male, 6 month-old pigs, weighing 91-115 kg. The animals were slaughtered in a licensed abattoir for a meat consumption in accordance with the European Union's and Bulgarian legislations. Specimens from the whole eyeball together with bulbar conjunctiva were processed by the classical histological methods. Serial histological and longitudinal sections of 5 μm thickness from material fixed in 10% aqueous solution of formalin were obtained.

Histochemical staining

Serial sections were stained by toluidine blue dye [50]and alcian blue dye with both pH 1.0 and 2.5 plus Safranin, then morphometric study was performed. Alcian blue staining at pH 2.5 visualizes all acid mucins: sulfated and carboxylated acid glycosaminoglycans, but at pH 1.0 – sulfated mucins only [18, 39, 40].

Micromorphometric study

The number of mast cells per microscopic field (x 200with an area of 0.163 mm^2) were estimated by light microscope (LEIKA DM1000) equipped with a digital camera (LEIKA DFC 290) and software (LAS V4.10.0 2016).

Statistical analysis

The morphometric data were processed by GraphPad Prism 6 for Windows (GraphPad Software, Inc., USA) via one-way analysis of variance (one-way ANOVA) followed by

Tukey-Kramer's post-hoc test and are presented as mean ± SD. P-values < 0.05 were considered statistically significant.

Results

In the current histochemical study three stainings were used: toluidine blue staining and alcian blue staining with both pH 1.0 and 2.5 in order to define mast cell distribution in the three tunics of the eyeball (*bulbus oculi*) and bulbar conjunctiva (*tunica conjunctiva bulbi*). The toluidine blue staining allowed detecting β-metachromasia in granules of the toluidine blue positive mast cell type ($MCTB^+$), but alcian blue staining in pH 1.0 and 2.5 marked the granules in light and dark blue, respectively in the cytoplasm of both alcian blue positive mast cell types: $MCAB1^+$ in pH 1.0 and $MCAB2.5^+$ in pH 2.5.

The bulbar conjunctiva showed that $MCTB^+$ were two times less than both MCAB1+ and $MCAB2.5^+$ ($p < 0.001$). No significant difference was observed between the number of $MCAB1^+$ and $MCAB2.5^+$ (**Table 1**). All mast cell types were localized in close proximity to the microcirculatory bed under the epithelium but not into the epithelium (**Fig. 1).**

In the fibrous tunic (*tunica fibrosabulbi***)** of the eyeball represented by sclera and cornea, no mast cells were identified (**Table 1**).

Mast cells were found to be localized mainly in ciliary part and iridial part of the vascular tunica (*tunica vasculosa*) (**Fig. 2)**. In the choroid no mast cells were observed (**Table 1**).

In the ciliary body (corpus ciliare) $MCTB^+$, $MCAB1^+$ and $MCAB2.5^+$ were detected near the capillaries and smooth muscle cells of the ciliary muscle (*musculusciliaris*). In the *orbiculusciliaris* mast cells were also

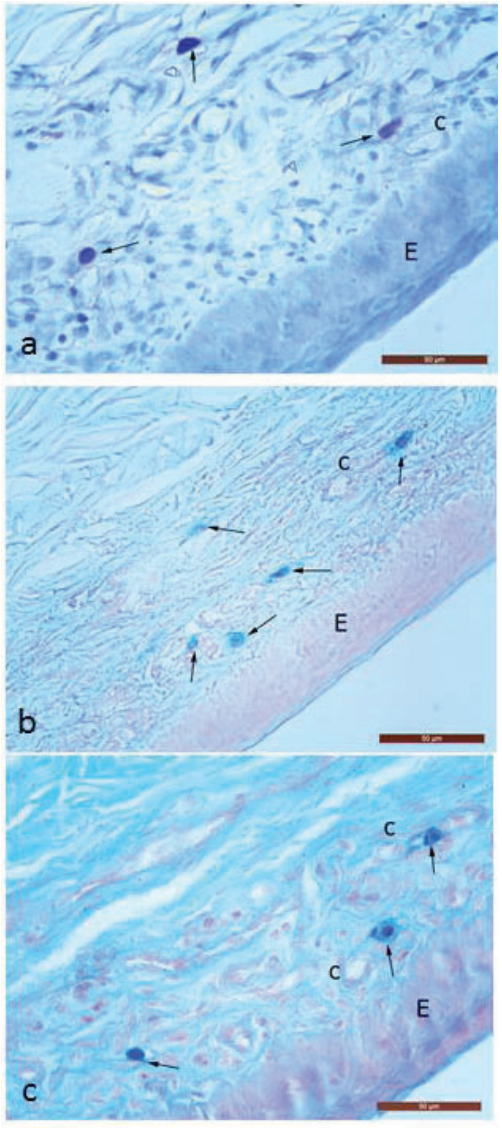

Fig. 1. Serial sections with toluidine blue positive mast cells (a) and alcian blue positive mast cells in pH 1.0 (b) and pH 2.5 (c) in the *lamina propria* of conjunctiva near the capillaries (c) and under the conjunctival epithelium (E). Arrows – mast cells. Bar = 50 μm.

observed close to pigment cells of its stroma. In the *corona ciliaris* the three types of mast cells were predominantly situated in the stroma of the anterior part near the capillaries and less in the central part near the pigment cells. The density of MCTB+ was lower than MCAB1+ and MCAB2.5^{+} density ($p < 0.001$) (**Table 1**). No significant difference was established between the density of MCAB1^{+} and MCAB2.5^{+}.

In the iris the number of MCTB^{+}, MCAB1^{+} and MCAB2.5 was higher in its posterior part than in its anterior part. In both parts of the iris the mast cells were localized in close proximity to the blood vessels and pigment cells of the iridal stroma. The number of MCTB+ was lower than that of MCAB1^{+} and MCAB2.5^{+} ($p < 0.001$) (**Table 1**). No significant difference was established between the density of MCAB1^{+} and MCAB2.5^{+}.

Table 1. Distribution of mast cells stained with toluidine blue (MCTB+), alcian blue pH 2.5 (MCAB2.5+) and alcian blue pH 1 (MCAB1+) in conjunctiva bulbi (Con B), cornea (Cor), sclera (Scl), corpus ciliaris (CCil), iris, choroidea (Ch), retina (Re) and nervusopticus (N).

Parameters	**Con B**	**Cor**	**Scl**	**CCil stroma**	**CCil Musculus Ciliaris**	**Iris Anterior Part**	**Iris Posterior part**	**Ch**	**Re**	**N**
Number of: MCTB+	4.50±0.51 **A4, B4**	-	-	1.44±0.51	8.05±0.80 **A4, B4**	2.22±0.42	3.22±0.42 **A4,B4**	-	-	-
MCAB2.5+	7.50±1.09	-	-	2.05±0.63	9.88±0.83	3.00±0.48	8.55±0.51	-	-	-
MCAB1+	8.05±0.80	-	-	2.16±0.71	10.17±1.04	3.00±0.59	8.61±0.50	-	-	-

Legend: (-) absence of staining
A4 – statistical significant difference between MCTB+ and MCAB2.5+
B4 – statistical significant difference between MCTB+ and MCAB1+

In the retina, lens and optic nerve mast cells were not detected.

When compared the mast cell density in all layers of eyeball we found that their number was the highest in the ciliary muscle, followed by posterior part of the iris, smaller – in the anterior part of the iris and the lowest - in the stroma of ciliary body.

The number of mast cells in bulbar conjunctiva was similar to that in the posterior part of the iris.

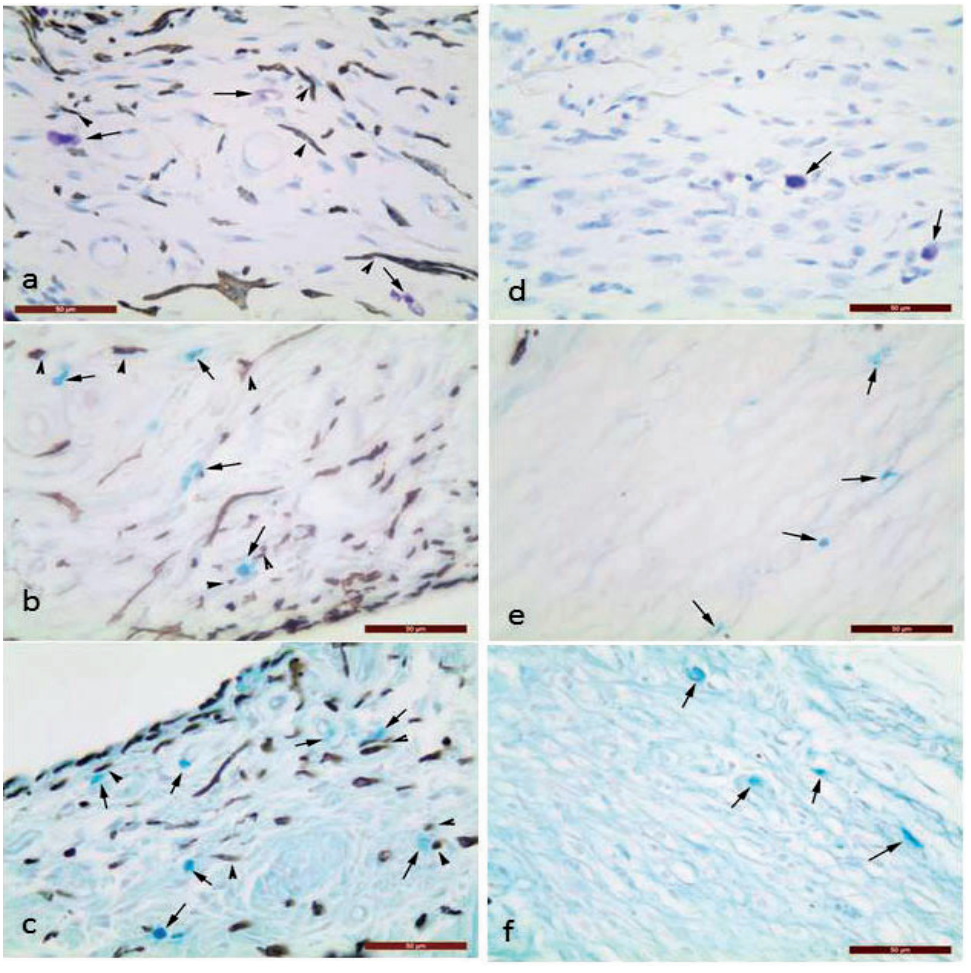

Fig. 2. Toluidine blue positive mast cells (a, d) and alcian blue positive mast cells in pH 1.0 (b, e) and pH 2.5 (c, f) in the stroma of the anterior part of the iris (a, b, c) and of the ciliary body (d, e, f) near the blood vessels (c) and pigment epithelium (arrowheads). Arrows – mast cells. Bar = 100 μm.

Discussion

In the current study the histochemical properties and distribution of mast cells in the porcine conjunctiva and eyeball were established for the first time. For this purpose toluidine blue and alcian blue dyes were used as specific markers of these cells [40, 50].

In this study we support the finding of Morgan et al. [37] about the existence of mast cells exhibiting staining that was resistant to formalin and suggest that they were connective-tissue type MCs. Morgan et al. [37, 38] used toluidine blue staining to demonstrate the presence of human conjunctival mast cells in normal tarsal conjunctiva and increased numbers in subjects with allergic conjunctivitis because of pollenosis. The

authors also revealed that the number of mast cells does not depend on the fixatives such as Camoy's fixative and formalin. These findings showed that MCs in the conjunctiva are not a static population but are involved in the pathogenesis of allergic eye disease.

We found that in all porcine conjunctiva specimens the presence of mast cell is obligatory. These results support the finding of other authors studying the distribution of mast cells in the human conjunctiva [6,21, 36, 37, 38]. In normal individuals, mast cells are abundant in the conjunctival stroma, particularly at the limbus, but are not present in the epithelium. In the conjunctival stroma, mast cells are localised in the subepithelial layer and vicinity of the blood vessels. The number of conjunctival mast cells increases in all chronic ocular allergic diseases, PAC, VKC, GPC, AKC and SAC [5].

The pro-inflammatory mediators released by mast cells include histamine, leukotriene (LTC4), prostaglandin (PGD2), tryptase, chymase, carboxypeptidase A, cathepsin G, platelet activating factor (PAF, a powerful eosinophil chemotactic agent), and other eosinophil and neutrophil chemoattractants [9]. The acute inflammatory response may also induce the influx of neutrophils and eosinophils into the conjunctiva.

It has been calculated that a single conjunctival mast cell contains 4.6 pg of histamine [36], signifying that the total potential amount of histamine that can be released with massive mast-cell degranulation is 23 ng/mm^3. In the tear film of normal subjects histamine was found at concentrations of 5 to 10 ng/ml, whereas tear samples of patients with active VKC contain significantly higher levels [1, 3]. Itching, hyperemia, tearing, and chemosis are the classic ocular manifestations of histamine release. SAC, acute conjunctival reactions, and acute palpebral edema are the clinical features of typical IgE-mediated massive mast-cell degranulation. A similar reaction can be induced using the standardized conjunctival allergen challenge model [2], with which an immediate response, or early phase reaction (EPR), and a late-phase reaction (LPR) have been widely studied. Either in nonactive allergic patients or in normal subjects, tear histamine levels are very low at baseline. Inducing an EPR by challenging allergic patients with specific allergen results in tear histamine levels that are significantly increased compared with baseline [23].

It has been shown that mast cells store and release the proinflammatory cytokines including interleukins (IL-4, IL-5, IL-6, IL-8, IL-13) and tumour necrosis factor α (TNFα) which are involved in the ocular allergic response [9].

Anti-allergic strategies for ocular diseases must remain focused on conjunctival mast cell activation and degranulation. A better knowledge of conjunctival mast-cell biology and functions will help in development of new antiallergic drugs and, consequently, in the management of ocular allergic diseases [28].

Leonardi [28] reported that mast-cell activation and release of the main mediator, histamine, has been described in all allergic ocular diseases: seasonal allergic conjunctivitis (SAC), perennial conjunctivitis (PAC), vernal keratoconjunctivitis (VKC), atopic keratoconjunctivitis (AKC), and contact lens-associated giant papillary conjunctivitis (GPC). Although ocular allergic reactions involve many cell types and mediators, mast cells play a crucial role in the common pathogenesis of these different forms of ocular allergy.

We did not find any mast cells in porcine choroid. In contrast, Smelser and Silver [45]reported that in human and animal mast cells are frequently found to be associated with vessels of the choroid. In addition, the choroid of the ferret is highly vascular, yet in this species very few mast cells were found, although large numbers were seen in the other membranes. Smith and Trokel [44] revealed that histamine released from the mast

cells of the choroid is believed a likely explanation for large vessel dilatation. These experiments are an *in vivo* demonstration of the reactions of the ocular mast cells, and suggest that these cells may be significant in ocular inflammation.

Our finding about the distribution of $MCTB^+$, $MCAB1^+$ and $MCAB2.5^+$ near the pigment cells and microcirculatory bed in the porcine iris contradicted the results of Smelser and Silver [45] who claimed that although the iris also is a vascular structure, no mast cells were found in that tissue. The same localization was observed in the ciliary body. The mast cell localization near the pigment cells can be explained by the study of Yoshito et al. [2000] who examined the effects of histamine on cultured human melanocytes. The increases in melanin content of the histamine-treated melanocytes indicated an elevation of melanin synthesis by tyrosinase activation. It was observed an increase in the intracellular cAMP contents of human melanocytes induced by histamine via the H2 receptors. Therefore, histamine induces melanogenesis of human cultured melanocytes by protein kinase A activation via H2 receptors. Recently, Arai et al. [7] reported that mast cells might influence retinal pigment epithelial (RPE) cells via secreted mediators rather than cell contact-dependent mechanisms, because only a few mast cells are observed around the choroidal capillaries near Bruch's membrane despite the high number of these cells in the choroid. The authors evaluated interactions between RPE cells and mast cells via secreted mediators. They found that H1R was expressed by RPE cells, suggesting that mast cell degranulation in the choroid could have a strong impact on RPE cells via histamine release, but the role of histamine in this setting is not well known. The histamine enhances IL-8 production by RPE cells, raising the possibility that histamine released from mast cells may contribute to RPE inflammation.

It is known that the iris pigment epithelium is the layer of pigmented cells forming the posterior layer of the iris [11]. There is a remarkable resemblance between IPE and retinal pigment epithelial cells (RPE) due to their shared embryonic development [24, 43]. *In vitro*, IPE and RPE share functional properties such as phagocytosis and synthesis of cytokines and growth factors [41,49].Rezai et al. [41] showed that IPE elicited phagocytic activity similar to RPE. Non-immune cells, such as IPE and RPE, form an interface between the eye and the environment that is not readily accessible to myeloid cells. By virtue of their ability to detect signals via innate immune receptors, such as toll-like receptors, they are able to recruit myeloid cells, such as neutrophils and macrophages to the site of injury and induce inflammation.

Expression of TLRs has been reported in a number of ocular tissues such as cornea, conjunctiva, sclera and retina [8, 25]. Studies have emphasized the importance of the LPS receptor complex (TLR4 and co-receptors CD14 and MD2) expression in ocular tissues and cells such as corneal epithelial cells, cornea stroma fibroblasts, human ciliary body, human iris endothelial cells (TLR4 only), RPE and resident antigen presenting cells in human uvea [8]. It has been shown that human RPE express TLRs and are considered to play an important role in posterior ocular inflammation due to their ability to secrete several inflammatory mediators [20].

Mast cell modulation is a fundamental target for antiallergic components. In fact, most of the ocular antiallergic drugs have been designed as mast cell stabilizers. The mechanism of the most widely used ocular mast-cell stabilizers such as sodium cromoglycate, lodoxamide, nedocromil, and pemirolast involves a decrease of calcium influx into the cytoplasm. An advance in the treatment of ocular allergy comes from newly designed ocular anti-allergic compounds, such as olopatadine and ketotifen

[54]. These drugs have a dual activity as antihistamines and mast-cell stabilizers [4], probably due to their effect on calcium mobilization or on phospholipid cellular membrane. However, the most successful effects in terms of therapeutic response in chronic allergic diseases are obtained by topical corticosteroids. For example, cyclosporine may act on various mast-cell protein kinases, thus reducing calcium influx, degranulation, and cytokine gene expression.

Conclusion

The current study showed that the mast cells are resident cells in the ciliarystroma and muscle, iris and ciliary body participating in maintaining the homeostasis in the porcine eye.

References

1. **Abelson, M. B., R. S. Baird, M. R. Allansmith**. Tear histamine levels in vernal conjunctivitis and other ocular inflammations. – *Ophthalmology*, **87**, 1980, 812-814.
2. **Abelson, M. B., W. Chambers, L. M. Smith**. Conjunctival allergen challenge. – *Arch. Ophthalmol*., **108**, 1990**,** 84-88.
3. **Abelson, M. B., A. Leonardi, L. M. Smith, I. A. Fregona, M. A. George, A. G. Secchi**. Histaminase activity in patients with vernal keratoconjunctivitis. – *Ophthalmology*, **102**, 1995, 1958-1963.
4. **Abelson, M. B., L. Spitalny**. Combined analysis of two studies using the conjunctival allergen challenge model to evaluate olopatadine hydrochloride, a new ophthalmic antiallergic agent with dual activity. – *Am. J. Ophthalmol*., **125**, 1998, 797-804.
5. **Allansmith, M. R., R. S. Baird**. Percentage of degranulated mast cells in vernal conjunctivitis and giant papillary conjunctivitis associated with contact-lens wear. – *Am. J. Ophthalmol*., **91**, 1981, 71-75.
6. **Allansmith, M. R., J. V. Greiner, R. S. Baird**. Number of inflammatory cells in the normal conjunctiva. – *Am. J. Ophthalmol*, **86**, 1978, 250-259.
7. **Arai, R., A.Usui-Ouchi, Y. Ito, KeMashimo, A. Murakami, N. Ebihara**. Effects of secreted mast cell mediators on retinal pigment epithelial cells: Focus on mast cell tryptase. – *Mediators Inflamm*., **2017**, 3124753.
8. **Chang, J. H., P. McCluskey, D. Wakefield**. Expression of toll-like receptor 4 and its associated lipopolysaccharide receptor complex by resident antigen-presenting cells in the human uvea. – *Invest..Ophthalmol. Vis. Sci.,* **45**, 2004, 1871-1878.
9. **Church, M. K., Y. Okayama, P. Bradding**. The role of the mast cell in acute and chronic allergic inflammation. – *Ann. NY Acad. Sci*., **725**, 1994**,** 13-21.
10. **Enerback, L**. Mast cell heterogeneity: the evolution of the concept of a specific mucosal mast cell. In: *Mast cell differentiation and heterogeneity*. (Eds. A.D. Befus, J. Bienenstock, J. A. Denburg), New York, Raven Press, 1986**,** pp. 1-26.
11. **Freddo, T. F.** Intercellular junctions of the iris epithelia in Macacamulatta. – *Invest. Ophthalmol. Vis. Sci.*, **25**, 1984, 1094-1104.
12. **Galli, S. J.** New approaches for the analysis of mast cell maturation, heterogeneity, and function. – *Fed. Proc.*, 1987, **46**, 1906-1914.
13. **Galli, S. J., N. Borregaard, T. A. Wynn**. Phenotypic and functional plasticity of cells of innate immunity: macrophages, mast cells and neutrophils. – *Natur. Immunol.*, **12**, 2011,1035–1044.

14. Gilfillan, A. M., M. A. Beaven. Regulation of mast cell responses in health and disease. – *Crit. Rev. Immunol.,* **31**, 2011, 475–529.
15. Gilger, B. C., E. M. Abarca, J. H. Salmon, S. Patel. Treatment of acute posterior uveitis in a porcine model by injection of triamcinolone acetonide into the suprachoroidal space using microneedles. – *Invest. Ophthalmol. Vis. Sci*., **5**, 2013**,** 2483-2492.
16. Godfrey, W. A. Characterisation of the choroidal mast cell. – *Trans Am. Ophthalmol. Soc.,* **85**, 1987, 557-599.
17. Gordon, J. R., P. R. Burd, S. J. Galli. Mast cells as sources of multifunctional cytokines. – *Immunol. Today*, **11**, 1990**,** 458-463.
18. Greiner, J. V., T. A. Weidmanz, D. R. Korb, M. R. Allansmith. Histochemical analysis of secretory vesicles in nongobletconjunctival epithelial cells. – *Acta Ophthalmol. (Copenh)*, **63**, 1985, 89-92.
19. Gtsuka, H., J. Denburg, J. Dolovich, D. Hitch, P. Lapp, R. S. Rajan, J. Bienenstock, D. Befus. Heterogeneity of metachromatic cells in the human nose: significance of mucosal mast cells. – *J. Allergy Clih..Immunol*., **76**, 1985, 695-702.
20. Holtkamp G. M., A. Kijlstra, R. Peek, A. F. de Vos. Retinal pigment epithelium-immune system interactions: cytokine production and cytokine-induced changes. – *Prog. Retin. Eye Res*., **20**, 2001, 29-48.
21. Irani A. M., S. I. Butrus, K. F. Tabbara, L. B. Schwartz. Human conjunctival mast cells: distribution of MCT and MCTC in vernal conjunctivitis and giant papillary conjunctivitis. – *J. Allergy Clin. Immunol*., 1990, **86**, 34-40.
22. Jorpes, E., H. Holmgren, O. Wilander. Uber das vorkommen von heparin in den gefasswanden und in den augen. – *Z. Mikr. Anat. Forsch*., **42**, 1937, 279.
23. Kari, O., O. P. Salo,L.Hamepuro, K. Suvilehto. Tear histamine during allergic conjunctivitis challenge. – *Graefes Arch. Clin. Exp .Ophthalmol*., **223**, 1985, 60-62.
24. Kociok N, H. Heppekausen, U. Schraermeyer, P. Esser, G. Thumann, S. Grisanti, K Heimann. The mRNA expression of cytokines and their receptors in cultured iris pigment epithelial cells: a comparison with retinal pigment epithelial cells. – *Exp. Eye Res*., **67**, 1998, 237-250.
25. Kumar, A., F-S. X. Yu. Toll-like receptors and corneal innate immunity. – *Curr. Mol. Med*., **6**, 2006**,** 327-337.
26. Kyhn, M. V., J. F. Kiilgaard,A. G. Lopez, E. Scherfig, J. U. Prause, M. la Cour. Functional implications of short-term retinal detachment in porcine eyes: Study by multifocal electroretinography. – *Acta Ophthalmol.,* **86**, 2008,18-25.
27. Lee T. D. G, M.Swieter, J.Bienenstock, A. D.Befus. Heterogeneity in mast cell populations. – *Clin. Immunol. Rev*., **4**, 1985, 143-199.
28. Leonardi, A. The Central Role of Conjunctival Mast Cells in the Pathogenesis of Ocular Allergy. – *Curr. Allergy Asthma Rep*., **2**, 2002, 325-331.
29. Levene, R. Z. Mast cells and amines in normal ocular tissues. – *Invest. Ophthalmol. Vis. Sci.*, **1**, 1962, 531-543.
30. Li, Q, Y. Fujino, R. R. Caspi, F. Najafian, R. B. Nussenblatt, C. Chan. Association between mast cells and the development of experimental autoimmune uveitis in different rat strains. – *Clin. Immunol. Immunopathol*., **65**, 1992, 294-299.
31. Li, Q., S. M. Whitcup, Y. Fujino, R. B. Nussenblatt, C. C. Chan. The role of mast cells in endotoxin-induced uveitis. – *Invest. Ophthalmol. Vis. Sci.,* 1993**, 34**, 256-259.
32. Louden, C., J. A. Render,W. W.Carlton. Mast cell numbers in normal and glaucomatous canine eyes. – *Am. J. Vet. Res*., **51**, 1990, 818-819.
33. Mcmenamin, P. G. The distribution of immune cells in the uveal tract of the normal eye. – *Eye,* **11**, 1997, 183-193.
34. McMenamin, P. G., W. J. Krause. Development of the eye in the North American opossum (Didelphisvirginiana). – *J. Anat*., **183**, 1993**,** 343-358.
35. Mcmenamin, P. G, E. Poll. Mast cells are present in the choroid of the normal eye in most

vertebrate classes. – *Vet. Ophthalmol*., **16**,2013, Supplement 1, 73-78.
36. Miller, S., E. Cook, F. Graziano, J. Spellman, J. Yanni. Human conjunctival mast cell responses in vitro to various secretagogues. – *Ocul. Immunol. Inflamm*., **4**, 1996, 39-49.
37. Morgan, S. J., J. H. Williams, A. F. Walls, M. K. Church, S. T. Holgate, J. I. McGill. Mast cell numbers and staining characteristics in the normal and allergic human conjunctiva. – *J. Allergy Clin. Immunol*., **87**, 1991a,111-116.
38. Morgan, S. J., J. H. Williams, A. F. Walls, S. T. Holgate. Mast cell hyperplasia in atopic keratoconjunctivitis. An immunohistochemical study. – Eye, **5**,1991b, 729-735.
39. Mowry, R. W. The special value of methods that color both acidic and vicinal hydroxylgroups in the histochemical study of mucins. With revised directions for the colloidal iron stain, the use of alcian blue G8X and their combinations with the periodic acid-Schiff reaction. – *Ann. NY Acad Sci*., **106**, 1963, 404-423.
40. Pearse, A. G. *Histochemistry theoretical and applied*. 2nd edition, London, J. & A. Churchil Ltd, 1962, pp. 432-434.
41. Rezai, K. A., A. Lappas, L. Farrokh-siar, L. Kohen, P. Wiedemann, K. Heimann. Iris pigment epithelial cells of long evans rats demonstrate phagocytic activity. – *Exp. Eye Res*., **65**, 1997, 23-29.
42. Sachs, H. G., F. Gekeler, H. Schwahn, W. Jakob, M. Kohler, F. Schulmeyer, J. Marienhagen, U. Brunner, C. Framme. Implantation of stimulation electrodes in the subretinal space to demonstrate cortical responses in Yucatan minipig in the course of visual prosthesis development. – *Eur. J. Ophthalmol*., **15**, 2005, 493-499.
43. Semkova, I., F. Kreppel, G. Welsandt, T. Luther, J. Kozlowski, H. Janicki, S. Kochanek, U. Schraermeyer. Autologous transplantation of genetically modified iris pigment epithelial cells: a promising concept for the treatment of age-related macular degeneration and other disorders of the eye. – *Proc. Natl. Acad. Sci. U. S. A*., **99**, 2002, 13090-13095.
44. Smith, R. S., S. Trokel. Effects of Mast-Cell Degranulation on the Choroid. – *Arch. Ophthal*., **75**, 1966, 390-394.
45. Smelser, G. K., S. Silver. The Distribution of Mast Cells in the Normal Eye. A Method of Study. – *Exp. Eye Res*., **2**, 1963, 134-140.
46. Stead, R. H., J. Bienenstock. Cellular interactions between the immune and peripheral nervous system: a normal role for the mast cells. In: *Cell to cell interaction* (Eds. M. M. Burger, B. Sordat, R. M. Zinkernagel), Basel, Karger, 1990**,** 170-187.
47. Stricker-Krongrad A, C. R. Shoemake, G. F. Bouchard. The Miniature Swine as a Model in Experimental and Translational Medicine. – *Toxicol. Pathol*., **44**, 2016, 612-623.
48. Strobe1 S., H. R. P. Miller, A. Ferguson. Human intestinal mucosal mast cells: evaluation of fixation and staining techniques. – *J. Clin. Pathol*., 34, 1981, 851-858.
49. Thumann, G. Development and cellular functions of the iris pigment epithelium. – *Surv. Ophthalmol.,* **45**, 2001, 345-354.
50. Tsandev, N., A. Vodenicharov, G. Kostadinov, I. Stefanov. Mast cell istribution in the terminal part of porcine ureter. – *Acta Morphol. Anthropol*., **26** (1-2), 2019, 52-55.
51. Rosolen, S. G., F. Rigaudiere, J. F. Le Gargasson. A new model of induced ocular hyperpressure using the minipig. – *J. Fr. Ophtalmol*., **26**, 2003, 259-267.
52. Vannas, S. Mast cells in glaucomatous eyes. – *Acta Ophthalmol. (Copenh),* 37, 1959**,** 330-339.
53. Xu L. R., M. M. Carr, A. P. Bland, G. A. Hall. Histochemistry and morphology of porcine mast cells. – *Histochem. J.,* **25**, 1993, 516-522.
54. Yanni, J. M., S. T. Miller, D. A.Gamache, J. M. Spellman, S. Xu, N. A. Sharif. Comparative effects of topical ocular anti-allergy drugs on human conjunctival mast cells. – *Ann. Allergy Asthma Immunol*., **79**,1997, 541-545.

Institute of Experimental Morphology, Pathology and Anthropology with Museum
Bulgarian Anatomical Society

Acta morphologica et anthropologica, 29 (1-2)
Sofia ● 2022

Biodiversity of Endoparasites in Domestic Cats and Dogs from the Sofia city, Bulgaria

Mariana S. Panayotova-Pencheva

Institute of Experimental Morphology, Pathology and Anthropology with Museum, Bulgarian Academy of Sciences, Sofia, Bulgaria

* Corresponding author e-mail: marianasp@abv.bg

During the period 2019-2021 fecal samples of domestic cats and dogs from the regions of Sofia, Bulgaria, were investigated by the ovoscopical methods of Fulleborn, serial sedimentations and modified technique of Bearman. Most of the registered parasites were nematodes (22% in cats; 23.8% in dogs), followed by protozoa (8% in cats; 9.5% in dogs), and cestodes (4% in cats; 4.8% in dogs). Parasites were found in 30% of the 50 fecal samples obtained from cats: *Aelurostrongylus abstrusus* (10%), *Capillaria aerophila* (2%), *Toxocara cati* (16%), *Dipylidium caninum* (4%), *Cystoisospora* sp. (8%). Parasites were found in 38% of the 21 samples from dogs: *Toxascaris leonina* (9.5%), *Trichuris vulpis* (9.5%), *Uncinaria stenocephala* (14.3%), *D. caninum* (4.8%), *Cystoisospora* sp. (9.5%). Morphometric features of eggs and larvae of the established parasites were described in present materials. Some of data concerning *A. abstrusus* were supplied for the first time in materials from Bulgaria.

Key words: Aelurostrongylus abstrusus, Capillaria aerophila, Toxascaris leonina, Toxocara cati, Trichuris vulpis, Uncinaria stenocephala, Dipylidium caninum, Cystoisospora sp.

Introduction

Carnivores are involved in the emergence and circulation of some viral, bacterial and parasitic infections, in most of the cases, they appear to be the leading factors in the distribution of them [16]. Many of the parasite species, specific to cats and dogs, parasitize other groups of animals, such as herbivores, omnivores, rodents. Examples are endoparasites of *Taenia* spp., *Toxocara* spp., *Hydatigera* spp., *Ancylostoma* spp. and others. Carnivores are hosts for a number of parasites that cause disease also in humans. According to Baneth et al. [1] some of the most important zoonoses transmitted from pets (dogs and cats) to humans in Europe are parasitic in nature, such as toxoplasmosis, leishmaniasis, giardiasis, cystic echinococcosis, alveolar echinococcosis, heartworm disease and toxocarosis. In 2012 alone, 320 people were

diagnosed with cystic echinococcosis in Bulgaria [8], and in the period 2006-2014 our country ranked first in the European Union in the number of confirmed cases of cystic echinococcosis [3]. Large part of the dogs' and cats' owners are unfamiliar with pet parasites and do not know how they are transmitted or what zoonotic risk they pose. Katagiri and Oliveira-Sequeira [9] suggest that low awareness, together with the high percentage of zoonotic parasites in dogs found in their study, show a high risk of infecting people with zoonotic parasites even in developed parts of the world. Children and the elderly are most at risk of infestations with parasites transmitted by carnivores, and protozoa of the genera *Cryptosporidium*, *Giardia* and *Toxoplasma* are particularly dangerous for people with compromised immune systems and pregnant women [15].

In order to succeed in the fight against parasitoses, special attention must be paid to their accurate diagnosis, to develop adequate guidelines for epidemiological studies and to obtain reliable data that enable health services to determine current ways to prevent and control them. In this regard, the aim of the present work was set, namely: to perform diagnostic parasitological studies of domestic cats and dogs by tracking the biodiversity and morphometric features of the established parasites, as well as some aspects of the observed parasitoses.

Materials and Methods

Fecal samples from 50 cats and 21 dogs were investigated for parasites in the period 2019-2021. The samples have been brought to several veterinary practices in Sofia by the animals‘ owners with a complaint of their pets being sick or a desire for preventive testing. Ovoscopical methods of Fulleborn, serial sedimentations and modified technique of Bearman were used to examine the feces in the laboratory [11]. The imaging and measurement of the parasite forms were performed using a Motic Images Plus 3.0 camera connected to an Amplival microscope, with accompanying software. The helminth eggs, larvae and protozoan oocysts were identified morphologically according to the descriptions of Thienpont et al. [18] and Foreyt [4].

Results

Parasite diversity

The biodiversity of the found parasites are pointed out in **Table 1**. Eight parasite taxa were diagnosed: *Aelurostrongylus abstrusus, Capillaria aerophila*, *Toxascaris leonina*, *Toxocara cati*, *Trichuris vulpis*, *Uncinaria stenocephala*, *Dipylidium caninum*, and *Cystoisospora* spp. Nematodes were most commonly found both in cats and dogs, followed by protozoa and cestodes. Single infections were more common. Co-infections were found in three cats, they were: *T. cati* + *Cystoisospora* sp.; *T. cati* + *A. abstrusus*; *T. cati* + *C. aerophila* + *Cystoisospora* sp. Two dogs were co-infected, both of them with *T. leonina* and *U. stenocephala*.

Clinical symptoms of the disease with concomitant detection of parasites in the feces were observed in 18% of the cats and 28.6% of the dogs. The main clinical symptoms that have led the owners to bring their pets for examination have been cough and diarrhea. Cough was observed in all cats infected with *A. abstrusus*, two

infected with *T. cati* and one with *C. aerophila*. Animals infected with *Cystoisospora* spp., *T. vulpis*, *U. stenocephala*, and some with *T. cati* had diarrhea. Diarrhea was particularly severe, with content of blood in feces, in two dogs - one of them with *Cystoisospora* sp. infection and other one with *T. vulpis* infection, as well as one cat with triple infection by *T. cati*, *C. aerophila*, and *Cystoisospora* sp.

Morphometric data

Morphometric characteristics of the detected parasites are presented in **Fig. 1** and **Table 2**. Here, we also provide some more morphometric data for *A. abstrusus* first stage larvae (L1) in the present materials: Body fusiform, 337.99 – 402.65 (av. 372.25) μm long and 15.18 – 21.00 (av. 17.41) μm maximal wide. Oesophagus with two dilatations – elongate, at the anterior and bulbous at the posterior end (**Fig. 2a**), 134.51 – 160.72 (av. 152.53) μm long and 7 – 10.51 (av. 8.77) μm maximal wide. Tail end of the body spirally curved, 5.08 – 7.38 (av. 6.13) μm long, with a small spike on the dorsal side (**Fig. 2b**). Distance between posterior body end and anus 31.96 – 52.19 (av. 37.53) μm.

Discussion

As can be seen from **Table 1** prevalence of infections with nematodes, cestodes and protozoa, as well as the overall prevalence of parasite infections was similar in cats and dogs. There were differences in the species composition of parasites in cats and dogs, most of which were due to host specificity (*A. abstrusus*, *T. vulpis*, *U. stenocephala*).

Targeted studies in Bulgaria and Europe, as well as reports of clinical cases provide data on the parasitofauna of domestic cats in our country [2, 6, 7, 14, 17, 19, 20]. Stoichev et al. [17] have found seven helminth species in cats from different villages in the country, and 3 of them were found in the present study (*D. caninum, T. cati* and *A. abstrusus*). Infestation of domestic cats in Bulgaria with helminthes of genera *Capillaria, Toxocara* and *Dipylidium* was reported in the international study by Rehbein et al. [14] with the values of the prevalence of infection were much higher than those found by us (4.3%, 53.2%, and 27.7% respectively). A higher prevalence of infection with *T. cati* (23.78%) and *D. caninum* (5.59%) has been also found in cats from the region of Stara Zagora [7]. The lungworm *A. abstrusus* has been established in cats of different categories from the regions of Sofia and Stara Zagora [2, 6, 20]. According to Giannelli et al. [6] the prevalence of cats' lungworm infections in Europe varied between the sampled sites, with the highest were recorded in Bulgaria (35.8%) where *A. abstrusus*, *Troglostrongylus brevior*, and *Eucoleus aerophilus* were found species. The name of the last mentioned species is synonymous with *C. aerophila* which we found in the present study.

The parasites we have identified in dogs are among the most prevalent parasitic agents in these animals from Bulgaria according to different scientists during the last two decades [7]. The prevalence of the registered infections in a comparative aspect is shown in **Table 3**. Our results about *T. vulpis, U. stenocephala, D. caninum* and *Cystoisospora* sp. are relatively close to those obtained in a study of dogs from shelters and owners from the regions of Sofia and Stara Zagora, which could be explained by the same studied region [13] and category of the dogs [7]. The present results differ to a greater extent from those of Georgieva et al. [5] and Kirkova et al. [10]. This could

be due to the fact that the first study covered only non-dewormed stray dogs [5], and the second studied a much larger number of animals of different categories from all over Bulgaria [10]. According to Iliev et al. [7] overall prevalence of infections with parasites in dogs from the region of Stara Zagora was 47.49%, by about 10% higher than established by us in this study.

The analysis of the morphometric data with respect to the identified parasitic species showed the following: The length and width of L1 of *A. abstrusus* measured by us correspond to those reported by Thienpont et al. [18]: 360-400 / 15-20 μm. The minimum and maximum length of the larvae established by us falls within the range indicated in materials from the region of Stara Zagora, Bulgaria: 234.9-417.6 μm [6] and the average length we have obtained is slightly higher than those pointed out in materials from the regions of Stara Zagora (350.8 μm) [6] and Lisbon, Portugal (350 μm) [12]. As can be seen from **Table 2** the egg sizes of the helminths we found generally correspond to those given by Thienpont et al. [18] and Foreyt [4]. Within the exceptions that are observed, the values we found are closer to the lower ones indicated by Thienpont et al. [18] and Foreyt [4]. Metric values for *D. caninum* egg packets are lower than those reported in the literature. Diversity in the metric features observed in the analysis most likely due to the peculiarities of the separate parasite populations from different parts of the world.

Conclusion

The parasite species found in domestic cats and dogs in the study were usual for these animals. In general, the prevalence of parasite infections was lower than this found in other studies from Bulgaria, especially when in them stray animals have been covered. In some cases the infestation of the animals was accompanied by a clinical manifestation of the disease. It should be borne in mind that some of the parasites found, such as *C. aerophila*, *T. cati, U. stenocephala* and *D. caninum*, have zoonotic potential.

References

1. **Baneth, G., S. M. Thamsborg, D. Otranto, J. Guillot, R. Blaga, P. Deplazes, L. Solano-Gallego.** Major parasitic zoonoses associated with dogs and cats in Europe. – *J. Comp. Pathol*., **155**, 2016, S54-S74.
2. **Borisov, B., R. Rafailov, D. Hadzhimitev, G. Marinov, N. Zlateva, Ev. Magkrioti.** *Aelurostrongylus abstrusus* in cats – diagnosis and treatment. – *Tradit. Mod. Vet. Med*., **3**, 2018, 91-96.
3. **Chakarova, B.** Cystic echinococcosis in people from the Stara Zagora region during the period 2006-2016. Scientific-practical conference «Epidemiological aspects of echinococcosis, leishmaniasis and heartworm disease in Bulgaria», November 22, Sofia, 2017. Available at http: //corhv.government.bg [in Bulgarian].
4. **Foreyt, W. J.** *Veterinary Parasitology: Reference Manual. 5th Edition*. Iowa, Blackwell Publishing, 2017, 235 pp.
5. **Georgieva, D., A. Ivanov, P. Prelesov.** Studies on the parasitic fauna in stray dogs in the Stara Zagora region. – *Bulg. J. Vet. Med*., **2**, 1999, 121-124.

6. **Giannelli, A., G. Capelli, A. Joachim, B. Hinney, B. Losson, Z. Kirkova, M. René-Martellet, E. Papadopoulos, R. Farkas, E. Napoli, E. Brianti, C. Tamponi, A. Varcasia, A. Margarida A., L. Madeira de Carvalho, L. Cardoso, C. Maia, V. Mircean, A. D. Mihalca, G. Miró, M. Schnyder, C. Cantacessi, V. Colella, M. A. Cavalera, M. S. Latrofa, G. Annoscia, M. Knaus, L. Halos, F. Beugnet, D. Otranto.** Lungworms and gastrointestinal parasites of domestic cats: a European Perspective. – *Int. J. Parasitol.*, **47**, 2017, 517-528.
7. **Iliev, P., Z. Kirkova, A. Ivanov, P. Prelezov, A. Tonev, I. Kalkanov.** Retrospective analysis on helminthic and protozoan infections in dogs and cats in Bulgaria. – *Bulg. J. Vet. Med*., **20**, Suppl. 1, 2017, 389-393.
8. **Kanchev, K., K. Salamitova, P. Radeva, R. Rafailov.** Cestodes in domestic dogs - should we worry? – Scientific-practical conference «Epidemiological aspects of echinococcosis, leishmaniasis and heartworm disease in Bulgaria», November 22, Sofia, 2017. Available at http: //corhv.government.bg [in Bulgarian].
9. **Katagiri, S., T. C. G. Oliveira-Sequeira.** Prevalence of dog intestinal parasites and risk perception of zoonotic infection by dog owners in Sao Paulo State, Brazil. – *Zoonoses and public health*, **55**, 2008, 406-413.
10. **Kirkova, Z., P. Iliev, C. Silaghi, S. Rehbein, M. Knaus.** Fecal examinations in dogs (*Canis familiaris*) in Bulgaria. – *Proceedings of Parasitologie and Parasitäre Krankheiten*, Gießen, 2013, 30-31.
11. **Koinarski, V., A. Ivanov, P. Prelezov, Z. Kirkova.** *Manual for Veterinary Parasitology*. Stara Zagora, 2009, 256 pp. [in Bulgarian].
12. **Nabais, J., A. M. Alho, L. Gomes, J. Ferreira da Silva, T. Nunes, G. Vicente, L. Madeira de Carvalho.** *Aelurostrongylus abstrusus* in cats and *Angiostrongylus vasorum* in dogs from Lisbon, Portugal. – *Acta Parasitol. Portug*., **20**, 2014, 35-40.
13. **Radev, V., N. Lalkovski, P. Zhelyazkov, T. Kostova, P. Sabev, N. Nedelchev, R. Vassileva.** Prevalence of gastrointestinal parasites and *Dirofilaria* spp. in stray dogs from some regions in Bulgaria. – *Bulg. J. Vet. Med*., **19**, 2016, 57-62.
14. **Rehbein, S., B. Capári, G. Duscher, D. Keidane, Z. Kirkova, S. Petkeviˇcius, D. Rapti, A. Wagner, T. Wagner, S. T. Chester, J. Rosentel, E. Tielemans, M. Visser, R. Winter, K. Kley, M. Knaus.** Efficacy against nematode and cestode infections and safety of a novel topical fipronil, (S)-methoprene, eprinomectin andpraziquantel combination product in domestic cats under field conditions in Europe. – *Vet. Parasitol*., **202**, 2014, 10-17.
15. **Robertson, I. D., R. C. Thompson.** Enteric parasitic zoonoses of domesticated dogs and cats. – *Microbes Infect.*, **4**, 2002, 867-873.
16. **Salkova, D., M. Panayotova-Pencheva, V. Dakova, Z. Hurnikova, M. Miterpakova, B. Víchová, V. Čabanová.** Carnivores and ixodid ticks as important factors in the emergence, circulation and distribution of dangerous infections. – *Acta Morphol. Anthropol.*, **26**, 2019, 145-152.
17. **Stoichev, I., J. Janchev, D. Svilenov.** Helminths and pathomorphological lesions in cats from villages of Bulgaria with human endemicnephropathy. – *Zentralbl. Vet. med. B*, **29**, 1982, 292-302.
18. **Thienpont, D., F. Rochette, O. Vanparijs.** *Diagnosing helminthiasis through coprological examination. 3th Edition.* Belgium, Jansen Animal Health, 2003, 215 pp.
19. **Tonev, A., Z. Kirkova, P. T. Iliev, A. Roussenov, T. Chaprazov, R. Roydev, N. Pirovski**. Clinical case of life-threatening co-infection due to *Dirofilaria immitis* and *Aelurostrongylus abstrusus* in a cat: First report of feline heartworm disease in Bulgaria. – *Helminthologia*, **58**, 2021, 106-114.
20. **Tonev, A., P. Iliev, R. Mileva**. First study on the efficacy of abamectin in a combined formulation with praziquantel against *Aelurostrongylus abstrusus* in cats. – *Bulg. J. Vet. Med*., 2022, Online first, doi: 10.15547/bjvm.2435.

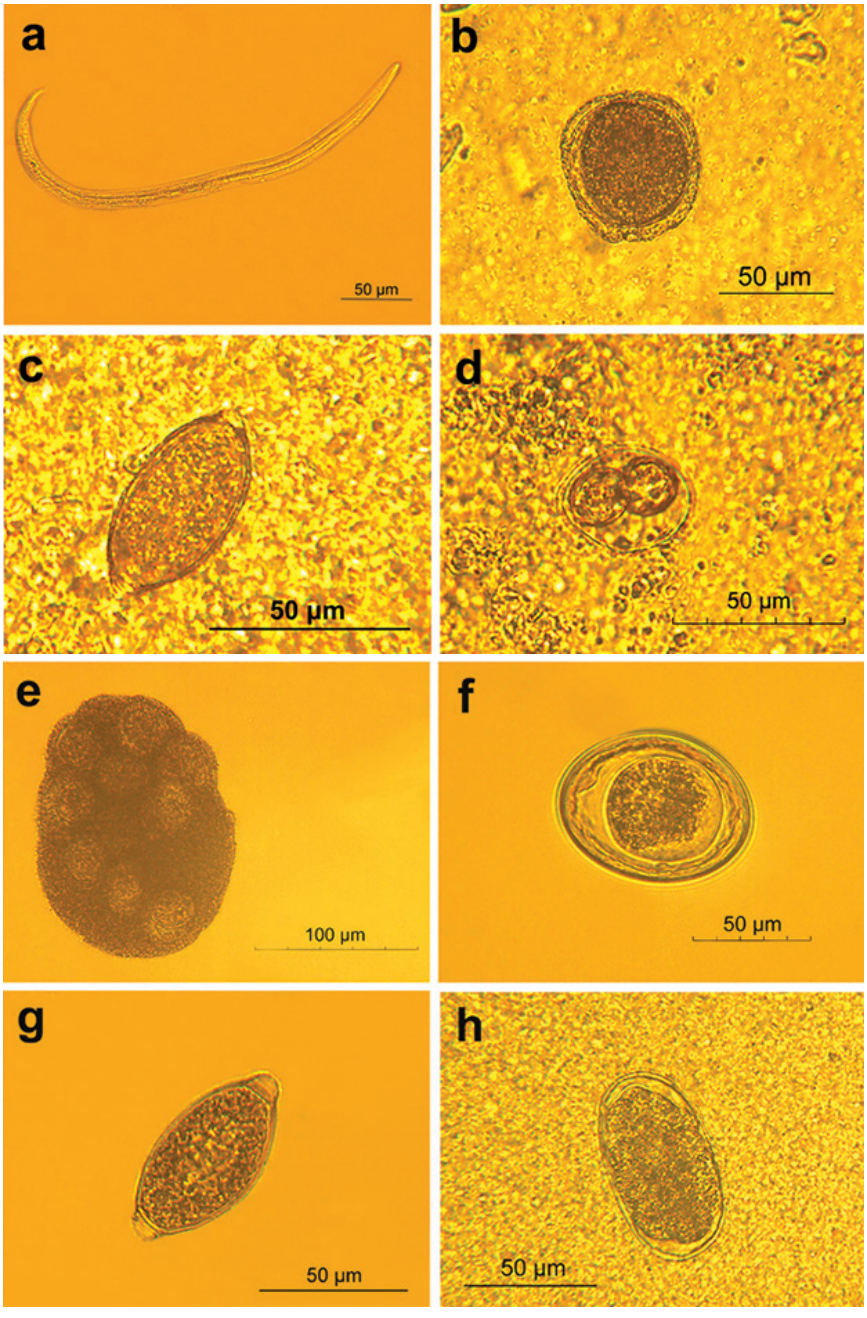

Fig. 1. Parasites detected in domestic cats (a-d) and dogs (e-h) from the Sofia city, Bulgaria, 2019-2021. **a)** *Aelurostrongylus abstrusus* larva first stage. **b)** *Toxocara cati* egg. **c)** *Capillaria aerophila* egg. **d)** *Cystoisospora* sp. oocyst. **e)** *Dipylidium caninum* egg packet. **f)** *Toxascaris leonina.*egg. **g)** *Trichuris vulpis* egg. **h)** *Uncinaria stenocephala* egg. Original pictures.

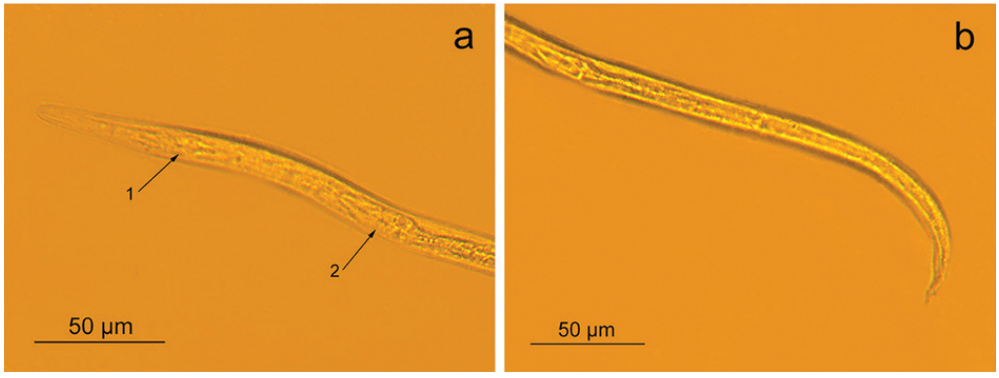

Fig. 2. *Aelurostrongylus abstrusus* first stage larvae detected in domestic cats. **a)** Anterior end. 1 – elongate dilatation of oesophagus. 2 – bulbous dilatation of oesophagus. **b)** Posterior end. Original pictures.

Table 1. Prevalence of parasite infections in domestic cats (n=50) and dogs (n=21) from the Sofia city, Bulgaria, 2019-2021.

	Cats	**Dogs**
Aelurostrongylus abstrusus	10 %	0
Capillaria aerophila	2 %	0
Toxascaris leonina	0	9.5 %
Toxocara cati	16 %	0
Trichuris vulpis	0	9.5 %
Uncinaria stenocephala	0	14.3 %
Nematodes	22 %	23.8 %
Dipylidium caninum	4 %	4.8 %
Cestodes	4 %	4.8 %
Cystoisospora sp.	8 %	9.5 %
Protozoa	8 %	9.5 %
Overall parasites	30 %	38 %
Single infections	24 %	28.6 %
Co-infections	6 %	9.5 %

Table 2. Metric data (in µm) on parasites from domestic cats and dogs from different sources

Parasite	Host	Length				Width			
		Thienpont et al. (2003)	Foreyt (2017)	Present data		Thienpont et al. (2003)	Foreyt (2017)	Present data	
				min-max	average			min-max	average
Capillaria aerophila eggs	cat	60-65	60	55.63-62.07	57.83	29-30	30	25.98-29.87	27.78
Toxascaris leonina eggs	dog	85	80	73.58-85.68	78.34	75	70	61.55-77.22	64.65
Toxocara cati eggs	cat	75	75	59.89-70.69	67.52	65	65	50.08–63.31	56.07
Trichuris vulpis eggs	dog	70-90	75	70.78-76.81	74.2	32-41	40	35.83-36.77	36.12
Uncinaria stenocephala eggs	dog	63-80	74	69.2-76.66	72.88	32-50	45	42.23-46.56	43.92
Dipylidium caninum egg packet	dog	200	200	157.5-183.5	169.3	120	150	94.37-25.42	114.28
Cystoisospora sp. oocysts	cat	–	13-42	38.79-40.66	39.77	–	10-31	30.95- 4.45	32.3
Cystoisospora sp. oocysts	dog	–	13-36	23.06-23.54	23.32	–	10-30	21.58-22.23	21.8

Table 3. Prevalence (%) of some parasite infections in domestic dogs from Bulgaria

Sources	Regions	Category of dogs	Parasite species				
			T.l.	**Tr. sp.**	**U. s.**	**D. c.**	**Cyst. sp.**
Georgieva et al., 1999	Stara Zagora	Stray	30	60	60	50	10%
Kirkova et al., 2013	Various regions of Bulgaria	Client-owned; From shelters	1	24.15	37.8*	0.3	1**
Radev et al., 2016	Sofia	Stray; From shelters	–	12.5	1	5.0	7,5
Iliev et al., 2017	Stara Zagora	Client-owned	–	10.42	–	1.93	–
Present data	Sofia	Client-owned	9.5	9.5	14.3	4.8	9.5

T.l. – Toxascaris leonina; Tr. sp. – *Trichuris* sp.; *U. s. – Uncinaria stenocephala*; *D. c. – Dipylidium caninum; Cyst.* sp. – *Cystoisospora* sp.; *hookworms; **Coccidia

Institute of Experimental Morphology, Pathology and Anthropology with Museum
Bulgarian Anatomical Society

Acta morphologica et anthropologica, 29 (1-2)
Sofia ● 2022

Oral Florid Papillomatosis Associated with Malignant Acanthosis Nigricans – a Case Report with a Review of the Literature

*Valentina Broshtilova[1], Tzetomila Vuteva[1], Vesel Kantardjiev[1], Mary Gantcheva[2,3]**

[1]Department of Dermatology and Venereology, Military Medical Academy, Sofia, Bulgaria
[2]Institute of Experimental Morphology, Pathology and Antropology with Museum, Bulgarian Academy of Science, Sofia
[3]Acibadem City Clinic Mladost, Sofia

*Corresponding author e-mail: mary_gant@yahoo.com

Oral florid papillomatosis is best defined as a type of verrucous carcinoma with local invasion and minimal dysplasia as well as a low incidence of metastases. Human papilloma virus infection is considered to trigger and perpetuate the disease, hence, its role in the the pathogenesis of the oncogenic process is still obscured. Herein, a very anecdotal case of HPV-driven oral florid papillomatosis in association with some clinical features of malignant acanthosisnigricans is presented. A comprehensive review of literature with a deductive clinical comparison of the two paraneoplastic syndromes is highlighted.

Key words: oral florid papillomatosis, HPV, paraneoplastic syndrome, acanthosis nigricans maligna, oral cavity

Introduction

Oral florid papillomatosis (OFP) is considered a locally aggressive form of verrucous carcinoma with a low metastatic potential. OFP affects predominantly the mouth; however, the larynx, nose, and genitalia can also be involved [5]. It manifests with cracking and enlargement of the lips, tongue and buccal mucosa. Interestingly, the oral form of acanthosis nigricans corresponds to the same clinical picture. Thus, the verification of the two prodromal neoplastic conditions is extremely difficult and relies only on histological grounds.

Herein, we report a case of OFP in association with darkening and thickening of the skin on the neck, clinically corresponding to acanthosis nigricans. A speculation on the probability of co-existence and common pathogenetic pathways of two paraneoplastic syndromes is presented.

Case Report

A 66-year-old man complained of verrucous lesion that appeared a month ago on the lips, oral commissures, buccal mucosa, and the tongue. He claimed on cracking of the lips, whitening of the tongue, and dry mouth. The lesions were sensitive when eating spicy food, which causes functional impairment. The patient noticed hoarsening of the voice with one-month duration and suffered dry cough for 4-5 months. He had a Covid-19 infection 7 months ago, after which he lost 5 kg from his body weight. He was a heavy smoker for more than 40 years.

On physical examination, confluent hyperplastic papules were detected on the buccal mucosa, oral commissures, lips and tongue. Hyperpigmented, velvet-like plaques extended on the flexular aspect of the neck. The distal phalanges of the fingers were thickened and larger (**Fig. 1**); there were accentuated dermatoglyphic ridges of the palms (**Fig. 2**). A 4-mm punch biopsy specimen of the buccal mucosa demonstrated pseudoepitheliomatous hyperplasia (**Fig.3**). The κeratinocytes were large, with centrally located nuclei and cytoplasm, filled with eosinophilic particles that stained positive with p16 (**Fig. 4**). Histological picture corresponds to HPV-associated epithelial lesion in the context of oral florid papillomatosis. A bronchoscopy verified a mild interstitial fibrosis with suspected tumor infiltration that required additional VATS (video-assisted thoracic surgery) examination. The patient was referred to thoracic surgery department for staging and appropriate treatment.

Fig. 1.

Fig. 2

Fig. 1. Raised formations, velvety white, rough thickening of the skin of the hands; enlargement of the distal parts of the tips of the nails and fingers.

Fig. 2. Velvety white, rough thickening of the skin of the palms with an emphasis on normal dermatoglyphic ridges.

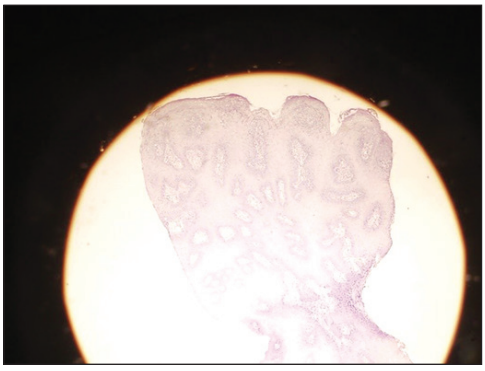

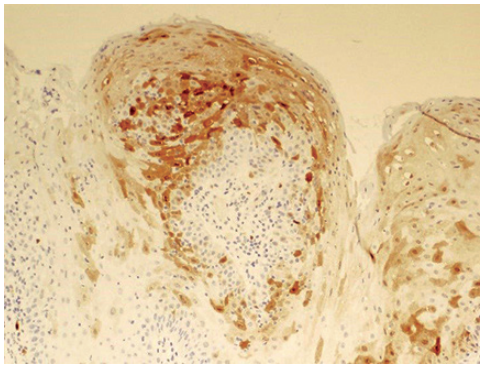

Fig. 3. **Fig. 4.**

Fig. 3. Pseudoepitheliomatous hyperplasia (H&E, x 200).

Fig. 4. Immunohistochemical staining for P16 is positive in 50% of the keratinocytes.

Discussion

OFP is a rare neoplasm that occurs in adults in their 4-5 decade with a very low incidence of 1-3 / 1 million persons each year [3, 7]. It was first reported by Lauren V. Ackerman under the term: oral verrucous carcinoma [11]. The condition represents an uncommon low-grade squamous cell carcinoma that is clinically evident as a slowly but relentlessly enlarging warty tumor, histologically characterized by local invasion with minimal, if any dysplasia, and biologically characterized by a low incidence of metastases. Even large, long-durated and infiltrative tumors do not evolve distant metastases [1].

The suspected pathogenetic factors encompass infection with human papillomavirus (HPV) and tobacco use. Perhaps, chemical and HPV viral co-carcinogens work together [12]. A number of HPV types are associated with squamous cell carcinoma, including HPV types 16 and 18 [6]. Hypothetically, the oncogenic potential of HPV exerts via two oncoproteins, E6 and E7 that promote the degeneration of p53 by means of a ubiquitin-dependent pathway. The E7 oncoprotein can similarly complexed with retinoblastoma (Rb) and inactivate it. OFP is a disease of cells that escape the control mechanisms of orderly cell growth and acquire the ability to proliferate and invade normal tissues [2].

Other risk factors are chronic inflammation or irritation, caused by poorly fitted dentures, alcoholism, immunosupression [3].

Surgical treatments for OFP are probably best and radiation therapy is generally considered a last resort. In oral verrucous carcinomas, irradiation is reported to produce highly malignant behavior with metastases, but some still use this treatment with confidence [3]. Safe therapeutic outcome with no evidence of anaplastic transformation after radiation is reported [13]. Many believe that radiation is an excellent choice for small and large oral and other types of verrucous carcinomas, with results comparable to surgery**.** Combined radiochemotherapy with vinblastine, methotrexate, and bleomycin is effective in the treatment of verrucous carcinoma of the head and neck [4]. It could be

successfully used with inoperable verrucous carcinoma or as an alternative to surgery. Photodynamic therapy using a topical application of 20% 5-aminolevulinic acid followed by multiple 3-min fractionated irradiations with a light-emitting diode (LED) red light may be an effective and successful treatment modality for oral verrucous carcinoma**.** Photodynamic therapy with systemic administration of the photosensitizer photocarcinorin proves to be equally beneficial. Bleomyciniontophoretic therapy, intra-arterial bleomycin, oral and intra-arterial methotrexate have been used with some success in small groups of OFP patients [9].

We report a clinical amalgam of OFP and acanthosis nigricans, evolving in the context of unspecified pulmonary malignancy. Acanthosis nigricans maligna (ANM) is a paraneoplastic syndrome, defined as a condition that arises in association with a malignancy elsewhere in the body but without malignant nature per se. It is a rare dermatopathy that occurs in men and women over age 40, without racial predilection or known familial association.

Clinically, ANM showed symmetric, hyperpigmented plaques with variable amounts of epidermal hypertrophy, ranging in color from yellow to brown or black, often with overlaid papillomas. The most common body sides affected are flexural zones and the posterior neck, but also mucosal surface involvement is frequent and may be the only clinical symptom present. Any mucosal surface can be involved, and as regards the oral cavity, disease affects the lips, tongue, palate, buccal and gingival mucosa.

ANM is primarily associated with adenocarcinomas. Accordingly, the progression of the tumor leads to ANM worsening, while tumor regress resorbs the skin changes [10]. The ANM suspected pathogenetic mechanism is related to a substance secreted either by the tumor or in response to the tumor, which closely correlates to transforming growth factor (TGF)-alpha that is structurally similar to epidermal growth factor. TGF-alpha and epidermal growth factor have been identified in lesional skin cells. Reports of urine and serum TGF-alpha levels normalizing after surgical tumor removal exist, with subsequent regression of skin lesions [8]. Remarkably, the oral form of ANM and OFP are clinically undistinguishable. Both conditions feature papillomatous proliferation, which is due to oversecretion of growth factors synthesis. The verification rests on identification of HPV inclusion bodies that are proven to present in our case by the p16 stain positivity.

The comparative analysis of the epidemiological, clinical and therapeutic characteristics of both entities is summarized on **Table 1**.

Table 1. Comparative analysis of the epidemiological, clinical and therapeutic characteristics

	Oral florid papillomatosis	**Acanthosis nigricans maligna**
Etiology	HPV 6,11,16,18,33	Paraneoplasia
Age	in adults	mostly in adults, but also in young
Manifestation	independent disease	paraneoplastic process

Table 1

	Oral florid papillomatosis	Acanthosis nigricans maligna
Localization	oral cavity, genitals, extremities	predilection sites (side parts of the neck, body folds, axillae, groin), oral cavity
Treatment	surgical excision, laser therapy, cryotherapy	underlying disease, local treatment, systemic treatment, surgical excision
Prognosis	poor	very bad/lethal

Conclusions

The reported association of OFP and ANM is a rare combination of peculiar paraneoplastic syndromes that requires thorough systemic work-up to verify underlying malignancy. The clinical similarities can be related to the overexpression of growth factors caused either by the neoplastic process or by the viral-induced keratinocytic hyperproliferation. Dermatological prodromes should be well-identified and rapidly diagnosed, since they facilitate an early identification of the related malignancy. Accummulation of clinical cases may further elucidate the intimate pathogenetic mechanisms and give some helpful clues for more specific verification of the underlying process.

References

1. Ackerman L. Verrucous carcinoma of the oral cavity. – *Surgery*, **4**, 1948, 670-678.

2. Agrawal, G., P. Joshi, A. Agrawal. Role of HPV-16 in pathogenesis of oral epithelial dysplasia and oral squamous cell carcinoma and correlation of p16INK4A expression in HPV-16 positive cases: an immunohistochemical study. – *Int. Scholar Resear. Notices*, **7**, 2013, 8070952.

3. Bouquot, J. Oral verrucous carcinoma. Incidence in two US populations. – *Oral Surg. Oral Med. Oral Pathol. Oral Radiol. Endod.*, **86**, 1998, 318- 324.

4. Chen, H., C. Chen, H.Yang, M. Lee, M. Kuo,Y. Kuo,Y. Wang, T. Tsai, C. Chiang. Successful treatment of an extensive verrucous carcinoma with topical 5-aminolevulinic acid-mediated photodynamic therapy. – *J. Oral Pathol. Med*., **4**, 2005, 253-256.

5. Dias-Polak, D., Z. Kra-oz, M. Szwarcwort-Cohen, A. Barzilai, R. Bergman. A Case of oral florid papillomatosis (verrucous carcinoma) with lack of evidence for human papilloma virus involvement. – *Am. J. Dermpath*., **8**, 2019, 617-619.

6. Fliss, D., S. Noble-Topham S, M. McLachlin M, J. Freeman, A. Noyek, A. van Nostrand, R. Hartwick. Laryngeal verrucous carcinoma: a clinicopathologic study and detection of human papilloma virus using polymerase chain reaction. – *Laryngoscope*, **104**, 1994, 146-152.

7. Kamath, V., R. Varma, D. Gadewar, M. Muralidhar. Oral verrucous carcinoma. Ananalysis of 37 cases. – J. *Craniomaxillofac. Surg*., **7**, 1989, 309-314.
8. Krawczyk, M., J. Mykala-Ciesla, A. Kolodziej-Jaskula. Acanthosis nigricans as a paraneoplastic syndrome. Case reports and review of literature. – *Pol. Arch. Med. Wewn*., **3**, 2009, 180-183.
9. Lu, Y., J. Wu, X. Lei X, T. Zhu, Y. He, L. Chen, Q. Cheng. Treatment of oral florid papillomatosis with systemic administration of photocarcinorin: an effective photodynamic therapy. – *Photomed. Laser Surg*., **6**, 2010, 831-833.
10. Mascitti, M., A. Santarelli, A. Albanese, G. Campisi, L. Muzio. Paraneoplastic acanthosis nigricans maligna. – *Ann. Stomatol. (Roma*), **4**, 2013, 29.
11. Schwartz, R. Verrucous carcinoma of the skin and mucosa. – J. *Am. Acad. Dermatol*., **32**, 1995, 22-24.
12. Shroyer, K., R. Greer, C. Fankhouser, W. McGuirt, R. Marshall. Detection of human-papilloma virus DNA in oral verrucous carcinoma by polymerase chain reaction. – *Mod. Pathol.,* **6**,1993, 669-672.
13. Wu, C.,C. M. Chen, Y. Shen, I. Huang, C. H. Chen, C. Y. Chen, T. Shieh, M. Sheen. Effective eradication of oral verrucous carcinoma with continuous intra arterial infusion chemotherapy. – *Head Neck,* **5**, 2008, 611-617.

Institute of Experimental Morphology, Pathology and Anthropology with Museum
Bulgarian Anatomical Society

Acta morphologica et anthropologica, 29 (1-2)
Sofia ● 2022

Review Articles

Free Radicals and Oxidative Stress as the Main Mechanism of Heavy Metal Toxicity in the Male Reproductive System

I. Ilieva, I. Sainova

Dept. Experimental Morphology, Institute of Experimental Morphology, Pathology and Anthropology with Museum, Bulgarian Academy of Sciences, Sofia, Bulgaria

* Corresponding author e-mail: iilieva@abv.bg

Heavy metals and metalloids such as lead, arsenic, mercury, and cadmium are dense elements with potential toxicity, widespread in the environment. One of the ways of toxic actions of these metals is related to their ability to generate reactive oxygen species (ROS) and oxidative stress (OS), causing cell damage, inflammatory processes, and apoptosis in various biological systems. The purpose of this review is to discuss ROS/OS, as one of the main factors and mechanisms by which metals/metalloids influence or contribute to the appearance and development of pathological processes in the male reproductive system. Studies on the mechanisms of heavy metals associated with augmentation ROS production, as well as their complex effect on the male reproductive system (in particular on spermatozoa), are essential in elucidating male infertility.

Keywords: Heavy metals/ Pb, Cd, Hg, As, reactive oxygen species, oxidative stress, male infertility

Introduction

The production of reactive oxygen species (ROS) in the organism can be accelerated by various exogenous factors, such as radiation, heavy metals, bacteria, and their toxins, viruses, or xenobiotics (including some drugs). Many metals, like zinc (Zn), iron (Fe), manganese (Mn), magnesium (Mg), and copper (Cu), perform vital functions and are toxic only in cases of overdose, but other as lead (Pb), arsenic (As), cadmium (Cd) and mercury (Hg) show high toxicity to living organisms. The toxicity of a metal depends on its physicochemical properties, but mainly on its preference for certain ligands (chemical elements/molecules donors of electrons in complex compounds). The so-called „soft“ transition metals, such as cadmium and mercury, prefer sulfur as their ligand, while „hard“ as chromium (Cr), Mn, but also the metalloids As,

antimony (Sb), and selenium (Se), prefer more oxygen in their higher oxidation states and sulfur in the lower oxidation states. Cobalt (Co), nickel (Ni), Fe, Pb, Cu, and Zn may use oxygen, sulfur, or nitrogen as ligands [39]. Toxic heavy metals are difficult to metabolize, respectively they can accumulate in the body, as well as combine and inhibit vital cellular functions [4]. At the cellular level, heavy metals/metalloids interfere with membrane function and nutrient assimilation, perturb protein function and activity, cause DNA damage, and/or impair DNA repairs mechanisms [39]. On the one hand, heavy metals can directly cause oxidative damage to biomolecules, but on the other indirectly, through the action of the intracellular ROS induced by them, which through changes in signaling pathways and epigenetic modifications mediate multiple abnormal changes in cellular behavior.

The most often circulating forms of ROS are these, which contain active oxygen atoms, as superoxide anions ($O_2^{\cdot}$), hydroxyl radicals ($OH^{\cdot}$), hydroperoxyl/peroxyl radicals ($HOO^{\cdot}/ROO^{\cdot}$), hydrogen peroxide (H_2O_2), etc [27]. Other organic atoms/molecules may be included in the class of ROS, such as carbon-containing radicals (or lipid peroxide radicals), which are derived by removing hydrogen from the unsaturated fatty acids as the result of lipid peroxidation. Nitrogen (peroxynitrite/ONOO−, nitric oxide/NO• or nitrogen dioxide/NO_2•) and other types of free radicals have also been described [59]. Another type is the thiol radicals (•SH), which are also derived from endogenous chemical substances, containing thiol (SH-) groups as glutathione (GSH), formed by hydrolytic breaking of disulfide (S-S-) bridges in the protein molecules. The strong toxicity of the thiol radicals has been proposed to be due to their possibility to react with oxygen species, which often leads to the formation of additional novel free radicals. All cells in the organism maintain metal homeostasis within physiological or sub-toxic levels, respectively, and utilize metal detoxification mechanisms. Glutathione is the most common circulating source of non-protein SH-groups in mammalian cells [45]. The reduced form of GSH is a tri-peptide (γ-glutamylcysteinyl-glycine), which performs important physiological and metabolic functions in all cells, particularly being detoxification of free radicals, metals, and other electrophilic compounds [22]. GSH is one of the main cellular factors that act on the first line of defense against oxidative stress (OS). Normal GSH content of a cell that is imperative to maintain a balance between depletion and synthesis ranges from 1 to 10 mM [8].

One of the ways of toxic action of metals is based on the fact that they are all redox elements and thus, can generate ROS and/or OS, causing cellular damage in a variety of biological systems [30, 50]. OS is a common factor in about half of infertile men, illustrating the role of heavy metals in activating transduction signaling pathways to initiate protective responses or to lead to oxidative damage in cells and tissues. ROS not only damages nucleic acids and inhibits DNA repair, and/or initiates membrane lipid peroxidation, but ROS can also inhibit the production of sulfhydryl antioxidants, as well as cause inflammatory processes in many organs, including the testes [27]. Any damage in the DNA of the sperm results in the impairment of fertility and could induce men infertility, cancer, or other disadvantages in the long term [2]. It is well documented that metal-induced generation of ROS can attack polyunsaturated fatty acids (PUFA), such as phospholipids. Lipid peroxidation (LP, a chain reaction in which ROS generates more new free radicals) is a biomarker for OS since the free radicals collect electrons from lipid molecules present inside the cell membrane [23], which ultimately destroys the plasmalemma and other membrane structures. Malondialdehyde (MDA) is a major

aldehyde product of LP and it serves as a marker for this process. The mechanism of free radical generation is specific to the type of heavy metal.

Our previous reviews have shown a lot of literature data about the negative influence of toxic heavy metals on human health particularly, on the male reproductive system [27, 28]. Despite this, the mechanisms of the harmful effects of these elements on the male reproductive tract and fertility are not yet sufficiently elucidated. The purpose of this review is to discuss ROS/OS, as one of the main factors and mechanisms by which metals/metalloids influence or contribute to the appearance and development of pathological processes in the male reproductive system.

Lead toxicity. The variety of adverse effects due to increased tissue ROS levels is mainly related to Pb exposure [50]. This metal causes toxicity in living cells by following the ionic mechanism and that of OS. Pb induces OS by promoting H_2O_2 generation. [47, 61]. Generally, proteins are not easily damaged by H_2O_2 and other simple oxidants unless transition metals are available. Thus, protein damage is usually metal-catalyzed and involves oxidative scission, tyrosine cross-links, loss of histidine residues, the introduction of carbonyl groups, and the formation of protein-centered alkyl (R•), alkoxyl (RO•), and alkyl peroxyl (ROO•) radicals [19]. Epidemiological studies on the male reproductive system show a positive correlation between Pb levels in seminal plasma (ejaculate) and ROS in germ cells [36], leading to a premature course of capacitation and acrosome reaction, processes related to the fertilizing ability of spermatozoa [26, 32, 36]. For example, a study on rat sperm exposed to ROS *in vitro* has demonstrated premature acrosome reactions and reduced penetration rate in the zona pellucida of the oocyte [26]. Data from a study of rats exposed to Pb for a long time showed an increase in the concentration of lipid peroxides in the reproductive organs, suggesting that LP is an important molecular mechanism that disrupts reproductive processes, either in hormonal stages or during spermatogenesis [44]. Pb-induced OS has been shown to have a dose-dependent effect (from low to high doses of Pb) and shows different responses in various target sites of testicular tissue, including sperm [26]. Other experiments reported an increase in lipid peroxide concentration in the reproductive organs in rats chronically exposed to Pb [44]. However, exposure to Pb leads to an increase in ROS in the cells, but at the same time to a decrease in antioxidant levels. For example, one of the antioxidants, glutathione exists in both reduced (GSH) and oxidized (GSSG) states, the reduced form of glutathione gives its reducing equivalents ($H^+ + e^-$) from the thiol groups in cysteine of ROS and is thus stable. In the presence of the enzyme glutathione peroxidase, this reduced form (after donating the electron) readily binds with another molecule and forms glutathione disulfide, which is its oxidized form – GSSG. Under OS, the concentration of the oxidized form of glutathione exceeds the concentration of the reduced form, while under normal conditions, GSH represents 90% of the total glutathione content and GSSG represents 10% [23]. Nevertheless, in people with protracted exposure to Pb, increased activity of superoxide dismutase (SOD) has been observed, which suggests an adaptive mechanism against the increased amount of ROS production induced by lead [32]. In this way, the possible oxidative cellular damage in reproductive tissues is closely associated with ROS production. The mechanism of the lead-induced carcinogenic process is also postulated to induce DNA damage, and disrupt the DNA repair system and cellular tumor regulatory genes through the generation of ROS. Research data

show that the ROS generation by Pb is a key point in the change in chromosome structure and sequence as a result of impaired transcription when Pb replaces Zn in certain regulatory proteins [57]. Therefore, the findings of the studies indicate that Pb-induced OS is an important molecular mechanism associated with both morphological and hormonal disorders during spermatogenesis leading to male infertility.

Cadmium toxicity. The main manifestation of toxicity through which Cd causes tissue damage in the organism is its ability to produce ROS to a very large extent (mostly OH•, HOO•, O_2• radicals, but also H_2O_2, NO•, and NO_2•) and/or by suppression of the components of the antioxidant system in the testes, leading to OS. Through the mechanism of accumulation of free radicals and OS, cadmium can be the cause of male infertility associated with damaged testicular tissue (including Sertoli cells/SCs and blood-testis barrier/BTB) and spermatogenesis, decreased cell proliferation, morphological abnormalities in germ cells, decreased number and motility of spermatozoa, and damage to Leydig cells (LCs) with reduced TE synthesis [28]. For example, a characteristic feature of Cd intoxication is increasing OS through activating processes of peroxidation and NO• formation, leading to lower levels of antioxidants in the testis, including SOD, peroxidase, catalase, GR, and GPx [2, 10, 21, 49]. On the other hand, studies by Elmallah et al. (2017) show that nuclear factor erythroid-derived 2-like 2 (NFE2L2 or NRF2) is significantly reduced, while heme oxygenase (HMOX1) is significantly increased in the testis tissue of intoxicated with Cd rats [21]. NFE2L2 is known to be a transcription factor that can regulate the expression and activity of antioxidant proteins (or elements of the antioxidant response) that protect cells from oxidative damage. HMOX1 is also a protein with a cytoprotective effect against induced OS and probably its increased expression, in this case, is related to the adaptive response of cells to the toxic action of Cd. These authors have also established increased levels of tumor necrosis factor-α (TNF-α) together with the noted decreased content of proliferating cell nuclear antigen (PCNA) in germ cells on the influence of Cd. PCNA is a nuclear protein that is involved in replication and DNA repair mechanisms and is involved in the process of cell proliferation. In addition, PCNA in the testes is used as a proliferative marker to quantify the effectiveness of spermatogenesis. Moreover, through the mechanism of OS, Cd indirectly reduces cell proliferation by increasing the expression of the proapoptotic BCL-2-associated-X-protein/Bax and tumor necrosis factor-α (TNF-α) but decreases the expression of the antiapoptotic gene/Bcl2 in the testis. Thus, Cd-induced oxidative damage to testicular tissue is accompanied by depletion of active DNA content in dividing spermatogenic cells [21, 15]. Furthermore, ascorbic acid (Vit. C) content is also significantly declined in the testes of Cd-exposed mice [2,10]. The injured prooxidant-antioxidant balance leads to injuries in the membrane structures (plasmalemma, cell-cell contacts, etc.) and cellular organelles (mitochondria or microsomes), but also in the spermatogenic epithelium of the seminiferous tubules, abnormal function of SCs and germ cells with decreased sperm count and increased sperm abnormality [2]. Mahmoudi et al., (2018) have also confirmed the availability of increased ROS production and significantly increased levels of malondialdehyde (MDA) in the testicular tissue with decreased numbers of spermatogonia, SCs, and LCs, but also decreased sperm motility and count, as well as inhibition of TE synthesis in rats treated with cadmium chloride. In fact, Cd exposure causes atrophy and swelling of the tubules, the height of the germ layer decreases (respectively reduces the diameter of the seminal tubule), and many spermatogonia cells

are lost. The authors have also revealed ameliorated sperm defects in cadmium chloride intoxicated rats after experimental application of green tea and reduced effects of ROS by the protection mechanism of green tea [43]. According to another study, generated ROS and increased MDA, but decreased testicular antioxidant activity (SOD, catalase, and ascorbic acid) lead to BTB disruption. However, the results of this study show that high doses of ascorbic acid can protect BTB destruction via suppressed Cd-induced OS (by decreasing the levels of ROS and MDA) and by inhibiting the TGF-β3/p38 MAPK signaling pathway in the testis of Cd-exposed rats [10].

Through the mechanism of OS, cadmium could cause degeneration of Leydig cells and to inhibit the testicular steroidogenesis [38, 49]. In the investigation of OS in the testis of adult male rats exposed to Cd-acetate is established that Cd generated ROS by elevating testicular MDA and decreased activities of the antioxidant enzymes SOD, catalase, glucose 6 phosphate dehydrogenase, and glutathione-S-transferase in the mitochondrial and/or post-mitochondrial fractions. Thus, the activities of LC steroidogenic enzymes 3β and 17β-hydroxysteroid dehydrogenase (Hsd3b1 and Hsd17b3) are also remarkably reduced, leading to altered TE production [49]. In other experiments with rats, tumors were found in Leydig cells as a result of a significant increase in lipid peroxidation and H_2O_2 formation and a decrease in the activity of antioxidant enzymes (catalase and GR) in LCs, after prolonged Cd treatment [38]. According to the results of Khanna et al, (2016), LCs of rats, *in vitro*-exposed to Cd, have had a simultaneous increase in the intracellular calcium (Ca^{2+}) and reduced mitochondrial membrane polarization, followed by significant induction of ROS and MAPK–extracellular-regulated kinases with concurrent GSH depletion and cell death (both necrotic and apoptotic), as well as decreased transcription of Hsd3b1 [34]. A similar *in vitro* study of SC-germ cell co-culture found that free radicals produced by Cd reduced GSH and caused cytochrome c release, caspase-3 activation, and SC apoptosis [34].

Arsenic toxicity. The metabolism of the element As in the cells, similarly to the other heavy metal, leads to the generation of ROS in them [63]. Arsenic induces the formation of singlet oxygen ($^1O_2$), $O_2^{-\bullet}$, H_2O_2, $^{\bullet}OH$, and $ROO^{\bullet}$ in different cell lines during the reduction of the molecular oxygen [54]. Under physiological conditions, the formation of ROS by arsenic lay on the oxidation of inorganic arsenite (iAs III) to arsenate (iAs V) [16]. In humans, inorganic As can be methylated to organic matter by S-adenosyl-L-methionine (SAM), including monomethyl-arsonic acid (MMA) and dimethyl-arsic acid (DMA) with trivalent (MMA III and DMA III) and pentavalent forms (MMA V and DMA V), respectively [1]. Intermediate As forms, such as dimethyl arsenic peroxyl radicals, could be generated during the metabolic processing of DMA. In addition, the release of redox-active Fe from ferritin is caused by methylated types of As. Other mechanisms of ROS generation, induced by As toxicity in cell activity, have also been described [20]. Arsenic induces significant ROS generation mainly through the mitochondrial (Mit) electron transport chain, inhibiting the activity of enzyme succinic dehydrogenase and thus uncoupling oxidative phosphorylation with the production of O_2^{-}• (which gives rise to other forms of ROS) [13], and/or by activation of enzyme nicotine adenine disphosphonucleotide oxidase/Nox, which also contributes to O_2^{-}• generation [20]. The endoplasmic reticulum is also thought to be a source of ROS caused by DMA III [46].

Arsenic (like Pb) has been shown to bind to glutathione and several antioxidant enzymes, thus decreasing the protective capacity of cells and inducing OS [59]. According to several studies, the interference of As with cellular antioxidants such as GSH, SOD, catalase and other GSH-related enzymes [11,48] indirectly results in increased ROS levels. Furthermore, As can alter signal transduction pathways (for example, the influence of extra- and/or intracellular signaling molecules on genes functions) via ROS alteration or reversible oxidation of SH-groups in proteins, which could lead to activation or inhibition of transcription factors, regulating in this way gene transcription [52]. Many studies have shown that the major ROS-affected pathways in response to As including signaling pathways, mitogen-activated protein kinases (MAPKs), microRNAs (miRNAs), tyrosine phosphorylation system, mitophagy pathway, Nrf2-antioxidant response element (ARE), nuclear factor κB (NF-κB), and activator protein-1 (AP-1) [17, 60].

These results suggest that oxidative stress generated by As and As compounds (like many other heavy metals) can damage testicular tubules, leading to reduced cell proliferation, and/or could cause gonadal dysfunction through reduced testosterone synthesis, apoptosis, and/or necrosis. Monomethylated and dimethylated arsenicals increase the production of ROS and OS associated with many cytotoxic and genotoxic effects, including oxidative DNA damage and chromosomal aberrations [37, 18]. Methylated trivalent metabolites are highly reactive and are more potent inhibitors of GSH reductase and thioredoxin reductase compared with arsenite or pentavalent metabolites [58]. In the Japanese eel, low doses (0.1 ~ 1 μM) of arsenic have been shown to inhibit spermatogenesis by suppressing steroidogenesis, and at high doses (100 μM), As mediates OS and induces germ cell apoptosis [12]. At 10 μM arsenic trioxide (As_2O_3) effectively induced ROS cytotoxicity and apoptotic cell death in murine TM4 Sertoli cells. *In vivo* studies have shown that oral exposure to inorganic As causes dysfunctions in spermatogenesis, decreased testosterone and gonadotropins, but also impaired steroidogenesis [35]. Additionally, in male rats, exposed to sodium arsenite, have been assessed decreased weights of the testes and of the accessory sex glands, but also reduced epididymal sperm counts [31]. Experiments with mice exposed to As have also shown dose-dependent gradual reductions in seminiferous tubular diameter and various gametogenic cell populations, such as resting spermatocytes, pachytene spermatocytes, and elongated spermatids [55]. It has also been found that the lack of transcriptional intermediary factor 1β, a key molecule associated with heterochromatin structures in Sertoli cells and round spermatids, as well as the formation of meiotic chromosomes [62], leads to a significant defect in spermatogenesis associated with failure to release spermatids and testicular degeneration [25, 29]. Other studies complete the toxic effects of arsenic on male fertility concerning inhibition of steroidogenesis and sperm maturation [35].

Mercury toxicity. Mercury (both organic and inorganic) generated ROS and affects the antioxidant defense system of the cells by connection with thiol groups (or SH-containing residues). The main mechanism of biochemical action of Hg^{2+} is connected with the strong affinity of this ion to SH-groups (with high stability constants), which are the main components for the structure and functions of different biomolecules (as GSH, cysteine, metallothionein, N-acetylcysteine, S-adenosyl-methionine, albumin and other proteins, including enzymes), presenting in both extra- and intracellular

membrane structures, as well as in the cellular organelles [51]. In this way, Hg alters the intracellular thiol status, leading to free radical generation and abnormal synthesis of many proteins, including such, which affect the membrane permeability, causing functional anomalies in the cells and/or cellular apoptosis [42]. Hg can cause disruption to the mitochondrial membrane potential and interrupt with intracellular calcium homeostasis. Besides that, the binding of Hg may also occur in other sites - e.g., ligands containing amino or carboxyl groups are generally less favorable (with almost 10 times lower Hg binding constant) than to SH-groups. Mercury generates mainly H_2O_2 and $O_2\bullet^-$, which in the presence of redox-active transition metals are converted into highly reactive OH• radical (by the reactions of Fenton and Haber-Weiss) [59]. Hg has been shown to induce cellular malignant growth through the generation of free radicals, inducing OS, as well as through disruption of DNA molecular structure, or the repair and maintenance system [14]. The molecular interactions of Hg with the SH-groups of SH-containing molecules are involved in the mechanisms of transport, accumulation, and toxicity of mercury ions in the tissues, including seminiferous tubules. On the one hand, GSH neutralizes the harmful action of Hg, but it is also a major factor in cellular protection against OS, on the other. GSH increases the antioxidant capacity of mitochondria, thus providing their protection against H_2O_2, singlet oxygen, hydroxyl radicals, and lipid peroxides generated by Hg. In this relation, differences between the exposition of the influence of Hg and the chemical nature of the Hg, accepted in the organism, have been proved. Methylmercury (MeHg, organic form) is usually bounded to one -SH-group to form a complex with thiol-containing molecules, while Hg^{2+} (inorganic mercury) binds to two GSH molecules by sulfur atom on the cysteinyl residue of GSH molecule [7]. Additionally, GSH facilitates the formation of metal complexes via non-enzymatic reactions. Hg^{2+} mediated depletion of GSH (reduced GSH) creates an OS condition characterized by increased sensitivity of the mitochondrial membrane to iron-dependent lipid peroxidation. The depletion of mitochondrial GSH and the increase of H_2O_2 in the inner mitochondrial membrane contribute to the acceleration of the exchange of Ca^{2+} and Mg^{2+} [41], which hampers mitochondrial function. These mechanisms cause membrane lipid peroxidation, leading to dysfunction and abnormal morphology of spermatozoa, but also to oxidative damages in their DNA, decreased mobility, and abnormal acrosome reaction [5]. The injured membrane integrity of the cell could also lead to increased membrane permeability and decreased compatibility to regulate the intracellular concentrations of ions, which are responsible for the control of the male germ cell's movement [6]. On the other hand, an increase in GSSH level leads to the progression of OS, promoting the oxidation of cellular protein cysteinyl thiols, which ultimately leads to impaired protein function. Thiol-disulfide balance in the cell regulates metabolic pathways by activating or inactivating key enzymes. Because thiol transfer reactions are bidirectional, the balance is determined by the redox state of the cell. A lot of enzymes in the antioxidative protective systems prevent the disbalance between prooxidants and antioxidants. Antioxidant enzymes such as GSH reductase (GR), GSH peroxidase (GPx), SOD, etc., containing SH-groups in their active centers, and also main metal ions in the role of co-factors (for instance, Zn, Se, etc.), are more prone to be attacked by Hg, which ultimately leads to the cessation of their activity [40]. The data have shown a disbalance between the prooxidant and antioxidant systems, which could cause a significant reduction of the activity of two main antioxidant enzymes in the testis – SOD and catalase, as well as

increased lipid peroxidation, leading to OS in exposure to Hg and/or its compounds in animals (mice, rats, etc.), [53, 56]. Hg has also been proved to cause strong interstitial oedema and vasodilatation in the testes of the individuals, exposed to its influence, which could lead to suppressed spermatogonia differentiation or induce apoptosis of these cells, but also to spermatocyte degeneration and degradation of the embryonic epithelium in the seminiferous tubules in rats [3, 9].

According to many review publications, the intoxication with Hg and/or its compounds, together with the induced OS besides affecting the spermatogenesis, also leads to abnormal steroidogenic functions (androgens deficiency) in the testes of male experimental animals and men [33]. Because LCs are the main testosterone-producing source in the testes, Hg intoxication modulates the functions of these cells by reducing the production of steroid hormones in the treated animals [24].

Conclusion

The data presented in the current review show that the main pathway of heavy metal toxicity is the induction of ROS, increased lipid peroxidation, and induction of OS in the reproductive organs. Together with their general properties, various types of free radicals influence various specific mechanisms, which distinguishes them from one another, and hence, their investigation could be useful for the development of easily-applying methods for laboratory analyzes and technologies for assessing these metabolic products in different biological materials (tissue probes, body fluids, etc.). Oxidative stress is a powerful mechanism that can lead to DNA damage in the germ cell lines during spermatogenesis, to the production of dysfunctional germ cells, and ultimately to male infertility. The diagnosis of abnormalities in the spermatogenesis process as a result of excessive ROS production is an important step in determining the etiology of male infertility and the development of appropriate therapeutic strategies.

Reference

1. **Abernathy, C. O., Y. P. Liu, D. Longfellow, H. V. Aposhian, B. Beck, B. Fowler, R. Goyer, R. Menzer, T. Rossman, C. Thompson, M. Waalkes.** Arsenic**.** Health effects, mechanisms of actions, and research issues. – *Environ. Health Perspect.,* **107**, 1999, 593-597.
2. **Acharya, U. R., M. Mishra, J. Patro, M. K. Panda**. Effect of vitamins C and E on spermatogenesis in mice exposed to cadmium. – *Reprod. Toxicol.* 25, 2008, 84-88.
3. **Agarval, A., R. A. Saleh, M. A. Bedaiwy**. Role of reactive oxygen specie in the pathophysiology of human reproduction. – *Fertil. Steril*., **79**, 2003, 829-843.
4. **Ali, H. M., Qater, A-N. A. Kanaem, M. O. Selman**. Relation of Some Heavy Metals with Male Infertility. – *Medico-legal Update*, **20**(1), 2020, 1440-1445.
5. **Arabi, M., M. S**. Heydarnejad. In vitro mercury exposure on spermatozoa from normospermic individuals. – *Pak J. Biol. Sci*., **10**, 2007, 2448-2453.
6. **Baumber, J., B. A. Ball., C. G. Gravance, V. Medina, M. C. G. Davies-Morel**. The effect of reactive oxygen species on equine sperm motility, viability, acrosomal integrity, mitochondrial membrane potential and membrane lipid peroxidation. – *J. Androl*., **21**, 2000, 895-902.
7. **Becker, A., K. F. A. Soliman**. The role of intracellular glutathione in inorganic mercury-induced toxicity in neuroblastoma cells. – *Neurochem. Res.,* **34,** 2009, 1677-1684.

8. Biswas, S. K., I. Rahman. Environmental toxicity, redox signalling and lung inflammation: Role of glutathione. – *Mol. Aspects Med.,* **30**, 2009, 60-76.
9. Boujbiha, M. A., K. Hamden, F. Guermazi, A. Bouslama, A. Omezzine, A. Kammound, A. E. Feki. Testicular toxicity in mercuric chloride treated rats: association with oxidative stress. – *Reprod. Toxicol*., **28**, 2009, 81-89.
10. Chen, N., P. Su, M. Wang, Y. M. Li. Ascorbic acid inhibits cadmium-induced disruption of the blood-testis barrier by regulating oxidative stress-mediated p38 MAPK pathways. – *Environ. Sci. Pollut. Res. Int.*, **25**, 2018, 21713-21720.
11. Chouchane S., E. T. Snow. In vitro effect of arsenical compounds on glutathione-related enzymes. – *Chem. Res. Toxicol.,* **14**, 2001, 517-522.
12. Celino, F. T., S. Yamaguchi, C. Miura, T. Miura. Arsenic inhibits in vitro spermatogenesis and induces germ cell apoptosis in Japanese eel (Anguilla japonica). – *Reproduction.,* **138,** 2009, 279-287.
13. Corsini, E., L. Asti, B. Viviani, M. Marinovich, C. L. Galli. Sodium arsenate induces overproduction of interleukin-1alpha in murine keratinocytes: Role of mitochondria. – *J. Investig. Dermatol.*, **113**, 1999, 760-765.
14. Crespo-Lopez, M. E., G. L. Macedo, S. I. Pereira, G. P. Arrifano, D. L. Picanco-Diniz, J. L. De Nascimento, **A. Herculano**. Mercury and human genotoxicity: Critical considerations and possible molecular mechanisms. – *Pharmacological Research*, **60**(4), 2009, 212-220.
15. Dai, X., G. Nie, H. Cao, C. Xing, G. Hu, C. Zhang. In vivo assessment of molybdenum and cadmium co-induced the mRNA levels of heat shock proteins, inflammatory cytokines and apoptosis in shaoxing duck (*Anas platyrhyncha*) testicles. – *Poultry Science*, **98**(11), 2019, 5424-5431.
16. Del Razo, L.M., B. Quintanilla-Vega, E. Brambila-Colombres, E.S. Calderon-Aranda, M. Manno, A. Albores. Stress proteins induced by arsenic. – *Toxicol. Appl. Pharmacol.,* **177**, 2001, 32-148.
17. Demers-Lamarche, J., G. Guillebaud, M. Tlili, K. Todkar, N. Bélanger, M. Grondin, A.P. Nguyen, J. Michel, M. Germain. Loss of Mitochondrial Function Impairs Lysosomes. – *J. Biol. Chem.,* **291**, 2016, 10263-10276.
18. Dopp, E., L. M. Hartmann, U, von Recklinghausen, A. M. Florea, S. Rabieh, U. Zimmermann, B. Shokouhi, S. Yadav, A. Hirner, A. Rettenmeier. Forced uptake of trivalent and pentavalent methylated and inorganic arsenic and its cyto-/genotoxicity in fibroblasts and hepatoma cells. – *Toxicological Sciences,* **87**, 2005, 46-56.
19. Eaton, J. W., M. W. Qian. Molecular bases of cellular iron toxicity. – *Free Radical Biology Medicine*, **32**, 2002, 833-840.
20. Ellinsworth, D. C. Arsenic, reactive oxygen, and endothelial dysfunction. – *J. Pharmacol. Exp. Ther.*, **353**, 2015, 458-464.
21. Elmallah, M. I. Y., M. F. Elkhadragy, E. M. Al-Olayan, A. E. Abdel Moneim. Protective effect of fragaria ananassa crude extract on cadmium-induced lipid peroxidation, antioxidant enzymes suppression, and apoptosis in rat testes. – *Int. J. Mol. Sci.*, **18**, 2017, 957.
22. Eto, K., Y. Takizawa, H. Akagi, K. Haraguchi, S. Asano, N. Takahata, H. Tokunaga. Differential diagnosis between organic and inorganic mercury poisoning in human cases – Pathologic point of view. – *Toxicol. Pathol.,* **27**, 1999, 664-671.
23. Flora, G., D. Gupta, A. Tiwari. Toxicity of lead: A review with recent updates. – *Interdiscip. Toxicol.,* **5**(2), 2012, 47-58.
24. Guraya, S. S. Cellular and molecular biology of capacitation and acrosome reaction in spermatozoa. – *Int. Rev. Cytol*., **199**, 2000, 1-64.
25. Herzog, M., O. Wendling, F. Guillou, P. Chambon, M. Mark, R. Losson, F. Cammas. TIF1β association with HP1 is essential for post-gastrulation development, but not for Sertoli cell functions during spermatogenesis. – *Dev. Biol.,* **350**, 2011, 548-558.

26. Hsu, P.C., Y.L. Guo. Antioxidant nutrients and lead toxicity. – *Toxicology*, **180**, 2002, 33-44.
27. Ilieva, I. N., I. B. Sainova, B. A. Nikolov. Free radicals, male reproductive diseases and male infertility: A review. – *Journal of Biomedical and Allied Research*, **1**(1), 2019, 1-22.
28. Ilieva, I., I. Sainova, K. Yosifcheva. Toxic effects of heavy metals (lead and cadmium) on sperm quality and male fertility. – *Acta morphol. anthropol.*, **27**(3-4), 2020, 61-73.
29. Ilieva, I., I. Sainova, K. Yosifcheva. Toxic effects of heavy metals (mercury and arsenic) on the male fertility. – *Acta morphol. anthropol.*, **28**(1-2), 2021, 64-75.
30. Jan, A. T., M.Azam, K. Siddiqui, A. Ali, I. Coi, Q. Haq.. Heavy metals and human health: Mechanistic insight into toxicity and counter defense system of antioxidants. **–** *Int. J. Mo.l Sci.*, **16**(12), 2015, 29592-29630**.**
31. Jana, K., S. Jana, P.K. Samanta. Effects of chronic exposure to sodium arsenite on hypothalamo-pituitarytesticular activities in adult rats: Possible an estrogenic mode of action. – *Reprod Biol Endocrinol.* **16**, 2006, 4-9.
32. Kasperczyk, S., E. Birkner, A. Kasperczyk, J. Zalejska-Fiolka. Activity of superoxide dismutase and catalase in people protractedly exposed to lead compounds. – *Ann Agric. Environ. Med*., **11**, 2004, 291-296.
33. Keck, C., M. Bergman, E. Ernst, C. Muller, S. Kliensch, E. Nieschlag. Autometallographic detection of mercury in testicular tissue of an infertile men exposed to mercury vapour. – *Reprod. Toxicol*., **7**, 1993, 469-475.
34. Khanna, S., S. Mitra, P.C. Lakhera, S. Khandelwal. N-acetylcysteine effectively mitigates cadmium-induced oxidative damage and cell death in Leydig cells *in vitro*. – *Drug Chem. Toxicol.*, **39**, 2016, 74-80.
35. Kim, Y-J., J-M. Kim. Arsenic Toxicity in Male Reproduction and Development. *Dev. Reprod.,* **19**(4), 2015, 167-180
36. Kiziler, A. R., B. Aydemir, I. Onaran, B. Alici, H. Ozkara, T. Gulyasar, M. Akyolcu. High levels of cadmium and lead in seminal fluid and blood of smoking men are associated with high oxidative stress and damage in infertile subjects. – *Biol Trace Elem. Res*., **120**, 2007, 82-91.
37. Kligerman, A.D., A. H. Tennant. Insights into the carcinogenic mode of action arsenic. – *Toxicology and Applied Pharmacology.* 2007; 222:281-288.
38. Koizumi, T., Z. G. Li. Role of oxidative stress in single-dose, cadmium-induced testicular cancer. – *J. Toxicol. Environ. Health*, **37**, 1992, 25-36.
39. Lemire, J. A., J. J. Harrison, R. J. Turner. Antimicrobial activity of metals: Mechanisms, molecular targets and applications. – *Nat. Rev. Microbiol.,* **11**, 2013, 371-384.
40. Leong, C. C., N.I. Syed, F. L. Lorscheider. Retrograde degeneration of neurite membrane structural integrity of nerve growth cones following *invitro* exposure to mercury. – *Neuroreport*, **12**, 2001, 733-737.
41. Lund, B. O., D. M. Miller, J. S. Woods. Mercury induced H_2O_2 production and lipid peroxidation *invitro* in rat kidney mitochondria. – *Biochem. Pharamacol.*, **42**, 1991, S181-187.
42. Magos, L., T. W. Clarkson. Overview of clinical toxicity of mercury. – *Ann. Clin. Biochem*., **43**, 2006, 257-268.
43. Mahmoudi, R., A. Azizi, S. Abedini, V. Hemayatkhah Jahromi, H. Abidi, M. J. Barmak. Green tea improves rat sperm quality and reduced cadmium chloride damage effect in spermatogenesis cycle. – *J. Med. Life,* **11**, 2018 371-380.
44. Marchlewicz, M., B. Wiszniewska, B. Gonet, I. Baranowska-Bosiacka, K. Safranow, A. Kolasa, **W. Glabowski, R. Kurzawa, K. Jakubowska, M. Rac.** Increased lipid peroxidation and ascorbic acid utilization in testis and epididymis of rats chronically exposed to lead. – *Biometals*, **20**, 2007, 13-19.
45. Meister, A. Glutathione metabolism and its selective modification. **–** *J. Biol. Chem.*, **263**, 1988, 17205-17208.

46. Naranmandura, H., S. Xu, S. Koike, L. Q. Pan, B. Chen, Y. W. Wang, K. Rehman, B. Wu, Z. Chen, N. Suzuki. The endoplasmic reticulum is a target organelle for trivalent dimethylarsinic acid (DMAIII)-induced cytotoxicity. – *Toxicol. Appl. Pharmacol.*, **260**, 2012, 241-249.

47. Ni, Z., S. Hou, C. H. Barton, N. D. Vaziri. Lead exposure raises superoxide and hydrogen peroxide in human endothelial and vascular smooth muscle cells. – *Kidney Int*., **66**, 2004, 2329-2336.

48. Nordenson, I., L. Beckman. Is the genotoxic effect of arsenic mediated by oxygen free radicals? – *Hum. Hered.*, **41**, 1991, 71-73.

49. Pandya, C., P. Pillai, L. P. Nampoothiri, N. Bhatt, S. Gupta, S. Gupta. Effect of lead and cadmium co-exposure on testicular steroid metabolism and antioxidant system of adult male rats. – *Andrologia*, **44**, (Suppl. 1), 2012, 813-822.

50. Patrick, L. Mercury toxicity and antioxidants: Part 1: role of glutathione and alpha-lipoic acid in the treatment of mercury toxicity. – *Altern. Med. Rev*., **7**(6), 2002, 456-471.

51. Patrick, L. Lead toxicity part II: the role of free radical damage and the use of antioxidants in the pathology and treatment of lead toxicity. – *Altern. Med .Rev*., **11**(2), 2006, 114-27.

52. Platanias, L. C. Biological responses to arsenic compounds. – *J. Biol. Chem.,* **284**, 2009, 18583-18587.

53. Rao, M. V., P. S. Sharma. Protective effect of vitamin E against mercuric chloride reproductive toxicity in male mice. – *Reprod. Toxicol*., **15**, 2001, 705-712.

54. Shi, H., X. Shi, K.J. Liu. Oxidative mechanism of arsenic toxicity and carcinogenesis. – *Mol. Cell. Biochem.,* **255**, 2004, 67-78.

55. Sanghamitra, S., J. Hazra, S. Upadhyay, R. Singh, R. Amal. Arsenic induced toxicity on testicular tissue of mice. – *Indian J. Physiol. Pharmacol.,* **52***,* 2008, 84-90.

56. Sener, G., O. Sehirli, A. Tozan, A. Velioglu-Ovunc, N. Gedik, G. Z. Omurtag. *Gingko biloba* extract protects against mercury(II)-induced oxidative tissue damage in rats. – *Food Chem. Toxicol*., **45**, 2007, 543-550.

57. Silbergeld, E. K., M. Waalkes, J.M. Rice. Lead as a carcinogen: Experimental evidence and mechanisms of action. - *American Journal of Industrial Medicine*, **38**(3), 2000, 316-323.

58. Styblo, M., S. V. Serves, W. R. Cullen, D. J. Thomas. Comparative inhibition of yeast glutathione reductase by arsenicals and arsenothiols. – *Chem. Res. Toxicol*. **10**,1997, 27-33.

59. Valko, M., H, Morris, M. T. Cronin. Metals, toxicity and oxidative stress. – *Curr. Med. Chem.,* **12,** 2005, 1161-1208.

60. Valko, M., K. Jomova, C.J. Rhodes, K. Kuca, K. Musilek. Redox- and non-redox-metal-induced formation of free radicals and their role in human disease. – *Arch. Toxicol.*, **90**, 2016, 1-37.

61. Vaziri, N. D., M. Khan. Interplay of reactive oxygen species and nitric oxide in the pathogenesis of experimental lead-induced hypertension. – *Clin. Exp. Pharmacol. Physiol,*, **34**, 2007, 920-925.

62. Weber, P., F. Cammas, C. Gerard, D. Metzger, P. Chambon, R. Losson, M. Mark. Germ cell expression of the transcriptional co-repressor TIF1beta is required for the maintenance of spermatogenesis in the mouse. – *Development,* **129**, 2002, 2329-2337.

63. Yamanaka, K., H. Hayashi, M. Tachikawa, K. Kato, A. Hasegawa, N. Oku, S. Okada. Metabolic methylation is a possible genotoxicity-enhancing process of inorganic arsenics. – *Mutat. Res.*, **394**, 1997, 95-101.

Institute of Experimental Morphology, Pathology and Anthropology with Museum
Bulgarian Anatomical Society

Acta morphologica et anthropologica, 29 (1-2)
Sofia ● 2022

ANTHROPOLOGY AND ANATOMY 29 (2)

Original Articles

Stunting is Associated with Low Birth Weight Among 3-12 Years Old Boys in Purba Medinipur, West Bengal, India

*Pikli Khanra[1], Kaushik Bose[1], Raja Chakraborty[2]**

[1] Department of Anthropology, Vidyasagar University, Midnapore, West Bengal, India
[2] Department of Anthropology and Tribal Studies, Sidho-Kanho-Birsha University, Purulia, West Bengal, India

*Corresponding author e-mail: rajanth2003@yahoo.co.uk

Stunting is a serious public health issue. It raises the risk of sickness in infancy and childhood. Low- and middle-income nations, notably India, have been battling for years to overcome this major issue, which is also connected to many socioeconomic and biological issues. However, understanding the interaction pattern of undernutrition with these determinants is critical for efficient policies and execution. Stunting (low height-for-age) in newborns and children is a well-known and simple indicator of undernutrition. The current study sought to determine the relationship among stunting, socioeconomic, demographic, and birth-related variables. The research was conducted in the Haldia municipality and Deshopran block (West Bengal, India). The participants were 291 (50.5%) urban and 285 (49.5%) rural boys aged 3-12 years. Stunting was defined as height-for-age 'Z Score' < -2. Overall, 13.88% boys were stunted. Stunting was significantly associated with low birth weight (LBW), controlling for all other significant variables.

Key Words: India, children, stunting, low birth weight

Introduction

Body height or stature is a linear anthropometric measurement influenced by genetic, socioeconomic, demographic and dietary factors in a population [25, 33]. Stunting, defined as low height for age (HAZ), is a well-recognized indicator of linear growth

in children. A child is said to be stunted if the age and sex-specific z-score for height is less than -2 [82]. The state of stunting was suggested to reflect a chronic nutritional deficiency, often connected with socioeconomic and environmental adversities [3]. In 2016, an estimated 144 million children less than five years in low- and middle-income countries (LMIC) were stunted [81]. In India, 38.4% of children were found stunted in the fourth National Family Health Survey (NFHS) 2015-16. In particular, 28% and 34% of children aged less than 5 years in urban and rural areas, respectively, were reportedly stunted in the Indian state of West Bengal [27]. Numerous studies have already reported the prevalence (%) of stunting in India ranging from 10.9 to 55.9 in boys and 18 to 58.4 in girls [1, 12, 17, 46, 62, 71], and in West Bengal [5, 6, 20, 43, 57, 64].

Stunting is considered to be a marker of the underlying processes responsible for poor growth and other adverse outcomes both in early and later life [16]. Stunting at an early stage of development leaves a long-lasting or permanent detrimental effect **on** later life. Stunted children often experience delayed skeletal maturation and usually become short adults and perform sub-optimal functions later in life [45]. Besides, it has long-term consequences **on** cognitive development, learning ability, and productivity during adulthood [16]. It also leads to reduced immune functions and increased susceptibility to infectious diseases. Stunting in childhood was also found to be associated with a higher incidence of non-communicable diseases, such as diabetes, hypertension, heart failure and other cardiovascular diseases during adulthood [10]. Stunted adolescents are often likely to develop overweight and obesity in adulthood [33, 66]. Long-term follow-up studies on children from five low- and middle-income countries, namely Brazil, Guatemala, India, the Philippines, and South Africa, found that childhood stunting was linked to short adult stature, lower lean body mass, less schooling, decreased mental functions, lower-income, and lower birth weight of infants born to women who had been stunted as children [77]. Thus, identifying stunting at an early stage in life could lead to improved population health in the long run.

Mothers' health and nutritional status are closely linked with those of their offspring. Children born to short women were at greater risk of mortality than children having mothers of normal height. Infants born to underweight or stunted women were highly likely to be underweight or stunted. In this way, undernutrition passes from one generation to another like an inherited attribute [55]. Several studies confirmed that poor height attainment due to undernutrition among women of childbearing age had a greater risk of adverse pregnancy outcomes or intrauterine growth retardation in the fetus [8, 77]. Low birth weight (LBW) and preterm birth are associated with short height in mothers [22, 39]. About twenty million infants are born each year with LBW, and many of them are from LMIC [74]. Moreover, the prevalence of stunting has been generally considered irreversible and difficult to reduce in a recurrent process. In childhood, women who were themselves stunted tend to have stunted offspring, creating an inter-generational cycle of poverty and reduced human capital [58]. The associations between poor socioeconomic, demographic and environmental conditions and chronic nutritional deficiencies are currently well known [9, 12, 35, 36, 46, 62, 65, 71]. Increased risk of stunting has been associated with both poor socioeconomic conditions and early exposure to adverse conditions, such as illness and inappropriate feeding practices [36, 70]. The results of a large survey from India revealed that undernutrition (indicated by anthropometry) was associated with birth-order, duration

of breastfeeding, place of delivery of the child, wealth index of the household, mother's BMI and mother's education in both urban and rural areas [34].

Apart from all those factors as described above, the phenomenon of undernutrition may also have genetic mechanisms [18]. Stunting is a derivative of height, and the latter also has a strong heritability component [44]. It was recently claimed that stunting might not always be, or in every context, should be equated with undernourishment in children [67], indicating that stunting might have causal factors other than those responsible for undernourishment, in general. With the same dataset used in the present study, it was already recently reported that low levels of mothers' education in rural areas and lower family income with poor housing in urban areas were associated with a higher prevalence of undernourished children [35, 36]. Therefore, the present study aimed to re-assess the roles of socioeconomic and demographic factors, the already known contributors of stunting, maternal nutritional status, and birth-related factors, particularly birth weight. We hypothesized that factors, such as birth weight, shall have a significant effect relative to all other probable factors in predicting the prevalence of stunting among boys aged 3-12 years.

Materials and Methods

Participants and settings

This cross-sectional study was conducted between December 2014 and April 2016 in selected areas under Haldia Municipality and Deshopran Block (rural) areas of Purba Medinipur district of West Bengal state, India. Among the 615 (urban: 307; rural: 308) participants of the study, 576 (93.7%) provided complete information. Out of them, 291 (50.5%) were urban, and 285 (49.5%) were rural boys aged between 3 and 12 years. In the public education system of the state, children begin to attend the care centers to receive a mid-day meal and some pre-nursery type education approximately around 3 years of age. On the other hand, since the study was intended to restrict within the preadolescent stage of the boys, the upper age was restricted to 12 years. A detailed description of the sample recruitment procedure was described elsewhere [35, 36]. Data were collected from one rural and one urban area of Purba Medinipur District (PMD). The rural boys were recruited from three villages, namely Kultalia, Sikdarchak and Uttar Amtalia, under Desopran Block of Contai Subdivision of PMD and the urban boys from three settlement colonies (CPT, IOC and HREL) and Rairarchak area under Haldia Municipality. The study abode by the ethical guidelines as per Helsinki Declaration, 2000 [72].

Demographic, socioeconomic and birth-related information

Demographic, socioeconomic, maternal health and childbirth-related data were collected directly from the parents, in most cases, from mothers, through a structured questionnaire. The information included social category (general- or scheduled caste), place of residence (urban or rural), number of family members, numbers of elder- and/or younger sisters and brothers, number of living rooms, house ownership, family income, parental education, type of cooking fuel and dirking water facility. Information regarding mother's age at child birth, place of delivery, birth weight, duration of breast

feeding and infant's age during the introduction of supplementary feeding were also recorded. Information about birth weight and the age of introducing supplementary food was obtained from the mothers. Low birth weight was defined as < 2500g of body weight of newborns [80].

Anthropometry

One researcher (PK) recorded all anthropometric measurements from all children. Height (cm) was measured for each child to the nearest millimeter, following standard procedure [42]. Prior to the commencement of the main survey, one researcher (PK) measured 30 individuals for standardization of protocol. The intra-individual technical errors of measurements were computed [73] and found within the acceptable limits, and thus, not incorporated in analyses of the main data set. Height-for-age 'Z Score' (HAZ) was computed to identify stunting among the children. The Z-Scores were derived using the WHO Anthro 3.2.2 and Anthro Plus 1.0.4 software. Stunting was defined as HAZ less than -2 [82].

Statistics

Percentages were used to report the distribution of the population according to categories of different variables. Mean and standard deviation (SD) statistics were used to describe continuous variables. Binary logistic regression (BLR) analyses (univariate model) were performed for each independent factor to assess whether it is significantly associated with stunting. In each BLR, odds ratio (OR) with 95% confidence interval (CI) was calculated to show the magnitude of association of a particular category of a predictor with stunting relative to the other category of the variables. Factors significantly associated in the bivariate analyses were further included in stepwise multivariate logistic regression analyses (enter method) to estimate their effects relative to each other and to identify the most effective predictor variables, if any. In all regression analyses, the dependent/outcome variable, namely, stunting was coded as 1 for 'stunted' and 0 for 'non-stunted'. The predictor variables in the present study were categorized as follow: social category (general or scheduled castes), place of residence (urban or rural), family size (≤5 or >5 members), Number of elder siblings or younger siblings (Nil vs. either or both present), number of living rooms (≤2 or >2 rooms), house ownership (own or rental), monthly family income per capita (≤2000 or >2000), parental education (both above secondary level or not), type of cooking fuel (smoky or smokeless), dirking water facility (tube well or municipal supply), mother's age at childbirth (≤20- or >20 years), place of delivery (institutional vs. home), birth weight (<2500gm vs. ≥ 2500gm), duration of breastfeeding (≤2 or >2 years) and infant's age on the introduction of supplementary feeding (≤ 6- or > 6 months). For each of these predictors, the superior alternatives (such as, smokeless fuel) or the higher values (such as birth weight ≥ 2500gm), were coded '0', whereas the respective poorer conditions or qualities (such as smoky fuel) or the lower values (such as birth weight ≥ 2500gm), were coded '1', respectively.

Family size, number of living rooms, number of younger and elder sisters and brothers, duration of breastfeeding and parity data were categorized on the basis cut off based on respective 50th percentiles. Mother's age at childbirth, birth weight and place of delivery and date of birth were confirmed from the vaccination record. Duration

of breastfeeding, the introduction of supplementary food and birth weight data were classified following appropriate guidelines [80]. Mother's nutritional status was determined using body mass index (BMI) calculated as weight in kilograms divided by height in meters squared (kg/m^2). Based on BMI values, the nutritional status of the mother were classified as undernourished (BMI <18.5 kg/m^2) or normal (>18.5 kg/m^2). A p-value of <0.05 is considered to be statistically significant. All statistical analyses were performed through SPSS-16 software.

Results

The overall prevalence of stunting among the boys in this study was 13.9%. **Tables 1 and 2** present the percent distribution of the participants according to categories of all independent factors as well as the significance of the association of each of these factors with stunting through the results of univariate BLR analyses. The results of BLR indicated that the risk of stunting was significantly higher (ORs = 2.53, $p<0.05$) among the boys whose parents were less educated. Poor household income was also significantly associated with a higher prevalence of stunting (ORs = 2.02, $p<0.05$). Boys who were very low weight at birth were significantly (ORs= 2.70, $p<0.01$) more likely to be stunted. Boys who had younger sisters and brothers were significantly (ORs=1.61, $p<0.05$) more likely to be stunted. Boys delivered at home were more likely to be stunted than those delivered at health institutions (ORs= 2.03, $p<0.01$). The risk of stunting was also found to be significantly (ORs=1.60, $p<0.05$) higher among boys whose mothers had less than 149.2cm height.

Table 3 presents the results of multivariate BLR analysis to identify independent risk factors predicting stunting. Boys who were low weight at birth were significantly ($p<0.005$) more likely to be stunted than boys who had a normal or healthy weight, independent of all other potential predictors. Other factors that show a significant effect on the prevalence of stunting in univariate BLR analyses did not reveal a significant impact in multivariate BLR analysis.

Discussion

The present study showed a significant association of stunting with parental education and family income when their effects were assessed separately. No other socio-demographic characteristic showed a statistically significant association. In contrast to their higher levels, lower parental income and educational levels were associated with a higher prevalence of stunting, respectively. However, this trend was not very surprising, since the previous studies, based on the same data set showed that mothers' education level in rural children, and the family economic condition in the urban counterpart, were the most important independent determinants of undernutrition among these 3-12 years old children [35, 36]. However, these studies used a composite index of anthropometric failure (CIAF), but not stunting, as the measure of undernourishment. Numerous previous researches showed that various measures of socioeconomic status, such as income, educational level and family assets, were associated with nutritional status in children [50, 52, 77]. The independent importance of both education and

Table 1. Frequency distribution and factors associated (binary logistic regression) with stunting among respondents by different socioeconomic and demographic characteristics

Variables	Categories	Total	(%)	Prevalence of stunting	B	Wald	p	OR	95 % CI for OR	
				N (%)					Lower	Upper
Place of residence	Urban®	291	50.5	45 (15.5)				1		
	Rural	285	49.5	35 (12.3)	-0.27	1.21	0.27	0.76	0.47	1.23
Social category	General®	389	67.5	56 (14.4)				1		
	Reserved	187	32.5	24 (12.8)	-0.13	0.25	0.61	0.87	0.52	1.46
Parental education	Both ≥ secondary*	117	20.3	8 (6.8)				1		
	Both < secondary	459	79.7	72 (15.7)	0.93	5.74	0.01	2.53	1.18	5.42
Family size	≤ 5 members*	418	72.6	61 (15.6)				1		
	> 5 members	158	27.4	19 (12.0)	-0.22	0.63	0.42	0.8	0.46	1.38
House ownership	Own*	458	79.5	62 (13.5)				1		
	Rental	118	20.5	18 (15.2)	0.14	0.23	0.63	1.15	0.65	2.03
Number of living rooms	> 2 rooms*	128	22.2	14 (10.9)				1		
	≤ 2 rooms	448	77.8	66 (14.7)	0.34	1.19	0.27	1.4	0.76	2.59
Cooking fuel type	Smokeless*	273	47.4	40 (14.6)				1		
	Smoky	303	52.6	40 (13.2)	-0.12	0.25	0.61	0.88	0.55	1.42
Drinking water	Tube well*	425	73.8	60 (14.1)				1		
	Tap	151	26.2	20 (13.2)	-0.07	0.07	0.79	0.92	0.54	1.6
Per capita income	Rs.>2000*	279	48.4	27 (9.7)				1		
	Rs. ≤2000	297	51.6	53 (17.8)	0.71	7.8	0.01	2.02	1.23	3.33
Per capita expenditure	Rs.>1750*	280	48.6	28 (10.0)				1		
	Rs.≤1750	296	51.4	52 (17.6)	0.65	6.73	0.01	1.92	1.17	3.13

® – reference category; CI – confidence interval, Binary logistic regression analysis (univariate model) considering effect of one predictor variables

Table 2. Frequency distribution and factors associated (binary logistic regression) with stunting among respondents by child and maternal issues

Variables	Categories	Total	(%)	Prevalence of stunting	B	Wald	p	OR	95.0% CI for OR	
				N (%)					Lower	Upper
Weight at birth	2500 & above*	518	89.9	64 (12.3)				1		
	<2500	58	10.1	16 (27.6)	0.93	9.49	0.01	2.7	1.43	5.08
Elder sisters & brothers	None*	337	58.5	46 (13.6)				1		
	Either or both	239	41.5	34 (14.2)	0.05	0.04	0.84	1.05	0.65	1.69
Younger sisters & brothers	None*	373	64.8	44 (11.8)				1		
	Either or both	203	35.2	36 (17.7)	0.48	3.83	0.05	1.61	0.99	2.6
Birth order	1st*	342	59.4	46 (13.4)				1		
	≥ 2nd	234	40.6	34 (14.5)	0.09	0.13	0.71	1.09	0.67	1.76
Mother age at child birth	≥ 20 years*	362	62.8	43 (11.9)				1		
	<20 years	214	37.2	37 (17.3)	0.44	3.26	0.07	1.55	0.96	2.49
Place of delivery	Institutional*	346	60.1	36 (10.4)				1		
	Home	230	39.9	44 (19.1)	0.71	8.56	0.01	2.03	1.26	3.28
Mothers' nutritional status	Normal*	520	90.3	74 (14.2)				1		
	Undernourished	56	9.7	6 (10.7)	0.32	0.52	0.47	0.72	0.29	1.74
Mothers' height	≥149.2cm*	288	50	32 (11.1)				1		
	<149.2cm	288	50	48 (16.7)	0.47	3.67	0.05	1.6	0.98	2.58
Period of breast feeding	≥ 2 years*	306	53.1	44 (14.4)				1		
	< 2 years	270	46.9	36 (13.3)	0.09	0.13	0.72	0.92	0.57	1.47
Introduction of supplementary food	≤ 6 months*	456	79.2	65 (14.2)				1		
	> 6 months	120	20.8	15 (12.5)	0.15	0.24	0.62	0.86	0.47	1.57

*Reference category; CI – confidence interval; Binary logistic regression analysis (univariate model) considering effect of one predictor variable

Table 3. Results of a multivariate logistic regression model (enter method) to predict stunting

Variables	B	Wald	p	OR	95.0% CI for OR	
					Lower	Upper
Parental education	0.546	1.547	0.21	1.727	0.73	4.08
Per capita income	0.42	1.099	0.294	1.51	0.699	3.263
Younger sisters and brothers	0.84	0.97	0.755	1.087	0.643	1.839
Weight at birth	0.947	7.856	0.005	2.579	1.33	5.003
Place of delivery	0.385	2.045	0.153	1.47	0.867	2.493
Mother height	0.318	1.567	0.211	1.375	0.35	2.262

CI – confidence interval

economic condition of the family for healthy growth of children were revealed in numerous previous studies, especially from low and middle-income countries [13, 32, 54, 57, 78]. There are plenty of evidence showing a positive association between low income and prevalence of stunting [31, 33, 37, 51, 57]. Therefore, improvement of the economic condition along with education seemed to be an effective measure to reduce child undernutrition, including stunting.

Similar to income and parental education, lower birth weight and birth at home, rather than in institutional health facilities, also showed association with higher chances of being stunted among the 3-12 years old boys in the present study. It is, however, worth mentioning that having one or more younger siblings and low mother's height was also very close to be significantly associated with stunting (Wald: 3.83 and 3.67, respectively, both p=0.05). Researchers have reported that the risk of stunting was higher among children born underweight. In this study, the direction of a relationship between birth weight and childhood undernutrition was in line with the results of other studies that showed that low birth weight had a significant higher risk of stunting in childhood [53, 60]. As mentioned above, the present study also revealed a close linkage between stunting and having younger brothers and sisters. This could, however, be the result of relatively increased attention towards the younger children by the parents in a resource-constrained setting, particularly in terms of food distribution and health care. Indeed, previous studies in similar populations in the same Indian state showed that a higher risk of stunting was associated with the presence of younger sisters and brothers [7, 51]. Place of delivery was a significant predictor of stunting in the present study, as also was reported in another study in Malawi [12]. In the present study, the relatively short mothers (<149.2 cm) had more stunted boys, although this association was not statistically significant, although closely to be. Studies identified mother's height to be closely linked with birth weight and length of offspring [84]. Evidence showed that maternal malnutrition was a risk for survival, health, and development among the offspring and may create an intergenerational cycle of malnutrition in the future where a stunted female child would become a stunted mother and would, in turn, deliver another stunted child [19].

However, all the above associations disappeared in the multiple regression analyses, whereas only the birth weight showed a significant independent association with the prevalence of stunting, allowing for all other potential factors. Boys with lower birth weight showed higher chances of being stunted at 3-12 years. Even family income or parental education did not qualify for a significant statistical effect on the stunting prevalence, as shown in our previous studies with the same data set, in rural and urban counterparts, respectively [35, 36]. In a study in Indonesia, LBW was the major predictor of stunting among infants aged 12-23 months. LBW infants showed 1.74 times higher likelihood to be stunted (95% CI 1.38-2.19) compared to those born with normal weight [4]. In the pre-school children in Bangladesh, birth size was one of the important determinants of stunting [59]. Another study from Zimbabwe showed decreased growth in LBW babies than normal-weight babies, and significant length differences appeared at 12 months of age [47]. The major factors responsible for undernutrition in under-five children in Pakistan were size at birth, previous birth interval, mothers' BMI at birth and parental education [61]. In the present study, mothers' nutritional status (BMI) was not associated with stunting.

LBW and stunting together were held responsible for more than two million deaths and ninety million disability-adjusted life years or DALYs [41]. India alone suffered 0.6 million deaths and 24.6 million DALYs from countries across the world due to stunting and IUGR/LBW [41]. LBW can result from preterm delivery or intrauterine growth restriction (IUGR) or a combination of the two. The global prevalence of LBW is 15.5%, which means that about 20.6 million infants with LBW are born each year, 96.5% of them in developing countries [79]. Globally, 14.6 percent of babies were born with low birth weight out of 20.5 million new born in 2015 [75]. India alone, with an estimated 33% of all newborns weighing < 2500g at birth, contributed 40% of the world's LBW population [30]. The prevalence of low birth weight in India was 21.4% in 2017 [29]. As per NFHS-3, the prevalence of LBW in West Bengal was 22% [28]. The causes of LBW are numerous and multifaceted. It depends on complex interactions of numerous factors like genetic, reproductive, socio-demographic, cultural, political and surrounding physical environmental conditions [3] and regional factors [46, 56, 71]. The etiology of LBW is maximally related to maternal [14, 15, 21, 26, 63], and socioeconomic and psychological factors [2, 69, 49]. Stunting is generally regarded as an expression of chronic deprivation from nutritional requirements at the population level. To determine the state of stunting, the importance of birth weight is independent of other important determinants. This indicates that improvement of maternal health and obstetric care, and socioeconomic development might improve the nutritional health of children. It might also have a long-term impression extended to adulthood. The observed correlations and linear associations between birth size and adult height have been consistent in several studies, although from the high-income countries [38, 40, 76].

Undoubtedly, undernourishment occurs from food deprivation or due to a diet deficiency in essential nutrients. Growing children starkly exhibit its consequences. Stunting is widely regarded as one of the efficient proxy measures of chronic undernutrition in children. However, there is adequate debate in recent times over the unquestionable acceptance of short stature, particularly in children, as a perfect proxy to undernourishment [67]. There are also evidence indicating that nutritional interventions did not always improve relative body size in children in terms of stature [22], or if at all, with a small effect size [48]. Even stunting or small stature in children

often poorly correlate with other anthropometric measures of nutritional/energy stores in the body [24, 67, 68]. Keeping in view these lines of arguments and recent evidence, including the present one, it appears that stunting (short stature) is not essentially a product of undernutrition. Maternal and prenatal health and nutritional conditions also influence body height in childhood through the size at birth.

The WHO has set a goal of reducing LBW and stunted children aged 5 years by 40% between 2010 to 2025 [83]. However, to fulfil this sacred ambition, further extensive studies, preferably with longitudinal designs in varied ecological contrasts, might assess the appropriateness of stature as a measure of undernourishment in children, especially in India. It was earlier proposed that the small size could adapt to unique mother-child ecology in a chronically resource-constrained situation rather than a clinical condition [11].

The study has some inherent limitations. As this study included only boys, the impact of birth weight in girls, allowing for socioeconomic factors that might have different impacts on two genders, is worth investigating in further studies. The current investigation also lacked detailed information on food intake and the composition of the diet and no information on the physical exercise pattern. However, if supported by some further evidence from similar populations, the results of this study could have direct policy implications in terms of interventions to reduce the burden of undernutrition in Indian children.

Conclusion

In this study, stunting in school going boys aged 3-12 years in Purba Medinipur district of West Bengal was significantly associated with LBW. Among the potential factors, LBW was the most dominant concomitant of stunting. Programmes for the reduction of stunting should focus on the socioeconomic improvement, particularly, on spreading education, and on the health of women, particularly before and during pregnancy.

Acknowledgement: All participants and their parents are sincerely acknowledged for allowing for data collection. Block Development Officer and Child Development Programme Officer of Desopran Block are also gratefully acknowledged for giving their permissions.

Authors' contributions: PK collected and analyzed the data and prepared the draft manuscript. KB designed and supervised the study, analyzed the data and provided intellectual inputs to the manuscript. RC designed the study and prepared the final manuscript.

References

1. Abbasi, S., H. Mahmood, A. Zaman, Z. D. Farooq, A. Mallk, Z. Saga. Indicators of malnutrition in under 5 Pakistani children: A DHS data secondary analysis. – *J. Med. Res. Health Edu.*, **2**(3), 2018, 1-10.

2. Agarwal, G., S. Ahmad, K. Goel, V. Kumar, P. Goel, M. Garg, A. Punj. Maternal risk factors associated with low birth weight neonates in a Tertiary care hospital, Northern India. – *J. Commut. Med. Health Educ.*, **2**(09), 2012, 177.

3. Aries, M., H. Hardinsyah, H. Tuhiman, Determinants of underweight and stunting on children aged 0-36 month based on conditional cash transfer family program (CCTFP) 2007. – J. *Food Nutr. Res.,* **7**(1), 2012, 19-26.

4. Aryastami, N. K., A. Shankar, N. Kusumawardani, B. Besral, A. B. Jahari, E. Achadi. Low birth weight was the most dominant predictor associated with stunting among children aged 12–23 months in Indonesia. – *BMC Nutr*., **3**(16), 2017, 1-6.
5. Bisai, S., C. Mallick. Prevalence of undernutrition among Kora-Mudi children aged 2-13 years in Paschim Medinipur District, West Bengal, India. – *World J. Clin. Pediatr.* **7**(1), 2010, 31-36.
6. Bisai, S., K. Bose, A. Ghosh. Prevalence of undernutrition of Lodha children aged 1-14 years of Paschim Medinipur District, West Bengal, India. – *Iran. J. Pediatr.,* **18**(4), 2008, 323-329.
7. Biswas, S., S. Koziel, R. Chakraborty, K. Bose. Sibling composition and household room sharing are associated with menarcheal status among rural Bengalee girls of West Bengal, India. – *Hum. Biol.*, **85**(4), 2013, 607-618.
8. Blossner, M., M. De, Onis, A. Pruss-Ustun. Malnutrition: quantifying the health impact at national and local levels, 2005, World Health Organization.
9. Bogale, B., B. T. Gutema, Y. Chisha. Prevalence of stunting and its associated factors among children of 6-59 months in Arba Minch health and demographic surveillance site (HDSS), Southern Ethiopia: A community-based cross-sectional study. – *J. Environ. Public Health*, 2020, 1-8.
10. Bryce, J., D. Coitinho, I. Darnton-Hill, D. Pelletier, P. Pinstrup-Andersen. Maternal and child undernutrition: effective action at national level. – *The Lancet*, **371**(9611), 2008, 510-526.
11. Chakraborty, R., K. Bose. Defining malnutrition in India: how much is too little, how much is too much? – *Curr. Sci.*, **106**(5), 2014, 670-672.
12. Chirande, L., D. Charwe, H. Mbwana, R. Victor, S. Kimboka, A. I. Issaka, S. K. Baines, M. J. Dibley, K. E. Agho. Determinants of stunting and severe stunting among under-fives in Tanzania: evidence from the 2010 cross-sectional household survey. – *BMC Pediatr.*, **15**(1), 2015, 1-13.
13. Cruz, L. P. G., G. G. Azpeitia, D. R. Suarez, A. S. Rodriguez, J. L. Ferrer, L. Serra-Majem. Factors associated with stunting among children aged 0 to 59 months from the central region of Mozambique. – *Nutrients*, **9**(491), 2017, 1-16.
14. Dasgupta, A., R. Basu. Determinants of low birth weight in a block of Hooghly, West Bengal: a multivariate analysis. – *Int. J. Biol. Med. Res.*, **2**(4), 2011, 838–842.
15. Demelash, H., A. Motbainor, D. Nigatu, K. Gashaw, A. Melese. Risk factors for low birth weight in Bale zone hospitals, South-East Ethiopia: a case-control study. – *BMC Pregnancy Childbirth*, **15**(1), 2015, 264–274.
16. Dewey, K. G., K. Begum, Long-term consequences of stunting in early life. – *Matern. Child Nutr*., **7**(3), 2011, 5–18.
17. Dubey, P. K., N. Tiwari, R. P. Jha. Regional disparity in nutritional status in India: An examination. – *Int. J. Health Sci. Res*., **8**(6), 2018, 249-258.
18. Duggal. P., W. A. Petri. Does malnutrition have a genetic component? – *Annu. Rev. Genom. Hum. Genet*., **19**(1), 2018, 247-262.
19. Felisbino-Mendes, M. S., E. Villamor, M. G. Velasquez, I. Vikbladh, O. Saxtrup. Association of maternal and child nutritional status in Brazil: A population based cross-sectional study. – *PLoS ONE*, **9**(1), 2014, e87486.
20. Giri, S. P., S. Biswas, K. Bose. Prevalence of undernutrition among Bengalee preschool children of Sundarban South 24 Parganas, West Bengal, India. – *Human Biology Review*, **6**(4), 2017, 284-300.
21. Golestan, M., K. S. Akhavan, R. Fallah. Prevalence and risk factors for low birth weight in Yazd, Iran. – *Singapore Med. J.*, **52**(10), 2011, 730-733.
22. Goudet, S., P. Griffiths, B. Bogin, N. Madise. Interventions to tackle malnutrition and its risk factors in children living in slums: a scoping review. – *Ann. Hum. Biol.*, **44**(1), 2017, 1-10.

23. Han, Z., O. Lutsiv, S. Mulla, S. D. McDonald. Maternal height and the risk of preterm birth and low birth weight: A systematic review and meta-analyses. – *J. Obstet. Gynaecol. Can.*, **34**(8), 2012, 721-746.
24. Hermanussen, M., J. M. Wit. How much nutrition for how much growth? – *Horm. Res. Paediatr.*, **88**(1), 2017, 38–45.
25. Herrador, Z., L. Sordo, E. Gadisa, J. Moreno, J. Nieto, A. Benito, A. Aseffa, C. Cañavate, E. Custodio. Cross-sectional study of malnutrition and associated factors among school aged children in rural and urban settings of Fogera and Libo Kemkem Districts, Ethiopia. – *PLoS ONE.*, **9**(9), 2014, p.e105880.
26. Hossain, N., N. Khan, N. H. Khan. Obstetric causes of stillbirth at low socioeconomic settings. – *J. Pak. Med. Assoc.*, **59**(11), 2009, 744-747.
27. International Institute for Population Sciences (IIPS). National family health survey (NFHS 4) 2015-2016. 2017, Mumbai: IIPS.
28. International Institute for Population Sciences (IIPS). National family health survey (NFHS 3) 2005-2006. 2008, Mumbai: IIPS.
29. Indian Council of Medical Research (ICMR). *Media report "release of India state-level malnutrtion" department of health research* – Ministry of health & family welfare government of India. 2019
30. Jain, V., A. Singhal. Catch up growth in low birth weight infants: Striking a healthy balance. – *Rev. Endocr. Metab. Disord.*, **13**(2), 2012, 141–147.
31. Katoch, O. R., A. Sharma. Prevalence and determinants of underweight: A study on school-going children of farming households in rural areas of district Doda, Jammu & Kashmir, India. – *Int. J. Recent Sci. Res.*, **8**(6), 2016, 17360-17363.
32. Kavosi, E., Z. H. Rostami, A. Nasihatkon, M. Moghadami, M. Heidari. Prevalence and determinants of under-nutrition among children under six: A cross-sectional survey in Fars Province, Iran. – *Int. J. Health Policy Manag*., **3**(2), 2014, 71-76.
33. Keino, S., G. Plasqui, G. Ettyang, B. van den Borne. Determinants of stunting and overweight among young children and adolescents in sub-Saharan Africa. – *Food Nutr. Bull.,* **35**(2), 2014, 167-178.
34. Khan, R. E. A., M. A. Raza. Child malnutrition in developing economies: a case study of Bangladesh. – *Qual Quant*, **48**(3), 2014, 1389–1408.
35. Khanra, P., K. Bose, R. Chakraborty. Mother's education level is associated with anthropometric failure among 3- to 12-year-old rural children in Purba Medinipur, West Bengal, India. – *J. Biosoc. Sci.,* **53**(6), 2021, 856-867.
36. Khanra, P., R. Chakraborty, K. Bose. Factors affecting anthropometric failure in urban Bengalee children of Purba Medinipur, West Bengal, India. – *Human Biology Review*, **9**(4), 2020, 309-327.
37. Kirk, A., T. Kilic, C. Carletto. Composition of household income and child nutrition outcomes evidence from Uganda. – *World Dev.*, **109**(2018), 2018, 452-469.
38. Knight, B., B. M. Shields, M. Turner, R. J. Powell, C. S. Yajnik, A. T. Hattersley. Evidence of genetic regulation of fetal longitudinal growth. – *Early Hum. Dev.*, **81**(10), 2005, 823-831.
39. Kozuki, N., J. Katz, A. C. C. Lee, J. P. Vogel, M. F. Silveira, A. Sania, G. A. Stevens, S. Cousens, L. E. Caulfield, P. Christian, L. Huybregts, D. Roberfroid, C, Schmiegelow, L. S. Adair, F. C. Barros, M. Cowan, W. Fawzi, P. Kolsteren, M. Merialdi, A. Mongkolchati. Short maternal stature increases risk of small-for-gestational-age and preterm births in low- and middle-income countries: Individual participant data meta-analysis and population attributable fraction. – *J. Nutr.*, **145**(11), 2015, 2542-2550.
40. Kuh, D., M. Wadsworth. Parental height: childhood environment and subsequent adult height in a national birth cohort. – *Int. J. Epidemiol.*, **18**(3), 1989, 663-668.

41. Kumar, B. P. R., S. R. Dudala, A. R. Rao. Kuppuswamy's socioeconomic status scale – a revision of economic parameter for 2012. – *Int. J. Res. Dev.,* **1**(1), 2013, 2-4.
42. Lohman, T. G., A. F. Roche, R. Martorell, *Anthropometric standardization reference manual*. 1988, Chicago, IL Human Kinetics Books.
43. Mandal, S., J. Pal, R. Parthasarathi, R. Biswas, Vr. Prabhakar. An assessment of nutritional status of children aged 0-14 years in a slum area of Kolkata. – *Int. J. Public Health*, **4**(2), 2014, 159-162.
44. Marouli, E., M. Graff, C. Medina-Gomez, K. S. Lo, A. R. Wood, T. R. Kjaer, R. S., Fine, Y. Lu, C. Schurmann, H. M. Highland, S. Rueger, G. Thorleifsson, A. E. Justice, D. Lamparter, K. E. Stirrups, V. Turcot, K. L. Young, T. W. Winkler, T. Esko, T. Karaderi. Rare and low-frequency coding variants alter human adult height. – *Nature*, **542**(7640), 2017, 186-190.
45. Martorell, R., L. K. Khan, D. G. Schroeder, Reversibility of stunting: epidemiological findings in children from developing countries. – *Eur. J. Clin. Nutr.*, **48** (Suppl.), 1994, S45-S57.
46. Mazengia, A. L., G. A. Biks, Predictors of stunting among school-age-children in Northwestern Ethiopia. – *J. Nutr. Metab*., Article ID 7521751, 2018, 1-7.
47. Mbuya, M. N. N., M. Chidem, B. Chasekwa, V. Mishra, V. *Biological, social, and environmental determinants of low birth weight and stunting among infants and young children in Zimbabwe*. Zimbabwe Working Papers, No.7. Calverton, Maryland, 2010, USA: ICF Macro.
48. McGregor, G. S. M., L. C. H. Fernald, R. M. C. Kagawa, S. Walker. Effects of integrated child development and nutrition interventions on child development and nutritional status. – *Ann. N. Y. Acad. Sci.*, **1308**(1), 2014, 11-32.
49. Meshram, I., M. Rao, C. Reddy, M. Ravindranath, S. Kumar, K. Sreerama, H. Kumar, R. Venkaiah, A. Laxmaiah, A. Prevalence of under nutrition and its predictors among under 5 year children in Surat Region, Gujarat, India. – *J. Clin. Nutr. Dietetics*, **02**(01), 2016, 1-12.
50. Mohammed, F. A., H. F. Farhood, M. Abdul-AtheemWtwt. Prediction of malnutrition using modified subjective global assessment-dialysis malnutrition score in patients on chronic hemodialysis. – *J. Commut. Med. Health Educ.*, **04**(03), 2014, 1000291.
51. Mondal, N., B. Basumatary, J. Kropi, K. Bose. Prevalence of double burden of malnutrition among urban school going bodo children aged 5-11 years of Assam, Northeast India. – *Epidemiol. Biostat. Public Health*, **12**(4), 2015, e11497.
52. Nguyen, P. H., R. Avula, M. T. Ruel, K. K. Saha, D. Ali, L. M. Tran, E. A. Frongillo, P. Menon, R. Rawat. Maternal and child dietary diversity are associated in Bangladesh, Vietnam, and Ethiopia. – *J. Nutr*., **143**(7), 2013, 1176-1183.
53. Ntenda, P. A .M., Y. C. Chuang. Analysis of individual-level and community-level effects on childhood undernutrition in Malawi. – *Pediatr. Neonatol.*, **59**(4), 2018, 380-389.
54. Owoaje, E., O. Onifade, A. Desmennu. Family and socioeconomic risk factors for undernutrition among children aged 6 to 23 months in Ibadan, Nigeria. – Pan. Afr. Med. J., **17**(161), 2014, 1-7.
55. Ozaltin, E., K. Hill, S. V. Subramanian. Association of maternal stature with offspring mortality, underweight, and stunting in low- to middle-income countries. – *JAMA*, **303**, 2010, 1507–1516.
56. Pal, A., S. Manna, P. C. Dhara. Comparison between the motor function of school-aged children with normal birth weight and children with low birth weight: a cross-sectional study. – *Turk. J. Pediatr.*, **61**(3), 2019, 374-385.
57. Pal, A., A. K. Pari, A. Sinha, P. C. Dhara. Prevalence of undernutrition and associated factors: A cross-sectional study among rural adolescents in West Bengal, India. – *Int. J. Pediatr. Adolesc. Med.*, **4**(1), 2017, 9-18.

58. Prendergast, A. J., J. H. Humphrey. The stunting syndrome in developing countries. – *Paediatr. Int. Child Health*., **34**(4), 2014, 250-265.
59. Rahman, A., S. Chowdhury. Determinants of chronic malnutrition among preschool children in Bangladesh. – *J. Biosoc. Sci.*, **39**(2), 2007, 161-173.
60. Rahman, M. S., T. Howlader, M. S. Masud, M. L. Rahman. Association of low-birth weight with malnutrition in children under five years in Bangladesh: Do mother's education, socioeconomic status, and birth interval matter? – *PLoS ONE*, **11**(6), 2016, e0157814.
61. Rayhan, Md. I., M. S. H. Khan. Factors causing malnutrition among under five children in Bangladesh. – *Pak. J. Nutr.*, **5**(6), 2006, 558-562.
62. Rengma, S. M., K. Bose, N. Mondal. Socioeconomic and demographic correlates of stunting among adolescents of Assam, North- east India. – *Anthropol. Rev.*, **79**(4), 2016, 409-425.
63. Sachin, S. M., M. Girish, D. Rajesh, Y. Surekha, K. T. Madhav, P. Kiran. Maternal risk factors associated with term low birth weight neonates: a matched-pair case control study. – *Indian Pediatr.,* **49**, 2012, 25-28.
64. Sarkar, S. Cross-sectional study of child malnutrition and associated risk factors among children aged under five in West Bengal, India. – *Int. J. Popul. Stud.*, **2**(1), 2016, 89-101.
65. Sarma, H., J. R. Khan, M. Asaduzzaman, F. Uddin, S. Tarannum, Md. M. Hasan, A. S. Rahman, T. Ahmed. Factors influencing the prevalence of stunting among children aged below five years in Bangladesh. – *Food Nutr. Bull.*, **38**(3), 2017, 291-301.
66. Savanur, M. S., P. S. Ghugre. BMI, body fat and waist-to-height ratio of stunted v. non-stunted Indian children: a case–control study. – *Public Health Nutr*., **19**(8), 2016, 1389-1396.
67. Scheffler, C., M. Hermanussen, B. Bogin, D. S. Liana, F. Taolin, P. M. V. P. Cempaka, M. Irawan, L. F. Ibbibah, N. K. Mappapa, M. K. E. Payong, A. V. Homalessy, A. Takalapeta, S. Apriyanti, M. G. Manoeroe, F. R. Dupe, R. R. K. Ratri, S. Y. K. P. V. Touw, B. J. Murtani, R. Nunuhitu. Stunting is not a synonym of malnutrition. – *Eur. J. Clin. Nutr.*, **74**(3), 2019, 377-386.
68. Scheffler, C., L. M. Krutzfeldt, P. Dasgupta, M. Hermanussen, M. No association between fat tissue and height in 5019 children and adolescents, measured between 1982 and 2011 in Kolkata/India. – *Anthropol. Anz*, **74**(5), 2018, 403-411.
69. Siza, J. E. Risk factors associated with low birth weight of neonates among pregnant women attending a referral hospital in northern Tanzania. – *Tanzan. J. Health Res.*, **10**(1), 2008, 5-8.
70. Soekatri, M. Y. E., S. Sandjaja, A. Syauqy. Stunting was associated with reported morbidity, parental education and socioeconomic status in 0.5-12-year-old Indonesian children. – *Int. J. Environ. Res. Public Health*, **17**(17), 2021, 6204.
71. Titaley, C. R., I. Ariawan, D. Hapsari, A. Muasyaroh, M. J. Dibley. Determinants of the stunting of children under two years old in Indonesia: A multilevel analysis of the 2013 Indonesia basic health survey. – *Nutrients*, **11**(5), 2019, 1106-1119.
72.. Touitou, Y., F. Portaluppi, M. H. Smolensky, I. Rensing, L. Ethical principles and standards for the conduct of human and animal biological rhythm research. – *Chronobiol. Int.*, **21**(1), 2004, 161-170.
73. Ulijaszek, S. J., D. A. Kerr. Anthropometric measurement error and the assessment of nutritional status. Br J Nutr 1999; 82:165-77.
74. UNICEF, WHO. *Low Birth weight: Country, regional and global estimates*, 2004, New York.
75. UNICEF-WHO. *Low birth weight estimates,* 2019. Available at: https://data.unicef.org/topic/nutrition/low-birthweight/pdf

76. Utami, N. H., I. R. Rachmalina, A. Irawati, K. Sari, B. C. Rosha, N. Amaliah, M. Besral. Short birth length, low birth weight and maternal short stature are dominant risks of stunting among children aged 0-23 months: Evidence from Bogor longitudinal study on child growth and development. – *Indones. J. Hum. Nutr.*, **24**(1), 2018, 11-23.

77. Victora, C. G., L. Adair, C. Fall, P. C., Hallal, R. Martorell, L. Richter, H. S. Sachdev. Maternal and child undernutrition: consequences for adult health and human capital. – *The Lancet*, **371**(9609), 2008, 340-357.

78. Vollmer, S., K. Harttgen, R. Kupka, S. V. Subramanian. Levels and trends of child- hood undernutrition by wealth and education according to a composite index of anthropometric failure: evidence from 146 demographic and health surveys from 39 countries. – *BMJ Glob. Health*, **2**(2), 2017, e000206.

79. WHO Guidelines on optimal feeding of low birth-weight infants in low- and middle-income countries, 2011, Geneva: World Health Organization.

80. WHO. Healthy food and nutrition for women and their families, 2001, regional office for UNICEF Geneva.

81. WHO. Malnutrition 2020 Available at: https://www.who.int/en/news-room/fact-sheets/detail/malnutrition.

82. WHO. *Physical status: The Use and interpretation of anthropometry. Report of a WHO expert committee.* – WHO Technical Report Series; 854. 1995, Geneva World Health Organization.

83. WHO. WHA Global nutrition targets 2025: Stunting policy brief WHO, 2014. Available at: https://www.who.int/nutrition/topics/globaltargets_stunting_policybrief.pdf.

84. Zhang, G., J. Bacelis, C. Lengyel, K. Teramo, M. Hallman, O. Helgeland, S. Johansson, R. Myhre, V. Sengpiel, P. R. Njolstad, B. Jacobsson, L. Muglia. Assessing the causal relationship of maternal height on birth size and gestational age at birth: A Mendelian randomization analysis. – *PLoS Med.*, **12**(8), 2015, e1001865.

Institute of Experimental Morphology, Pathology and Anthropology with Museum
Bulgarian Anatomical Society

Acta morphologica et anthropologica, 29 (1-2)
Sofia ● 2022

Morphometric Study of Umbilicus Position in a Young Adult Nigcrian Population

Godson Emeka Anyanwu [1], Benedeth Igboke Chikaodili[2], Terkuma Chia[3]*

[1] Department of Anatomy, Faculty of Basic Medical Sciences, College of Medicine, University of Nigeria Enugu Campus, Enugu State, Nigeria.
[2] Department of Anatomy, Faculty of Basic Medical Sciences, Enugu State University of Science and Technology, Enugu State, Nigeria.
[3] Department of Anatomy, Faculty of Basic Medical Sciences, College of Health Sciences, Nile University of Nigeria, Abuja, Nigeria.

*Corresponding author e-mail: anyanwugemeks@yahoo.com

The umbilicus is a prominent feature on the abdominal wall whose position is a determining factor for body proportion among others. The umbilicus position is known to vary across population and genders. Using a sample of young adults in Nigeria, this study was conducted to determine the position of the umbilicus and other related parameters. The round and protruding types of umbilicus were most common in the studied populations. Similarly, most of the participants had their umbilicus located along the midline. Overall there were no significant differences in the umbilicus of males in comparison to those of females. Proper positioning of the umbilicus is essential in maintaining individual identity. However, recognizing its variation across populations, gender and age are the first in achieving the most appropriate position.

Key words: umbilicus, umbilicoplasty, abdominoplasty, morphometry, human variation

Introduction

The umbilicus is a scarred tissue remnant of the umbilical stump that connected an infant to its mother during fetal life [13]. The umbilicus presents centrally in the anterior abdominal wall, but this is an inconstant position, as it may be at a higher or lower position in a small proportion of population [9, 11] or even not at the midline [19] but typically it lies at the high point level of iliac crest, opposite to the disc between third and fourth lumbar vertebrae [10, 20] or it lies matching one of tendinous transverse intersection of rectus abdominis muscle [6].

This variation in the position of the umbilicus becomes more evident between genders, age groups and possibly race. For instance, the umbilicus is more inferiorly placed in men when compared with women and the distance of the iliac crest to the umbilicus is shorter in women specifically due to wider hip in women [21]. In young adults it lies on the level with the disc between the third and fourth lumbar vertebrae and in old individuals it sinks to a lower position [15]. According to Visconti and Salgarello [2] abdominal changes which start before the age of 18 cause initially round-shaped umbilicus to become vertical oval, anchoring of the umbilicus in the deep muscle fascia planes which increases umbilical depth and creation of a horizontal fold after the age of 18. The variation in the position of the umbilicus among different populations and age groups has clinical implications for numerous surgical procedures. This is even more important now that the umbilicus is gaining attention for aesthetics thereby requiring surgical procedures to go around it.

With the variations in the position of the umbilicus in several populations, there is need to determine the position of the umbilicus in the Nigeria population. Therefore, the key objective in this study is to define umbilicus position in Nigerian young adult males and females through morphometric measurements. The study will also characterize other parameters associated with the umbilicus - shape, type, height and width.

Materials and Methods

This study was an observational, cross-sectional study conducted using 125 adult (50 male and 75 female) volunteers. Ethical clearance was obtained from the ethical committee of the Enugu State University of Science and Technology, Enugu, Nigeria. Participants voluntarily consented to participate in their study as extensive explanations were given.

For collection of umbilicus parameters, the subjects were asked to be in a supine anatomical position and restrict the movement of their abdomen (**Fig. 1**). The following parameters were measured: (A) the distance between the inferior part of the xiphoid process and the center of the umbilicus; (B) the distance between the center of the umbilicus and the upper part of the pubis; (C) the distance between the umbilicus and the right anterior superior iliac spine (ASIS), (c′) distance between the umbilicus and the left anterior superior iliac spine; (D) the distance between the center of the umbilicus and the straight line going through the top of the iliac crests; and (E) the distance between the anterior superior iliac spines. The shape of the umbilicus was noted and recorded. The shape of the umbilicus was described based upon the 6 shapes reported by Delpierre et al [7] namely, T-shaped, vertical oval, horizontal oval, round, deformed, and protruded. Measurement of anatomical landmarks to determine the position of the umbilicus was done using a metric tape. To locate the umbilicus, measurements were taken from the xiphoid process, the middle of upper border of the pubis symphysis and the two central iliac spines. Navel height and width were measured using metric tape and the navel depth was determined using a wooden rod which was inserted, marked and drawn out and measured using a plastic ruler. Other parameters collected from participants included age, height (in cm), weight (in kg), and BMI.

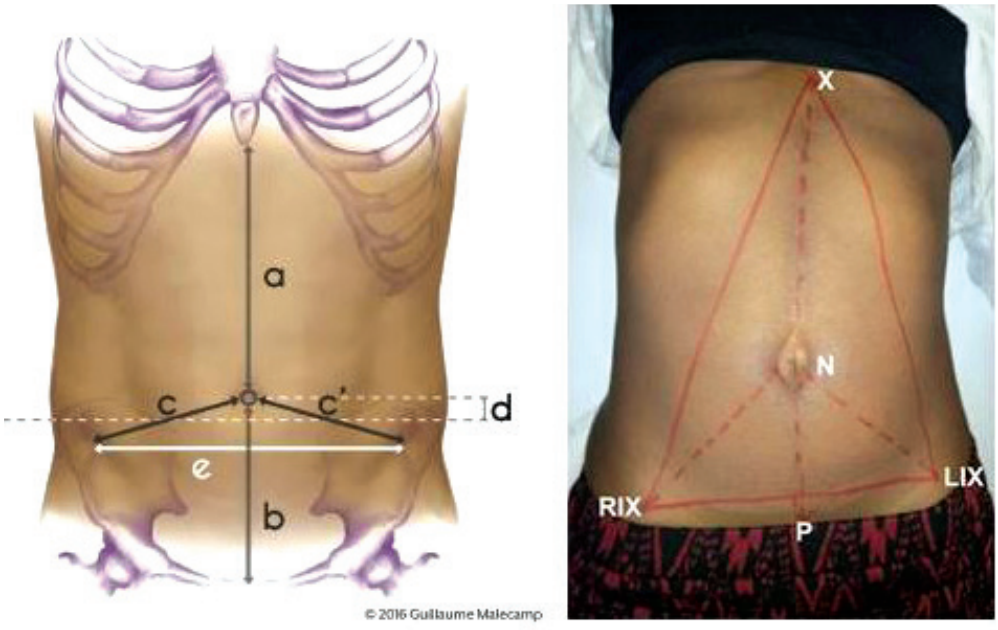

Fig. 1. The standardized measures of the umbilicus and anatomical landmarks used in demonstrating the position of the umbilicus

The measurements were in a prepared data collection sheet and later transferred for statistical analysis using Statistical package for social sciences SPSS version 21.0. Statistical analysis performed on the conducted data included measures of central tendency and variability (mean and standard deviation) as well as frequency distribution.

The exclusion criteria were as follows: any abnormality, deformity or lesion of umbilicus, pregnancy or history of pregnancy, intra-abdominal masses, anterior abdominal wall pathologies, and history of abdominal surgery.

Results

Population and measurements

The study consisted of 125 participants including 50 (40%) males and 75 (60%) females aged between 22 to 26 years. Mean age of the participants was 22.96±3.36 years for males and 21.13±1.64 years for females. Mean height was 174.52 cm, and 165.39 cm in males and females respectively. Males had a mean weight of 70.63 kg while females had 62.18 kg. Males had a mean BMI of 23.36 kg/m^2 and 22.69 kg/m^2 in females. Mean hip circumference and waist circumference was 48.48 cm and 41.33 cm in males while 68.79 cm and 92.15 cm in females respectively. Both the hip and waist circumference showed statistically significant differences between male and female subjects (p = 0.000). **Table 1** displays the details of these measurements.

Table 1. Measurements data

Parameters	Male (n=50)		Female (n=75)			Total (n=125)	
	Mean	**± SD**	**Mean**	**± SD**	***P* value**	**Mean**	**± SD**
Age (Years)	22.96	3.36	21.13	1.64	.000	21.86	2.62
Height (cm)	174.52	8.02	165.39	5.57	.000	169.04	8.01
Weight (Kg)	70.63	10.68	62.18	10.51	.000	65.56	11.33
BMI (Kg/m^2)	23.36	4.40	22.69	3.38	0.341	22.96	3.82
HC (cm)	48.48	24.53	92.15	17.09	.000	74.68	29.56
WC (cm)	41.33	21.52	68.79	13.65	.000	57.81	21.83
ASIS (cm)	22.88	2.41	22.56	2.04	0.433	22.67	2.19
XP (cm)	31.36	3.23	33.10	3.49	0.005	32.41	3.48
XU (cm)	22.01	2.89	22.15	3.06	0.796	22.09	2.98
LIU (cm)	14.33	1.62	15.26	4.67	0.173	14.89	3.73
RIU (cm)	14.78	1.74	14.67	2.10	0.807	14.72	2.56
LIX (cm)	31.97	3.39	31.39	4.09	0.407	31.62	3.82
RIX (cm)	32.30	3.45	31.49	4.65	0.297	31.81	4.21

Abbreviations: BMI=Body Mass Index; SD=Standard Deviation; HC=Hip Circumference, WC=Waist Circumference, ASIS=Anterior Superior iliac spine, XP=Xiphisternum to Pubis, XU=Xiphisternum to Navel, LIU=Left anterior iliac spine, RIU=Right anterior iliac spine, LIX=Left iliac spine to Xiphisternum, RIX=Right iliac spine to Xiphisternum. *P*-value≤0.005

Umbilicus Position

The vertical distance from the lower border of the xiphisternum to the umbilicus process (XU) was 22.01±2.89 cm in males and 22.15±3.06 cm in females while the distance from the lower border of the xiphisternum to the upper border of the pubis (XP) was 31.36± 3.23 cm for males, 33.10± 3.49 cm for females denoting a ratio of XU:XP of 70.18% in males and 66.14% in females. The subjects all together had an XU:XP ratio of 68.16%.

Umbilicus Type and dimensions

With respect to the umbilicus type, the round type was predominant in females (25.6%) followed by the protruding umbilicus type (18.4%). On the contrary, in males the predominant umbilicus type was the protruding type (19.2%) followed by the round type (16.8%). A significant difference was noted between the umbilicus depth of males and females (p =0.000). Overall, the most common umbilicus types in the subjects were the round type (42.4%) and protruding type (37.6%). Umbilicus height, width and depth in the subjects put together were 2.88±0.62 cm, 2.92±0.83 cm and 1.53±0.97 cm respectively. Further details of the umbilicus type and dimensions are shown in **Fig. 2** and **Table 2**.

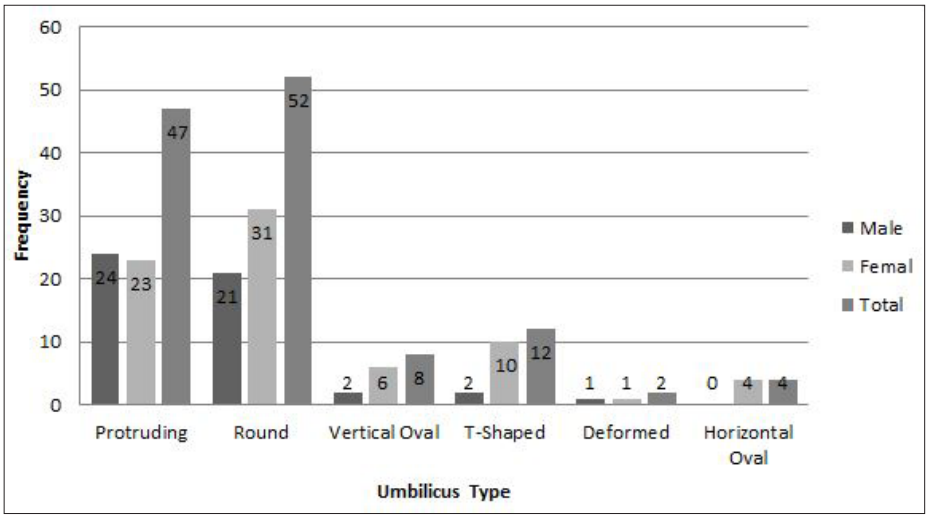

Fig. 2. Distribution of umbilicus types

Table 2. Mean Distribution of Various Measurements around the Umbilicus Based on Gender

	Male (n=50)		**Female (n=75)**			**Total (n=125)**	
	Mean	± SD	**Mean**	± SD	***p* Value**	**Mean**	± SD
Umbilicus Height (cm)	2.82	0.63	2.92	0.61	0.335	2.88	0.62
Umbilicus Width (cm)	2.81	0.66	2.99	0.93	0.216	2.92	0.83
Umbilicus Depth (cm)	0.96	0.55	1.91	1.01	0.000	1.53	0.97

p-value=0.005

Umbilicus Midline Positioning

Measurement of the position of the umbilicus relative to a line extending from the center of the sternal notch found that the umbilicus was central in 72% of the subjects and lateralized to the right and left in 11.2% and 16.8% subjects respectively. Of these 44% females of the subjects were central while only 28% of males were central. **Fig. 3** displays further details of these.

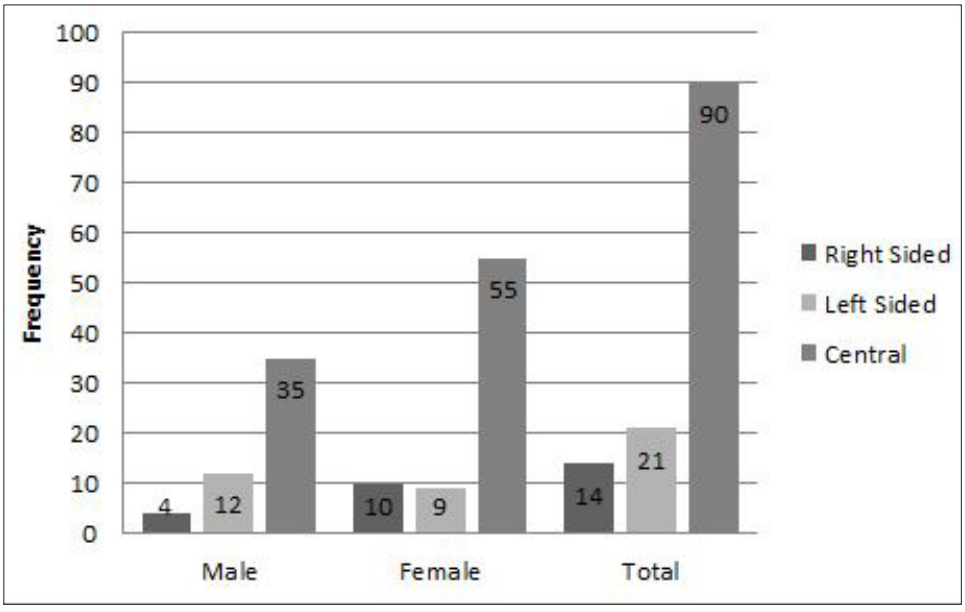

Fig. 3. Distribution of midline positioning of the umbilicus

Discussion

This study was set out to characterize the umbilicus in terms of position, shape and its dimensions in a population of young Nigerians. This information is useful for abdominoplasty and umbilicoplasty planning without which reconstruction of the umbilicus may not be appealing [4]. According to Craig et al [5] the size, shape and location of the umbilicus contribute to an ideal umbilicus. Şentürk et al [18] noted that a normal umbilicus is located on the cranial tangential line of the bilateral iliac crest and the median line of the abdominal wall. On the basis of shape, Choudhary and Taams [3] identified as the ideal. Opinions differ as to what an ideal umbilicus is. The aesthetic nature of the umbilicus however cannot be disputed. Philosophers and artists refer to the ideal proportion of umbilicus height versus body weight as the Golden ratio, also called the Divine proportion. That is, an ideal umbilicus height is about 62% of the body height and is said to exhibit a special beauty as the legs and torso appear in sound proportion [6].

The findings of this study contrast that of Yu et al [21] where the umbilicus was located more inferiorly in men compared to women. This study also affirms like most other studies that the umbilicus is not always in the midline [8, 12, 16]. Rohrich et al [17] reported up to 80% laterality of the umbilicus in their own study. Craig et al [5] photographed 147 women a round umbilicus with superior hooding (T-shaped) was present in 37%, oval shape in 22%, linear in 17%, and horizontal in 14%. The remaining 10% were distorted. Lee et al [14] assessed the umbilical position on photographs and they a ratio of xiphoid-umbilicus-pubic symphysis of 46:54. Their results differ from the present study where the same ratio was closer to the 62% proposed by Davari et al [6] as being ideal. It also affirms the variability of the umbilicus as proposed by Catteau [1].

Conclusion

The umbilicus is a prominent landmark on the anterior abdominal wall and its appearance is influenced by many factors. Knowing where the umbilicus is placed is critical for the reconstruction of the umbilicus to maintain its aesthetic nature. In every clime, the plastic surgeon needs this evidenced based approach to benchmark their techniques and self-assessment to provide patients with acceptable results.

References

1. **Catteau, J. F.** Of the umbilicus and its modifications in cases of distension of the abdomen – *Doctoral dissertation*, Faculty of Medicine of Paris. 1876. [in French]
2. **Correia, N., L. Jayyosi, S. Chiriac, Y. Renard, E. Raimond, M. L. Poli-Merol, et al.** Morphometric analysis of the umbilicus according to age. – *Aesthetic Surgery Journal*, **38**(6), 2018, 627-634.
3. **Choudhary, S., K. O. Taams.** Umbilicosculpture: a concept revisited. – *British Journal of Plastic Surgery*, **51**(7), 1998, 538-541.
4. **Visconti, G., M. Salgarello.** The divine proportion "ace of spades" umbilicoplasty: a new method of navel positioning and plasty in abdominoplasty. – *Annals of Plastic Surgery*, **76**(3), 2016, 265-269.
5. **Craig, S. B., M. S. Faller, C. L. Puckett.** In search of the ideal female umbilicus. - *Plastic and Reconstructive Surgery*, **105**(1), 2000, 389-392.
6. **Davari, H., M. Nazam.** The normal position of umbilicus in the newborn: an aid to improve cosmetic result in exomphalos major. – *Journal of Research in Medical Sciences*, **1**, 2004, 34-38.
7. **Delpierre, V., D. Coquerel-Beghin, A. Aktouf, I. Auquit-Auckbur, P. Y. Milliez.** Biometric and morphometric analyse of the umbilicus: about 70 cases. In: *Annales de Chirurgie Plastique et Esthetique*, **57**(6), 2011, 575-579.
8. **Dini, G. M., L. M. Ferreira.** Putting the umbilicus in the midline. – *Plastic and Reconstructive Surgery*, **119**(6), 2007, 1971-1973.
9. **Du-Plessis, D. J.,** A Synopsis of Surgical Anatomy. 11th ed. Bristol, John Wright and Son Ltd, 1975.
10. **Farquharson, M., J. Hollingshead, B. Moran.** Farquharson's Textbook of Operative General Surgery (9th edn). London, United Kingdom, Hodder Arnold, 2005, 201.
11. **Fawkner-Corbett, D., J. A. Nicholson, T. Bullen, P. Cross, D. Bailey, M. H. Scott.** Anatomical variation in the position of the umbilicus and the implications for laparoscopic surgery. – *International Journal of Surgery*, **7**(8), 2010, 540.
12. **Golcman, R., B. Golcman.** *Tummy tucks with reduced scars*. Plastic surgery fundamentals and arts: cosmetic surgery. Rio de Janeiro: Medsi, 2003, 625-628. [in Portuguese]
13. **Hegazy, A. A.** Anatomy and embryology of umbilicus in newborns: a review and clinical correlations. – *Frontiers of Medicine*, **10**(3), 2016, 271-277.
14. **Lee, S. J., S. Garg, H. P. Lee.** Computer-aided analysis of the "beautiful" umbilicus. – *Aesthetic surgery journal*, **34**(5), 2014, 748-756.
15. **Psillakis, J. M.** Abdominoplasty: The Role of the External Oblique Muscle. In: *New Concepts on Abdominoplasty and Further Applications,* Springer, Cham, 2016, 497-509.
16. **Ribeiro, R. C., R. Saltz, C. Ramirez, L. F. de Cordova.** Anatomical position of umbilicus in Latin-American patients. – *European Journal of Plastic Surgery*, **42**(4), 2019, 351-358.
17. **Rohrich, R. J., E. S. Sorokin, S. A. Brown, D. L. Gibby.** Is the umbilicus truly midline? Clinical and medicolegal implications. – *Plastic and reconstructive surgery*, **112**(1), 2003, 259-263.

18. Şentürk, S., A. Özkan, K. Gemici, D. Efe. The dome procedure: a new technique for the reconstruction of the umbilicus. – *Hernia*, **20**(4), 2016, 505-508.
19. Smith, T., C. Pinnock, T. Lin, R Jones. *Fundamentals of Anaesthesia*. Cambridge University Press. 2009, 77-104.
20. Williams, A. M., J. L. Brain. The normal position of the umbilicus in the newborn: an aid to improving the cosmetic result in exomphalos major. **–** *Journal of Pediatric Surgery*, **36**(7), 2001, 1045-1046.
21. Yu, D., W. M. Novicoff, T. J. Gampper. The average size and position of the umbilicus in young men and women. – In: *Adult Umbilical Reconstruction*, Springer, Cham, 2017, 43-47.

Institute of Experimental Morphology, Pathology and Anthropology with Museum
Bulgarian Anatomical Society

Acta morphologica et anthropologica, 29 (1-2)
Sofia ● 2022

Shape Differences in the Auricula of the Human Foetus: A Geometric Morphometric Approach

Yasin Demiraslan[1], İhsan Hiz[2], Berfu Özdemir[2], Soner Albay[2], Ahmet İhsan Aytek[3], Özcan Özgel[l]*

[1] Burdur Mehmet Akif Ersoy University, Department of Anatomy, Faculty of Veterinary Medicine, Burdur, Turkey
[2] Süleyman Demirel University, Department of Anatomy, Faculty of Medicine, Isparta, Turkey
[3] Burdur Mehmet Akif Ersoy University, Department of Antropology, Faculty of Arts and Science, Burdur, Turkey

*Corresponding author e-mail: yasindemiraslan@hotmail.com

The aim of the study is to analyse the auricula of human foetus using geometric morphometric methods based on the foetal age groups and, thus, to determine the presence of shape differences. For this purpose, the foetuses having a gestational age of 23-40 weeks were divided in three groups based on intrauterine gestational age and analysed. After performing photography, landmarking and dataset formation stages for geometric morphometric analysis, the principal component, and discriminant and regression analyses were made. The first principal component accounted for 26.461% of the total shape difference based on foetal age. The most apparent shape changes were observed on helix (superior), crus helicis, tragus and antitragus points. Consequently, the variations concentrated especially around cavum concha.

Key words: auricle, hearing, morphoJ, tragus

Introduction

Humans have the most complex and efficient communication system among mammals and this ability is one of the fundamental concept for surviving during the evolution of humankind. Hearing is one of the key abilities for communication and can be examined by aid of malleus, stapes and incus (unique to mammals) in fossil specimens since auricula cannot be fossilized. Although it is known that *Homo sapiens* (anatomically modern human) has the most complex auditory system among human species, a recent study points out that the closest modern human relative, *Homo neanderthalensis*, could have had similar auditory capacity as modern humans [12].

Auricle is a cartilaginous and fibroelastic structure covered by a thin skin [3]. Auricle grows throughout lifetime and males have greater increase then females [30]. It

is also highly variable body part among individuals and populations. The surface of this structure is characterized by protrusions and depressions [47]. Auricula is composed of three main components: helix-antihelix, cavum concha and lobulus auriculae [31].

The studies have emphasized [26, 44] that the six hillocks originating from the first and second pharyngeal arches are responsible for the development of auricula. These hillocks located as three on both sides of meatus acusticus externus, three on each side, form auricula by expanding and combining asymmetrically. Lobulus auriculae are the last part developing in auricula [29, 46].

It is a complicated process that the principal structures of auricula combine in the foetal periods. For this reason, the development anomalies of auricula are common [5]. It is an important question which structures contribute to the development of auricula by changing shape on which side. Therefore, it is important to know the normal shape changes of auricula in the foetal period to clearly figure out the effect of anomalies on auricula.

Geometric morphometrics is a method helping many different disciplines such as anthropology, anatomy, zoology and botany in the recent years. In this method, landmarks (LM) are digitized at *Cartesian* coordinates in accordance with the geometric structure of objects [33]. Thus, two- or three-dimensional shape of the sample and the shape changes are analysed using the location differences between objects [27, 48, 50]. Also, the analysis results are interpreted by being mapped based on the size and direction of the change in the coordinates of the landmarks [7].

There are a limited number of studies in the literature for auricula by using geometric morphometric methods in adult human beings [31, 33]. However, no study has been found in which auricula is analysed with geometric morphometric methods based on the foetal period. For this reason, the aim of the study is to analyse the auricula of human foetus by using geometric morphometric methods based on the foetal age groups.

Materials and Methods

Samples

The foetuses which were obtained from Isparta Maternity and Child Hospital and found in Süleyman Demirel University Medical Faculty Anatomy Department laboratory by obtaining the permission of the families between 1996 and 2010 were used in this study. Approval was obtained from the Medicine Clinical Research Ethics Committee. The ages of the foetuses kept in formaldehyde solution (10%) were between the 23-40 gestational weeks and they did not have any anomaly or pathological condition. They were divided into three groups based on the intrauterine gestational age. Twelve foetuses had a gestational age of 23-28 weeks in the first group, 9 foetuses had a gestational age of 29-34 weeks in the second group, and 11 foetuses had a gestational age of 35-40 weeks in the third group.

Data collection and Landmarking

The left auricle of samples was photographed in the way that the camera (18x55 lens, Canon Eos, 600D, Japan) and the focus were on the same plane (camera resolution

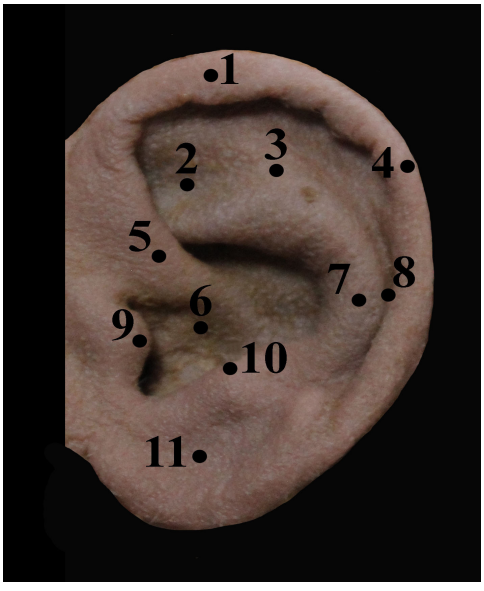

Fig. 1. Landmarks, 1. Helix (superior), 2. Fossa triangularis, 3. Crus antihelices (intersection of crus antihelices), 4. Helix (posterior, crus antihelices), 5. Crus helicis, 6. Cavum concha, 7. Antihelix, 8. Scapha (antihelix), 9. Tragus, 10. Antitragus, 11. Lobulus auriculae (mid point)

890 x 1065 pixels). Cavum concha was determined as the focus in the photographing. The distance between the focus and lens were standardized at 30 cm. These photos were converted into tps format using TpsUtil (Version 1.79) [41].

The eleven homolog LMs [25, 36] (**Fig. 1**) were marked on the photos by TpsDig2 programme (Version 2.31) [40]. Thus, the *x, y Cartesian* coordinates of LMs were determined. Before the statistical analysis, it was important to determine whether or not the new tangent space was small enough to demonstrate that it was a good representation of the Procrustes data in a Euclidean space. This confirmation test was made in TpsSmall (Version 1.34) [39] software by determining the correlations of the tangent and Procrustes distances. The test results (uncentred correlation: 0.999, root mean square error: 0.000149) confirmed that the correlation data were quite close for both space distances.

Statistical analysis

As there are differences in the auricula such as size, position and direction, General Procrustes Analysis (superimposition) was performed [45]. Principal component analysis (PCA) was performed on the new coordinates obtained as a result of Procrustes analysis. Thus, the degree of split upof samples based on the age groups between the factors was determined using covariance analysis [50].

The potential size and shape differences between the age categories were analysed with one-wayanalysis of variance (ANOVA). PAST (Version 4.02) [17] software was used for these analyses.

It was determined at which landmark and in which direction the shape difference was located based on the PCA. To assess the allometric effect based on the foetal age on the shape change, a multivariable regression of Procrustes coordinates was performed using a permutation test with 10.000 repetitions [13, 16]. As CS (centroid of size) corresponds to the square root of total of the distances of the squares from each turning point to the central point [38], the CS of the landmark configurations was used as a representative for the dimension measurement. Discriminant function analysis (DA) was performed on the procrustes coordinates to see the grouping properties of the samples. MorphoJ [28] software was used for all these analyses.

Results

Table 1 shows the results related to the PCA. Accordingly, the first principal component accounted for 26.461% of the total shape variance based on foetal age. The difference based on foetal age in terms of the first and second principal component was shown in the plot in **Fig. 2**. Based on the plot, it was observed that the foetuses in the first group fall mostly negative half of *y* axis and the individuals in the third group fall mostly positive half of *y* axis. The foetuses in the second group were located on the centre of the plot.

Table 1. Values obtained as a result of the PCA, PC: principal component

PC	Eigenvalue	% Variance	PC	Eigenvalue	% Variance
1	0,005162	26,461	12	0,000342	1,7546
2	0,003726	19,1	13	0,000238	1,2221
3	0,002559	13,116	14	0,000137	0,7029
4	0,002053	10,524	15	0,000112	0,57421
5	0,001232	6,3134	16	8,94E-05	0,45851
6	0,001036	5,3103	17	6,61E-05	0,33878
7	0,000694	3,5568	18	4,55E-05	0,23333
8	0,00061	3,1288	19	2,61E-05	0,13367
9	0,000528	2,7077	20	4,05E-16	2,07E-12
10	0,000492	2,5228	21	1,75E-16	8,97E-13
11	0,000359	1,8414	22	1,31E-16	6,71E-13

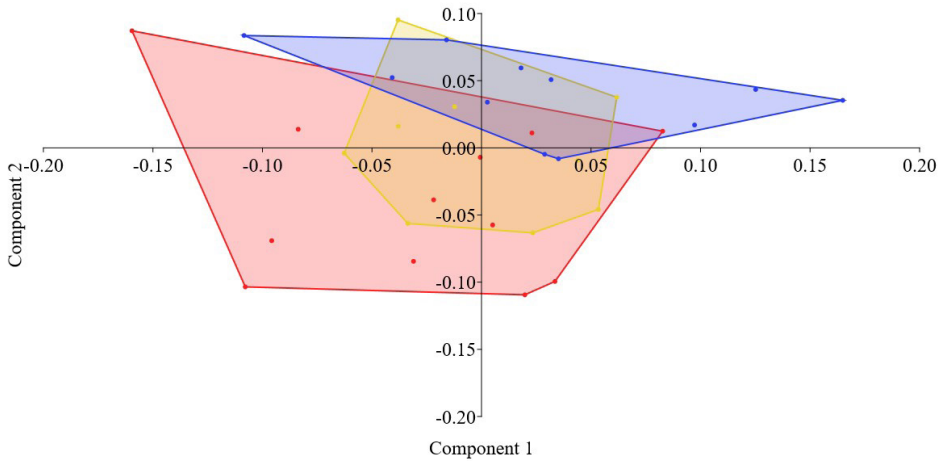

Fig. 2. In the graphic presentation of the results obtained based on the first and second principal component, the red points represent the first group individuals (foetal age of 23-28 weeks), the yellow points represent the second group (foetal age of 29-34 weeks) and the blue points represent the third group individuals (foetal age of 35-40 weeks).

Table 2 shows the results of ANOVA test made to determine the difference between the Procrustes coordinate values of the landmarks based on the foetal age groups. Table 3 shows the statistically significant landmark data ($p<0.05$) as a result of the Post-hoc (Tukey) test. Based on the tables, there were statistically significant differences between the groups related to the location of helix (posterior point), antitragus and lobulus auriculae on *x* axis and the location of crus helicis, scapha (antihelix) and lobulus auriculae on *y* axis.

Table 2. Results of Anova test. Co: Coordinates, SS: Sum of squares, Df: Degrees of freedom, MS: Mean square, F: F-value, P: P-value

Co	SS	Df	MS	F	P
X1	0,000558	2	0,000279	0,1779	0,8379
Y1	0,000722	2	0,000361	0,3107	0,7354
X2	0,001945	2	0,000973	2,745	0,08092
Y2	0,001804	2	0,000902	1,653	0,209
X3	0,002011	2	0,001005	2,867	0,07308
Y3	0,005954	2	0,002977	2,999	0,06548
X4	0,007927	2	0,003963	12,84	0,0001
Y4	0,001404	2	0,000702	1,23	0,3072
X5	0,004803	2	0,002402	2,861	0,07346
Y5	0,005209	2	0,002604	3,736	0,036
X6	9,61E+00	2	4,80E+00	0,06676	0,9356
Y6	0,002111	2	0,001055	1,224	0,3087
X7	0,000591	2	0,000295	0,5219	0,5989
Y7	0,002341	2	0,001171	1,627	0,2139
X8	0,004653	2	0,002326	2,575	0,09346
Y8	0,003848	2	0,001924	4,529	0,01943
X9	0,001917	2	0,000958	0,658	0,5255
Y9	0,001386	2	0,000693	1,147	0,3316
X10	0,017777	2	0,008888	7,527	0,00233
Y10	0,000422	2	0,000211	0,2347	0,7923
X11	0,005458	2	0,002729	4,761	0,0163
Y11	0,01378	2	0,00689	4,403	0,02138

Table 3. The landmarks with $p < 0.05$ as a result of the post-hoc test of Procrustes coordinates

Landmark	Group	Axis	P-value
LM4	1x2	X	0.001
	1x3		0,000
LM5	1x2	Y	0,048
LM8	1x2	Y	0,047
	1x3		0,036
LM10	1x3	X	0,002
LM11	1x2	X	0,033
	2x3		0,024
	1x3	Y	0,016

Figure 3 shows at which landmarks the shape differences occurred based on the PCA. Accordingly, an apparent shape differentiation was observed superioposteriorly in LM1, inferioposteriorly in LM5 and LM6, superioanteriorly in LM8 and LM10 and inferiorly in LM9.

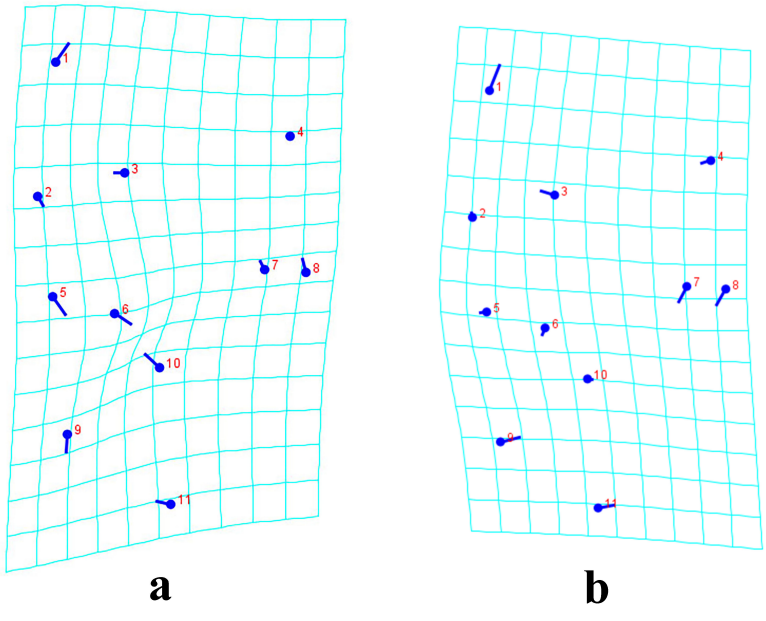

Fig. 3. The point demonstration of the shape differences occurred at the landmarks based on the PC1 (a) and PC2 (b). Point represents the average shape. Set scale factor: 0.1.

Table 4 shows the distinction obtained with the discriminant function analysis implemented to observe the classification of the foetal age groups. Accordingly, it was observed that group 1 was completely separated from the other groups. Also, **Fig. 4** shows the discriminant score graphic obtained as a result of the discriminant function analysis and **Fig. 5** shows the shape variation plot. Accordingly, among all the groups, apparent shape differences were observed at LM8, LM9 and LM11. In addition, in the comparisons of group 1 and group 3, a significantshape change was observed at LM6, LM7, LM8, LM9, and LM11 (**Fig. 5**).

Table 4. Discriminant function analysis of the foetal age groups. The number of the samples was presented for each group.

Group	**1 (23-28 week)**	**2 (29-34 week)**	**Total**
1 (23-28 week)	12	0	12
2 (29-34 week)	1	8	9
Group	**1 (23-28 week)**	**3 (35-40 week)**	**Total**
1 (23-28 week)	12	0	12
3 (35-40 week)	0	11	11
Group	**2 (29-34 week)**	**3 (35-40 week)**	**Total**
2 (29-34 week)	8	1	9
3 (35-40 week)	1	10	11

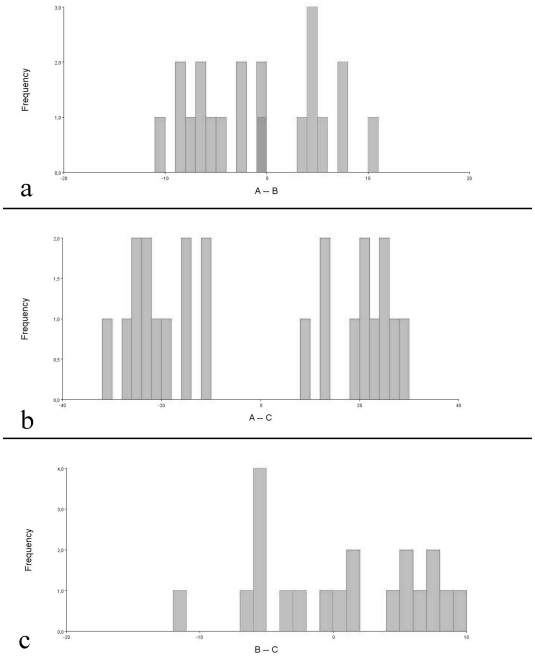

Fig. 4. The classification plot obtained with discriminant function analysis based on the foetal age groups, a. 1x2, b. 1x3, c. 2x3, A: Group 1 (23-28 weeks), B: Group 2 (29-34 weeks), C: Group 3 (35-40 weeks)

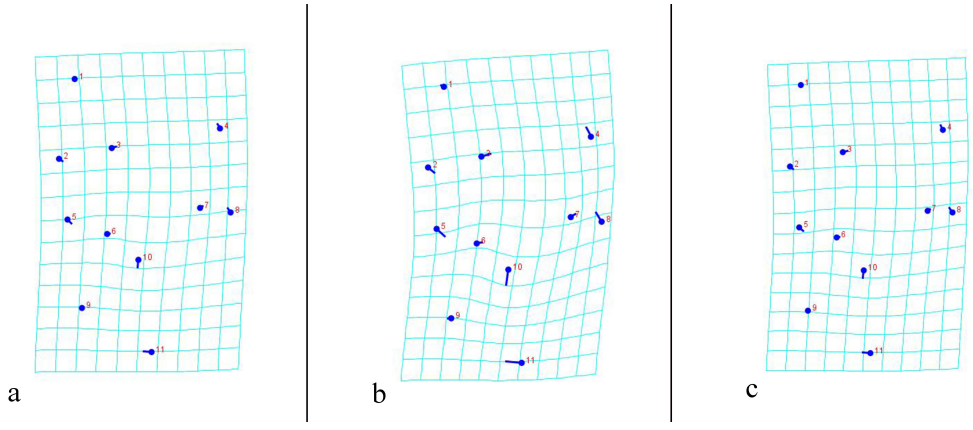

Fig. 5. The shape variation plot obtained with discriminant function analysis based on the foetal age groups, A. 1x2 (point represents group 1), B. 1x3 (point represents group 1), C. 2x3 (point represents group 2). Set scale factor: 1.0.

In the study, the statistical allometric effect of Procrustes coordinates (dependent variable) on dimension (log CS, independent variable) was observed only in group 2 (P value: Group 1: 0.652; Group 2: 0.0104; Group 3: 0.8722). Dimension explained 7.2556%, 24.9918%, and 4.7198% of the total shape difference in groups 1, 2, and 3, respectively and the groups were separated apparently (**Fig. 6b**).

In the assessment performed in terms of the rates of the allometric shape variation at landmark (**Fig. 6a**), it was observed that an apparent shape differentiation occurred in LM8, LM9, and LM11 together with the increase in the foetal age.

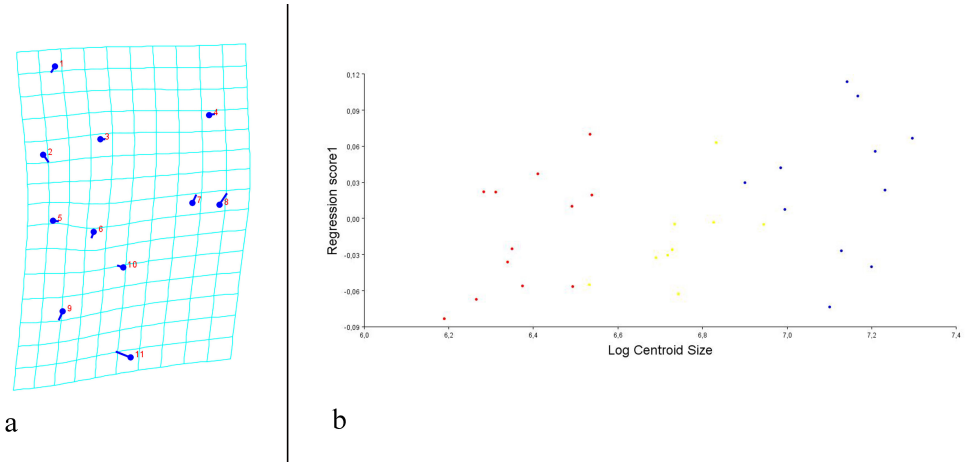

Fig. 6. Regression plot of Procrustes coordinates based on the foetal age groups (a, set scale factor: 0.5) and shape variation (b), Red: Group 1 (23-28 weeks), Yellow: Group 2 (29-34 weeks), Blue: Group 3 (35-40 weeks)

Discussion

At the end of the twentieth week of the foetal period, auricula takes its adult shape and this development continues averagely until the age of 9 in the postnatal period [49]. It has been suggested that the factors such as skin elasticity [35], strength of connective tissue [21], gravity force [37], genetics [32], age [2], sex[6], geographical location [14], chemicals and radiation exposure[18], uterus and placenta functions [4] may affect this development. However, the effects of these factors on the anatomic structures contributing the 'whole auricula shape' are not clear yet. In the present study, in the foetuses with the gestational age of 23-40 weeks, the first five components, based on the PCA, explained 75.5144% of the total shape variation. Different fetal age groups are separated in the PCA graph. Based on the PCA plot, it was remarkable that the foetus group with the gestational age of 29-35 weeks were gathered in the transition areas of the other two foetus groups. It was interpreted that this situation may be due to the fact that the shape change occurred gradually based on the foetal age groups. Also, considering that it is nearly impossible to standardize the above mentioned factors, affecting the general form of auricula, in practice, it was significant that the foetal age groups formed an important shape variation in terms of the "whole auricula shape" based on the PCA.

The effective and appropriate analysis of auricula shape helps us to understand the anatomic changes caused by the pathological disorders [15]. Foetal auricula, which is an important criterion for pediatrists, is useful in the assessment of some congenital malformations [10, 24, 37] and syndromes [37]. Kalcıoğlu *et al.* (2003) [23] reported in their study on auricula morphometry that the measures from tragus to helix and antihelix may be determinant in the diagnosis of abnormal auricula structure. Auricula is also an indicator of abnormal development in the pharyngeal region due to the fact that it has a close relationship with pharyngeal arcus and it develops from different origins [9, 43]. Therefore, the development of the foetus auricula and its general shape are highly important. We investigated which landmarks produced the most significant changes in the shape of the auricle in normal fetuses. In the present analysis performed for this purpose, it was observed that the most apparent shape changes were on helix (superior), crus helices, tragus and antitragus points.

Lobulus auriculae areolar, which has a connective tissue and fatty tissue quality [3] is the last part developing in auricula [5]. The most apparent changes in auricula together with the aging process occur in lobulus auriculae [8]. In the study, the general shape of auricula was focused rather than the general form of lobulus auriculae. For this reason, a single landmark representing lobulus auriculae was determined. In the present study, there was an anterior apparent variation in the landmark (LM11) representing lobulus auriculae based on the foetal age groups. However, whether or not there is a change in the general shape of lobulus auriculae or the degree of the variation may be examined in another study.

Among the hillocks, responsible for the formation of auricula, the first hillock contributes to the development of tragus, the second hillock contributes to the development of crus helices, the third hillock contributes to the development of helix, the fourth and fifth hillock contribute to the development of helix, scapha and antihelix and the sixth hillock contributes to the development of helix and antitragus. The combination of these hillocks occurs in the 6th and 8th weeks of the embryological development and they grow at different growth rates and provide that auricula takes

its normal shape [22]. In accordance with the literature [22], it was also determined in the present study that the anatomic formations of foetus auricula had different growth rates with the result of the discriminant function analysis. Accordingly, the fastest and apparent variation was observed at tragus (LM9), scapha (antihelix, LM8) and lobulus auriculae (LM11).

Morphologically, auricula is different in certain degrees in primates. It is known that this difference is one of the determinant criteria in terms of phylogenetic relations [11]. The auriculae of the anthropoid and non-anthropoid primates may be distinguished in terms of morphological differences but it is not known whether the auriculae of these species have the similar or different developmental stages in foetal period. When viewed from this point of view, no study similar to the present study was found in the literature not only on human beings but also on primate order.

The helix-antihelix complex of auricula allows collecting and directing sounds. Concha intensifies the collected sounds and increases their frequencies [1]. An adult human being has the ability to hear the sounds at the frequencies ranging between 20 Hz and 20 000 Hz. Some authors [42] have reported that the hearing frequency range in newborns was 500-1000 Hz. Hepper and Shahidullah (1994) [19] reported in their study that one foetus responded to 500 Hz tone of voice in the 19th gestational week. In the same study, it was revealed that as the foetal age increased, the degree of the sound frequency respond also increased. Hepper & Shahidullah (1994) [19] stated that all of the foetuses responded to 1000 Hz of tone in the 33th gestational week and 3000 Hz of tone in the 35th gestational week. In the present study, the shape variations of auricula, which is known to function as directing sound and increasing its frequency, based on foetal age groups were examined and it was observed that certain variations formed in many anatomic points. In the literature [19], it has been stated that the direct proportion between the age of responding to sound and frequency height may be related to the fact that all the structures included in the hearing function develop. The contribution of the shape variation in auricula to the relationship between the age of responding to sound and frequency is not known. However, in accordance with the present study, that the shape variation intensified around cavum conchae in terms of increasing foetal age suggested that the shape change in auricula may be one of the determinant factors in the relationship between the response age and frequency.

Özkoçak (2017) [33] stated in the study conducted with adult human beings that LM2, LM4, LM5 and LM6 included a shape change outwards, and LM10 and LM11 included a shape change inwards. In this study, it was assumed that the shape change stated to be outwards or inwards referred to the situation compared to the centre of the grid map. In the present study, the vectoral side of the shape changes was defined in accordance with the anatomic expressions.

When x or y coordinate values of the landmarks were statistically compared in terms of the foetal age groups in the present study, significant differences were observed in LM4, LM5, LM8, LM10, and LM11. Accordingly, it was concluded that the anterioposterior (x) or superioinferior (y) movement of helix (posterior point), antitragus, crus helicis, scapha (antihelix) and lobulus auriculae among the foetal age groups was significant. These differences also supported the variation plot data obtained as a result of the discriminant function analysis substantially.

Honkura *et al*., (2020) [20] stated that meatus acusticus externus of human foetuses had a funnel-like shape in the postnatal period together with cavum conchae based on

the development of cartilage and muscles in the foetal period. The authors [20] have interpreted the variation using the knowledge that different cartilage reaches this shape with different growth rates [22]. In the present study, the shape variation, especially between group 1 and group 3, around cavum concha supports this information.

Conclusion

Consequently, the shape variations in the foetus auricula were investigated in the study based on the middle and late gestational ages. According to the results of the present study, there were apparent shape variations in different anatomic points based on the foetal age groups. These variations concentrated, especially, around cavum concha. Statistical allometric effect based on the foetal age in terms of size and shape was observed only in group 2.

The allometric effect was quite weak in the other two groups. We do not ignore that shape variations are assessed on more foetuses by including the factors such as symmetry or sex. However, we consider that the results obtained as a result of the study will make a new effect together with the limited number of auricula studies conducted with geometric morphometric method.

Author Contributions: Demiraslan Y, Aytek Aİ and Özgel Ö designed and directed the study. Demiraslan Y and Aytek Aİ conducted geometric morphometric application. Hız İ, Özdemir B and Albay S provided and prepared the material for study. Demiraslan Y, Aytek Aİ, Hız İ, Özdemir B, Albay S and Özgel Ö co-wrote the overall paper.

References

1. Akyıldız, N. *Balance and hearing physiology, ear diseases and microsurgery-1*. Bilimsel Tıp Yayınevi, Ankara, 1998. [in Turkish].

2. Alexander, K. S., D. J. Stott, B. Sivakumar, N. Kang. A morphometric study of the human ear. – *J Plast Reconstr. Aesthet. Surg*., **64,** 2011, 41-47.

3. Arıncı, K., A. Elhan. *Anatomy (6th ed.)*. Güneş Tıp Kitabevleri, Ankara, 2016.[in Turkish].

4. Avery, M. E., H. W. Taeusceh. Intrautarin growth retardation. In: *Schaffer's diseases of the newborn (Eds. M. E. Avery,& H W. Taeusceh),* Philadelphia, WB Saunders Co, 1984, 92-100.

5. Başaklar, A. C. *Langman's Medical embryology (7th ed.),* Ankara, Palme Yayıncılık, 1996. [in Turkish].

6. Beasley, N. J., N. S. Jones. Otoplasty: the problem of the deep conchal bowl. – *J. Laryngol. Otol*., **110**, 1996, 864-868.

7. Bigoni, L., J. Veleminska, J. Bruzek. Three-dimensional geometric morphometric analysis of cranio-facial sexual dimorphism in a Central European sample of known sex. - *Homo*, **61**, 2010, 16-32.

8. Brucker, M. J., J. Patel, P. K. Sullivan. A morphometric study of the external ear: age- and sex-related differences. – *Plast. Reconstr. Surg*., **112**, 2003, 647-652.

9. Carlson, B. M. *Human embryology and developmental biology (5th ed.)*, Philadelphia, Elsevier, 2014.

10. Chang, C. H., F. M. Chang, C. H. Yu, R. I. Liang, H. C. Ko, H. Y. Chen. Fetal ear assessment and prenatal detection of aneuploidy by the quantitative three-dimensional ultrasonography. – *Ultrasound MedBiol*., **26,** 2000, 743-749.

11. Coleman, M. N., C. F Ross. Primate auditory diversity and its influence on hearing performance. – *Anat. Rec. Part A Discov. Mol. Cell Evol. Biol*., **281,** 2004, 1123-1137.

12. **Conde-Valderde, M., I. Martinez, R.M. Quam, M. Rosa, A.D. Velez, C. Lorenzo, P. Jarabo, J. M. Bermudez de Castro, E. Carbonell, J. L. Arsuaga.** Neanderthals and Homo sapiens had similar auditory and speech capacities. – *Nat. Ecol. Evol*., **5**, 2021, 609-615.
13. **Edgington, E. S.** *Randomization Tests*. New York, Marcel Dekker, 1995.
14. **Ferro-Luzzi, A.** Environment and physical growth. In: *Genetic and environmental factors during the growth period* (Ed. C. Susanne) New York, Plenum Publ. Corp, 1984, 169-198.
15. **Fritscher, K. D., R. Pilgram, R. Leuwer, C. Habermann, A. Muller, R. Schubert**. Analyzing inter-individual shape variations of the middle ear cavity by developing a common shape model based on medial representation. Computer sssisted radiology and surgery. Proceedings of the 18th International Congress and Exhibition. International Congress Series 1268 Elsevier, Chicago, 2004, 243-248.
16. **Good, P.** *Permutation Test: A Practical guide to resampling methods fortTesting hypotheses*. New York, Springer-Verlag, 1994.
17. **Hammer, Q., D. A. T. Harper, P. D. Ryan.** PAST: Paleontological statistics software package for education and data analysis. – *Palaeontol. Electron*., **4**, 2001, 9.
18. **Hauspie, R., M. C. Lauwers, C. Susanne.** Effect of industrial pollution on somatic and neuropsyhological development. *In, Genetic and environmental factors during the growth period* (Ed. C. Susanne), New York, Plenum Publ. Corp,1984, 221-233.
19. **Hepper, P. G., S. Shahidullah.** Development of fetal hearing. – *Arch. Dis. Childh*., **71**, 1994,81-87.
20. **Honkura, Y., S. Hayashi, J.H. Kim, G. Murakamid, H. Abee, J. F. Rodriguez-Vazquez,Y. Katoria.** Development and growth of auricular cartilage and muscles: A study using human fetuses. – *Int. J. Pediatr. Otorhinolaryngol*., **133**, 2020.
21. **Ito, I., M. Imada, K. Sueno, T. Arikuni, A. Kida.** A morphological study of age changes in adult auricular cartilage with special emphasis on elastic fibres. – *Laryngoscope*, **111**, 2001, 881-886.
22. **Kagurasho, M., S.Yamada, C. Uwabe, K. Kose, T. Takakuwa.** Movement of the external ear in human embryo. – *Head Face Med*., **8**, 2012,1-9.
23. **Kalcıoğlu, M. T., M. C. Miman, Y. Toplu, C. Yakıncı, O. Özturan.** Anthropometric growth study of normal human auricle. – *Int. J. Pediatr. Otorhinolaryngol*., **67**, 2003, 1169-1177.
24. **Kalcıoğlu, M. T., Y. Toplu, O. Özturan, C. Yakıncı.** Anthropometric growth study of auricle of healty preterm and term newborns. – *Int. J. Pediatr. Otorhinolaryngol*.,**70**, 2006, 121-127.
25. **Kapil, V., J. Bhawana, K. Vikas.** Morphological variation of ear for individual identification in forensic cases: A study of an Indian population. – *Res. J. Forensic Sci*., **2**, 2014,1-8.
26. **Karmody, C. S., D. J. Annino.** Embryology and anomalies of the external ear. – *Facial Plast Surg*., **11**, 1995, 251–256.
27. **Kimmerle, E. H., A. Ross, D. Slice.** Sexual dimorphism in America: geometric morphometric analysis of the craniofacial region. – *J. Forensic Sci*., **53**, 2008, 54-57.
28. **Klingenberg, C. P.** MorphoJ: an integrated software package for geometric Morphometrics. – *Mol. Ecol. Resour*., **11**, 2011, 353–357.
29. **Moore, L. K., N. V. T. Persuad, M. G. Torchia.** *The Developing human clinically oriented embryology(10th Ed.)*, H. Dalçık (Translation). Nobel Tıp Kitabevleri, İstanbul, 2016. [in Turkish].
30. **Niemitz, C., M. Nibbrig,V. Zacher.** Human ears grow throughout the entire lifetime according to complicated and sexually dimophic patterns-conclusions from a cross-sectional analysis. – *Anthropol. Anz*., **65**, 2007, 391-413.
31. **Ocakoğlu, G., S.Turan Özdemir, İ. Ercan, A. Etöz.** The shape of the external human ear: a geometric morphometric study. – *Türkiye Klinikleri J. Med. Sci*., **33**, 2013,184-190.

32. Olowe, S. Standards of intrauterine growth for an African population at sea level. – *J. Pediatr*., **99**, 1981, 459-495.
33. Özden, B. Geometric morphometric analysis of Iran dwarf honey bee (Apis flore Fabricius) populations. *Master Thesis*, Karaelmas University, Institute of Science and Technology, Zonguldak,2008. [in Turkish].
34. Özkoçak, V. Estimation of age with geometric morphometry analysis from human ear. *PhD Thesis*, Ankara University, Institute of Social Sciences. Ankara, 2017.[in Turkish].
35. Pasquali-Ronchetti, I., M. Baccarani-Contri. Elastic fibre during development and aging. – *Microsc. Res. Tech*., **38**, 1997, 428-435.
36. Pflug, A., C. Busch. Ear biometrics: a survey of detection, feature extraction and recognition methods. – *IET Biom*., **1**, 2012, 114-129.
37. Purkait, R., P. Singh. Anthropometry of the normal human auricle: a study of adult Indian men. – *Aesthetic. Plast. Surg*., **31**, 2007, 372-379.
38. Rohlf, F. J. Geometric morphometrics simplified. – *Trends Ecol. Evol*., **20**, 2005,13-14.
39. Rohlf, F. J. TpsSmall Version 1.34.Ecology & Evolution, SUNY at Stone Brook, USA 2017.http://life.bio.sunysb.edu/morph/index.html
40. Rohlf, F. J. TpsDig Version 2.31. Ecology & Evolution, SUNY at Stone Brook, USA 2018. http://life.bio.sunysb.edu/morph/index.html
41. Rohlf, F. J. TpsUtil program Version 1.79.Ecology & Evolution, SUNY at Stone Brook, USA 2019.http://life.bio.sunysb.edu/morph/index.html
42. Rubel, E. W. Auditory system development. In: *Measurement of audition and vision in the first year ofpostnatal life: a methodological overview*. (Eds. G. Gottlieb,& N.A. Krasnegor), New Jersey, Ablex, 1985, 53-90.
43. Sadler, W. T. *Langman's Medical embryology (12th ed.)*, Philadelphia, Lippincott Williams & Wilkins, a Wolters Kluwer, 2012.
44. Siegert, R., H. Weerda, S. Remmert. Embryology and surgical anatomy of the auricle. – *Facial Plast. Surg*., **10**, 1994, 232-243.
45. Slice, D. E. Geometric morphometrics. – *Annu. Rev. Anthropol*., **36**, 2007, 261–281.
46. Som, P. M., H. D. Curtin, K. Liu, M. F. Mafee. Neurographics. – *Head Neck*., **6**, 2016, 332-349.
47. Standring, S. *Gray's Anatomy: The anatomical basis of clinical practice (40th ed.)*. Elsevier Churchill Livingstone, New York, 2008.
48. Viscosi, V., A. Cardini. Leaf morphology, taxonomy and geometric morphometrics: A simplified protocol for beginners. – *PLoS One*., **6**, 2011, e25630.
49. Weerda, H. Embryology and structural anatomy of the external ear. – *Facial Plast. Surg*., **2**, 1985, 85-91.
50. Zelditch, M. L., D. L. Swiderski, H. D. Sheets. *Geometric morphometrics for biologists: a primer*. Amsterdam, Academic Press, 2012.

Institute of Experimental Morphology, Pathology and Anthropology with Museum
Bulgarian Anatomical Society

Acta morphologica et anthropologica, 29 (1-2)
Sofia ● 2022

Anthropometric Characteristics of Limbs and Body Circumferences in Bulgarians with Type 1 Diabetes Mellitus

Atanas Baltadjiev[1], Maria Orbezova[2], Stefan Sivkov[1], Maria Semerdjieva[3], Tsvetanka Petleshkova[1], Maria Ilieva-Gerova[2]*

[1]*Department of Anatomy, Histology and Embryology, Faculty of Medicine, Medical University of Plovdiv, Plovdiv, Bulgaria*
[2]*Department of Endocrinology, Faculty of Medicine, Medical University of Plovdiv, Plovdiv, Bulgaria*
[3]*Department of Management of Healthcare, Faculty of Public Health, Medical University of Plovdiv, Bulgaria*

*Corresponding author e-mail:dr_atanas@abv.bg; atanas.baltadjiev@mu-plovdiv.bg

The purpose of the study was to examine certain limb and body circumferences in Bulgarians with type 1 Diabetes Mellitus and to compare them with healthy subjects. The study included 120 patients aged 20-40 years and 80 healthy Bulgarians at the same age. Measured circumferences: neck, arm, forearm, waist, hip, thigh, and calf. Calculated indices: Waist-to-hip ratio (WHR), Waist-to-thigh ratio (WTR). The circumferences of neck, arm, forearm, hip, thigh, and calf in the healthy men were significantly greater than in male patients. The circumferences of neck, arm, forearm waist and calf in the female patients were significantly greater than in the healthy controls. The value of WHR was significantly greater in the patients of both sexes than in healthy people. Reduction of subcutaneous, but not of visceral adipose tissue in the male patients was detected. The amount of both subcutaneous and visceral adipose tissue was greater in female patients than in healthy women.

Key words: T1DM, Bulgarians, circumferences, WHR, adipose tissue

Introduction

Diabetes mellitus is a chronic metabolic disease, characterized with hyperglycaemia, which is due to impaired insulin secretion, insulin action or both. An estimated 537 million people are affected by the disease worldwide (8.8% of the adult population). Type 2 diabetes makes up about 90% of the cases [9]. Rates are similar in women and men [18]. This number is predicted to rise to 643 million by 2030 and 783 million by 2045 [19]. Diabetes mellitus is the 7th leading cause of death globally [1]. Type 1 diabetes makes up 5 to 15 percent of diabetic patients and often involves children. Type 1 diabetes

mellitus (T1DM) is an autoimmune disease that leads to the destruction of insulin-producing pancreatic beta cells [16]. Autoimmune destruction of β-cells has multiple genetic predispositions and is also related to environmental factors (that are still poorly defined). The destruction of the beta cells in the pancreatic islets over months or years causes an absolute deficiency of insulin. Insulin is an essential anabolic hormone that exerts multiple effects on glucose, lipid, protein, mineral metabolism, and last but not least growth.The chronic hyperglycemia is associated with long-term damage and failure of various organs, especially eyes, kidneys, nerves, heart and blood vessels [2,10].

Most anthropological studies have been performed in patients with type 2 Diabetes mellitus. It is associated with the obesity in these patients. Not many anthropological surveys have been conducted in patients with type 1 Diabetes mellitus worldwide. This anthropological study is original for Bulgarian patients suffering from T1DM.

The **aim** of the study was to examine certain limb and body circumferences in Bulgarians with type 1 Diabetes mellitus and to compare them with healthy subjects. It will clarify the distribution of adipose connective tissue in the bodies of Bulgarian patients with T1DM.

Material and Methods

Patients. The study included 60 female patients and 60 male patients with type 1 Diabetes mellitus aged 20-40 years. The study was conducted in the Clinic of Endocrinology and Metabolic Diseases at the University Hospital «St. George» – Plovdiv, Bulgaria in the period 2019-2022. The mean age of female patients was 29.09±1.29 and 30.08±1.16 of male patients.

The inclusion criteria were: Bulgarian ethnicity, type 1 Diabetes mellitus, duration of the disease no less than one year, clinically compensated diabetes at the time of the study. The exclusion criteria were: previous or existing metabolic, oncological and other disorder that could compromise the anthropological study: thyroid related diseases, adrenal glands related diseases, carcinoma, type 2 Diabetes mellitus, pregnant and lactating women, the presence of heart, respiratory, renal or hepatic failure, proliferative retinopathy, diabetic macroangiopathy, the presence of acute decompensation of metabolic disease at the time of the study, hormonal (contraceptive) therapy less than 3 months prior to the start of the study, treatment of chronic concomitant pathology that could affect hormonal indices.

The present study included 40 healthy Bulgarian women and 40 healthy Bulgarian men at the same age range (controls). The mean age of healthy women was 30±0.47 years and 31.01±0.31 years for healthy men.

All participants have given their written consent in accordance with the Declaration of Helsinki, as the study was approved by the Scientific Ethics Board of the Research Council at the Medical University – Plovdiv.

Methods. We used the anthropological methodic of Martin-Saller, modified by Y. Yordanov.

*Directly measured parameters***.** The following circumferences were measured: neck, arm relaxed (right, in the middle), arm contracted (right, at the greatest diameter), forearm (right, proximal), waist (between the 12th rib and the iliac crest), hip (between

the widest part of the gluteal region and the pubic symphysis), thigh (right, proximal third) and calf (right, the greatest circumference).

Calculated indices. Waist-to-hip ratio (WHR), Waist-to-thigh ratio (WTR)

Statistics. Data were analyzed using statistical software SPSS version 23 (SPSS Inc., Chicago, IL). Statistical significance was considered high at $p \leq 0.001$, moderate – at $p \leq 0.01$, low – at $p \leq 0.05$ and no significance – at $p > 0.05$.

Results

Eight significant differences between the means of measured circumferences in male patients and healthy controls were found. The circumferences' values of thigh and calf in the healthy men were significantly greater than in the male patients ($p<0.001$). The circumferences' values of neck, arm relaxed, arm contracted, forearm and hip in the healthy men were also significantly greater than in male patients, but the degree of statistical significance was low ($p<0.05$). Opposite, the value of waist circumference in male patients was significantly higher than in healthy men ($p<0.05$). These results are shown in **Table 1**.

Table 1. Limb and body circumferences in male patients with type 1 Diabetes mellitus and healthy men

circumferences	Male patients				Healthy men				P
	N	Mean	SE	SD	N	Mean	SE	SD	
Neck	60	38.08	0.49	2.81	40	39.06	0.26	1.63	p<0.05
Arm relaxed	60	27.77	0.66	3.77	40	29.48	0.46	2.86	p<0.05
Arm contracted	60	31.62	0.71	4.10	40	33.75	0.50	3.13	p<0.05
Forearm	60	26.72	0.40	2.28	40	27.66	0.25	1.56	p<0.05
Waist	60	84.46	1.76	10.13	40	80.57	1.08	6.74	p<0.05
Hip	60	95.38	1.28	7.37	40	98.76	1.06	6.59	p<0.05
Thigh	60	53.45	1.21	6.96	40	58.50	0.83	5.20	p<0.001
Calf	60	35.93	0.54	3.12	40	38.40	0.40	2.51	p<0.001

The values of both indices W/H ratio and W/T ratio were significantly higher in the male patients than in healthy men, shown in **Table 2**. The degree of statistical significance was high ($p<0.001$).

Our team found five statistically significant differences between the means of circumferences in female patients and healthy women. The circumferences' values of neck, forearm and waist in the female patients were significantly greater than in healthy controls ($p<0.001$). The circumference's values of arm contracted and calf in female patients were significantly greater than in healthy women ($p<0.05$). The results are shown in **Table 3**.

Table 2. Calculated indices in male patients with type 1 Diabetes mellitus and healthy men

Indices	Male patients				Healthy men				P
	N	Mean	SE	SD	N	Mean	SE	SD	
W/H ratio	60	0.88	0.01	0.06	40	0.82	0.06	0.04	p<0.001
W/T ratio	60	1.59	0.03	0.15	40	1.39	0.01	0.06	P<0.001

Table 3. Limb and body circumferences in female patients with type 1Diabetes mellitus and healthy women

circumferences	Female patients				Healthy women				P
	N	Mean	SE	SD	N	Mean	SE	SD	
Neck	60	33.72	0.36	1.20	40	31.27	0.29	1.70	p<0.001
Arm relaxed	60	26.81	0.69	3.80	40	25.61	0.46	2.71	p>0.05
Arm contracted	60	29.12	0.72	3.97	40	26.55	0.46	2.70	p<0.05
Forearm	60	24.38	0.36	1.96	40	22.97	0.26	1.52	p<0.001
Waist	60	75.67	1.54	8.43	40	67.98	1.07	6.22	p<0.001
Hip	60	99.17	1.65	9.02	40	98.62	1.28	7.46	p>0.05
Thigh	60	57.99	1.29	6.93	40	55.33	1.81	1054	p>0.05
Calf	60	35.68	0.60	3.26	40	33.85	1.01	5.88	p<0.05

The value of W/H ratio was significantly greater in the female patients than in healthy women. The degree of statistical significance was high (p<0.001), shown in **Table 4**.

Table 4. Calculated indices in female patients with type 1 Diabetes mellitus and healthy women

Indices	Female patients				Healthy women				P
	N	Mean	SE	SD	N	Mean	SE	SD	
W/H ratio	60	0.76	0.01	0.05	40	0.69	0.01	0.05	p<0.001
W/T ratio	60	1.31	0.02	0.10	40	1.28	0.07	0.38	p>0.05

Discussion

Anthropological measurements of certain body's circumferences are used for assessment of deposition of adipose connective tissue in different parts of the human body. Waist circumference is very important. Its value is indirectly related to the deposition of visceral adipose tissue intra-abdominal. The values of anthropological parameters waist circumference, hip circumference and thigh circumference are used for calculating the following indices: waist-to-hip ratio (WHR) and waist-to-thigh ratio (WTR). These indices are mainly used to evaluate the degree of obesity in humans. WHR is closely related to the deposition of visceral fat tissue into abdominal cavity. Obesity, particularly visceral, is very common in patients with T2DM [3, 11, 14].

Although the impaired glucose metabolism is essential for both type 1 and type 2 Diabetes mellitus, the pathogenesis is very different between the two conditions. The examined anthropological parameters waist circumference (WC) and WHR are useful to predict the presence of metabolic syndrome in adult patients with T1DM [7, 13]. Some authors reported about the relationship between central obesity and retinopathy, as well as other complications in patients with T1DM [8, 15].

We found that the values of the following circumferences: neck, arm (both contracted and relaxed), forearm, hip, thigh, and calf were significantly lower than the same in healthy men. In our opinion these findings are related to some reduction of subcutaneous connective fat tissue. On the contrary, the waist circumference in male patients was greater than in healthy controls. The values of WHR and WTR were significantly greater in men with DMT1than in healthy men. In our opinion the accumulation of visceral fat tissue is greater in the male patients than in the controls. It didn't occur any reduction of intra-abdominal fat tissue in the body of male patients. Similar results were reported by Fernández-Miró et al. [6].

Not the same results were found for female patients in the current study. The values of the measured circumferences: neck, arm contracted, forearm, waist and calf were significant lyreater in female patients than in healthy women. Cho et al. reported that the large neck circumference had a negative impact in the development of DM [4]. This is the result of more subcutaneous fat deposition in these parts of the female body. We found that the value of WHR was higher in female patients than in healthy women. It is in accordance with significant greater value of waist circumference in female patients than in the controls. In our opinion the accumulation of visceral fat tissue is greater in the female patients than in the healthy women. Darabian et al., and Momesso et al. reported close to our results concerning the accumulation of visceral fat tissue in patients with T1DM [5,12]. Wegeberg et al. reported lack of reduction of subcutaneous fat tissue in patients with T1DM [17].

The values of measured circumferences can be used for calculating of the somatotype's components of Bulgarian patients suffering from T1DM.

Conclusion

The data of the survey show that healthy men have greater circumferences of neck, arm (contracted and relaxed), forearm, hip, thigh, and calf than in men diagnosed with type 1 Diabetes mellitus. The circumference of waist is greater in male patients.

Opposite, the circumferences of neck, arm (contracted), forearm, waist and calf are greater in female patients with type 1 DM than in the healthy women. The values of WHR were higher in the patients with type 1 DM of both sexes in comparison to healthy individuals. Reduction of subcutaneous, but not of visceral adipose tissue in male patients suffering from T1DM was detected. The amount of both subcutaneous and visceral adipose tissue was greater in female patients than in healthy women.

Acknowledgements: This study is supported by Medical University of Plovdiv, Bulgaria. This article is part of a scientific project № HO - 03/2019 "Morpho-anthropological characteristics of patients suffering from type 1 Diabetes mellitus", Medical University of Plovdiv, Bulgaria.

References

1. "The top 10 causes of death". www.who.int*.,* 2020.
2. American Diabetes Association. Diagnosis and classification of diabetes mellitus. *Diabetes Care*. **33** Suppl., 2010, 62-69.
3. Andreenko, E., M. Nikolova. Age features in the development of the subcutaneous fat tissue, muscularity and muscle-fat rations in men with different physical activity. – *Glasnik, Antropološkog društva Srbije*, **43**, 2008, 478-487.
4. Cho, N., T. Oh, K. Kim, S. H. Choi, J. H. Lee, K. S. Park, H. C. H. Jang, J. Y. Kim, H. K. Lee. Neck circumference and incidence of diabetes mellitus over 10 years in the Korean genome and epidemiology study (KoGES). – *Sci.* Rep., **5**, 2015**,** 18565.
5. Darabian, S., J. Y. C. Backlund , P. A. Cleary , N. Sheidaee, I. Bebu. Significance of epicardial and intrathoracic adipose tissue volume among type 1 diabetes patients in the DCCT/EDIC: A pilot study. – *Plos One*, **11**(7), 2016
6. Fernández-Miró, M., J. J. Chillarón, M. Albareda, S. Fontserè, C. Colom, L. Vila, J. Pedro-Botet, J. A. Flores LE-Roux. TEST-T1D study group. Hypertriglyceridemic waist in type 1 diabetes patients: prevalence and related factors. – *Minerva Endocrinol*., **42**(1), 2017, 1-7.
7. Ferreira-Hermosillo, A., C. Ramírez-Rentería, V. Mendoza-Zubieta, M. A. Molina-Ayala. Utility of the waist-to-height ratio, waist circumference and body mass index in the screening of metabolic syndrome in adult patients with type 1 diabetes mellitus. – *Diabetology & Metabolic Syndrome,* **6**, 2014, 2-10.
8. Hägg, S., L. M. Thorn, C. M. Forsblom, D. Gordin, M. Saraheimo, N. Tolonen, J. Wadén, R. Liebkind, J. Putaala, T. Tatlisumak, Per-Henrik Groop. Different risk factor profiles for ischemic and hemorrhagic stroke in type 1 diabetes mellitus. – *Clinical Sciences*, **45**, 2014, 2558-2562.
9. IDF Disbetes Atlas Ninth Edition 2019/2021"(PDF). www.diabetesatlas.org*.,* 2021.
10. Lucier, J., R. S. Weinstock. Diabetes mellitus type 1. In: StatPearls [Internet]. Treasure Island (FL): StatPearls Publishing; 2022. Available from: https://www.ncbi.nlm.nih.gov/books/NBK507713/
11. Mladenova, S., M. Nikolova, D. Boyadzhiev. Body mass index, some circumference indices and their ratios for monitoring of physical development and nutritional status of children and adolescents. – *Acta morphol. anthropol.,* **10**, 2005**,** 226-229.
12. Momesso, D. P., I. Bussade, M. A. Epifanio, C. D. S. Schettino, L. Au. T. Russo, R. Kupfer. Increased epicardial adipose tissue in type 1 diabetes is associated with central obesity and metabolic syndrome. – *Diabetes Research and Clinical Practice*, **91**(1), 2011, 47-53.

13. Mutter, S., E.B. Parente, V. Harjutsalo, A. J. Ahola, C. Forsblom, P. H. Groop. Waist-height ratio and waist circumference are the best estimators of visceral fat in type 1diabetes independently of diabetic nephropathy. – *EASD, VM*, 2020.
14. **Nikolova, M., S. Mladenova.** Anthropometric indicatoris for assessment of body composition. – *Acta morphol. anthropol.*, **10**, 2005, 218-225.
15. **Parente, E., V. Harjutsalo, C. Forsblom, Per-Henrik Groop.** Waist-height ratio and the risk of severe diabetic eye disease in type 1 diabetes: A 15-year cohort study. – *The Journal of Clinical Endocrinology & Metabolism*, **107(2)**, 2022, 653-662.
16. **Vos T, A. D. Flaxman, M. Naghavi, R. Lozano, C. Michaud, M. Ezzati M.**"Years lived with disability (YLDs) for 1160 sequelae of 289 diseases and injuries 1990-2010: a systematic analysis for the Global Burden of Disease Study 2010". – *Lancet,* **380** (9859), 2012, 2163-2196.
17. **Wegeberg, A. M., T. Meldgaard, A. Baek, A. M. Drewes, M. Vyberg, N. Jessen, B. Brock, C. Brock**. Subcutaneous adipose tissue composition and function are unaffected by liraglutide-induced weight loss in adults with type 1 diabetes. – *Basic Clin. Pharmacol. Toxicol*., **128**(6), 2021, 773-782.
18. What is Diabetes?. *Centers for Disease Control and Prevention.* 2020.

Institute of Experimental Morphology, Pathology and Anthropology with Museum
Bulgarian Anatomical Society

Acta morphologica et anthropologica, 29 (1-2)
Sofia ● 2022

Morton's toe Frequency among the Bulgarian Population and its Association with High Arched Foot

Desislava Marinova, Meglena Angelova, Veselina Zhekova*

Department of Anatomy and Cell Biology, Medical University "Prof. Dr. Paraskev Stoyanov", Varna, Bulgaria

*Corresponding author e-mail: angelovameglena@gmail.com

The human foot must be enough flexible to absorb the ground reaction forces and stiff enough for weightbearing. The medial foot arch has been recognized as a key component in the overall function of the foot. We studied the Morton's toe frequency in Bulgaria among randomly selected men and women aged 18 to 60 years. The foot arch height was investigated. For this purpose we used the common and well established method based on footprints. We combined the measurements of the Clarke angle and the Chippaux-Smirak index to divide the footprints into three groups: normal, high arched and flat foot. Our results show a high prevalence of Morton's toe in the Bulgarian population and a higher frequency of a high arched foot compared to flat one. The statistical data analysis (the χ^2 test) proved an association between the high arched foot and Morton's toe ($p \leq 0.05$).

Key words: foot arch, brachimetatarsia, Morton's toe

Introduction

The human foot plays a key role in supporting the weight of the body, in keeping a stable upright posture and in providing the locomotion. It must be enough flexible to absorb the ground reaction forces and stiff enough for weightbearing. These unique functions of the human foot are defined by its anatomical structure and mainly by its three arches. The medial longitudinal arch is higher than the lateral one and is composed of the calcaneus, the talus, the navicular, the three cuneiforms, and the first, second, and third metatarsals bones. Elasticity is the main characteristic of this arch. The medial arch has an important role in shock absorption and the propulsion during walking and running, so its features have been recognized as a key component in the overall function of the foot during gait [3].

Adequate foot diagnostics requires modern and repeatable technics for assessment of foot construction, based on strictly defined, reliable and repeatable methods of measurement. Morphological examinations use common, simple methods based on

footprint (plantogram) analysis: Arch index, Staheli arch index, Chipaux-Smirak index, Sztriter-Godunow Index, Clarke angle, [7, 9, 12], etc. According to these indices the foot types are classified as normal, high arched foot and flat foot.

The features and shape of the human foot have aroused interest since ancient times. Several types of soles are described according to their shape and toe length. One of the most common is the Greek foot, which can be seen in many statues from ancient Greece: Venus de Milo and also in the Michelangelo's David. This type of foot is characterized with longer second toe compared to the first one. The condition is named Morton's toe after the orthopedic surgeon Dudley J. Morton (1884–1960) in the early 20th century [11].

Morton's toe is a congenital condition with brachimetatarsia [8]. In these cases the first metatarsal bone is shorter than the second one. It is usually asymptomatic, but in some occasions the hypermobility or instability of the first metatarsal bone can result in gait changes, in caluses formation and hammertoes [11].

Materials and Methods

Footprints (plantograms) of randomly selected 102 Bulgarian men and women, without malformations, surgery or traumas of the foot, aged 18 to 60 years were collected after their written consent. The study was approved by the Research Ethics Committee at the Medical University "Prof. Dr. P. Stoyanov" with protocol №140/01.07.2021 and will continue until 600 participants are gathered.

The footprints representing second toe longer with at least 1,5 mm than the first one, were described as Morton's toe positive.

The collected footprints were examined by measuring the Clarke angle and the Chippaux-Smirak index.

Clarke's angle is defined as the angle obtained by a tangent line joining the medial edges of the first metatarsal head and the heel, and the second line that connects the first metatarsal head and the acme of the medial longitudinal arch concavity [3] (**Fig. 1A**). Based on the Clarke's angle value the foot is normal with Clarke's angle between 42° and 54°, flat when the angle is less than 41° and with high medial arch when the Clarke's angle is more then 54°.

Chippaux-Smirak index is the ratio of the maximum support width of the metatarsals to the minimum support width of center of the arch (**Fig. 1B**) [7]. Thus, Chippaux-Smirak index = AB/CD×100 % (**Fig. 1B**) [7]. In the cases with Chippaux-Smirak index between 25% and 45% the foot is considered as normal. If the Chippaux-Smirak index is more than 45% the foot is described as flat (pes planus) and when the index is less than 25% – as high arched foot.

According to these observations and measurements, study participants were divided into three groups: normal, high arched and flat foot, based on both Clarke's angle and Chippaux-Smirak index values. The frequency of Morton's toe in each group was studied.

The statistical data analysis was performed using the χ^2 test and $p \leq 0.05$ was accepted as statistical reliability.

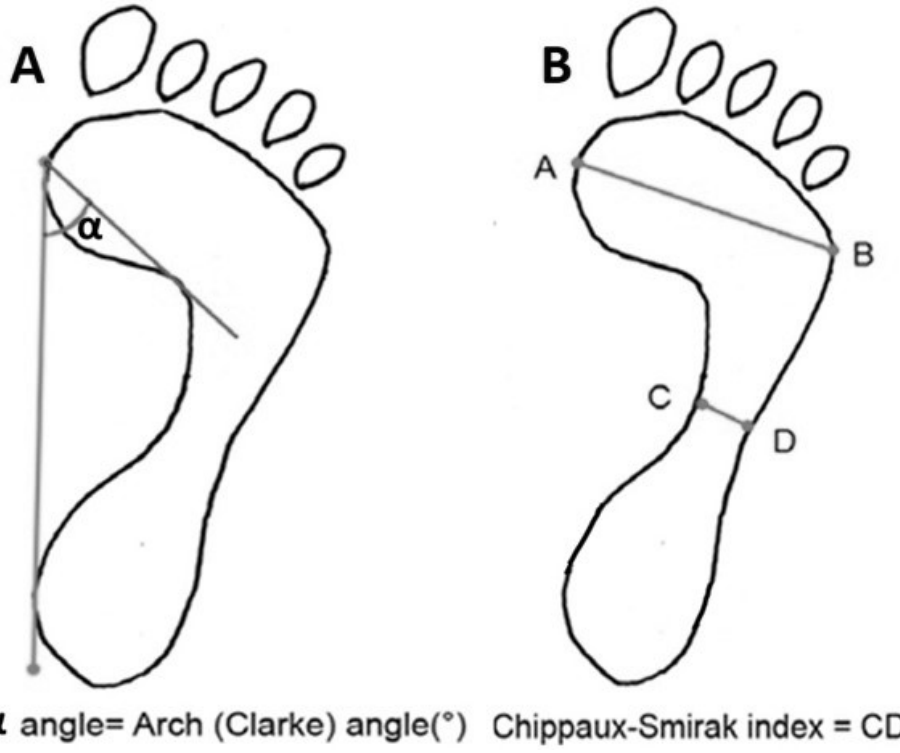

Fig. 1. A. Clarke's angle (α angle) is obtained by a tangent line joining the medial edges of the first metatarsal head and the heel, and the second line that connects the first metatarsal head and the acme of the medial longitudinal arch concavity. **B.** Chippaux-Smirak index is the ratio of the maximum support width of the metatarsals (AB line) to the minimum support width of center of the arch (CD line). Thus, Chippaux-Smirak index = AB/CD×100 % [7].

Results

Forty six (46) out of 102 plantograms were positive for Morton's toe or 45% of the participants were with shorter first toe compare to the second one (**Fig 2**.).

According to the values of Clarke's angle and Chippaux-Smirak index 85 were with normal, seven – with flat and ten persons with high arched foot. Expressed in percentages these results show that 6,86 % of the included footprints are characterized as flat ones and 9,80% as high arched foot.

Within the Morton's toe positive group, 17,40 % of the foot prints were with high medial arch. In the Morton's toe negative group this percentage was 3,58 %.

The further statistical analysis (the χ^2 test) proved an association between the high arched foot and Morton's toe ($p \leq 0.05$) and showed no association between the flat foot condition and the Morton's toe (**Fig. 3**).

Fig. 2. A. Morton's toe negative footprint. **B.** Morton's toe positive footprint (second toe is longer than the first one). α – Clarke's angle. AB line – the maximum support width of the metatarsals; CD line - the minimum support width of center of the arch. Chippaux-Smirak index = AB/CD×100 %.

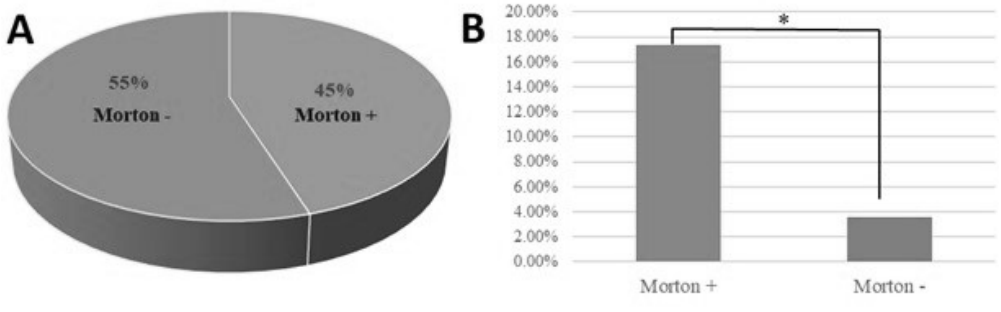

Fig. 3. A. 45% of all plantograms in our study are Morton's toe positive. B. In 17,40 % in the Morton's toe positive group the foot prints were with high medial arch. In the Morton's toe negative group this combination is observed only in 3,58 % ($\chi 2$ test, $p \leq 0.05$).

Discussion

Morton's toe is a congenital shortening of the first metatarsal bone. The secondary ossification center is different in this bone and in the other four metatarsal bones. It appears in the proximal end of the first metatarsal and in the distal ends of the second to fifth metatarsal bones. The premature closure of the epiphysis of the first metatarsal causes Morton's toe condition.

The Morton's toe has been observed with varying prevalence in different populations. The results show frequency of the condition between 0,05% and more than 50% [11]. Our data show a high prevalence of Greek foot in the Bulgarian population.

Static foot assessment is one of the commonly used methods to get information and make clinical decisions in order to identify possible etiological factors of the lower extremity dysfunctions and injuries. The results when using only one method are quite variable and in practice the combined use of several parameters in the evaluation of plantograms is preferred. The accuracy of the Clarke's angle itself is estimated to be 68% and the accuracy of the Chippaux-Smirak index – 80%. The experimental results using a combination of indicators show that an accuracy of the result is up to 93% more than the single index [1]. For this reason we combined these two measurements.

The results of this study show that the high arched foot is more common in Bulgarian population than the flat foot. This type of foot is often underestimated as a cause of complaints and problems involving the entire lower limb.

The data showed a higher frequency of high arched foot in Morton positive participants. This is a combination of two conditions that lead to impaired morphology and function of the medial arch, which can disturb the distribution of body weight during gait and result in compensatory changes in adjacent joints of the lower limb and predisposition to low energy trauma. Common complication is metatarsalgia (a pain under heads of metatarsals), predominantly under second toe due to increased weight forces during the propulsive phase of gait. This is because the second metatarsal head is farthest forward and the force is transferred through it. Along with high medial arch, which makes the foot rigid with less surface area for absorbing impact, there is excessive pressure on rearfoot and forefoot areas. This can make the leg susceptible to foot conditions such as heel pain, plantar fasciitis and metatarsalgia [4, 5, 6, 10].

Conclusions

Morton's toe, which is primarily a genetically determined condition, is very common in the Bulgarian population. The high arched foot is significantly more common than the flat foot. We found that Morton's toe is associated with a higher incidence of high arched foot.

Acknowledgements: We thank the colleagues from the Medical Center for Rehabilitation and Sports Medicine -1, Varna for the opportunity to use their base.

References

1. **Aruntammanak, W., Y. Aunhathaweesup, W. Wongseree, A. Leelasantitham, S. Kiattisin.** Diagnose flat foot from foot print image based on neural network. – *Computer Science*, **1** 2013. Available at https//DOI:10.1109/BMEICON.2013.6687684Corpus ID: 27733508
2. **Ayub, A., S. H. Yale, C. Bibbo.** Common foot disorders. – *Clin. Med. Res.,* **3**, 2005, 116-119.
3. **Gray, H.** *Anatomy of the human body* (Ed. W.H.Lewis), 20th edition, NY, 2000. Available at http://www.Bartleby.com.
4. **Hong, W. H., Y. H. Lee., H. C. Chen, Y.C. Pei, C. Y. Wu**. Influence of heel height and shoe insert on comfort perception and biomechanical performance of young female adults during walking. – *Foot Ankle Int.,* **26**, 2005, 1042-1048.
5. **Kouchi, M., M. Kimura, M. Mochimaru.** Deformation of foot cross-section shapes during walking. – *Gait Posture,* **30**, 2009, 482-486.
6. **Lee, Y. H., W. H. Hong.** Effects of shoe inserts and heel height on foot pressure, impact force, and perceived comfort during walking. – *Appl. Ergon.,* **36**, 2005, 355-362.
7. **Open University of Cyprus. Nicosia.** Cyprus Available at://www.omim.org/entry/189200
8. **Ozer, C. M.** Evaluation of the sole morphology of professional football players. – *International Sportmed Journal*, **13**, 2012, 1, 8-17.
9. **Papaliodis, D. N., M. A. Vanushkina, N. G. Richardson, J. A. DiPreta**. The foot and ankle examination. – *Med. Clin. N. Am*., **98**, 2014, 181–204.
10. **Umberto, A. M., C. Valentina, L. Mangiavini, M. Palmucci.** Is it still current to talk about frst ray hypermobility? – *Acta Biomed.*, **90**, 2019, Supplement 1, 32-35.
11. **Vounotrypidis, P., P. Noutsou**. Greek foot: is it a myth or reality? An epidemiological study in Greece and connections to past and modern global history. – *British Journal of Rheumatology*, **54**(suppl_1), 2015, i182-i183.
12. **Xiong, S., R. S. Goonetilleke, C. P. Witana, T. W. Weerasinghe, E. Au.** Foot arch characterization: a review, a new metric and a comparison. – *J. Am. Podiatr. Med. Assoc.,* **100**, 2010, 14-24.

Institute of Experimental Morphology, Pathology and Anthropology with Museum
Bulgarian Anatomical Society

Acta morphologica et anthropologica, 29 (1-2)
Sofia ● 2022

Study of the Facial Index in Young Bulgarians by 3D laser Scanning

Tsvetanka Petleshkova[1], Stefan Sivkov[1], Atanas Baltadjiev[1], Hristo Manev[2], Ralitza Raycheva[3], Pavel Timonov[4], Vasilena Beleva[5]*

[1]Department of Anatomy, Histology and Embryology, Faculty of Medicine, Medical University of Plovdiv, Plovdiv, Bulgaria
[2]Department of Medical Physics and Biophysics, Faculty of Pharmacy, Medical University of Plovdiv, Plovdiv, Bulgaria
[3]Department of Social Medicine and Public Health, Faculty of Public Health, Medical University of Plovdiv, Plovdiv, Bulgaria
[4]Department of Forensic Medicine and Deontology, Faculty of Medicine, Medical University of Plovdiv, Plovdiv, Bulgaria
[5]Student, Faculty of Medicine, Medical University of Plovdiv, Plovdiv, Bulgaria

*Corresponding author e-mail: Tsvetanka.Petleshkova@mu-plovdiv.bg

The aim of the present study was to provide information about the type of face in young Bulgarian adults. The three-dimensional coordinates of several soft-tissue landmarks on the face were obtained using hand-held laser scanner in 95 healthy individuals (46 males and 49 females) of Bulgarian origin aged 21-30 years. From the landmarks bizygomatic breadth and morphological face height were calculated and averaged for sex. The face was classified into five different types based on the values of facial index, according to the categories of Garson. For morphological facial index most of the males fell in the categories mesoprosop – 30.43 % and leptoprosop – 26.09 % and females in the category leptoprosop - 38.78%. Equal percentages of the females fell in the categories mesoprosop and hyperleptoprosop - 26.53%. The data obtained in the present study can be used in aesthetic and maxillofacial surgery, forensic anthropology.

***Key words**:* 3D laser scanning, facial index, Bulgarians

Introduction

The quantitative facial characteristics have been subject of research in many studies of gender differences and ethnic characteristics in different populations [2, 17, 21].

Data providing information on the shape, size and proportions of the face are used in fields of medicine - rhinoplasty, maxillofacial and aesthetic surgery. The methods of identification in forensic medicine are based on the anthropological characteristics of the subject and must be based on reliable comparative measurements [7, 12, 14].

The data on the facial morphology in different age groups of the Bulgarian population obtained so far have been compiled by the methods of classical direct cephalometry [10, 11, 20]. With the development of new computer technologies, creation of three-dimensional digital images of the face became possible. Digital cephalometry is a fast and non-invasive method that avoids the compression of soft tissues, the possibility of making mistakes when repeatedly collecting data from the subjects [15].

The **aim** of this study was to evaluate the facial index in young Bulgarians and to determine the dominant facial type using 3D laser scanning.

Material and Methods

Subjects: The sample included 95 healthy Bulgarians (46 males and 49 females) aged 21-30 years, who had no history of surgery, facial injury, craniofacial anomalies, and mental disorders. Subjects with different ethnicity were excluded from the study. The study was conducted in accordance with the **Declaration of Helsinki Ethical** Principles for research involving human subjects. The participants gave their informed consent to participate in the study after the aim and procedures had been priorly explained.

Collection of three-dimensional landmarks*:* Three-dimensional images were obtained from each subject using a hand-held laser scanner (FastSCAN Cobra, Polhemus Inc., Colchester VT). The scanner incorporates motion tracking technology to achieve 3D computer reconstruction of the subject's face. Two sensors, one attached to the optics and another to a headband, are used to track both the position of the optics and any movement of the subject's head. Following instruction to keep eyes (for safety) and mouth (for uniformity) closed and to maintain a blank expression, the stripe of low intensity laser light is manually swept smoothly over the subject's face. Four vertical sweeps are generally used to record the entire facial surface. Captured data are postprocessed to produce a single surface dataset; postprocessing parameters can be varied to alter the resolution of the final surface [4].

On each of the obtained images a set of anthropometric landmarks were placed: nasion (n); gnathion (gn); zygion (zy_r, zy_l) [18]. The procedure was performed by a single operator (**Fig. 1**). Using these three-dimensional landmarks, the bizygomatic breadth (zy_r-zy_l) and morphological facial height (n-gn) were measured (**Table 1**). The measurements were used to calculate **the morphological facial index** = morphological facial height (n-gn) / bizygomatic breadth (zy_r-zy_l) × 100. According to the values obtained for morphological facial index the subjects were divided into categories after Garson [Cited by 20].

Males	*Females*
Hypereuriprosop = x – 78.9	**Hypereuriprosop** = x – 76.9
Euriprosop = 79.0 – 83.9	**Euriprosop** = 77.0 – 80.9
Mesoprosop = 84.0 – 87.9	**Mesoprosop** = 81.0 – 84.9
Leptoprosop = 88.0 – 92.9	**Leptoprosop** = 85.0 – 89.9
Hyperleptoprosop = 93.0 – x	**Hyperleptoprosop** = 90.0 – x

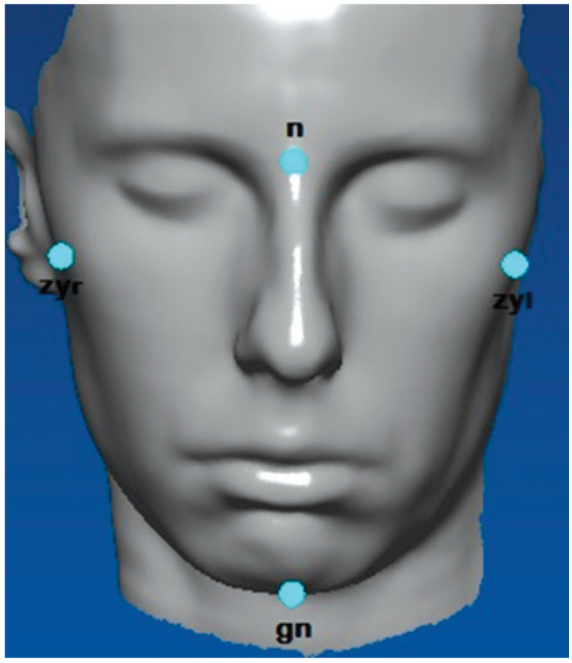

Fig. 1. Facial landmarks on three-dimensional image**.**

Table 1. Description of the facial landmarks and measurements

Landmarks/ Measurements	**Description**
Nasion (n)	A point located on the soft tissue contour at the base of the root of the nose at the level of the frontonasal suture.
Gnathion (gn)	The lowest point in the middle of the lower border of the chin.
Zygion (zy_r, zy_l)	The most lateral point of the soft tissue contour on each of the zygomatic arches.
Bizygomatic breadth	The linear distance between the two points zygion (zy_r-zy_l)
Morphological face height	The linear distance between nasion to gnation (n-gn)

Statistics: Descriptive statistics (mean±standard deviation / proportion±standard error), independent samples t-test (to compare the means between two unrelated groups on the same continuous normally distributed variables), Mann-Whitney U test (to compare two distributions in independent samples) and two-samples z-test (to compare two independent proportions) were used for the data analysis. Statistical significance was set at $\alpha \leq 0.05$. Intra-rater reliability was measured with Cohen's kappa coefficient (κ) in SPSS (Kappa value = 0.823.3).

Results

The measurements of the bizygomatic breadth (zy_r-zy_l) and morphological facial height (n-gn) of the sample subjects are presented on **Table 2.** These were used to determine the morphological facial index in males and females (**Table 2**). The values of the morphological facial index allowed to define the incidence of the facial phenotypes. The results from the categorization of males and females according to the morphological facial index are shown in **Table 3**.

Table 2. The craniofacial parameters of the examined subjects

Variable	Sex	Mean	SD	Min	Max	Statistical significance
Morphological face height (mm)	males	126.18	6.73	113.46	136.56	p<0.001
	females	117.99	7.18	103.99	134.04	
Bizygomatic breadth (mm)	males	146.25*	11.24**	129.68	168.07	p<0.001***
	females	135.41*	7.16**	123.47	151.26	
Morphological facial index	males	85.90	6.08	72.45	101.82	p>0.05
	females	87.20	4.80	76.68	101.48	

* median – in case of incorrect distribution of data
** interquartile range
*** Mann-Whitney U test

Table 3. Morphological facial index. Distribution of the individuals into categories (after Garson)

Categories	Males n, (%)	Females n, (%)	Statistical significance
hypereuriprosop	6, (13.04)	1, (2.04)	**p<0.05**
euriprosop	9, (19.57)	3, (6.12)	**p<0.05**
mesoprosop	14, (30.43)	13, (26.53)	p>0.05
leptoprosop	12, (26.09)	19, (38.78)	p>0.05
hyperleptoprosop	5, (10.87)	13, (26.53)	p>0.05
Total	**46 (100)**	**49 (100)**	

Most of the males fell into the categories mesoprosop – 30.43 % and leptoprosop – 26.09%. In the categories euriprosop, hypereuriprosop and hyperleptoprosop the males were at lower percentages – 19.57%, 13.04% and 10.87%, respectively. Most of the female subjects were in the category leptoprosop – 38.78%. Equal percentages

were found for categories mesoprosop and hyperleptoprosop – 26.53%. Only 6.12% and 2.04% of the females fell into the categories euriprosop and hypereuriprosop. Statistically significant differences between genders were found in two of the categories – hypereuriprosop (z=2.1, p=0.040) and euriprosop (z=2.0, p=0.049).

Discussion

The morphological facial index gives an idea of the length-width proportions of the face. So far, the study of the faces of Bulgarian males and females has been carried out using the methods of classical direct cephalometry. The results obtained by us through this new three-dimensional method for analysis of facial morphology are close to those obtained in previous studies [20]. The largest percentage of males in both studies fall into the categories of mesoprosop and leptoprosop. In the previous study, the highest percentage of males was with medium, long and very long faces. In our results, the highest percentage of males was with medium, long and wide faces. In both studies, the largest percentage of females has long, very long and medium faces.

In a study of the morphological facial index in Serbian males and females, the highest percentage of subjects were in the category leptoprosop – 76.6% and 87.06%, respectively. Mesoprosop and hyperleptoprosop facial types (medium and very long narrow faces) presented at low percentage. No euriprosops and hypereuriprosops (short broad face and very short broad face) were found [6]. In a study of the facial shape types in the Turkish population mesoprosops and euriprosops were found to be the dominant facial types (medium and short broad face). Hypereuriprosops (very short broad faces) occurred at a lower but still relatively high percentage [13]. In a study of Chinese students most of the females had leptoprosop facial type, while males presented mostly as mesopropops [1]. In a study of Nepalese males and females the dominant facial types were leptoprosop and hyperleptoprosop (long narrow face and very long narrow faces) [16]. The same dominant facial type was found in Indian males [3]. In a study evaluating the sexual difference and variation of facial index among Kashmiri population males were mostly with leptoprosopic face, while females with mesoprosopic face [8]. In Malaysian males and females, the dominant facial type was mesoprosop [19]. A research of three ethnic groups in Nigeria found that the dominant facial type in both genders was hyperleptoprosop (very long narrow faces), occurring at very high percentage in females [9]. In a study of Japanese students, the dominant facial type in females was euriprosop and mesoprosop [5]. These studies indicate that considerable ethnic and racial variation exists in facial index and in most populations significant sexual difference is present.

Conclusion

The results obtained in our study show that the most common facial type in males is mesoprosop and in females is leptoprosop. The second common facial type in males is leptoprosop and in females mesoprosop and hyperleptoprosop. The data for the facial proportional analysis in the different populations can be used in the planning and reporting the results in the aesthetic and maxillofacial surgery.

References

1. **Calvin, K., S. Susiana, H. Winsa**. Facial indices in Chinese ethnic students aged 20-22. – *Journal of Dentistry Indonesia*, **19(1)**, 2012, 1-4.
2. **Celebi, A. A., C. H. Kau, F. Femiano, L. Bucci, P. Perillo**. A three-dimensional anthropometric evaluation of facial morphology. – *J. Craniofac. Surg.,* **29 (2)**, 2018, 304–308.
3. **Doni, P. K., C. S. Janaki, V. Vijayaraghavan, U. Delhiraj**. A study on measurement and correlation of cephalic and facial indices in males of south Indian population. – *Int. J. Med. Res. Health Sci.*, **2(3)**, 2013, 439-446.
4. **Hennessy, R. J., A. Kinsella, J. L. Waddingtona**. 3D laser surface scanning and geometric morphometric analysis of craniofacial shape as an index of cerebro-craniofacial morphogenesis: initial application to sexual dimorphism. – *Biological Psychiatry,* **51(6)**, 2002, 507-514
5. **Hossain, M. G., A. Saw, F. Ohtsuki, P. E. Lestrel, T. Kamarul**. Change in facial shape in two cohorts of Japanese adult female students twenty years apart. – *Singapore Med. J.,* **52(11)**, 2011, 818-823.
6. **Jeremić, D., S. Kocić, M. Vulović, M. Sazdanović, P. Sazdanović, B. Jovanović, J. Jovanović, Z. Milanović, N. Donović, A. Simović, K. Parezanović-Ilić, A. Maliković, J. Toševski, I. živanović-Mačužić**. Anthropometric study of the facial index in the population of central Serbia. – *Arch. Biol. Sci*., **65 (3)**, 2013, 1163-1168.
7. **Koudelová, J., J. Dupej, J. Brůžek, P. Sedlak, J. Velemínská.** Modelling of facial growth in Czech children based on longitudinal data: Age progression from 12 to 15 years using 3D surface models. – *Forensic. Sci. Int.,* **248**, 2015, 33-40.
8. **Latoo, S. H., S. Gupta, M. Shafi Dar**. Study of prosopic index in Kashmir: A population based cross-sectional study. – *IAIM*, **7(12)**, 2020, 39-43.
9. **Maina, M. B., O. Mahdi, G. G. Kalayi.** Craniofacial forms among three dominant ethnic groups of Gombe state, Nigeria. – *Int. J. Morphol*., **30(1)**, 2012, 211-216.
10. **Nacheva, A., J. Zhecheva, I. Yankova, Z. Filcheva, Z. Mitova, Y. Yordanov.** *Physical development of children and youths in Bulgaria on the borderline between 20th and 21st century.* Sofia, Prof. Marin Drinov Academic Publishing House, 2012. [in Bulgarian]
11. **Nikolova, M., S. Mladenova**. Morphological peculiarities in the cephalic and facial structure in children and adolescents from three generations from the town of Plovdiv, *85th Aniversary of the Department of Anatomy and Histology, Anatomical collection, Medical University of Sofia*, 2003, 64-66.
12. **Ogawa, Y., B. Wada, K. Taniguchi, S. Miyasaka, K. Imaizumi**. Establishment of large-sample standard reference data for personal identification using a three-dimensional capture system. – *Forensic Sci. Int.,* 257, 2015, 511.e1-9.
13. **Ozsahin, E., E. Kizilkanat, N. Boyan, R. Soames, O. Oguz**. Evaluation of face shape in turkish individuals. – Int. J. Morphol., **34(3)**, 2016, 904-908.
14. **Ritz-Timme, S., P. Gabriel, J. Tutkuviene, P. Poppa, Z. Obertová, D. Gibelli, D. De Angelis, M. Ratnayake, R. Rizgeliene, A. Barkus, C. Cattaneo**. Metric and morphological assessment of facial features: a study on three European populations. – *Forensic Sci. Int.,* **207(1-3)**, 2011, 239.e1-8.
15. **Sforza, C., V. Ferrario.** Soft-tissue facial anthropometry in three dimensions: from anatomical landmarks to digital morphology in research, clinics and forensic anthropology. – *J. Anthropol. Sci*., **84**, 2006, 97-124.
16. **Shrestha, R., N. Shrestha, H. P. Upadhyay**. Prevalence of Leptoprosopic Type of Face among Dental Students: A Cross-Sectional study. – *J. Nepal Med. Assoc.,* **57(218)**, 2019, 216-220.
17. **Staka, G., F. Asllani-Hoxha, V. Bimbashi**. Facial anthropometric norms among Kosovo – Albanian adults. – *Acta Stomatal. Croat.,* **51(3),** 2017, 195-206.

18. Swennen, G. R. J., F. Schutyser, J. E. Hausamen. *Three-dimensional cephalometry: a color atlas and manual.* Heidelberg, Springer; 2006.
19. Yesmin, T, S. S. Thwin, S. Afrin Urmi, M. M. Wai, P. Zaini, K. Azwan. A study of facial index among Malay population. – *J. Anthropol*., 2014, 2014: 1-4.
20. Yordanov, Y., A. Nacheva, S. Tornjova-Randelova, N. Kondova, B. Dimitrova, D. Paskova-Topalova. *Anthropology of the Bulgarian population at the end of the 20th century (30-40 years old persons).* Sofia, Professor Marin Drinov Academic publishing house, 2006
21. Zacharopoulos, GV, A. Manios, C. H. Kau, G. Velagrakis, G. N.Tzanakakis, E. de Bree. Anthropometric analysis of the face. – *Craniofac. Surg.,* **27(1)**, 2016, e 71-75.

Institute of Experimental Morphology, Pathology and Anthropology with Museum
Bulgarian Anatomical Society

Acta morphologica et anthropologica, 29 (1-2)
Sofia ● 2022

Morphological and Craniometrical Studies on the Skull of the South Karaman Sheep

Zekeriya Özüdoğru[1], Dervis Özdemir[2], Bumin Emre Teke[3], Mesut Kirbas[3]*

[1] Balikesir University, Faculty of Veterinary Medicine, Department of Anatomy, Balıkesir, Turkey
[2] Atatürk University, Faculty of Veterinary Medicine, Department of Anatomy, Erzurum, Turkey
[3] Bahri Dagdas International Agricultural Research Institute, Konya, Turkey.

*Corresponding author e-mail: dozdemir2544@hotmail.com, dozdemir@atauni.edu.tr

In this study, it was aimed to determine the craniometric measurements of the skull of the South Karaman sheep breed and to reveal the differences between them and other sheep breeds. The skull length was 238.37±4.18, the frontal width (ectorbitale – ectorbitale), which is the widest part of the skull was 115.75 ± 4.45. The distance between the supraorbitales was determined to be 50.01±3.94. There is a strong negative correlation between L9 (akrokranio – bregma) and L14 (greatest length of the lacrimal (most lateral point of the lacrimal – the most oral point of the lacrimo-maxillary suture) and positive correlation was found among other features. As a result, it is thought that the difference between the craniometric values of the South Karaman sheep, which are accepted as the native breeds of Turkey in the study, and other sheep breeds, depending on the skull morphology, may be due to the breed of the sheep.

Keywords: craniometrical, morphology, skull, south Karaman

Introduction

The size of the skull can provide valuable information about changes in the breed over time [5, 8]. Therefore, it was noted that the differences in races were found in the head of the animal, and it was reported that the differences in skull level defined a species more than those found in the rest of the skeleton [2, 22]. Thus, craniocephalic topography provides topometric data that facilitates sex discrimination [14].

Morphometric analysis is a preferred method in zoo archaeological studies, osteological evaluations, to reveal shape differences due to internal and external factors and differences between sexes [4].

Many authors have used the geometric dimensions of the skull bones of small ruminants for species identification [11, 23, 25, 27]. Kaymakci [12] states that there are many types of Akkaraman race and the variety called “South Karaman” is found in the foothills of the Taurus Mountains facing Central Anatolia. He reported that the breed, which is grown in the Taurus Mountains, is highly productive in terms of meat

and milk, and is among the most preferred species in aquaculture, with its resistance to environmental conditions.

The Southern Karaman Sheep are small in general appearance, have white, gray, brown and mottled colours, the males are horned, the females are generally hornless and have a fat tail [18, 21].

To date, some studies on craniometric measurements Tuj and morkaraman sheep [19], Hemşin sheep [6], Suffolk Down Sheep [3], Kosava's Barkhoka sheep) [7], Zell sheep [13] although no craniometric studies were found on the South Karaman sheep breed, this study was concerned with the head structure of Turkey's native sheep breed, which is common in the Mediterranean region.

Materials and Methods

Material

In the study, eight South Karaman sheep (male) skulls, ranging in weight from 38-56 kg, obtained from Bahri Dagdas International Agricultural Research Institute were used. After the animals were duly slaughtered, the skulls were subjected to maceration. Measurements were made using Mitutoyo digital caliper from 46 points on the skull of the South Karaman sheep. The anatomical terms used were based on Nomina Anatomica Veterinaria [16]. This study was approved by the Experimental Animals Ethics Committee of Atatürk University (Ethical number: 23.10.2015, 8/148).

The following measurements by using definitions of measuring points [6, 7, 17, 19, 20] on the cranium were made:

L1. profile length (akrokranion – prosthion),
L2. condylobasal length,
L3. basal length (basion – prosthion),
L4. short skull length (basion premolare),
L5. premolare – prosthion,
L6. ossa cranii length (basion – nasion),
L7. ossa faciei length (nasion prosthion),
L8. median frontal length (akrokranion – nasion),
L9. akrokranion - bregma,
L10. frontal length (bregma – nasion),
L11. upper ossa cranii length: Akrokranion – supraorbitale,
L12. facial length (supraorbitale – prosthion),
L13. Akrokranion-infraorbitale of one side,
L14. greatest length of the lacrimal (most lateral point of the lacrimal – the most oral point of the lacrimo-maxillary suture,
L15. greatest length of the nasals (nasion-rhinion),
L16. short lateral facial length (entorbitale – prosthion),
L17. from the aboral border of one occipital condyle to the infraorbitale of the same side,
L18. dental length (postdentale – prosthion),
L19. oral palatal length (palatinoorale – prosthion),

L20. lateral length of the premaxilla (nasointermaxillare – prosthion),
L21 length of the cheektooth row (measured along the alveoli),
L22. length of the molar row (measured along the alveoli on the buccal side),
L23. length of the premolar row (measured along the alveoli on the buccal side),
L24. zygomatic width (the distance between two zygomatic arches),
L25. greatest inner length of the orbit (ectorbitale – entorbitale),
L26. greatest inner height of the orbit (measured in the same way as measurement),
L27. greatest mastoid breadth (otion – otion),
L28. greatest breadth of the occipital condyles,
L29. greatest breadth at the bases of the paraoccipital processes,
L30. greatest breadth of the foramen magnum,
L31. eight of the foramen magnum (basion – opisthion),
L32. least breadth of parietal: Least breadth between the temporal lines,
L33. greatest ossa cranii Breadth-Greatest breadth of the braincase (euryon – euryon),
L34. least breadth between the orbits (entorbitale – entorbitale),
L35. greatest breadth across the orbit-greatest frontal breadth-greatest breadth of skull (ectorbitale – ectorbitale),
L36. facial breadth (breadth across the facial tuberosities),
L37. greatest breadth across the nasals,
L38. greatest breadth across the premaxillae,
L39. greatest palatal breadth (measured across the outer borders of the alveoli),
L40. the distance from infraorbital foramen to facial tuberosity,
L41. the distance from facial tuberosity to root of alveolar tooth,
L42. distance between first premolar teeth,
L43. distance between first molar teeth,
L44. distance between the last molar teeth,
L45. distance from orbital arcus,
L46. supraorbital foramina distance.

Craniofacial indices [19]**:**

I1. Nasal index: greatest breadth across the nasals x 100/ greatest length of the nasals
I2. Facial index: zygomatic width x 100/viscerocranial length
I3. Ossa cranii index: maximum width of the ossa cranii x 100/Ossa cranii length
I4. Basal index: maximum width of ossa cranii x100/basal length
I5. Skull index: zygomatic width x 100/skull length
I6. Orbital index: Greatest inner height of the orbit x100/ Greatest inner length of the orbit
I7. Foramen Magnum index: the height of the foramen magnum× 100/the width of the foramen magnum

Statistical analysis

The mean values, standard deviations, coefficient of variations and craniofacial indices were calculated with SPSS (version 22). Independent samples *t* test was used for *p* values. The values determined are indicated in Tables 1-4.

Results

In the study, 46 morphometric measurements of South Karaman sheep were made. The reference points for these measurements are presented in **Figs. 1-6**, the morphometric values obtained are presented in **Table 1**, and the calculated index values are presented in **Table 2**.

In the study, as seen in **Table 1**, the skull length of the South Karaman sheep was 238.37±4.18, the condylus occipitalis 51.51±1.65, proc. The base of the jugularis is 72.37±3.79 and the smallest parietal width is 52.34±2.43 for the distance between the supraorbitales was determined as 50.01±3.94.

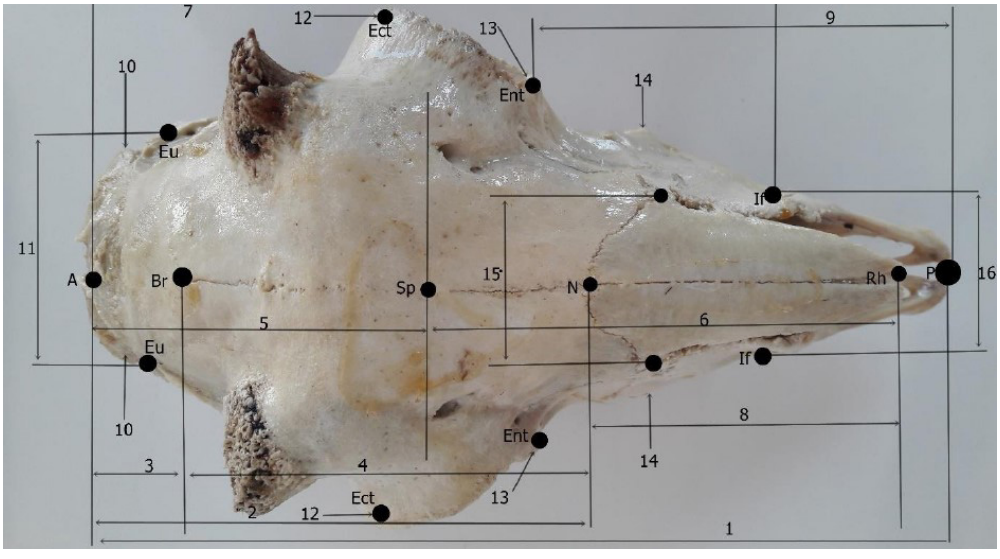

Fig. 1. Measurements of the skull of the South Karaman sheep (dorsal view). **1**. profile length, **2**. median frontal length, **3**. akrokranion-bregma, **4.** frontal length, **5**. upper ossa cranii length, **6.** facial length, **7.** akrokranion-infraorbitale of one side, **8.** greatest length of the nasals, **9.** short lateral facial length, **10.** least breadth of parietal: Least breadth between the temporal lines, **11**. greatest ossa cranii breadth-Greatest breadth of the braincase, **12**. greatest breadth across the orbit-greatest frontal breadth-greatest breadth of skull, **13**. least breadth between the orbits, **14.** facial breadth, **15.** greatest breadth across the nasals, **16**. greatest breadth across the premaxillae.

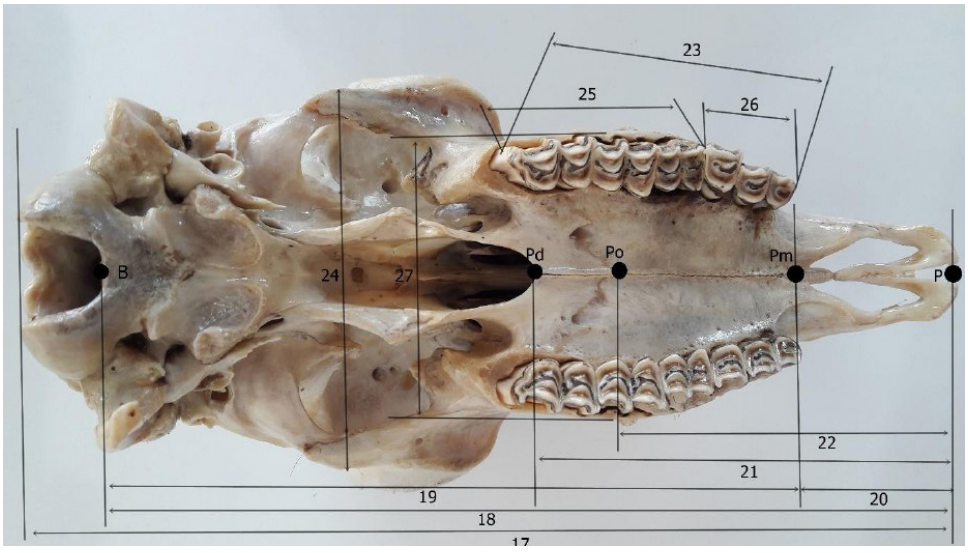

Fig. 2. Measurements of the skull of the South Karaman sheep (ventral view). **17.** condylobasal length, **18.** basal length, **19**. short skull length, **20.** premolare-prosthion, **21.** dental length, **22.** oral palatal length, **23.** Length of the cheektooth row, **24.** zygomatic width, **25.** Length of the molar row, **26.** Length of the premolar row, **27.** greatest palatal breadth.

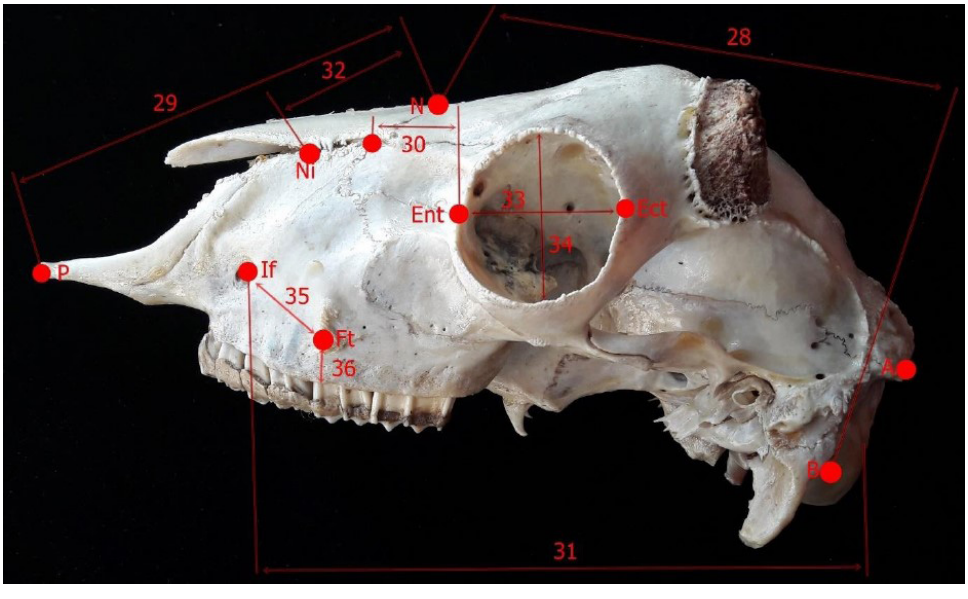

Fig. 3. Measurements of the skull of the South Karaman sheep (lateral view). **28.** ossa cranii length, **29.** ossa faciei length, **30**. greatest length of the lacrimal, **31.** from the aboral border of one occipital condyle to the infraorbitale of the same side, **32.** lateral length of the premaxilla, **33.** greatest inner length of the orbit, **34**. greatest inner height of the orbit, **35.** the distance from infraorbital foramen to facial tuberosity, **36.** the distance from facial tuberosity to root of alveolar tooth,

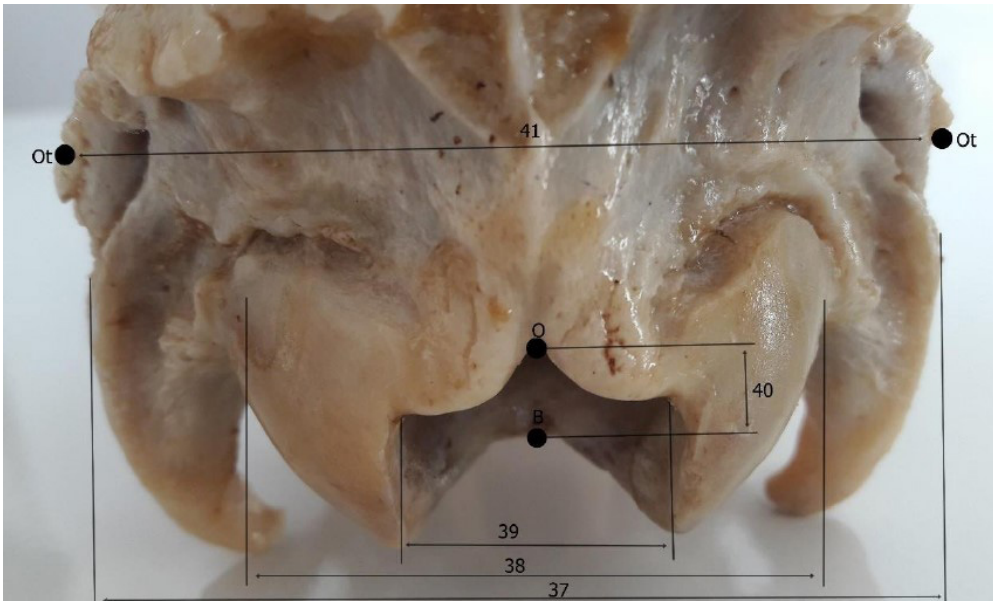

Fig. 4. Measurements of the skull of the South Karaman sheep (occipital view). **37.** greatest breadth of the bases of the paraoccipital processes, **38.** greatest breadth of the occipital condyles, **39.** greatest breadth of the foramen magnum, **40.** height of the foramen magnum, **41.** greatest mastoid breadth.

Fig. 5. Skull of the south Karaman sheep (ventral view). **42.** Supraorbital foramina distance, arrows. Naso-frontal suture like "U" shape; dashed arrows. Parieto-frontal suture like "V" shape.

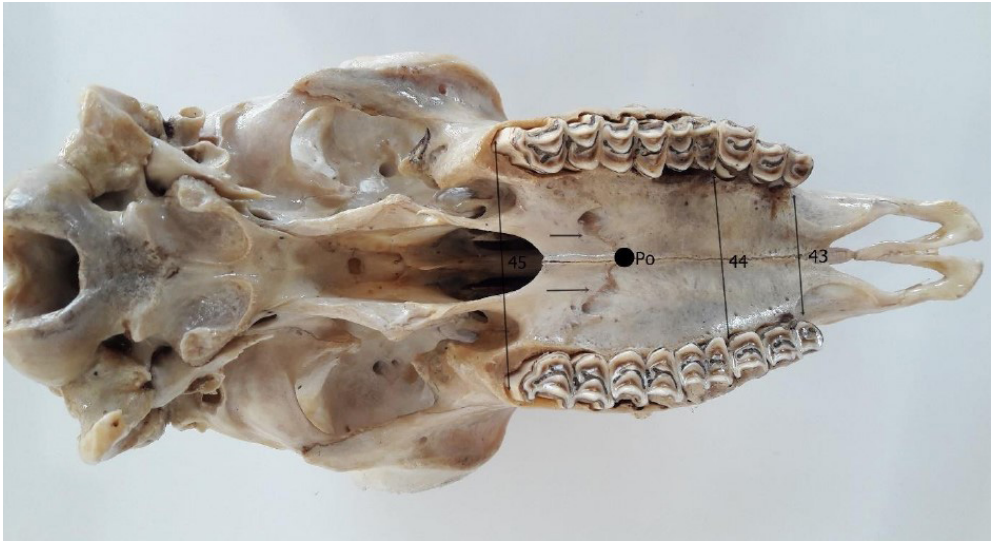

Fig. 6. Skull of the south Karaman sheep (ventral view) **43.** distance between first premolar teeth, **44.** distance between first molar teeth, **45.** Distance between the last molar teeth, arrows. "V" shape of the palatine bone with maxilla's palatine processes.

Table 1. The mean and standard deviations values of male South Karaman sheep.

Length	Mean ± Std Deviation	Length	Mean ± Std Deviation
L1	238.37 ± 4.183	L24	100.50 ± 2.850
L2	226.61 ± 6.874	L25	39.00 ± 1.589
L3	210.09 ± 7.835	L26	38.02 ± 2.222
L4	153.24 ± 6.599	L27	74.68 ± 3.047
L5	59.19 ± 2.124	L28	51.51 ± 1.653
L6	120.43 ± 6.081	L29	72.37 ± 3.788
L7	134.70 ± 3.203	L30	19.96 ± 2.308
L8	123.95 ± 5.259	L31	20.55 ± 1.882
L9	52.71 ± 6.503	L32	52.34 ± 2.433
L10	82.56 ± 5.313	L33	66.05 ± 2.170
L11	104.94 ± 4.951	L34	80.29 ± 3.758
L12	118.21 ± 4.453	L35	115.75 ± 4.450

L13	176.67 ± 5.557	L36	76.63 ± 2.386
L14	33.98 ± 1.516	L37	37.72 ± 3.572
L15	91.06 ± 3.188	L38	44.42 ± 3.769
L16	134.49 ± 4.157	L39	69.81 ± 3.020
L17	164.07 ± 6.539	L40	27.61 ± 2.412
L18	116.50 ± 4.057	L41	12.53 ± 3.126
L19	95.67 ± 3.930	L42	26.51 ± 2.716
L20	77.05 ± 4.012	L43	34.68 ± 2.603
L21	70.16 ± 3.771	L44	40.20 ± 1.164
L22	48.41 ± 1.993	L45	101.69 ± 5.465
L23	21.70 ± 1.655	L46	50.01 ± 3.935

Table 2. The mean and standard deviation values of craniofacial indices of male South Karaman sheep.

Craniofacial index	Mean ± Std Deviation
I1 Nasal index	74.61 ± 1.442
I2 Facial index	41.41 ± 3.612
I3 Ossa cranii index	54.98 ± 3.830
I4 Basal index	31.48 ± 1.663
I5 Skull index	42.16 ± 1.061
I6 Ortibal index	102.8 ± 6.048
I7 For. Mag. index	103.97 ± 14.659

When **Table 3**, which indicates the correlation between index values, is examined, it is seen that there is a statistically significant strong positive correlation between I3 (Ossa cranii index) and I4 (Basal index), but the relationship between other examined features is insignificant. Although the correlation between I3 and I6 index values was high (r=0.776), the correlation was found to be statistically insignificant (P=0.070). A similar situation was seen in I4 and I6 features (P=0.098).

Table 3. Correlation of craniofacial index.

	I1	I2	I3	I4	I5	I6
I2	-0.046					
I3	-0.616	-0.426				
I4	-0.615	-0.583	0.917**			
I5	0.312	-0.100	-0.310	-0.004		
I6	-0.690	0.094	0.776	0.732	0.016	
I7	-0.293	0.418	0.057	0.084	0.497	0.570

*: P<0.05; **: P<0.01

Statistically significant correlation values of skull measurements are shown in **Table 4**. When **Table 4** is examined, it is seen that there is a strong negative or positive correlation between the characteristics. It was determined that there was a strong negative correlation (-0.827) between L9 and L14 features, and positive correlation coefficients between other features. The highest positive correlation was observed between L7 and L34 features (0.992).

Table 4. The correlation values of skull male Güney Karaman sheep.

	L1	L2	L3	L4	L6	L7	L8	L9	L11	L12	L15	L16	L17	L18	L19	L20
L3		0.984 **														
L4		0.923 **	0.934 **													
L6		0.853*	0.823*													
L8	0.843*	0.894*	0.886*	0.849*	0.937 **											
L10					0.839*											
L12	0.917 **															
L14								-0.827*								
L15						0.915*										
L16	0.856*															
L18		0.965 **	0.972 **	0.848*												
L19	0.861*	0.935 **	0.933 **	0.919 **	0.836*		0.960 **							0.846*		
L20		0.887*	0.851*	0.935 **			0.842*		0.880*						0.932 **	
L22		0.838*												0.865*		
L25													0.846*			
L26			0.865*				0.810*							0.855*		
L27													0.902*			
L28									0.950 **							0.844*
L29					0.829*	0.830*			0.829*				0.815*			
L30										0.885*						
L31				0.863*					0.839*							0.809*
L32				0.913*					0.828*							0.895*
L34						0.992 **					0.924 **					
L35													0.894*			
L36					0.826*				0.879*			0.850*				
L37									0.974 **							0.915*
L38							0.902*								0.874	0.826*
L39												0.855*				

L41									0.945 **						0.882*
L42		0.962 **	0.946 **	0.886*	0.943 **		0.905*							0.920*	0.877*	
L43		0.894*	0.949 *	0.920 **			0.886*							0.869*	0.942 **	0.828*
L44						0.901*					0.891*					
L45													0.860*	0.868*		

*: P<0.05; **: P<0.01

Continuation of Table 4.

	L21	L22	L24	L25	L26	L27	L28	L29	L31	L32	L34	L36	L37	L38	L42
L22	0,938**														
L25	0,926**														
L29						0,868*									
L30					0,912*										
L31						0,824*									
L32									0,943**						
L34								0,859*							
L35						0,982**		0,924**							
L36								0,926**			0,832*				
L37							0,945**		0,818*	0,826*					
L38										0,843*					
L39		0,838*													
L41							0,922**						0,986**		
L42					0,864*										
L43					0,845*										0,843*
L44			0,908*								0,930**	0,851*			
L45	0,951**	0,932**		0,915*											
L46										0,848*				0,870*	

*:P<0.05; **: P<0.01

Discussion

In the study, the skull length was determined as 238.37±4.18 in South Karaman sheep. This value is 209±4.77 in Iranian domestic sheep [15], 200.6±0.6 in Mehraban sheep [11], 246.5±2.16 in Barbados Black Belly sheep [14], 246.5±2.16 in Tuj sheep [19], 198.08±7.69 and 241.20±25.17 in Hemsin sheep [6], Suffolk Down Sheep [3] 238.3±2.07, Kosava in Barkhoka sheep [7] 245.25±10.24, Zell sheep [13] 196.73±0.60 in Yankasa sheep [24] 325±0.99, in Ivesi sheep [28] was reported to be 241.30±14.01, in Xisqueta sheep [22] 265.51± 22.24 and in Sharri sheep [9] 247.47 ± 13.12. According to these reported values, it was observed that the skull length of the South Karaman sheep was smaller than the skull length of the Barkhoka sheep of Yankasa, Xisqueta, Barbados Black Belly, Sharri and Kosava, and it was almost equal to the Suffolk Down breed, but longer than all of the other breeds mentioned above.

Skull index value in morkaraman sheep [19] 51.36±0.69, Tuj sheep [19] 50.42±0.78, Mehraban sheep [11] 53.57±3.26, Avesi sheep [28] 47.77±3.23, Xisqueta sheep [22] 44.69± 4.29, Barkhoka sheep of Kosava [7] 41.69±1.74, Saanen goat [26] was measured as 53.45±1.55. This value was measured as 42.16 ± 1.06 in South Karaman sheep.

Yılmaz and Demircioglu [28] and Ozcan et al. [19] stated that the widest region of the skull in sheep is the frontal width (ectorbitale – ectorbitale) due to morphological differences. Accordingly, they reported that this length was 102.98±2.52 mm in Morkaraman sheep [19], 101.66±1.69 mm in Tuj sheep [19], and 115.07±7.74 mm in Avesi sheep [28]. In this study, it was determined that the widest region of the skull was the frontal width (ectorbitale – ectorbitale), similar to what the authors reported in sheep, and this distance was 115.75 ± 4.45 in South Karaman sheep.

The orbital region is a craniofacial structure that can be affected by many congenital, traumatic, neoplastic, vascular and endocrine disorders [1], as it plays a fundamental role in the assessment and recognition of the craniofacial complex [10].

Parés-Casanova et al. [22], in their study on the biometric appearance of the skull in Spanish Xisqueta sheep, reported that the orbital index value was 109.77±10.23. The mentioned orbital index was measured as 112.27±3.50 in Avesi sheep [28] and 93.46± 3.48 in Barkhoka sheep of Kosava [7]. In the study, it was determined that the measured value of 102.8 ± 6.048 in South Karaman sheep was greater than only Kosava's Barkhoka breed.

Although Sharri sheep [9], Bardhoka sheep of Kosovo [7] and Kagani goat [23] stated that the fronto-nasal sutura is in the form of the letter "V" sheep [6] has been reported to be in the shape of the letter "U". In the study, it was determined that the fronto-nasal sutura resembles the letter "U" in South Karaman sheep.

It is reported that the palato-maxillary sutura between the lamina horizantali of the os palatine and the processus palatinus of the os maxilla is in the form of the letter "U" in hellon sheep [11], and in the shape of the letter "V" in Bardhoka sheep of Kosovo [7] has been done. In the study, it was determined that the palato-maxillar sutura in South Karaman sheep resembles the letter "V" as in Bardhoka sheep. In addition, in the study, it was determined that the pariato-frontal suture was in the form of the letter "V", and this finding is consistent with the reports of Sharri sheep [9] that the sutura can be in the form of a straight line or the letter "V".

As reported in the correlation analysis of the measurements made on the skull index values of Hemsin sheep, it was determined that there is a statistically significant strong positive correlation between I3 (Ossa cranii index) and I4 (Basal index) in South Karaman sheep. However, there was no statistically positive correlation between nasal index (I1) and skull index [6], as reported in sheep. According to the statistical values of the skull measurements of the Southern Karaman Sheep, there is a strong negative correlation (-0.827) between L9 (akrokranio – bregma) and L14 (greatest length of the lacrimal (most lateral point of the lacrimal – the most oral point of the lacrimo-maxillary suture) and the correlation coefficients were positive among other features. The highest positive correlation value was observed between L7 and L34 features (0.992).

There is a positive strong correlation between the basal length and the short skull length in hemsin sheep while the greatest inner height of the orbit and the between the breadth of the occipital condyles there was a strong correlation in the negative direction.

This study is important because it is the first study on the mental structure of domestic sheep breeds in Turkey. It is thought that the difference between the skulls of South Karaman sheep and other sheep may be due to the breed of the sheep. In addition, this research will contribute to the scientific studies to be carried out in this direction and to the literature on the subject.

References

1. Acer, N., B. Sahin, H. Ergur, et al. Stereological estimation of the orbital volume: a criterion standard study. – *J. Craniofac. Surg.,* **20**, 2009, 921-925.

2. Agüera, S., F. Castejón, A. Diaz, F. Miró, J. López Rivero. Diferenciación radiológica en ovejas manchegas y merinas. – *Archivos de Zootecnia*, **37**, 1988, 205. [In Spanish]

3. Barra, R., A. M. Carvacal. Martinez. Variability of cranial morphometrical traits in Suffolk Down Sheep. – *Austral J. Vet. Sci.,* **52**, 2020, 25-31.

4. Cakır, A., I. G. Yildirim, O. Ekim. Craniometric measurements and some anatomical characteristics of the cranium in Mediterranean Monk Seal (Monachus monachus. Hermann 1779). – *Ankara Univ. Vet. Fak. Derg.,* **59**, 2012, 155-162.

5. Cobb, S., P. O´Higgins. The ontogeny of sexual dimorphism in the facial skeleton of the African apes. – *J. Hum. Evol.*, **53**, 2007, 176-190.

6. Dalga, S., K. Aslan, Y. Akbulut. A morphometric study on the skull of the Hemshin sheep. – *Van. Vet. J.*, **29**, 2018, 125-129.

7. Gundemir, O., S. Duro, T. Jashari, O. Kahvecioglu, I. Demircioglu, H. Mehmeti. A study on morphology and morphometric parameters on skull of the Bardhoka autochthonous sheep breed in Kosovo. – *Anat. Histol. Embryol.,* **49**, 2020, 365–371.

8. Ilayperuma, I. Evaluation of cephalic indices: A clue for racial and sex diversity. – *Int. J. Morphol.*, **29**, 2011, 112-117.

9. Jashari, T., S. Duro, O. Gundemir, T. Szara, V. Ilieski, D. Mamuti, O. P. Choudhary. Morphology, morphometry and some aspects of clinical anatomy in the skull and mandible of Sharri sheep. – *Biologia*, **77**, 2022, 423–433.

10. Ji, Y., Z. Qian, Y. Dong, et al. Quantitative morphometry of the orbit in Chinese adults based on a three-dimensional reconstruction method. – *J. Anat.,* **217**, 2010, 501-506.

11. Karimi, I., V. Onar, G. Pazvant, M. M. Hadipour, Y. Mazaheri. The Cranial Morphometric and Morphologic Characteristics of Mehraban Sheep in Western Iran. – *Global Veterinaria*, **6**, 2011, 111-117.

12. Kaymakci, M. *Advanced sheep breeding.* Bornova-İzmir, 2006. [In Turkish].

13. **Marzban, Abbasabadi B., O. Hajian, S. Rahmati.** Investigating the morphometric characteristics of male and female Zell sheep skulls for sexual dimorphism. – *A.S.J.,* **17**, 2020, 13-20.
14. **Mohamed, R., M. Driscoll M, N. Mootoo.** Clinical anatomy of the scull of the Barbados Black Belly sheep in Trinidad. – *Int. J. Curr. Res. Med. Sci.*, **2**, 2016, 8-19.
15. **Monfared, A. L.** Clinical anatomy of the skull of Iranian Native sheep. – *Global Veternaria*, **10**, 2013, 271- 275.
16. **NAV.** Nomina anatomica veterinaria, international committee on veterinary gross anatomical nomenclature. 5th Edition, Hannover, Columbia, Gent, Sapparo, USA, 2005.
17. **Onar, V., G. Pazvant.** Skull typology of adult male Kangal dogs. – *Anat. Histol. Embryol.,* **30**, 2001, 41–48.
18. **Ozdemir, D., Z. Ozudogru.** Macroanatomical investigations on renal arteries of southern Karaman Sheep. – *Turkish Journal of Agriculture - Food Science and Technology*, **8**, 2020, 1878-1881.
19. **Ozcan, S., G. Aksoy, I. Kurtul, I., K. Aslan. Z. Ozudogru.** A comparative morphometric study on the skull of the Tuj and Morkaraman sheep. – *Kafkas Universitesi Vet. Fak. Derg.*, **16**, 2010, 111-114.
20. **Ozkan, E., A. B. Siddiq, O. Kahvecioglu, M. Ozturk, V. Onar.** Morphometric analysis of the skulls of domestic cattle (*Bos taurus* L.) and water buffalo (*Bubalus bubalis* L.) in Turkey. – *Turkish J. Vet. Anim. Sci.,* **43**, 2019, 532–539.
21. **Ozudogru, Z., D. Ozdemir.** A Morphological study on sinus interdigitalis in south Karaman Sheep. – *Atatürk University J. Vet. Sci.,* **16**, 2021, 228-235.
22. **Parés-Casanova, P. M., S. Kamal, J. Jordana.** On biometrical aspects of the cephalic anatomy of Xisqueta sheep (Catalunya, Spain). – *Int. J. Morpol.*, **28**, 2010, 347-351.
23. **Sarma, K.** Morphological and craniometrical studies on the skull of Kagani goat (*Capra hircus*) of Jammu region. – *Int. J. Morphol.*, **24**, 2006, 449-455.
24. **Shehu, S., A. Bello, A. Danmaigiro, et al.** Osteometrical study on age related changes of the skull of Yankasa ram. – *J. Human Anat.,* **3**, 2019, 136.
25. **Von Den Driesch, A.** A guide to the measurement of animal bones from archaeological sites. Peabody Museum Bulletin 1. Cambridge, MA, Harvard University, 1976.
26. **Wang, X., A. Lıu, J. Zhao, F.M. Elshaer, D. Massoud.** Anatomy of the skull of Saanen goat. An anesthesiology and stereology approach. – *Int. J. Morphol.,* **39**, 2021, 423-429.
27. **Yalcin, H., M.A. Kaya.** Anadolu yaban koyunu ve akkaraman koyununun kafa kemikleri üzerinde karşılaştırmalı geometrik morfometri. – *Atatürk Univ. Vet. Bil. Derg.*, **4**, 2009, 105-116. [In Turkish].
28. **Yılmaz, B., I. Demircioglu.** Morphometric analysis of the skull in the Awassi Sheep (*Ovis aries*). – *Fırat* Üniv. *Sag. Bil. Vet. Derg.,* **34**, 2020, 1-6.

Institute of Experimental Morphology, Pathology and Anthropology with Museum
Bulgarian Anatomical Society

Acta morphologica et anthropologica, 29 (1-2)
Sofia ● 2022

Calot`s Triangle – and Hepatocystic triangle – Like Areas in Domestic Swine

Ivaylo Stefanov[1,2], Stefan Stefanov[3]*

[1]Department of Anatomy, Faculty of Medicine, Trakia University, Stara Zagora, Bulgaria
[2]Department of Anatomy, Histology and Embryology, Pathology, Burgas University Prof. Dr. Asen Zlatarov, Burgas, Bulgaria
[3]Fifth year student at Medical faculty, Trakia University, Stara Zagora, Bulgaria

*Corresponding author e-mail: ivstefanov@abv.bg

Due to the similarities to human anatomy the domestic swine is one of the most preferred species for experiments especially in developing new surgical techniques in the cholecystectomy in humans. The aim of the study was to establish the existence of both the Calot`s triangle and the hepatocystic triangle and the length of their borders in the domestic pigs. This research work was conducted on livers from 30 male pigs separated to different age groups. The results showed that Calot`s triangle – and the hepatocystic triangle-like areas were present. The borders of the triangles were identified, measured and statistically analyzed in immature and mature pigs and age dependent differences were identified. The similarities and differences in borders of triangles between pigs and humans were discussed. This study revealed that, like in humans, the Calot`s triangle and the hepatocystic triangle are presented and have important clinical significance.

Key words: Calot`s triangle, hepatocystic triangle, anatomy, morphometry, pigs

Introduction

The Calot`s triangle and hepatocystic triangle in humans are studied in detail because of the cholecystectomy surgery [18]. In order to develop new surgical techniques for gallbladder removing, the domestic swine is widely used as one of the most suitable experimental models for cholecystectomy [18]. Misinterpretation or lack of knowledge of this information contributes to intraoperative complications such as biliary injuries, which can cause serious morbidity and occasionally mortality [9]. Information about the presence of such triangles in animals was not found. The similarity in the anatomy of extrahepatic biliary tracts in both humans and pigs [10, 11] is well known. For example, both species possess a common hepatic duct, a common bile duct terminating in the duodenum by a papilla duodeni major and a cystic duct [10, 17]. Moreover, the cystic artery is a main vessel that supplies the gallbladder and has similar topography in both species.

Laparoscopic cholecystectomy became the preferred modern method for the treatment of symptomatic cholelithiasis [8]. Laparoscopic cholecystectomy has many

advantages over the standard open cholecystectomy: minimal trauma, decreased pain, shorter hospital stay, satisfactory cosmetic outcome, quick recovery, and return to work. However, numerous studies have shown that laparoscopic cholecystectomy is associated with a higher frequency of complications compared to the standard open cholecystectomy including lesions to the common bile duct, injury to the vascular and visceral structures [4]. Major complications (biliary and vascular) are life threatening and increase mortality rate, therefore creating the need for conversion to open surgical approach in order to treat them. The frequency of complications associated with laparoscopic cholecystectomy varies from 0.5 to 6% [4]. The most serious complications are associated with high mortality rate: injury of common bile duct with an incidence of 0.1-0.6% [12], injuries of large blood vessels 0.04-1.22% depending on the study [11]. They are more common in older age patients, male gender. During the cholecystectomy, Calot area was surgically opened, the vessel and duct of gallbladder were cut and clips applied, gallbladder was surgically removed from its adjoining area of liver.

The knowledge of anatomy of the borders and structures of Calot`s triangle can be very useful in preventing the intraoperative and postoperative complications during laparoscopic cholecystectomy in a treatment of cholelithiasis [4]. In 1891, the French surgeon Jean F. Calot described a triangular area formed by the cystic artery, common hepatic duct and the cystic duct. The borders of this triangle are as follows: the superior and inferior borders represented by the cystic artery and cystic duct, respectively which are equal and a little longer medial border, represented by the part of the hepatic duct, near the terminal part of the cystic duct. Later, Calot`s space was renamed as to hepatobiliary, hepatocystic or cystohepatic triangle; with a superior border given by the visceral surface of the liver, medial border – by the common hepatic duct and inferior border – by the cystic duct draining the gallbladder [6]. Therefore, the modern triangle appears to provide the surgeon with a more constant triangle boundary, one that would otherwise be variable, given the occasionally inconsistent pattern of the cystic artery [9]. The contents of cystohepatic triangle include the right hepatic arteria, cystic artery, lymph node of gallbladder, lymphatics and fibro-fatty connective tissue area. In patients without structural variations, laparoscopic removal of gallbladder stones is a routine technic for surgeons.

Laparoscopic surgery is a technique often chosen in case of gallbladder stones [9]. Vascular and ductal variations can disorientate the surgeon during performing of laparoscopic technic [1]. In this relation, the knowledge of Calot`s triangle anatomy is of significant importance for the operator especially when there are arterial and biliary anomalies [4].

The domestic swine as omnivorous, monogastric species is regarded as a suitable animal model for human diseases. There are a lot of similarities to humans in anatomy and functions of the immune system. Based on the facts that the porcine organs are anatomically comparable in size and the porcine immune system resembles human's in > 80%, in contrast to mice with only 10% [3], the pigs are currently thought to be the best candidates for organ donation in xenotransplantation. Moreover, the pigs are inexpensive and easy to maintain in pathogen-free facilities, have relatively short gestation periods, large litters, and are easy to breed making them readily available [7].

All mentioned studies provoked the question if these two triangles are present in domestic pigs.

Based on the facts above, we aimed to establish the existence of both the Calot`s triangle and the hepatocystic triangle as well as to define their borders in the domestic pigs.

Materials and Methods

Animals

This research work was conducted on male crossbred pigs (Landrace×Danube White). A set of fresh liver with gallbladder, stomach, spleen and cranial part of the duodenum was collected from 30 pigs divided in three age groups – 10 animals at the age of 2 months (24-32kg), 10 animals at the age of 6 months (91-115 кg) and 10 animals at the age of 3 years (250-310 кg), at a legal slaughterhouse. All measurements involved in the study were done at a slaughterhouse. All procedures were performed in accordance with the Bulgarian legislation regarding animal care (Ordinance 20 of 01.11.2012 on the minimum requirements for the protection and welfare of experimental animals and the requirements for the sites for use, breeding and/or delivery) and in accordance with Directive 2010/63 / EU of the European Parliament and of the Council of 22 September 2010 on the protection of animals used for scientific purposes.

Macromorphometric method

After removing the sets of organs from the porcine bodies, the connective tissue surrounding the extrahepatic bile ducts was dissected and removed in order to visualize and prepare them for a macromorphometric study. The studied macrometric parameters were the length (in millimeters) of the common hepatic duct (*ductus hepaticus commun*is), cystic duct (*ductus cysticus*), common bile duct (*ductus choledochus*) and of the right margin of quadrate lobe of liver as borders of Calot`s and hepatocystic triangles. The distance (in millimeters) between dorsal margin of the liver and the point of union of *ductus cysticus, ductus hepaticus communis* and *ductus choledochus* was estimated as well. The length measurements were performed using a digital electronic caliper (with accuracy 0.01 mm). The angles were measured by protractor (a half circle with marked degrees from 0 to 180).

Statistical analysis

Data were processed by GraphPad Prism 6 for Windows (GraphPad Software, Inc., USA) via one-way analysis of variance (one-way ANOVA) followed by Tukey-Kramer's posthoc test and were presented as mean ± standard deviation (SD). P-values lower than 0.05 were considered statistically significant.

The terminology was consistent with the Nomina Anatomica Veterinaria [10] and with Terminologia anatomica [17].

Results

In order to visualize the structures of Calot`s and hepatocystic triangles following steps are needed to be done for safe identification of the triangles` structures: the first step is the clearance of the HC triangle – the HC triangle should be cleared of all the adipose

tissue (**Fig. 1**). It allows further safe dissection and identification of the cystic duct arising from the gallbladder neck and of the cystic artery which is the second step. The cystic artery can pass cranially or caudally to *ductus hepaticus communis* and predominantly on the left side of the cystic duct. The third step is to find the union of cystic duct to common bile duct. This can be achieved by following the direction of cystic duct to the common bile duct. Once reached the point of union, the three extrahepatic bile ducts can be visualized: the ventral duct – *ductus cysticus,* the left duct – *ductus hepaticus communis* and the right duct – *ductus choledochus* which terminates into the wall of duodenum. These ducts together with cystic artery are the anatomical landmarks for identification of both triangle borders.

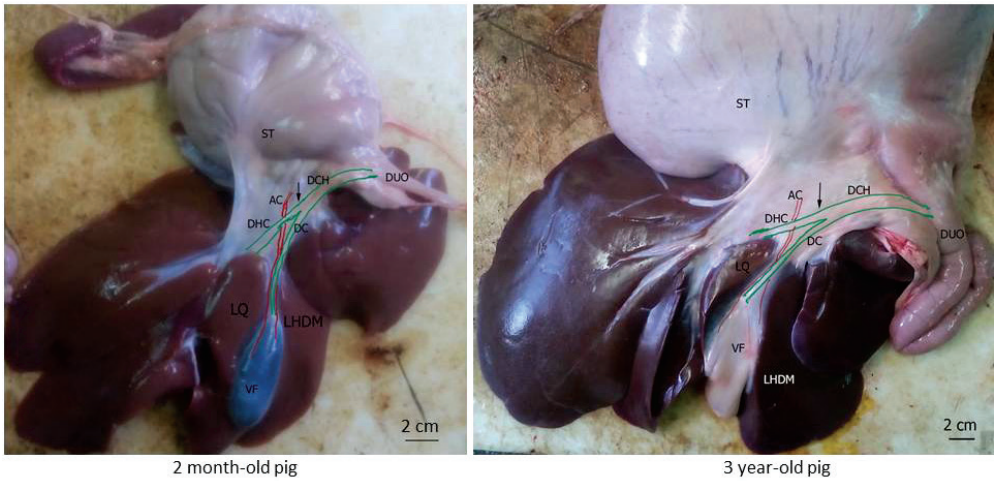

Fig. 1. Relevant anatomical structure before dissection – *(DC) ductus cysticus; (DHC) ductus hepaticus communis, (AC) a. cystica,(DCH) ductus choledochus, (LQ)lobus hepatis quadratus, (ST) stomach, (VF) vesica fellea; (DUO) duodenum; (arrow)* indicates the distance between the dorsal margin of the liver and the union of the bile ducts.

In this study, the borders of Calot`s triangle were visualized and their length was measured in the three aged groups (**Fig. 2, Table 1**):

1. The right border was represented by the cystic duct which length increased with age and a statistical significant difference was detected.

2. The left border was given by cystic artery which length increased with age without any statistical significant difference.

3. The dorsal border was represented by common hepatic duct which length increased with age without any statistical significant difference.

Calot`s triangle is referred to a scalene because none of the sides of the triangle have equal lengths. Its side represented by *ductus cysticus* was the longest, followed by that represented by *a. cystica* and *ductus hepaticus communis*, respectively. The Lymph node in the Calot`s triangle was not present, so that the main content was the adipose tissue.

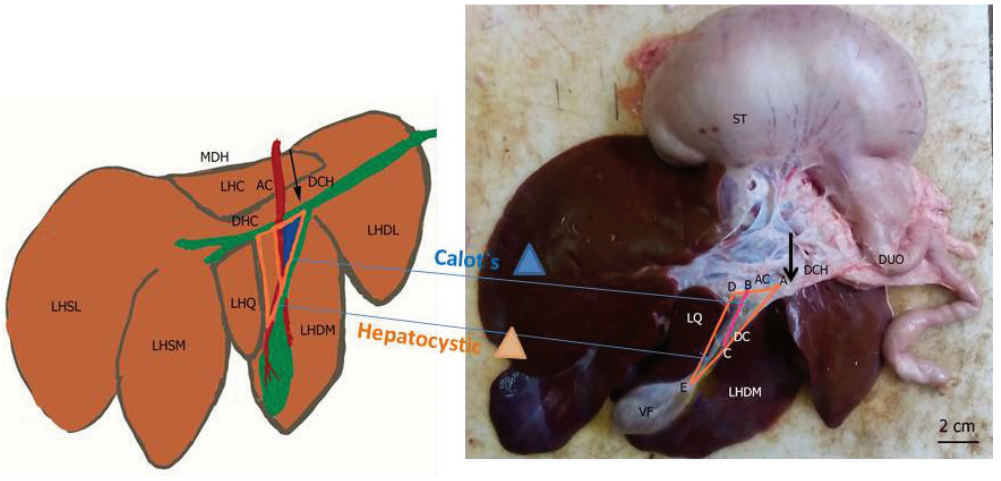

Fig. 2. Anatomy of hepatocystic and Calot's triangles in 6 month-old pig.
(Original figure, I. Stefanov) **Left:** Hepatocystic triangle (orange outline); **Right:** Calot's triangle (in blue); *(DC) ductus cysticus; (DHC) ductus hepaticus communis, (AC) a. cystica, (DCH) ductus choledochus, (LQ, LHQ) lobus hepatis quadratus, (LHSL, LHSM, LHDL, LHDM, LHC) lobus hepatis sinister lateralis, lobus hepatis sinister medialis, lobus hepatis dexter lateralis, lobus hepatis dexter medialis, lobus hepatis caudatus, espectively, (MDH) margo dorsalis hepatis;(ST) stomach, (VF) vesica fellea; (DUO) duodenum; (arrow)* indicates the distance between the dorsal margin of the liver and the union of the bile ducts.

The borders of the hepatocystic triangle also were visualized and their length was measured in the three aged groups (**Table 1**):

Table 1. The length (mm) of the borders of Calot`s triangle and hepatocystic triangle as well as the distance (mm) (MDH-UEBD) between *margo dorsalis hepatis* (MDH) and the union of the extrahepatic bile ducts (UEBD).

Calot`s triangle borders	**2 month-old pigs Length (mean±SD)**	**6 month-old pigs Length (mean±SD)**	**3 year-old pigs Length (mean±SD)**
ductus hepaticus communis Min-max	14.49±9.97**a1** 3.76-29.38	19.95±12.74 **a4, b1** 5.38-43.33	29.32±9.56 **a4** 15.23-44.98
ductus cysticus Min-max	35.71 ±4.16 **A2, B4** 29.71-40.28	60.71±13.26 **c2** 43.22-89.12	71.49 ±11.94 **c3** 52.67-92.12
arteria cystica Min-max	25.73±12.92 9.22-40.29	38.38±17.87 10.48-61.15	42.95±17.78 13.22-64.33
Hepatocystic triangle borders	**2 month-old pigs Length (mm) (mean±SD)**	**6 month-old pigs Length (mm) (mean±SD)**	**3 year-old pigs Length (mm) (mean±SD)**
ductus hepaticus communis Min-max	21.78±10.99 **a1** 6.28-32.19	35.35 ±13.87 **a4** 16.37-55.01	36.14±14.39 **a4** 16.92-57.22

Table 1.

ductus cysticus *Min-max*	39.07 ±4.11 **A3, B4** 31.28-44.15	65.28± 12.40 **d2** 50.18- 92.19	76.28±11.03 **d4** 58.73-94.28
lobus quadratus hepatis Min-max	32.98±14.48 **A1, B3** 13.27-49.92	50.00±14.40 19.77-69.87	51.87±15.88 21.22-71.88
Distance MDH-UEBD	23.92±3.77 **A4, B4** 16.11-27.72	36.84±5.44 28.43-44.38	36.71±5.55 29.88-43.28

Legend:
1,2,3,4 ($P < 0.05;0.01; 0.001;0.0001$, respectively)
A – Statistical significant difference against the age of 6 months
B – Statistical significant difference against against the age of 3 years
a – Statistical significant difference against the *ductus cysticus*
b – Statistical significant difference against the *a. cystica*
c – Statistical significant difference against the *a. cystica*
d – Statistical significant difference against the *lobus quadratus hepatis*

1. The right border was represented by the cystic duct which length increased with age and a statistical significant difference was detected.

2. The left border was given by the right margin of *lobus hepatis quadratus* which length increased with age and a statistical significant difference was detected.

3. The dorsal border was represented by common hepatic duct which length increased with age without any statistical significant difference.

The side of hepatocistic triangle represented by *ductus cysticus* was the longest, followed by that represented by *lobus hepatis quadratus* and *ductus hepaticus communis*, respectively.

Obviously, the area of hepatocystic triangle is bigger than that of the Calot`s triangle. So that the Calot`s triangle was formed as a part of hepatocystic triangle.

The main content of hepatocystic triangle is the large amount of adipose tissue and *arteria cystica* (**Figs 1, 2**).

In order to define more easily the union of the three extrahepatic bile ducts the distance between the dorsal margin (*margo dorsalis*) of the liver and the level of union was evaluated (**Table 1**). This distance in 6 month- and 3 year-old pigs was larger than in immature ones.

The angles of Calot`s triangle and of hepatocystic triangle were estimated (**Table 2**).

Table 2. Values (degrees ^{0}) of the angles (∠CAB, ABC, ACB, ADE and AED, see **Figs**. **1, 2**) of Calot`s triangle and of hepatocystic triangle in pigs from the three age groups as well as between the *ductus cysticus* and the *ductus choledochus* (∠DC-DCH), between the *ductus cysticus* and the neck of gallbladder (∠DC-GB) to the long axis (LA) of the gallbladder.

Angles	**2 month-old pigs (mean±SD)**	**6 month-old pigs (mean±SD)**	**3 year-old pigs (mean±SD)**
∠CAB	50.4 ±21 **A4, B4**	48.7±1.3	48.9 ±1.1
∠ABC	101.7±2.6 **A4, B4, a4**	109.4±1.3 C2,a4	112.0±1.7 a4
∠ACB	24.0±1.0	20.10±0.9	20.00±0.8

∠ADE	110.3±0.8**A4, B4**	114.9± 1.7 C4	116.4±1.4
∠AED	30.0±1.2	28.5±0.5	28.0±0.7
∠DC-DCH	125.5±9.84 110.0-140.0	130.3±17.33 110.0-162.0	133.0±20.17 110.0-170.0
∠DC-GB	126.5±12.70 115.0-153.0	126.0±23.07 90.00-166.0	135.5±23.62 100.0-173.0

Legend:
∠CAB – the angle between *ductus cysticus* and *ductus hepaticus communis*
∠ABC – the angle between *ductus hepaticus communis* and *a. cystica*
∠ACB – the angle between *ductus cysticus* and *a. cystica*
∠ADE – the angle between *ductus hepaticus communis* and *right margin of lobus hepatis quadratus*
∠AED – the angle between *ductus cysticus* and right margin *of lobus hepatis quadratus*
2, 4 ($P < 0.01$; 0.0001, respectively*)*
A – Statistical significant difference against the age of 6 months
B – Statistical significant difference against the age of 3 years
C – Statistical significant difference against the age of 3 years
a – Statistical significant difference between ∠ABC and ∠ADE

The angles between *ductus cysticus* and *ductus hepaticus communis*, between *ductus cysticus* and *a. cystica,* between *ductus cysticus* and right margin of *lobus hepatis quadrates* decreased with age*,* while the angles between *ductus hepaticus communis* and *a. cystic* as well as the angle between *ductus hepaticus communis* and right margin of *lobus hepatis quadrates* increased with age (**Figs. 1, 2, Table 2**).

In addition, the angles between cystic duct and common bile duct as well as between the cystic duct and the neck of gallbladder were evaluated (**Table 2**). The both angles showed similar values and were the largest in all age groups.

Discussion

In this study, for the first time, the borders of Calot`s triangle and of hepatocistic triangle were identified and their length was measured in the three aged groups of pigs. The similarities and differences between human and porcine triangles were discussed as well. It was found that the borders of Calot`s triangle in porcine liver are identical to that of Calot`s triangle in humans. In both pigs and humans the area of hepatocystic triangle is bigger than that of the Calot`s triangle. So that the Calot`s triangle is formed as a part of hepatocystic triangle. However, due to the different anatomical position of the body in both species the different terms are used in the definition of sides of the triangles in pigs and in humans. The right side of porcine Calot`s triangle was represented by the cystic duct, the left side was given by cystic artery, the dorsal side was represented by common hepatic and none of the sides of the triangle have equal lengths. In humans the superior and inferior borders of Calot`s triangle, represented by the cystic artery and cystic duct, respectively are equal and a little longer medial border, represented by the part of the hepatic duct, near the terminal part of cystic duct [6]. Therefore the Calot`s triangle in pigs is referred to as scalene but in humans it's referred to as isosceles.

The sides of hepatocystic triangle in humans and pigs are represented by similar structures. However, again due to the different anatomical position of the body in both species, the different terms are used in definition of the sides of triangles. In pigs, they are represented by the right margin of the visceral surface of *lobus hepatis quadratus* forming the left side, *ductus cysticus* forming the right side and *ductus hepaticus communis* forming the dorsal side. The cystohepatic triangle in humans has a superior (cranial) side given by the visceral surface of the liver, medial (right) side – by the common hepatic duct and inferior (caudal) border – by the cystic duct [6]. The right hepatic arteria, cystic artery, cystic lymph node, lymphatics and fibro-fatty connective tissue are the contents of cystohepatic triangle.

The borders and contents of the hepatobiliary triangle are the main landmarks used by surgeons when performing the laparoscopic technique. In humans, a detailed study regarding the anatomy of hepatobiliary triangle and its variations was carried out by Ahmad et al. [1] using a laparoscope. These authors found out that 63.6% of patients expressed cystic duct, cystic lymph nodes and cystic artery variations. Among them 12% depicted cystic duct variations, 32.2% of patients demonstrated cystic lymph nodes variations and 19.4% of the patients showed cystic artery variations. Fat deposition, fibrosis and adhesions were also observed in hepatobiliary areas of female patients. Ahmad et al. [1] revealed that 32.2% of the patients had cystic lymph node variations. Cystic lymph node was found posterior to cystic duct in 8.1%, anterolateral to cystic duct 8.1%, and outside hepatobiliary triangle in 8% of the patients. Normal cystic duct was documented in 83.85% of the patients. Percentages of cystic duct variations included broad cystic duct in 4%, long cystic duct in 3.67%, short cystic duct in 4.33%, absence of cystic duct in 0.33%, spiral cystic duct in 2.70%, double cystic duct in 0.33%, accessary cystic duct in 0.10%, adherent cystic duct in 0.33%, and parallel insertion of cystic duct to form common bile duct in its retroduodenal part in 0.15% cases. Bleeding and biliary injury force surgeon to do open abdominal operation especially when structural variations are encountered [15].

The cystic artery is the key structure clipped or ligated during laparoscopic or conventional cholecystectomy [5, 9]. Ahmad et al. [1] identified single cystic artery in hepatobiliary triangle in 76.02% of cases, double artery in hepatobiliary triangle – in 9.88%. In terms of syntopic relations of *a. cystica* to *ductus cysticus* in pigs, two variations were described by us in previous study [13]. The first type of variation (92% of cases) showed that a. *cystica* passed on the left of *d. cysticus* and caudally to v. *portae* and *d. hepaticus communis*. In this case *a. cystica* originated from *r. dexter medialis* and from *a. gastroduodenalis*. The second type of variation (8% of cases) represented the origin of *a. cystica* from the common trunk of *r. dexter lateralis* and *r. dexter medialis.* In this case*,* the beginning of *a. cystica* was located on the right of *ductus cysticus*. Then *a. cystic* directed ventrally passing cranially to *ductus choledochus* to the place of its division.

Anatomical variations increase the risk of structural injuries during the laparoscopic cholecystectomy can be prevented by precise operative technique, clear visualisation of anatomical landmarks, and careful dissection of tissues [11]. The risk is further increased when these variations are encountered during laparoscopic visualization rather than open surgery. Of all the structural injuries following a cholecystectomy, bile duct injury BDI is the most feared because it can result in high morbidity, long-term hospitalization, and may be life-threatening [2, 14]. The identification of the Calot's

triangle borders is very important in order to prevent bile duct injury (BDI) [2, 16]. The potential for BDI remains statistically greater with the laparoscopic approach [2, 8]. The incidence of BDI in open cholecystectomy is estimated at 0.1-0.25% whereas the figure is higher in the laparoscopic approach, at 0.5% [13, 14]. Other studies indicate that the cases of injuries to the common bile duct varies from 0.1 to 0.6% [12, 11].

Conclusion

This study revealed that, like in humans, the Calot`s triangle and the hepatocystic triangle with similar borders are presented. Full knowledge of the borders and contents of the Calot`s triangle as important anatomical landmarks can be very helpful for surgeons in developing new technics for safe execution of cholecystectomy and to avoid intraoperative and postoperative bleeding and biliary leakage.

R e f e r e n c e s

1. Andall, R. G., P. Matusz, M. du Plessis, R. Ward, R. S. Tubbs, M. Loukas. The clinical anatomy of cystic artery variations: a review of over 9800 cases. – *Surg. Radiol. Anat.,* 2016, **38**, 529-553.

2. Connor, S., O. J. Garden. Bile duct injury in the era of laparoscopic cholecystectomy. – *Br. J. Surg*., 2006**, 93**, 158-168.

3. Dawson, H. A comparative assessment of the pig, mouse and human genomes: structural and functional analysis of genes involved in immunity an inflammation. In: *The minipig in biomedical research* (Eds. A. D. Dayan, P. A. McAnulty, N.-Ch. Ganderup, K. L. Hastings), CRC Press, 2012**,** 664.

4. Fuller, J., B. S. Ashar, J. Carey-Corrado. Trocar-associated injuries and fatalities: an analysis of 1399 reports to the FDA. – *J. Minim. Invasive Gynecol*., 2005, **12,** 302-307.

5. Harris, H. W. Biliary system. In: *Surgery: basic science and clinical evidence* (Ed. J. A. Norton), editor, 2nd Ed. New York, Springer, 2008, 911-942.

6. Haubrich, W. S. Calot of the triangle of Calot. – *Gastroenterology*, 2002**, 123,** 1440.

7. Kemter, E., D. Joachim, W. Eckhard. "Will genetic engineering carry xenotransplantation of pig islets to the clinic?". – *Curr. Diab. Rep*., 2018, **18**(11), 1-12.

8. Lau, W. Y., E. C. Lai, S. H. Lau. Management of bile duct injury after laparoscopic cholecystectomy: A review. – *ANZ J. Surg.,* 2010**, 80**(1-2), 75-81.

9. Nagral, S. Anatomy relevant to cholecystectomy. – J. *Minim Access Surg*., 2005**, 1**, 53-58.

10. Nomina Anatomica Veterinaria. Sixth edition, prepared by the International Committee on Veterinary Gross Anatomical Nomenclature, published by the Editorial Committee Hanover (Germany), Ghent (Belgium), Columbia, MO (U.S.A.), Rio de Janeiro (Brazil), 2017**,** pp. 54, 55, 112.

11. Radunovic, M., R. Lazovic, N. Popovic, M. Magdelinic, M. Bulajic, L.Radunovic, M.Vukovic, M. Radunovic. Complications of laparoscopic cholecystectomy: our experience from a retrospective analysis. – *Open Access Maced. J. Med. Sci*., **4**, 2016, 641-646.

12. Singh, K., A. Ohri. Anatomic landmarks: their usefulness in safe laparoscopic cholecystectomy. – *Surg. Endosc*., **20**, 2006**,** 1754-1758.

13. Stefanov, I. S., N. S. Tsandev, A. P. Vodenicharov. Variations and some clinically relevant relations of a. cystica in pigs – a corrosion cast study. – *Bulg. J. Vet. Med.,* **24,** (3), 2021, 317-323.

14. **Strasberg, S. M.** Error traps and vasculo-biliary injury in laparoscopic and open cholecystectomy. – *J. Hepato-Biliary-Pancreat. Sci.,* **15**, 2008, 284-292.
15. **Talpur, K., A. A. Laghari, S. A. Yousfani, A. M. Malik, A. Memon, S. A. Khan.** Anatomical variations and congenital anomalies of extra hepatic biliary system encountered during laparoscopic cholecystectomy. – *J. Pak. Med. Assoc*., **60**, 2010, 89-93.
16. **Vollmer, C. M., M. P. Callery.** Biliary injury following laparoscopic cholecystectomy: Why still a problem? – *Gastroenterology,* **133**, 2007, 1039-1041.
17. **Whitmore, I.** Terminologia anatomica: new terminology for the new anatomist. – *Anat. Rec.*, **257**, 1999, 50-53.
18. **Zhu, H-Y, F. Li, K-W. Li, X-W. Zhang, J. Wang, F. Ji.** Transumbilical endoscopic cholecystectomy in a porcine model. – *Acta Cir. Bras*., **28**, 2013, 762-766.

Institute of Experimental Morphology, Pathology and Anthropology with Museum
Bulgarian Anatomical Society

Acta morphologica et anthropologica, 29 (1-2)
Sofia ● 2022

Traumatic Diastasis of Metopic Suture in an Adult Skull Victim of a Gunshot Wound: a Case Report

Lyubomir Gaydarski[1,3], Plamen Iliev[2], Alexandar Alexandrov[2], Boycho Landzhov[1],*

[1]*Department of Anatomy, Histology and Embryology, Medical University of Sofia, Sofia, Bulgaria*
[2]*Department of Forensic Medicine and Deontology, Medical University of Sofia, Sofia, Bulgaria*
[3]*Medical University of Sofia, Sofia, Bulgaria, medical student*

*Corresponding author e-mail: lgaidarsky@gmail.com

The metopic suture is a mid-sagittal plane variant of cranial syndesmosis, visualized from the nasion to the bregma. In most cases, the metopic suture closes during the first year of age; however, there are rare occurrences of persisting metopic suture in adults. Metopism is caused by incomplete fusion of the two embryological halves of the frontal bone. Usually, skull entry gunshot wounds are round or oval in shape and leave characteristic marks on the bone. Exit gunshot wounds to the skull are larger and more irregular. Herein we present a rare case of a human skull with a gunshot wound causing a traumatic diastasis of a complete, persisting metopic suture found during forensic examination. The gunshot wounds of the skull increase intracranial tension pressure and as a result an opening on the level of the nasion and nasofrontal suture was observed.

Key words: metopic suture, diastasis, gunshot wound

Introduction

The metopic suture is a vertical syndesmosis that connects the two halves of the frontal bone. This structure is a normal finding in the skulls of newborns, and between 3-9 months of age, it closes and allows complete fusion of the two halves of the frontal bone [14]. It is to be noted that the premature closure of the cranial sutures leads to the condition known as craniosynostosis [4]. There are two major variations of the metopic suture: complete – runs sagittal through the entire frontal bone; and incomplete that can be further subcategorized into upper – only present in the superior part of the frontal bone; middle – only present in the middle part of the frontal bone and it can be further subdivided into upper-middle and lower-middle; lower – present in the inferior part of the frontal bone [1]. The lower type shows variability in its course, and in accordance

with its shape, it can be further subdivided into linear; u-shaped;y-shaped; V-shaped; H-shaped; inverted Y-shaped; radiating types [1].

Gunshot wounds to the skull usually leave distinguishable marks and fractures to the adjacent bones. Entrance gunshot wounds to the skull vary in shape and diameter in accordance with the caliber of the projectile and the distance between the skull and the weapon. Typically, entrance wounds are round or oval in shape. Exit gunshot wounds to the skull are most commonly irregular in shape and with a wider diameter in comparison to the diameter of the entrance wound. Exit wounds normally exhibit an inward punch-out appearance [12].

Traumatic diastasis of cranial sutures is a pathological process of fracture of the suture consequently to a prior traumatic injury to the skull. This type of cranial fracture is more common in children due to the more flexible junctions at the sutures in comparison to the fully ossified adult skull [6].

Case report

During forensic examination in the Department of Forensic Medicine at the Medical University Sofia, of middle-aged human remains, it was determined that there was damage to the skull typical for a gunshot wound in the region of the head. To better assess the damage to the bones, the skull had undergone specific procedures for detachment of the remaining soft tissue. After the procedures, it was morphologically established that there were marks of gunshot damage on the skull, with an entrance wound, irregular ovoid in shape and around 9 mm in diameter, at the level of the left lateral supraorbital region. The exit wound is with irregular shape and larger in diameter than the entrance wound. Furthermore, a rare anatomical variation in the formation of the frontal bone was also present: – a continuous complete metopic suture. The atypical structure is situated in the sagittal plane, and it is a continuation of the sagittal suture, passes through the coronary suture, runs through the entirety of the frontal bone and ends inferiorly to the glabella below the level of the supraorbital margin, at the level of connection between the frontal bone and the nasal bone. As a result of the applied intracranial tension pressure, caused by the projectile, an opening of the distal part of the metopic suture, at the level of the nasion was observed. Traumatic diastases of the metopic suture and the frontonasal suture are illustrated on **Fig. 1**.

Fig.1. Photo of the skull of a gunshot wound victim with a persisting metopic suture. White arrow head – metopic suture; black arrow head – traumatic diastasis of metopic suture; white arrow – entrance gunshot wound; black arrow – traumatic diastasis of frontonasal suture, asterisk – exit gunshot wound**.**

A persisting metopic suture could be used to identify an individual by morphological criteria, if such peculiarity had been known and registered in the medical record of the given individual during his lifetime.

Discussion

Metopism, or the persistence of the frontal (metopic) suture in adults, is considered a rare anatomic variant [1; 3; 5; 13; 15]. The prevalence of this variation deviates throughout the literature. Furthermore, the incidence rate of metopism varies from race to race. According to Bergman [3], metopism has an incidence rate of 1-12%. According to Bryce [5], metopism is found in 8.7% of European skulls, 5.1% of Mongolian skulls, 1.2 of Negroid skulls and 1% of Australian skulls. According to Zdilla [15] the prevalence of metopism in European skulls is 8.06%; in 15.38% of Asian skulls; in 2.20% of Egypt skulls, 2.86% of Benga skulls. Moreover, metopism is more common in females (3.77%) than in males (1.79%) [15].

As anatomical variation, the persistent metopic suture has no immediate clinical significance. However, studies suggest link between the persistence of the metopic suture and the suppression of the development of the frontal sinus [4; 8-11]. According to the study of Guerram et al. [8], there was a statistical significance between metopism and hypoplasia of the frontal sinus: 50.8% of the skulls with persisting metopic suture were found to have bilateral hypoplasia of the frontal sinus, in comparison to the 9.4% of the normal skulls with this condition. According to Nikolova et al. [9], there was a statistically significant link between the persistence of the metopic suture and aplasia of the frontal sinus: 27,5% of the skulls with metopism had aplasia of the frontal sinus (20% unilateral and 7.5% bilateral) in comparison of 4.8% of the skulls in the control group exhibited aplasia of the frontal sinus. In another study, Nikolova et al. [10] found that 19.35% of the skulls with metopism exhibited aplasia of the frontal sinus (7.53% bilateral and 11.83% unilateral – 9.68% right and 2.15% left) in comparison to the 12.41% of the skulls in the control group with such condition. In 22,58% of the skulls with metopism exhibited hypoplasia of the frontal sinus (8.60% bilateral; 13.98 unilateral – 12.90% right and 1.08% left) in comparison to the 13.14% of the skulls from the control group with such condition. It is apparent that most commonly, the right frontal sinus is affected.

Gunshot wounds to the skull are associated with powerful pressure forces acting on the cranial bones. Initially the bullet causes inwards puncture pressure to entrance wound bone, which travels towards the adjacent bones and damages them. Afterwards the bullet causes intracranial tension pressure, when passing inside the skull. Lastly, the bullet causes outwards puncture pressure to the bone of the exit wound, which travels to the neighboring bones and damages them. The amount of pressure applied by the bullet depends on its mass, velocity, shape and trajectory [7]. As a result of the intracranial tension pressure caused by the bullet there might occur a traumatic diastasis of the coronary sutures.

Even though the persisting metopic suture is a rare anatomical variant without underlying pathology, it might be misinterpreted as a fracture of the frontal bone during

different radiological tests [2]. Therefore, knowledge of this ordinarily occurring deviation in the development of the frontal bone is paramount for radiologists, neurosurgeons and orthopedists.

Conclusion

The persisting metopic suture in adults – metopism is a standard anatomical variant with no primary underlying pathology. However, though, metopism might be the cause of suppressed development of the frontal sinus. Furthermore, the persisting metopic suture might mimic a frontal bone fracture and might be misinterpreted by inexperienced radiologists.

Acknowledgments: "The authors sincerely thank those who donated their bodies to science so that anatomical research could be performed. The results from such research can potentially increase mankind's overall knowledge that can then improve patient care. Therefore, these donors and their families deserve our highest gratitude."

Ethical Approval The article was performed in accordance with the ethical standards, approved by the Medico-Legal Office and Local Ethics Committee, Medical University of Sofia.

References

1. Ajmani, M. L., R. Mittal, S. Jain. Incidence of the metopic suture in adult Nigerian skulls. – *J. Anat.*, **137***,* 1983, 177-183.

2. Bademci, G., T. Kendi, F. Agalar. Persistent metopic suture can mimic the skull fractures in the emergency setting? – *Neurocirugia (Astur)*, **18(3)**, 2007, 238-240.

3. Bergman, R. A., A. K. Afifi, R. Miyauchi. Illustrated encyclopedia of human anatomic variation. Frontal bone [Internet] Anatomy Atlases, 2021. Available from: https://www.anatomyatlases.org/AnatomicVariants/SkeletalSystem/Text/FrontalBone.shtml

4. Bilgin, S., U. H. Kantarcı, M. Duymus, C. H. Yildirim, B. Ercakmak, G. Orman, B. C. Gunenc, M. Kaya, M. Gok, A. Akbasak. Association between frontal sinus development and persistent metopic suture. – *Fol. Morph.*, **72(4)**, 2013, 306-310.

5. Bryce, T. H. Osteology and Arthrology. – In: *Quain's Elements of Anatomy* (Eds. Schäfer, Symington, Bryce), 11th ed., London, Longmans Green, 1915, 177.

6. Campobasso, C. P., F. De Micco, V. Bugelli, A. Cavezza, W. C. Rodriguez 3rd, B. D. Pietra. Undetected traumatic diastasis of cranial sutures: a case of child abuse. – *Forensic Sci Int.*, **298(1)**, 2019, 307-311.

7. Fackler, M. L. Gunshot wound review. – *Ann. Emerg. Med*., **28(2)**, 1996, 194-203.

8. Guerram, A., J. M. Le Minor, S. Renger, **G. Bierry**. Brief communication: The size of the human frontal sinuses in adults presenting complete persistence of the metopic suture. – *Am. J. Phys. Anthropol*., **154(4)**, 2014, 621-627.

9. Nikolova, S., D. Toneva, I. Georgiev, **N. Lazarov**. Digital radiomorphometric analysis of the frontal sinus and assessment of the relation between persistent metopic suture and frontal sinus development. – *Am. J. Phys. Anthropol*., **165(3)**, 2018, 492-506.

10. Nikolova, S., D. Toneva, I. Georgiev. A persistent metopic suture –incidence and influence on the frontal sinus development (preliminary data). – *Acta morphol. anthropol*., **23(1)**, 2016, 85-92.

11. Nikolova, S., Toneva, D., Georgiev, I., **N. Lazarov**. Relation between metopic suture persistence and frontal sinus development. – *Challenging Issues on Paranasal Sinuses* (Ed. Tang-Chuan Wang), IntechOpen, 2018. Available at: https://www.intechopen.com/chapters/62423.
12. Quatrehomme, G., M. Y. Işcan. Gunshot wounds to the skull: comparison of entries and exits. – *Forensic Sci. Int*., **94(1-2)**, 1998, 141-146.
13. Vinchon, M. The metopic suture: Natural history. – *Neurochirurgie*, **65(5)**, 2019, 239-245.
14. Vu, H. L., J. Panchal, E. E. Parker, N. S. Levine, P. Francel. The timing of physiologic closure of the metopic suture: a review of 159 patients using reconstructed 3D CT scans of the craniofacial region. – *J. Craniofac. Surg*., **12(6)**, 2001, 527-532.
15. Zdilla, M. J. , M. L. Russell, A. W. Koons, K. N. Bliss, K. R. Mangus. Metopism: a Study of the Persistent Metopic Suture. – *J. Craniofac. Surg*., **29(1)**, 2018, 204-208.

Institute of Experimental Morphology, Pathology and Anthropology with Museum
Bulgarian Anatomical Society

Acta morphologica et anthropologica, 29 (1-2)
Sofia ● 2022

Review Articles

The Population of Serdica During the Late Antiquity (IV-VI A.D.) According to Anthropological and Archaeological Data

Vanyo Panchev

Institute of Experimental Morphology, Pathology and Anthropology with Museum, Bulgarian Academy of Sciences

*Corresponding author e-mail: vlpanchev1@gmail.com

Burial facilities and bone remains of people who lived in antiquity are a valuable source of archaeological and anthropological information: about the age and sex distribution of past population and the lifestyle of people who inhabited corresponding territory. Skeletal remains reveal traces of various pathological conditions, traumatic injuries and signs of medical treatment. Complex analysis finds clues for ethnic and religious affiliation and social status of the deceased. The current review aims to summarize available anthropological and archaeological data about population of Serdica and to assess its structure during the Late Antiquity (4th-6th c. AD). The paleoanthropological material from the Serdica's necropolises is insufficient to draw reliable conclusions about the demographic structure (age and sex distribution, age specific mortality and average life span), lifestyle of the ancient population, pathological processes and causes of death. It can be assumed that the average life expectancy in adults is not much different from that of the Roman period.

Key words: Serdica, paleoanthropology, Late antiquity, Western necropolis, Eastern necropolis

Introduction

During the Late Antiquity of the present Bulgarian territory (mostly parts from provinces Thracia and Moesia Inferior), dozens of towns have been established and nowadays are partially or completely studied. Serdica continues its development from previous period and is mentioned in historical sources throughout the whole Late Antiquity [26]. The history of the Roman town begins with the fall of Thracian lands under Roman authority after 45 AD. During the reign of emperor Traian the settlement received urban status and the name of emperor's family – *Ulpia Serdicae* [8]. The

town is important trade, administrative and spiritual center during the Roman and the Late Antique periods [9]. The chronological border of the study covers the time from the end of 3th-beginning of 4th to 6th c. AD. During this period many changes in the Roman Empire and in the Balkans took place, which had led to a positive change in the development of Serdica [5]. The new status of the capital of the province of Inner Dacia, the adoption of Christianity as equal (Milan edict of 313 AD), as well as the proclamation of Constantinople as capital by Constantine the Great accelerated the development of the ancient town. Historical events such as the Church council of 343 AD. and the invasions of Hun tribes from the middle of the 5th c. AD left their mark on the image of the city and its population [26].

From archaeological and anthropological perspectives, the burial facilities and bone remains of people who lived in past periods are a valuable source of information about the sex and age distribution of buried; about the life of the people who inhabited the corresponding territory; about various pathological conditions, traumatic injuries and signs of medical treatment (trepanations), about the ethnic and religious affiliation and social status of the deceased, etc.

The current review aims to summarize available anthropological and archaeological data for the town of Serdica and to assess the structure of its population during the Late Antiquity (4th-6th c. AD).

The study focusses on the published anthropological data from the East and West necropolises of Serdica [2, 3, 7, 12, 20, 24, 25], as well as from the Late Antique mausoleum and burials in the Lozenets district [10, 11, 18, 21, 23, 27]. In achievement of more detailed picture, the data from the already studied synchronous necropolises of on the territory of Bulgaria are also examined [14, 15, 16].

Archaeological data

Archaeological studies have so far contributed to the clarification of the main construction periods of the town [1, 4]. The topography and planning of the ancient city are largely clarified, and the cited two urban necropolises are localized and explored (still partially).

The Eastern Necropolis has been the subject of research since the end of the 19th century [24]. It is located about 170 meters from the fortified territory. The necropolis is used for a long period of time (from the last decades of 2th – the beginning of the 3th c. AD to the 16th-17th c. AD). During this long period, according to the available archaeological information it is assumed that various burial rites (pagan, Christian and Muslim) have been applied. In the center of the necropolis rises the iconic Church of St. Sophia, as a result from at least three major reconstructions [5].

Serdica‘s Western necropolis was discovered in the beginning of last century by B. Filov [1] and has been investigated for more than a century, but remains studied to a lesser extent [12]. It develops in Southwest direction, near the West city Gate. Like the Eastern one, the Western necropolis developed around on other basilica. The studies carried out so far have identified three vaulted tombs, dated to the late 4th and 5th c. AD, 38 burial facilities and seven tombstones – of the Early Christian community, some of them presenting church officials [12]. In 2018 part of Western necropolis is excavated at „Solen pasar“ site [25]. Remains of 24 individuals, buried as Christians are discovered and dated in 4th to 5th c. AD.

In the Lozenets district, during studies in 1954, a part of a massive building was discovered, which was interpreted as a basilica. In 2001, after a comprehensive study of the same building, it was established that it was a Late Antique family mausoleum of a wealthy citizens, which functioned from the last quarter of the 4th to the first decades of the 5th c. AD [10]. Excavated graves from mausoleum area in 2020 were published recently, as well as burials in its vicinity in Lozenets district [11, 18]. After these finds could be supposed that a necropolis developed also in South direction of ancient Serdica in Roman period and Late Antiquity, which is important addition to the information from already known Eastern and Western necropolises.

Another excavated mausoleum is located in present Stefan Karadzha district [6]. It is part of villa complex in vicinity of Serdica and includes four burial chambers. From architectural point of view it presents a similar plan as the one in Lozenets.

A number of epigraphic monuments in Latin and Greek, also provide valuable information about the population of Early Christian Serdica [17]. Most often, these are Christian tombstones and construction inscriptions with information about the origin, profession and religion of ancient inhabitants.

Anthropological data

The excavations of burial complexes provide anthropological material, which study contributes to the reconstruction of processes, which took place in the population of the Late Antiquity town. The paleoanthropological investigations provide detailed information about the age and sex of buried, their anthropological type and physical development. Human bones retain signs of various pathological changes and incidents of human influence on the body, conducted ante- or post-mortem.

Anthropological studies of the population of ancient Serdica have been carried out since the beginning of the 20th century [2, 3, 7]. Compared to the investigations of Late Antique populations studied from the other necropolises unearthed in the Bulgarian territory, those from Serdica are scarce. This is due to the location of the necropolises (under the modern center of the capital) and poor preservation of human bone remains of Late Antiquity in the specific soil conditions.

In the 20th century, major paleoanthropological studies were associated with excavations within the Eastern necropolis [2, 3, 7]. Skulls of eight individuals (a child and seven men) from a Christian tomb have been discovered and studied [7]. By the anthropological characteristics of the skulls, male individuals fall into the groups of adults (*Adultus,* 20-30 years) and maturs (*Maturus,* 40-50 years). Skulls are meso- and brachycrane and are not racially homogeneous. Due to their poor preservation, no more extensive analyses and conclusions have been made [7]. A partially preserved dolichocrane skull with trepanation has been studied. The probable reason of the procedure is the treatment of neuro-mental illness [3]. The patient did not survive the procedure. From historical sources it is known that surgical trepanations in the past have been carried out in connection with the treatment of traumatic wounds, nervous or mental illnesses. By metric and descriptive traits of the skull, the individual is identified as an adult man (between 25-30 years). Due to the absence of the facial skull, race identification is impossible. This is one of the few known cases of skull trepanation in Bulgaria and Serdica in particular and presents a technique which

has not been used in other known cases [22, 28]. The find shows advanced medical technique, practiced in the Roman Empire that the local Serdician medicals were familiar with [3].

In recent years paleoanthropological studies have also been carried out on the territory of the Western necropolis of the town, with the bone material from two tombs (II and III) and 7 graves [12, 13, 20]. The identified men split into the groups of adultus (20-40 years) and maturus (40-60 years) and women in the group of adults (20-40 years). In two of the buried (a male and a female), the age at death was defined at about 20 years, and for all others death occurred at the age of over 20 years. Traces of various pathological processes have been identified on the bone remains, the most common being dental pathologies (paradontosis and carious changes of the teeth), dystrophic changes of joint surfaces (spondylosis and arthrosis). Evidences for the anthropological type of buried are scarce, only height being achieved for a few male individuals due to incomplete and fragmented material [20]. It is reconstructed to vary between 165.8 and 172.52 cm (according to the Pearson-Lee formula) and 172.45 to 177.52 (according to the Trotter-Glaeser formula). Recently studied individuals from „Solen pasar“ site present a case of possible artificial deformation of the head in one child (gr. № 9, *Infans I*) and mongoloid influence in features of the skull of an adult male (gr. № 12) (unpublished material provided by Victoria Ruseva to whom I am grateful). These specifics could be a result of infiltration in Serdica of elements from arriving populations in Europe during the Great migration of peoples.

Paleoanthropological material from the Late Antique mausoleum in Lozenets district presents eight individuals – two children between 5 and 7 years (age group of *Infans I)*, one men in the senile age, at about 60-65 years, two men and two women at about 45-50 years at death (in the age group *Maturus*) and a woman at younger age, in group of adults, at about 35-40 years [27]. The height of the buried individuals is determined from the bones of the postcranial skeletons. Men fall into the category “tall” (182.05 cm /174.07 cm), and women in the category „medium“ (166.32 cm/157.58 cm), according to formulas mentioned above. According to the metric and descriptive traits of the skulls, the authors assign them to the Southern European racial type, with predominant of Dinaric-Mediterranean characteristics [27]. Latest anthropological analyzes from Lozenets mausoleum gives information about woman (30-40) who suffered from initial form of disability with limping gate acquired after trauma [21].

More detailed information about Late Antiquity populations from the present Bulgarian territory provide paleodemographic studies for other investigated urban necropolises such as those of Augusta Trayana, Abritus, Kabile, Kaliakra [14, 15, 16, 19]. From the analyses, the higher number of men in adult and elderly age, with life expectancy between 42 and 47 years makes an impression. On average, men in their 20^{s} lived up to 43.9 years. For women, life expectancy is lower, in average of four-seven years and they are expected to live up to 42.7 years. This observation is associated with their higher mortality rate in the age group of adults (20-40 years), explained with complications during pregnancy and childbirth [14, 19]. High infant mortality, specific for preindustrial populations is also reported, in average it varies between 25-30 and 40-45 % for buried at the age 0-14 years in most studied necropolises (Kabyle, Kaliakra, Augusta Traiana, Koprivlen). In most cases relative number of buried in the age group of *Infans* I, in the interval of 0-4 years

is higher [14, 15, 19]. It is assumed that high mortality rates are due to factors such as hygiene level, medical development and living environment [14]. In the studied populations, there are variations in the height of individuals. For men it is from medium (165.5 cm) to high (173.3 cm), and for women – below average (150.7 cm) and medium (153.7 cm). A pathological processes established among the Serdician society, have also been found in the other studied populations from Late Antiquity [16, 20, 21] – dental pathologies (presence of dental calculus, periodontal changes, and carious changes in the teeth), degenerative joint disease (spondyloarthrosis and arthrosis). Common in addolescent age (14-18 years) is the osteoporosis of the upper orbital wall (cribra orbitalia), which is associated with anemia of various origins. Pathological conditions are also traumas, mainly fractures of the long bones of the limbs, possibly a consequence of physical impact. Paleopathological findings are an indicator of living conditions, diet, work activity, lifestyle and social situation of the studied population [2, 3, 14, 15, 16, 19]. The study of pathological changes of bones can contribute in clarifying the causes of death or the state of health of the individual in life. Paleopathological analysis shows relatively good health of populations during Late Antiquity and the presence of favorable living conditions with high level of hygiene practices and medicine.

The carried out racial-typological analysis of the Ancient populations shows an affiliation with the Southern European racial types with a predominance of marks of the Mediterranean race.

The discovered and studied so far paleoanthropological material from the necropolises of Ancient Serdica is insufficient to draw reliable conclusions about the demographic structure (age-sex distribution, average life span) and lifestyle of the population of the ancient town, pathological processes and causes of death. It can be assumed that the average life expectancy of Late Antique Serdicians was not much different from that of the Roman period, according to the calculations of Boev, Kondova, Cholakov – 42 and 47 years. The estimated life span for men is 4-7 years higher than that of women. Men were medium to tall, and women were middle and below average stature. Dental pathologies (presence of dental calculus, periodontal changes and carious changes of the teeth), degenerative-dystrophic changes of joint surfaces and traumatic injuries were common. In general, the Late Antique populations, which inhabited our lands had a relatively good health condition. The individuals belonged to the Southern European racial type, and there are also dinaro-mediteran variants.

Acknowledgements: This work was supported by the Bulgarian Ministry of Education and Science under the National Research Programme "Young scientists and postdoctoral students" approved by DCM No 577 / 17.08.2018.

R e f e re n s e s

1. Bobchev, S. Revew of the ruins from Serdica, discovered in last fifty years – *Serdica. Arachaeological exavations and materials* 2, Sofia 1989, 37 – 59 (Бобчев С. Преглед на останките от Сердика, открити в течение на петдесет години – *Сердика. Археологически материали и проучвания.* 2, София 1989, 37-59) [In Bulgarian].

2. Boev, P. Anthropological studies of skulls from Serdica and ancient Sofia. *Biolog. and med. science*, BAS, 3, 1957, 13-23 (Боев, П. Антропологични изследвания на черепи от Сердика и Стара София. *Биологически и медицински науки*, БАН, 3 1957, 13-23) [In Bulgarian]
3. Boev, P. Trepanned skull from Sofia – *Archaeology journal*, 1961, book 4, 70-72 (Боев, П. Трепаниран череп от София – *списание Археология* 1961, книга 4, 70-72) [In Bulgarian]
4. Boyadzhiev, St. Serdica. Urban planning, fortification, public, private, cult and cemeterial buildings between II – IV c. – *Roman and early Bizantine towns in Bulgaria.* I. Sofia, 2002, 125-180 (Бояджиев, Ст. Сердика. Градоустройство, крепостно строителство, обществени, частни, култови и гробнични сгради през II – IV в. – *Римски и ранновизантийски градове в България*, I, София 2002; 125 – 180) [In Bulgarian]
5. Dinchev, V. „Saint Sofia" and Serdica, Sofia, 2014 (Динчев, В. „Св. София" и Сердика, София, 2014) [In Bulgarian]
6 Dinchev, V. Roman villas in today's Bulgarian territory, Sofia 1997, 52 (Динчев, В. Римските вили в днешната българска територия, София 1997, 52) [In Bulgarian]
7. Dronchilov, K. Skulls from old Christian tomb in Sofia – NBAC, 1919 – 1920, 58 – 69 (Дрончилов К. Черепи от старохристиянска гробница в София – В: ИБАД, 1919 – 1920, 58-69) [In Bulgarian]
8. Gerov, B. Studies on Western Thrace lands in roman time. Part II, 1967, 72 – 89 (Геров, Б. Проучвания върху Западнотракийските земи през римско време. Част II, 1967, 72 – 89) [In Bulgarian]
9. Gerassimov, T. Serdica. Archaeological materials and studies. I, 1964, 5-7 (Герасимов, Т. Сердика. Археологически материали и проучвания. I, 1964, 5-7) [In Bulgarian]
10. Ivanov, M. Elephantum ex musca! On the chronology, periodization and function of the Late Antique mausoleum in Lozenets residential district, Sofia. – *Archaeology journal*, XLIX, book 1-4, 2008, 149-159 (Иванов М. Elephantum ex musca! За хронологията, периодизацията и функцията на късноантичния мавзолей в кв. Лозенец, София. – *Археология* XLIX, Кн. 1- 4, 2008, 149 – 159.) [In Bulgarian]
11. Ivanov, M. Harizanov, Al. Late roman necropolis in Lozenets quarter, Sofia – *Archaeological discoveries and excavations in 2020.* Book II, Sofia 2021, 919-922 (Иванов, М. Харизанов, Ал. Късноримски некропол в кв. Лозенец, София – *Археологически открития и разкопки през 2020 г.* Книга II, София 2021, 919-922) [In Bulgarian]
12. Kirova, N. Tombs from Western necropolis of Serdica – *Archaeology journal* XLVIII, book 1 – 4, 2007, 38 – 45. (Кирова Н. Гробници от западния некропол на Сердика. *Археология* XLVIII, кн. 1 – 4, 2007, 38-45) [In Bulgarian]
13. Kirova N. Antique site in third rescue zone of HAR „Serdica - Sredets", Dame Gruev str. № 8, Sofia, in 2006 – *Archaeological discoveries and excavations in 2006.* Sofia, 2007, 314 – 317 (Кирова Н. Античен обект в трета спасителна зона на ИАР „Сердика - Средец", ул. Даме Груев № 8, София, през 2006 – *Археологически открития и разкопки през 2006г.*, София, 2007, 314 – 317) [In Bulgarian]
14. Kondova, N., P. Boev, S. Cholakov. Biological reconstruction of Late Antique populations from Bulgarian lands – *Bulgarian ethnography*, IX,2, 1984 . Sofia. 27 – 32 (Кондова, Н. Сл. Чолаков. Биологична реконструкция на късноантични популации от българските земи – *Българска етнография*, IX, 2, 1984, Sofia, 27-32) [In Bulgarian]
15. Kondova, N., S. Cholakov. Paleoanthropological data about demographic processes in Bulgarian lands during the Roman period – *Bulgarian Ethnography* XIV, 1 1989, 31-38 (Кондова, Н. Сл. Чолаков. Палеоантропологични данни за демографските процеси в българските земи през римския период – *Българска етнография*, XIV,1 1989, 31-38) [In Bulgarian]

16. Kondova, N., S. Cholakov, Paleodemographic and paleopathologic data of Late Antique population of Augusta Trayana. – *Acta cytobiol. et morphol*., 2, 1992, 8-16
17. Markov, K. Spiritual life in Bulgarian lands in Late Antiquity (IV – VI в.). Sofia, 1995 (Марков К. Духовен живот в българските земи през късната античност (IV – VI век), София 1995 [In Bulgarian]
18. Meshekov, Y., Stanev, Al. Rescue archaeological study of „Late Antiqe mausoleum" site, Lozenets quarter in Sofia – *Archaeological discoveries and excavations in 2020.* Book II, Sofia 2021, 915-918 (Мешеков, Юн. Станев, Ал. Спасително археологическо проучване на обект „Късноантичен мавзолей", кв. Лозенец в София – *Археологически открития и разкопки през 2020 г.* Книга II, София 2021, 915-918) [In Bulgarian]
19. Ruseva, V. Anthropological data on changes in mortality and life span on the territory of Bulgaria from neolithic to late antiquity. IEMPAM – BAS. (Abstract), Sofia, 2003 (Русева В. 2003: Антропологични данни за промените в смъртността и продължителността на живота на територията на България от неолита до късното средновековие. Автореферат, ИЕМПАМ – БАН, София 2003) [In Bulgarian]
20. Ruseva, V. Anthropological investigations of buried in the section of the Western cemetery of Serdica – *Interdisciplinary studies XX-XXI*, 2009, BAS, Sofia, 56-70 (Русева В. Антропологично проучване на погребаните в сектор от Западния некропол на Сердика – В: *Интердисциплинарни изследвания XX – XXI*, 2009, БАН, София 56-70) [In Bulgarian]
21. Russeva, V., N. Atanassova, G. Tomov. Anthropological investigations in 2020 (preliminary results) – Archaeological discoveries and axcavations in 2020, Book 1, Sofia 2021, 171-178 (Русева, В. Атанасова, Н. Томов, Г. Антропологични изследвания през 2020 г. (предварителни резултати) – Археологически открития и разкопки през 2020 г. Книга I, София 2021, 171-178 [In Bulgarian]
22. Russeva, V. Religion, magic or medicine? New finds of trepanned skulls from Southeast Bulgaria, XI-XIII c. – *Archaeologia Bulgarica*, XVI, 2, 2016, 1-28.
23. Shalganov, K., M. Ivanov. A recent excavated mausoleum in the Lozenets quarter, Sofia in 2001. – *Spartacus II (2075 years from the Spartacus uprising/ Thrace-Roman heritage/ 2000 years of Christianity).* International symposium 1 – 4 october 2002. Sandanski. Veliko Tarnovo, 2006, 314 – 324. (Шалганов К., М. Иванов. Новооткрит късноантичен мавзолей в кв. Лозенец през 2001г. – *Spartacus II (2075 години от въстанието на Спартак/ трако – римско наследство/ 2000 години християнство).* Международен симпозиум 1 – 4 октомври 2002г. Сандански. Велико Търново, 2006, 314 – 324) [In Bulgarian]
24. Shkorpil, K. Medieva churches and cemeteries in Sofia – *Collection of folk tales, science and literature*, book II, 1890, 46-60, table 1-5 (Шкорпил, К. Средновековни гробища и църкви в София. – *Сборник за народни умотворения и книжнина*, книга II, София 1890, 46 – 60) [In Bulgarian]
25. Vassileva, El., An. Cholakova. Western necropolis of Serdica – Rescue archaeological excavation of „Solen pasar" site, Sofia – *Archaeological discoveries and axcavations in 2018*. Sofia 2019, 428-431 (Василева, Ел. Чолакова, Ан. Западен некропол на Сердика – Спасително археологическо проучване на обект „Солни пазар", гр. София – *Археологически открития и разкопки през 2018 г.* София 2019, 428-431) [In Bulgarian]
26. Velkov, V. Town in Thrace and Dacia during Late Antiquity (IV – VIc.). Studies and materials, BAS, Sofia 1959 (Велков, В. Градът в Тракия и Дакия през късната античност (IV – VI в.). Проучвания и материали, БАН, София, 1959) [In Bulgarian]

27. Yordanov, Y., Br. Dimitrova, V. Ruseva. Anthropological data of the buried in the late antique mausoleum, Lozenets district, Sofia. – *Annual of NAIM – BAS*, Book II, 2002, 274 – 290 (Йорданов, Й., Бр. Димитрова, В. Русева. Антропологични данни за погребаните в късноантичния мавзолей, квартал Лозенец, София. *Годишник на НАИМ – БАН*, книга II, 2002, 274-290) [In Bulgarian]

28. Yordanov, Y., N. Atanassova, N. Dimitrov. Anthropological investigation of two skeletons with trepanations from Pliska (end of X-XI c.). – *From regional to national.* Jubilee corpus in honor of Prof. H. Haritonov, II, 43-60. (Йорданов Й., Н. Атанасова, Н. Димитров. Атропологично изследване на два скелета с трепанации от Плиска (края на X – XI в). – В: Харитонов, Х. От регионалното към националното. Юбилеен сборник в чест на ст.н.с.др Христо Харитонов, II част, 43-60.) [In Bulgarian]

Institute of Experimental Morphology, Pathology and Anthropology with Museum
Bulgarian Anatomical Society

Acta morphologica et anthropologica, 29 (1-2)
Sofia ● 2022

IN MEMORIAM

Professor Dr. Marlena Anastassova-Kristeva

On the 14th of January 2022, Professor Doctor Marlena Anastassova-Kristeva passed away at the age of 98 at her home in Los Angeles, USA.

Marlena Anastassova-Kristeva was born on the 17th of December 1923 in Berlin, Germany. She graduated Medical Faculty, Vienna University, (1944), as well as Higher Dental School (1948) and Higher Medical School (1952) at Medical Academy, Sofia, Bulgaria. In 1955 she started work as a researcher in histology and embryology, and later on, as a senior scientist at the Institute of Morphology, Bulgarian Academy of Sciences till 1979. Prof. Kristeva organized and managed research laboratories for Histochemistry, Tissue Cultures, Histoautoradiography and Karyotyping.

Between 1982 and 1990 Prof. Kristeva was honored as a professor in histology and developmental biology at the California State University Northridge (CSUN), USA. Between 1990 and 1994 Prof. Kristeva organized and managed Central Lab on AIDS research. She conducted research on BSL 3 Mouse-Human Chimeras at Core Faculty in Hematology-Oncology at University of California Los Angeles (UCLA). Since 1996 till 1999 Prof. Kristeva was teaching histology as a part time professor at School of Medicine, Department of Cell and Neurobiology, University of Southern California (USC).

Prof. Kristeva was Honorary Member of the Bulgarian Academy of Sciences (2006), The New York Academy of Sciences (1982) and Sigma Xi, USC (1981). She was a member of Union of Scientists in Bulgarian and European Cell Biology Organization, France. Since 2001 she was an official adviser in embryology for Journal of Chemotherapy and Stem cell Research, now renamed Stem Cells and Development.

Prof. Kristeva dedicated more than 50 years to students, graduated and post-graduate students. Her scientific work includes over hundred of publications and hundreds citations in journals with high impact factor.

Prof. Kristeva's major scientific achievements contributed to several areas of research: First priority was reproduction, particularly the origin of the primordial germ cells (PGC) in undifferentiated gonads, cell differentiation of germ and somatic cells, development and maturation of germ cells and meiosis. With her wide background in the field of embryology, cellular and molecular biology, Prof. Kristeva transferred her scientific activity in genetics, introducing modified method for human chromosome karyotyping. She described for the first time the changes in nucleolus that occurred during mitotic cycle in humans. She created nucleolar test for evaluation the number of satellite chromosome in plants and animals, widely cited and applied in molecular biology and pathology.

After retirement at 2000, Prof. Kristeva was completely devoted on theoretical science and published many articles in prestigious scientific journals. In 2003 she published an article entitled: "The origin and development of immune system with a view to stem cell therapy" in "Journal of Chemotherapy and Stem Cell Research". She reported her new concepts about hemopoiesis, lymphopoiesis and macrophage-monocyte systems. Comparative study on lymphopoiesis, hemopoiesis and macrophage system during phylogeny and ontogeny showed her contemporary concept that lymphocytes and macrophages originate in the bone marrow from a common hematolymphoid precursor.

In the paper "The secret of epigenetics and its implication for cell therapy" (2007), Prof. Kristeva postulates that since the morphogens selectively unlock new genes, it will be possible production of morphogens and selective trans-differentiation of adult patient cells *in vitro*.

Obtaining pluripotent embryonic cells from patient cells in vitro, and production of such nutrient medium, named "cloning medium" will be indisputably very profitable.

On the basis of her erudition and fundamental knowledge in embryology, cell differentiation and genetics, she published few articles in journal Stem Cells and Development, entitled: "Morphogens Reveal the Appearance and Function of IncRNAs" (2015) and "Correspondence on: A Hyaluronic Acid-Rich Node and Duct System in which Pluripotent adult Stem Cells Circulate" (2016). She hypothesized that the nuclear HOX proteins bind the mRNAs and suppress translation turning them into IncRNAs. This new compound (HOX protein + mRNA) is a morphogen, which explains in a very elegant manner the molecular mechanism of cell differentiation and the great and multifaceted repertoire of RNAs. According to Prof. Kristeva this scientific data open great possibilities for further research in the field of gene engineering giving the manner of producing morphogens *in vitro* for cell therapy. In this article she concluded that the transcripts of each gene may be coding or non-coding, depending on the proteins they bind. The morphogenesis (mRNAs bind with HOX proteins) in the embryonic cells (blastomere) are synthesized in the oocyte and during the cleavage

segregate in a special order in the blastomere, determining the body plan of the future embryo. The morphogens make the early embryo cell pluripotent. The two elements – HOX proteins and non-coding RNAs applied separately cannot work as morphogens.

Prof. Kristeva declared the great discovery she made studying the meiosis. She knew that her hypothesis will face extreme opposition within the scientific community. However, on the basis of her half-century-long scientific career, she was obligated to share her knowledge with younger scientists to achieve a deeper insight into the evolution of the immune system.

A remarkable Editorial's note on her last article was: "She was an accomplished embryologist who maintains a vigilant survey of the interpretation of key results in the field of phylogeny and ontogeny of hematopoietic, lymphopoietic and macrophage systems as well as of stem cell research".

Nevertheless, working in United States for many years, Prof. Kristeva always published her articles on behalf of Institute of Morphology, Bulgarian Academy of Sciences, thus presented our science in the world. She never lost her connections with all her former students and collaborators. With her vitality, enthusiasm, goodwill and encyclopedic knowledge, Prof. Kristeva never will be forgotten. By her death Bulgarian Academy of Sciences as well as Bulgarian Morphological School lost a great scientist.

Yordanka Martinova

Author Guidelines

Acta morphologica et anthropologica is an open access peer review journal published by Bulgarian Academy of Sciences, Prof. Marin Drinov Publishing House.
Corporate contributors are Bulgarian Academy of Sciences, Institute of Experimental Morphology, Pathology and Anthropology with Museum and Bulgarian Anatomical Society.

Acta morphologica et anthropologica is published in English, 4 issues per year.
The journal accepts manuscripts in the following **fields**: experimental morphology, cell biology and pathology, anatomy and anthropology.

Publication types: original articles, short communications, case reports, reviews, Editorial, letters to the Editors.

Acta morphologica et anthropologica is the continuation of Acta cytobiologica et morphologica

The **aim** of the Journal is to disseminate current interdisciplinary biomedical research and to provide a forum for sharing new scientific knowledge and methodology. The general editorial policy is to optimize the process of issuing and distribution of *Acta morphologica et anthropologica* in line with modern standards for scientific periodicals focusing on content, form, and function.

Scope – experimental morphology, cell biology and pathology (neurobiology, immunobiology, tumor biology, environmental biology, reproductive biology, etc.), new methods, anatomy and pathological anatomy, anthropology and paleoanthropology, medical anthropology and physical development.

Acta morphologica et anthropologica is published twice a year as one volume with 4 issues. For the first two issues (1-2) the deadline for manuscript submission is March 15th and for the next two issues (3-4), the deadline is September 15th. Electronic version for issues 1-2 is uploaded on the website till June 30th and for issues 3-4 – till December 30th.

Contact details and submission

Manuscript submission is electronical only. The manuscripts should be sent to the Managing Editor's e-mail address ygluhcheva@hotmail.com with copy to iempam@bas.bg
All correspondence, including notification for Editor's decision, requests for revision, is sent by e-mail.

Article structure

Manuscripts should be in English with total length not exceeding 10 standard pages, line-spacing 1.5, justified with 2.5 cm margins. The authors are advised to use Microsoft Word 97-2003, Times New Roman, 12 pt throughout the text. Pages should be numbered at the bottom right corner of the page.

The article should be arranged under the following headings: Introduction, Material and Methods, Results, Discussion, Conclusion, Acknowledgements and References.

Title page – includes:

- **Title** – concise and informative;
- **Author(s)' names and affiliations** – indicate the given name(s) and family name(s) of all authors. Present the authors' affiliation addresses below the names. Indicate all affiliations with a lower-case superscript after the author's name and in front of the appropriate address. Provide the full postal address information for each affiliation, including the country name.
- **Corresponding author** – clearly indicate who will handle the correspondence for refereeing, publication and post-publication. An e-mail should be provided.
- **Abstract** – state briefly the aim of the work, the principal results and major conclusions and should not exceed 150 words. References and uncommon, or non-standard abbreviations should be avoided.
- **Key words** – provide up to 5 key words. Avoid general, plural and multiple concepts. The key words will be used for indexing purposes.or indexing purposes.

Introduction – state the objectives of the work and provide an adequate background, avoiding a detailed literature survey or summary of the results.

Material and Methods – provide sufficient detail to allow the work to be reproduced. Methods already published should be indicated as a reference: only relevant modifications should be described.

Results – results should be clear and concise.

Discussion – should explore the significance of the results in the work, not repeat them. A combined *Results and Discussion* section is often appropriate. Avoid extensive citation and discussion of published literature.

Conclusions – the main conclusions of the study should be presented in a short section.

Acknowledgements – list here those individuals who provided help during the research and the funding sources.

Units – please use the International System of Units (SI).

Math formulae – please submit math equations as editable text, not as images.

Electronic artwork – number the tables and illustrations according to their sequence in the text. Provide captions for them on a separate page at the end of the manuscript. The proper place of each figure in the text should be indicated in the left margin of the corresponding page. **All illustrations (photos, graphs and diagrams)** should be referred to as "figures" and given in abbreviation "Fig.", and numbered in Arabic numerals in order of its mentioning in the manuscript. They should be provided in grayscale as JPEG or TIFF format, minimum 300 dpi. The illustrations should be submitted as separate files.

References – they should be listed in alphabetical order, indicated in the text by giving the corresponding numbers in parentheses. The "References" should be typed on a separate sheet. The names of authors should be arranged alphabetically according to family names. In the reference list titles of works, published in languages other than English, should be translated, original language must be indicated at the end of reference (e.g., [in Bulgarian]). Articles should include the name(s) of author(s), followed by the full title of the article or book cited, the standard abbreviation of the journal (according to British Union Catalogue), the volume number, the year of publication and the pages cited, for books - the city of publication and publisher. In case of more than one author, the initials of the second, third, etc. authors precede their family names. Ideally, the names of all authors should be provided, but the usage of "et al" after the fifth author in long author lists will also be accepted.

For articles: **Davidoff, M. S., R. Middendorff, G. Enikolopov, D. Riethmacher, A. F. Holstein, D. Muller**. Progenitor cells of the testosterone-producing Leydig cells revealed. – *J. Cell Biol.,* **167**, 2004, 935-944.

Book article or chapter: **Rodriguez, C. M., J. L. Kirby, B. T. Hinton. The development of the epididymis.** - In: *The Epididymis - from molecules to clinical practice* (Eds. B. Robaire, B. T. Hinton), New York, Kluwer Academic Plenum Publisher, 2002, 251-269.

Electronic books: **Gray, H.** *Anatomy of the human body* (Ed. W.H.Lewis), 20th edition, NY, 2000. Available at http://www.Bartleby.com.

PhD thesis: **Padberg, G**. Facioscapulohumeral diseases. *PhD thesis*, Leiden University, 1982, 130 p.

Website: National survey schoolchildren report. National Centre of Public Health and Analyses, 2014. Available at http://ncphp.government.bg/files

Page charges

Manuscript publication is free of charges.

Ethics in publishing

Before sending the manuscript the authors must make sure that it meets the Ethical guidelines for journal publication of Acta morphologica et anthropologica.

Human and animal rights

If the work involves the use of human subjects, the authors should ensure that work has been carried out in accordance with *The Code of Ethics of the World Medical Association* (Declaration of Helsinski). The authors should include a statement in the manuscript that informed consent was obtained for experimentation with human subjects. The privacy rights of human subjects must always be observed.
All animal experiments should comply with the *ARRIVE guidelines* and should be carried out in accordance with the U.K. Animals (Scientific procedures) Act, 1986 and the associated guidelines *EU Directive 2010/63/EU* for animal experiments, or the National Institutes of Health guide for the care and use of Laboratory animals (NIH Publications No. 8023, revised 1978) and the authors should clearly indicate in the manuscript that such guidelines have been followed.

Submission Details

Acta morphologica et anthropologica is published twice a year as one volume with 4 issues. For the first two issues (1-2) the deadline for manuscript submission is March 15th and for the next two issues (3-4), the deadline is September 15th. Electronic version for issues 1-2 is uploaded on the website till June 30th and for issues 3-4 – till December 30th.

Manuscript submission is electronical only.

The manuscripts should be sent to the Managing Editor email address ygluhcheva@hotmail.com with copy to iempam@bas.bg.
All correspondence, including notification for Editor's decision, requests for revision, is sent by e-mail.

Submission declaration

Submission of the manuscript implies that the work described has not been published previously, is not considered under publication elsewhere, that its publication is approved by all authors, and that if accepted, it will not be published elsewhere in the same form, in English or in any other language, including electronically, without the informed consent of the copyright-holder.

Contributors

The statement that all authors approve the final article should be included in the disclosure.

Copyright

http://www.iempam.bas.bg/journals/acta/Author%20Copyright%20Agreement_last.pdf

Upon acceptance of an article, the authors will be asked to complete a "**Copyright Transfer Agreemen**t".
http://www.iempam.bas.bg/journals/acta/Copyright_Transfer_Agreement_Form_AMA.doc

Peer review

Once a manuscript is submitted, the Managing Editor (or the Editor-in-Chief) briefly checks the manuscript for conformance with the journal's Focus, Scope, Policies and style requirements and decides whether it is potentially suitable for publication and can be processed for review, or rejected immediately, or returned to the author for improvement and re-submission.

Manuscripts are peer-reviewed by the Editors, Editorial Board members, and/or external experts before final decisions regarding publication are made. The entire editorial workflow is performed in the following steps:

1. The submitted manuscript is checked in the editorial office whether it is suitable to go through the normal peer review process.
2. If deemed suitable, the manuscript is sent to 2 reviewers for peer-review. The choice of reviewers depends on the subject of the manuscript, the areas of expertise of the reviewers, and their availability.

3. Each reviewer will have 2 weeks to provide evaluation of the manuscript. The Editor may recommend publication, request minor, moderate or major revision, or provide a written critique of why the manuscript should not be published (rejected).
4. In case only one reviewer suggests rejection of the manuscript, the latter is subjected to additional evaluation by a third reviewer.
5. The manuscript will be published in a revised form provided that the authors successfully answer the critics received. The Editor-in-Chief is the final authority on all editorial decisions.

Open Access

This journal provides immediate open access to its content on the principle that making research freely available to the public supports a greater global exchange of knowledge.

After acceptance

Proof correction

The corresponding author will receive proofs by e-mail in PDF format and will be requested to return it with any corrections within two weeks.

ISSN 1311-8773 (print)
ISSN 2535-0811 (online)